UNIVERSIDAD DE CONCEPCIÓN

FACULTAD DE FARMACIA

Doctorado en Ciencias y Tecnología Analítica

DEVELOPMENT OF PREDICTIVE METHODS BASED ON VIS-NIR SPECTROSCOPY AND ARTIFICIAL VISION TECHNIQUES FOR THE DETECTION OF WATER STRESS IN *Eucalyptus* spp. AND A STUDY OF THEIR RECOVERY

DESARROLLO DE MÉTODOS PREDICTIVOS BASADOS EN ESPECTROSCOPIA VIS-NIR Y TÉCNICAS DE VISIÓN ARTIFICIAL PARA LA DETECCIÓN DE ESTRÉS HÍDRICO EN *Eucalyptus* spp. Y ESTUDIO DE SU RECUPERACIÓN

Thesis submitted to the Faculty of Pharmacy of the University of Concepción

for the Degree of Doctor in Analytical Sciences and Technology

By: Pamela Alejandra Sanhueza Novoa

THESIS ADVISOR: Dra. Rosario del P. Castillo Felices

Concepción, Chile

2026

Authorization

Acknowledgments

I would like to express my sincere gratitude to the National Agency for Research and Development (ANID) for the funding that made this research possible, including the National Doctoral Scholarship No. 21221771 and the complementary benefits associated with the doctoral internship abroad and operational expenses. I also gratefully acknowledge the support provided by FONDECYT projects 1221387 and 1251201, FONDEQUIP project EQM230094, and FOVI220172, whose resources contributed substantially to the development of this work.

I am deeply grateful to my thesis advisor, Dr. Rosario Castillo, for giving me the opportunity to grow professionally in a field that was initially almost entirely unfamiliar to me, but which became an important space for both professional and personal growth. Thank you for always listening to my ideas, for your trust, and for generously sharing your experience, wisdom, and advice throughout this journey.

I would also like to sincerely thank Dr. Carolina Hernández and Dr. Marta Fernández, their unconditional support and guidance were essential to making this work possible. I am deeply grateful for the time, knowledge, and generosity they shared throughout this research.

To my colleagues and friends Macarena, Mario, Martín, and Cristian, thank you for your generosity, friendship, and constant support, both professionally and personally. I will always be grateful to have found such a remarkable group of people with whom I could share not only scientific challenges, but also learning experiences, meaningful moments, and many good memories.

I am also very grateful to Yasmin, Darlei, and José Amigo, who made my doctoral research stay abroad much easier and more enjoyable. Thank you for welcoming me so warmly and for sharing your knowledge, experience, and friendship with such generosity. That stage of my training would not have been the same without you.

To my family, thank you for being an essential source of emotional support throughout this stage of my life. Thank you for accompanying me, understanding me, and supporting me through every moment, especially during the most demanding ones.

And, most especially, to my husband Sebastián. Without you, quite simply, none of this would have been possible. Thank you for being by my side throughout every stage, for your patience, your unconditional support, and for believing in me so strongly, even in those moments when you believed in me more than I believed in myself. Thank you for always being there…I love you.

And, of course, to my faithful companion Goddard…

Abstract

Water deficit is a major constraint on the productivity, establishment, and adaptability of *Eucalyptus* plantations, creating a need for rapid and non-destructive analytical tools capable of detecting plant responses before severe visible damage occurs. The main objective of this Ph.D. thesis was to develop and evaluate spectral methodologies based on visible–near infrared hyperspectral imaging (VIS–NIR HSI) and portable near-infrared spectroscopy, combined with chemometrics, machine learning, physiological measurements, recovery assessment, and candidate gene-expression analysis, for monitoring water-deficit responses in juvenile *Eucalyptus* plants.

Two sequential controlled-environment assays were conducted. An initial assay involving four genotypes was used to evaluate the feasibility of VIS–NIR HSI for differentiating mild, moderate, and severe water-deficit conditions and to compare full-spectrum information with conventional vegetation indices. A second, expanded assay involving six genotypes integrated VIS–NIR HSI, portable NIR spectroscopy, physiological measurements, gene-expression analysis, and post-stress monitoring after rewatering. Principal component analysis was used to explore spectral structure, whereas ANOVA–simultaneous component analysis (ASCA) was applied to partition spectral variability associated with genotype, sampling day, treatment condition, biological replicate, and their interactions. Supervised classification models were evaluated for binary discrimination between control and pooled water-deficit samples and for multiclass discrimination among the control condition and three progressive water-deficit stages. Partial least squares-discriminant analysis, support vector machines, k-nearest neighbors, Random Forest, Extreme Gradient Boosting, and multivariate regression methods were evaluated within the analytical workflow.

VIS–NIR HSI detected spectral changes associated with progressive water deficit more effectively than the evaluated vegetation indices. In the initial assay, supervised models based on mean spectra achieved external-validation errors between 0 and 2%, while support vector machine classification generated the most consistent spatial reconstructions of stress progression. In the expanded assay, binary discrimination between control and water-deficit samples was effective for both spectral platforms, whereas direct classification of the control condition and the three progressive water-deficit stages was less accurate because adjacent stress stages showed

substantial spectral overlap. ASCA demonstrated that VIS–NIR HSI variability was dominated by genotype, which explained 30.2% of the spectral variance, whereas portable NIR variability was primarily associated with sampling day and treatment condition, explaining 40.2% and 10.6%, respectively. An ASCA-guided hierarchical HSI workflow achieved complete correct classification in the evaluated external-validation set, while portable NIR provided a more moderate but interpretable classification of water-deficit progression.

Physiological measurements confirmed coordinated reductions in net CO_2 assimilation, stomatal conductance, photosystem II performance, and plant water status. Recovery after rewatering was incomplete and strongly genotype dependent, with the six evaluated genotypes showing contrasting degrees of restoration of water status and physiological function during the monitored recovery period. Water deficit induced DHN1, LEA4, and TRDX expression in genotype-dependent patterns, although high transcript accumulation did not necessarily indicate greater physiological tolerance. VIS–NIR HSI showed its strongest association with non-photochemical quenching, whereas portable NIR spectroscopy showed the clearest relationship with plant water potential.

Overall, the results demonstrate that VIS–NIR HSI and portable NIR spectroscopy provide complementary, biologically meaningful information for non-destructive water-deficit monitoring in *Eucalyptus*. The proposed design-aware analytical framework supports controlled-environment phenotyping and genotype screening, although independent validation across new genotypes, experimental campaigns, nurseries, and field-like environments is required before operational implementation.

Resumen

El déficit hídrico constituye una de las principales limitaciones para la productividad, el establecimiento y la adaptabilidad de las plantaciones de Eucalyptus, lo que genera la necesidad de disponer de herramientas analíticas rápidas y no destructivas capaces de detectar las respuestas de las plantas antes de que se produzcan daños visibles severos. El objetivo principal de esta tesis doctoral fue desarrollar y evaluar metodologías espectrales basadas en imágenes hiperespectrales en el visible–infrarrojo cercano (VIS–NIR HSI) y espectroscopía portátil en el infrarrojo cercano, combinadas con quimiometría, aprendizaje automático, mediciones fisiológicas, evaluación de

la recuperación y análisis de expresión de genes candidatos, para monitorear las respuestas al déficit hídrico en plantas juveniles de Eucalyptus.

Se realizaron dos ensayos secuenciales bajo condiciones ambientales controladas. Un ensayo inicial, que incluyó cuatro genotipos, se utilizó para evaluar la viabilidad de VIS–NIR HSI en la diferenciación de condiciones de déficit hídrico leve, moderado y severo, y para comparar la información del espectro completo con índices de vegetación convencionales. Un segundo ensayo ampliado, que incluyó seis genotipos, integró VIS–NIR HSI, espectroscopía NIR portátil, mediciones fisiológicas, análisis de expresión génica y seguimiento posterior al estrés después del restablecimiento del riego. El análisis de componentes principales se utilizó para explorar la estructura espectral, mientras que el análisis ANOVA–componentes simultáneos (ASCA) se aplicó para particionar la variabilidad espectral asociada con el genotipo, el día de muestreo, la condición de tratamiento, la réplica biológica y sus interacciones. Los modelos de clasificación supervisada se evaluaron mediante una estrategia binaria, destinada a discriminar entre muestras control y muestras sometidas a déficit hídrico agrupadas, y una estrategia multiclase, destinada a discriminar entre la condición control y tres etapas progresivas de déficit hídrico. Dentro del flujo analítico se evaluaron análisis discriminante por mínimos cuadrados parciales, máquinas de vectores de soporte, k-vecinos más cercanos, Random Forest, Extreme Gradient Boosting y métodos de regresión multivariante.

VIS–NIR HSI detectó los cambios espectrales asociados con la progresión del déficit hídrico de manera más efectiva que los índices de vegetación evaluados. En el ensayo inicial, los modelos supervisados basados en espectros medios alcanzaron errores de validación externa entre 0 y 2%, mientras que la clasificación mediante máquinas de vectores de soporte generó las reconstrucciones espaciales más consistentes de la progresión del estrés. En el ensayo ampliado, la discriminación binaria entre muestras control y sometidas a déficit hídrico fue efectiva para ambas plataformas espectrales, mientras que la clasificación directa de la condición control y las tres etapas progresivas de déficit hídrico presentó una menor exactitud debido al considerable solapamiento espectral entre etapas de estrés adyacentes. ASCA demostró que la variabilidad de VIS–NIR HSI estuvo dominada por el genotipo, que explicó el 30,2% de la varianza espectral, mientras que la variabilidad de NIR portátil estuvo asociada principalmente con el día de muestreo y la condición de tratamiento, que explicaron el 40,2% y el 10,6%, respectivamente.

Un flujo de clasificación jerárquica mediante HSI guiado por ASCA alcanzó una clasificación completamente correcta en el conjunto de validación externa evaluado, mientras que NIR portátil proporcionó una clasificación más moderada, pero interpretable, de la progresión del déficit hídrico.

Las mediciones fisiológicas confirmaron reducciones coordinadas en la asimilación neta de CO_2, la conductancia estomática, el desempeño del fotosistema II y el estado hídrico de las plantas. La recuperación después del restablecimiento del riego fue incompleta y fuertemente dependiente del genotipo, y los seis genotipos evaluados mostraron distintos grados de restauración del estado hídrico y de la función fisiológica durante el periodo de recuperación monitoreado. El déficit hídrico indujo la expresión de DHN1, LEA4 y TRDX siguiendo patrones dependientes del genotipo, aunque una elevada acumulación de transcritos no necesariamente indicó una mayor tolerancia fisiológica. VIS–NIR HSI mostró su asociación más fuerte con la disipación no fotoquímica, mientras que la espectroscopía NIR portátil presentó la relación más clara con el potencial hídrico de las plantas.

En conjunto, los resultados demuestran que VIS–NIR HSI y la espectroscopía NIR portátil proporcionan información complementaria y biológicamente significativa para el monitoreo no destructivo del déficit hídrico en Eucalyptus. El marco analítico propuesto, que considera explícitamente el diseño experimental, constituye una herramienta de apoyo para el fenotipado en condiciones controladas y la evaluación de genotipos, aunque se requiere validación independiente en nuevos genotipos, campañas experimentales, viveros y condiciones más cercanas a campo antes de su implementación operativa.

Table of Contents

Table of Tables

Table of Figures

Chapter 1
Introduction.

1.1. Forestry sector, climate change and water deficit in *Eucalyptus* spp.

Species of the genus *Eucalyptus* are among the most widely planted forest trees worldwide because of their rapid growth, adaptability, and industrial relevance for pulp, paper, wood products, essential oils, biomass, and bioenergy (Saadaoui et al., 2017). In Chile, *Eucalyptus globulus* and hybrids between *Eucalyptus nitens* and *Eucalyptus globulus* are relevant to nursery propagation and genetic-improvement programs aimed at combining productivity and adaptive traits (Correia et al., 2014; INFOR, 2025).

However, the productivity and establishment of *Eucalyptus* plantations are strongly conditioned by water availability. Under drought or water-limited conditions, trees may experience reductions in carbon assimilation, stomatal conductance, photosynthetic efficiency, biomass accumulation, and growth (Berenguer et al., 2018; Merchant et al., 2007; Valdés et al., 2013). These responses can compromise plant quality during nursery production, reduce field performance after transplantation, and ultimately affect the productivity and sustainability of forest plantations (Correia et al., 2014a; Saadaoui et al., 2017).

This problem has become increasingly relevant in the context of climate change, as drought risk and drought- and heat-related tree mortality are expected to intensify under global warming (Allen et al., 2010; Hartmann et al., 2025; Vicente-Serrano et al., 2020). In Chile, where plantation forestry represents an important productive and export-oriented sector, water deficit is therefore not only a physiological constraint but also an operational and economic challenge, particularly in systems that depend on the early selection of vigorous and stress-tolerant plant material (INFOR, 2025).

A central feature of *Eucalyptus* responses to water deficit is their strong dependence on species, genotype, developmental stage, environmental origin, and stress duration (Berenguer et al., 2018; Merchant et al., 2007; Spokevicius et al., 2017). Different genotypes may display contrasting physiological and molecular strategies under water limitation, ranging from rapid stomatal closure and reduced growth to the activation of protective mechanisms associated with osmotic adjustment, antioxidant defense, and cellular stabilization (Ulloa et al., 2022; Valdés et al., 2013; Villar et al., 2011). This genetic variability is biologically relevant because it provides an opportunity to identify plant material with improved performance under drought. At the same

time, it is analytically challenging because genotype-related spectral differences may overlap with, mask, or amplify the spectral signatures associated with water deficit (Humphreys et al., 2008; Migacz et al., 2022).

Consequently, the development of monitoring tools for *Eucalyptus* spp. should not be limited to discriminating stressed from non-stressed plants. A more robust approach should determine whether the measured response is mainly driven by water status, genotype, sampling time, recovery stage, or interactions among these factors. This distinction is essential if spectral technologies are expected to support high-throughput phenotyping, nursery management, and decision-making in forestry breeding programs (Ibarra et al., 2023; Sanhueza-Novoa et al., 2026).

The analytical challenge is that drought response cannot be reduced to a single physiological variable. Plants exposed to water deficit undergo simultaneous changes in water status, stomatal regulation, photosynthetic performance, pigment composition, structural organization, biochemical metabolism, and molecular regulation (Saadaoui et al., 2017; Spokevicius et al., 2017; Valdés et al., 2013). Therefore, robust monitoring requires analytical strategies capable of capturing this multivariate response while preserving biological interpretability.

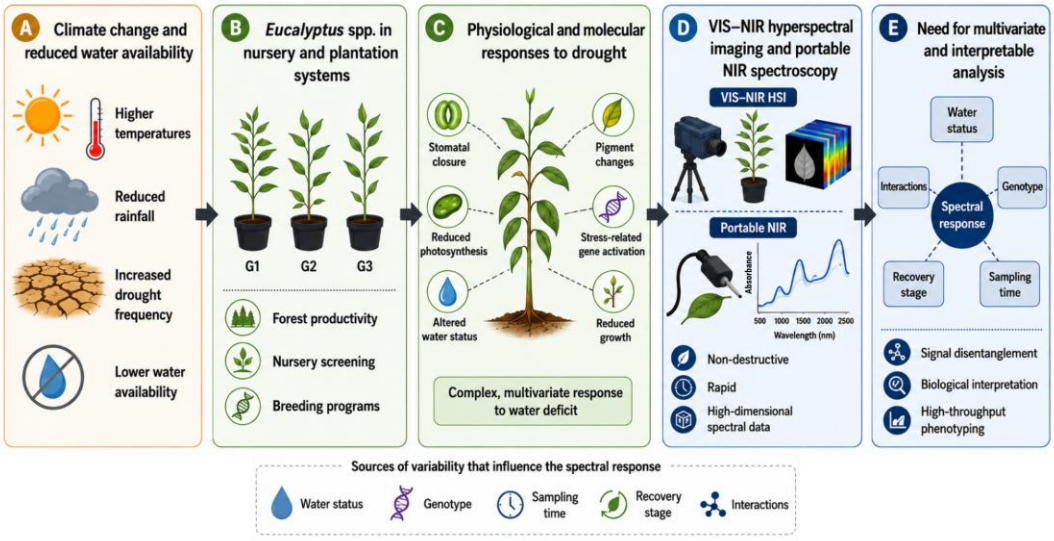

Figure 1.1 Water-deficit responses in *Eucalyptus* spp. and sources of variability affecting spectral monitoring.

1.2. Physiological and molecular responses of *Eucalyptus* to water deficit

Water-deficit stress occurs when soil water availability is insufficient to meet plant water demand. Under this condition, plants activate coordinated physiological, biochemical, and morphological mechanisms aimed at limiting water loss, maintaining cellular homeostasis, and preserving essential metabolic functions. One of the earliest responses is stomatal closure, which reduces transpiration and helps conserve water, but also restricts CO_2 uptake and photosynthetic carbon assimilation (Warren et al., 2011a; Zahra et al., 2023a). As water limitation progresses, reductions in photosynthetic rate, electron transport, photochemical efficiency, growth, and fresh biomass may occur (Berenguer et al., 2018; Correia et al., 2014a; Merchant et al., 2007). Under severe stress, tissue turgor decreases and visible wilting symptoms can become evident.

Physiological measurements provide valuable information about plant performance under water deficit. Variables such as water potential, stomatal conductance, net photosynthetic rate, chlorophyll fluorescence parameters, electron transport rate, non-photochemical quenching, leaf temperature, biomass, and plant height describe different dimensions of the plant response, including water status, gas exchange, photosynthetic efficiency, thermal regulation, and growth (Correia et al., 2014a; Pita & Pardos, 2001; Sobejano-Paz et al., 2020). However, these variables are often measured independently and may not fully capture the integrated nature of drought response. In addition, similar physiological alterations can be induced by other abiotic or biotic stresses, limiting their specificity when used as isolated indicators (Ejaz et al., 2023; Lee & Luan, 2012).

At the molecular level, drought induces transcriptional and metabolic changes associated with osmotic adjustment, reactive oxygen species control, protein stabilization, membrane protection, and stress signalling (Correia et al., 2016; Spokevicius et al., 2017; Valdés et al., 2013; Villar et al., 2011). Studies conducted in *Eucalyptus* have demonstrated that these responses may vary among species, tissues, and genotypes, indicating that drought adaptation involves different and partially genotype-dependent molecular strategies (Martins et al., 2018; Spokevicius et al., 2017; Villar et al., 2011).

In this context, DHN1, LEA4, and TRDX represent candidate genes associated with complementary protective processes. Functional studies in plant systems have shown that DHN1

can interact with phospholipid membranes, potentially contributing to the stabilization of membrane structures during dehydration (Koag et al., 2003). Group-4 LEA proteins have been directly associated with adaptation and tolerance to severe water deficit (Olvera-Carrillo et al., 2010), whereas thioredoxin systems participate in the regulation of metabolic and redox responses during drought and subsequent recovery (Da Fonseca-Pereira et al., 2019). Their expression may therefore provide mechanistic information about cellular protection, dehydration response, and redox regulation, while helping to identify contrasting response strategies among *Eucalyptus* genotypes.

Nevertheless, gene-expression analyses require destructive tissue collection, RNA extraction, laboratory processing, and appropriate normalization and quality-control procedures. These characteristics limit their suitability for routine high-throughput monitoring or for repeated assessment of the same plant. Their principal value in an integrated analytical framework is therefore to provide biological support for the interpretation of spectral and physiological patterns. Combining non-destructive spectral measurements with physiological variables and drought-responsive gene expression offers a more comprehensive strategy than relying on a single analytical domain.

1.3. Traditional methods for water-deficit assessment and their limitations

Traditional water-deficit assessment in forest plants commonly relies on visual evaluation, biomass and growth monitoring, plant water-status measurements, gas-exchange analysis, chlorophyll fluorescence, and multispectral vegetation indices. These approaches provide valuable reference information and have been widely used to characterize plant responses to drought. However, they present important limitations for early, selective, and large-scale stress detection. Visible symptoms commonly become evident after underlying physiological changes have already begun, whereas biomass and growth measurements represent cumulative responses and frequently require repeated measurements or destructive harvesting (Behmann et al., 2014a; Munns et al., 2010). Plant water potential, stomatal conductance, and photosynthetic rate provide more direct information about plant functioning, but conventional measurements are generally point-based, sensitive to measurement conditions, and difficult to scale to large plant populations (Jones, 2007; Munns et al., 2010).

Multispectral vegetation indices such as the normalized difference vegetation index (NDVI), photochemical reflectance index (PRI), and modified chlorophyll absorption ratio index (MCARI) provide rapid and non-destructive indicators related to canopy greenness, photosynthetic light-use efficiency, and chlorophyll-associated absorption, respectively (Gamon et al., 1992; T Daughtry et al., 1999). However, these indices are calculated from a small number of predefined wavelengths and therefore reduce complex spectral responses to simplified ratios. This simplicity facilitates rapid screening but may also reduce selectivity, because index values can be influenced by pigment concentration, canopy structure, leaf orientation, developmental stage, illumination, species, genotype, and environmental conditions. In juvenile *Eucalyptus* plants, different vegetation indices have also shown unequal sensitivity across genotypes and water-deficit stages, indicating that an individual index may not reliably describe the complete stress response (Sanhueza-Novoa et al., 2026).

A critical assumption that should be avoided is that a vegetation index, physiological variable, fluorescence parameter, or individual wavelength represents a specific marker of water deficit. No single water-status measurement is universally optimal, and its interpretation depends on the biological process and experimental conditions being investigated (Jones, 2007). Likewise, chlorophyll fluorescence responds to numerous abiotic and biotic factors and must be interpreted within an appropriate physiological context rather than as a drought-specific signal (Murchie & Lawson, 2013). In complex plant material, the measured response is generally produced by overlapping biochemical, structural, genetic, temporal, and environmental factors. Conventional physiological measurements and vegetation indices therefore remain essential as reference information, but they should be complemented by full-spectrum, multivariate, and biologically interpretable analytical approaches.

Behmann et al. demonstrated detection of drought-related changes before they became visible to the naked eye, while Munns et al. described traditional growth measurements as time-consuming and frequently destructive. Jones provides a particularly strong methodological basis for discussing the limitations and context dependence of plant water-status and physiological measurements.

Table 1.1 Reference approaches for assessing plant water-deficit responses and their main analytical limitations.

Approach	*Information provided*	*Main advantages*	*Main limitations*	*Representative references*
Visual symptoms	Wilting, chlorosis, leaf rolling, leaf damage and senescence	Simple, inexpensive and does not require specialized equipment	Subjective and poorly specific; symptoms may become visible only after physiological changes have begun	(Behmann et al., 2014a)
Biomass and growth	Changes in height, leaf area, fresh and dry biomass and biomass allocation	Directly related to accumulated plant performance and productivity	Cumulative rather than immediate response; often requires repeated measurements or destructive harvesting; limited suitability for early detection	Eziz et al., (2017); Munns et al., (2010)
Plant water potential	Energy status of water in plant tissues and hydraulic limitation	Physiologically meaningful and useful for defining drought intensity	Point-based; measurement timing and tissue selection affect interpretation; requires specialized equipment and trained operators	Jones, (2007); Oliveira et al., (2022)
Stomatal conductance and photosynthesis	Gas exchange, transpiration regulation and carbon assimilation	Direct functional indicators that can respond rapidly to water limitation	Sensitive to irradiance, temperature, vapour-pressure deficit and CO_2 concentration; leaf-chamber measurements are difficult to implement at high throughput	(Jones, 2007; Munns et al., 2010)
Chlorophyll fluorescence	PSII performance, photochemical efficiency and non-photochemical energy dissipation	Non-destructive and potentially sensitive to changes in photosynthetic function	Responds to multiple abiotic and biotic stressors; strongly dependent on measurement protocol and physiological context	Murchie & Lawson, (2013); Zhuang et al., (2020)
Vegetation indices	Greenness, chlorophyll-associated absorption and photochemical activity	Fast, simple, non-destructive and potentially scalable	Use few wavelengths; affected by pigments, architecture, illumination and genetic or developmental variability; limited stress specificity	Gamon et al., (1992); Sanhueza-Novoa et al., (2026); T Daughtry et al., (1999)
Gene-expression analysis	Activation of stress-responsive genes and protective or regulatory pathways	Provides mechanistic information and supports identification of genotype-dependent responses	Destructive tissue sampling; requires RNA extraction, normalization and laboratory processing; limited suitability for repeated routine monitoring	(Correia et al., 2018; Villar et al., 2011)

1.4. Spectral sensing as a non-destructive strategy: VIS–NIR HSI and portable NIR spectroscopy

Spectroscopic techniques offer an attractive alternative for plant-stress monitoring because they enable rapid and non-destructive measurements, generally require minimal sample preparation, and do not require chemical reagents during spectral acquisition. These characteristics make them

potentially adaptable to high-throughput phenotyping and operational screening workflows. In plant tissues, the measured spectral response results from wavelength-dependent absorption and scattering processes associated with pigments, water, proteins, carbohydrates, cellulose, lignin, and other organic constituents, as well as with tissue structure and sample geometry. Changes in these properties during water deficit may modify reflectance or absorbance patterns, generating multivariate spectral fingerprints associated with plant physiological status (Beć et al., 2020a; Manley, 2014; Türker-Kaya & Huck, 2017a). NIR spectroscopy is widely recognized as rapid and non-destructive, while its broad and overlapping bands generally require multivariate modelling for interpretation.

Visible–near infrared hyperspectral imaging (VIS–NIR HSI) combines spectroscopy and digital imaging, producing a three-dimensional data structure composed of two spatial dimensions and one spectral dimension. Consequently, each pixel contains a reflectance spectrum, allowing spectral and spatial variability to be evaluated simultaneously. For water-deficit assessment, VIS–NIR HSI can capture changes associated with pigment absorption, red-edge behaviour, tissue and canopy structure, and the heterogeneous spatial distribution of stress responses. Unlike conventional vegetation indices, which use a limited number of predefined wavelengths, HSI acquires numerous contiguous spectral bands and therefore retains a more detailed representation of plant optical properties (Behmann et al., 2014b; Blackburn, 2007a; Manley, 2014). HSI is particularly valuable because the spatial dimension allows spectral differences to be localized within heterogeneous biological material.

Portable near-infrared spectroscopy provides complementary information in a region dominated by overtones and combination bands of molecular vibrations involving O–H, C–H, N–H, and related bonds. These spectral features make NIR measurements sensitive to variations in tissue water and organic constituents, including carbohydrates, proteins, cellulose, and lignin. Strong water-associated absorption features have been described near 1450 and 1940 nm, although the broad and overlapping nature of NIR bands means that the resulting spectra should be interpreted as multicomponent signals rather than as compound-specific measurements (Beć et al., 2020a; Cen & He, 2007; J. Wang et al., 2009a). Portable NIR instruments have also demonstrated potential for predicting leaf water content and water-stress indicators in eucalypt material (Haynes et al., 2024a; Johnson, 2023a).

Compared with hyperspectral imaging, point-based portable NIR spectroscopy does not intrinsically provide spatial maps of spectral variability. Nevertheless, it offers operational advantages related to instrument portability, simpler acquisition, rapid measurement, and potential implementation under nursery or plant-screening conditions. The complementary use of VIS–NIR HSI and portable NIR spectroscopy can therefore provide information from two different but overlapping spectral domains. VIS–NIR HSI contributes spatially resolved information mainly associated with pigments, red-edge behaviour, and structural heterogeneity, whereas portable NIR measurements are more strongly influenced by water-related and organic X–H absorption features. Their combined use can provide a broader analytical description of water-deficit progression and recovery in juvenile *Eucalyptus* plants.

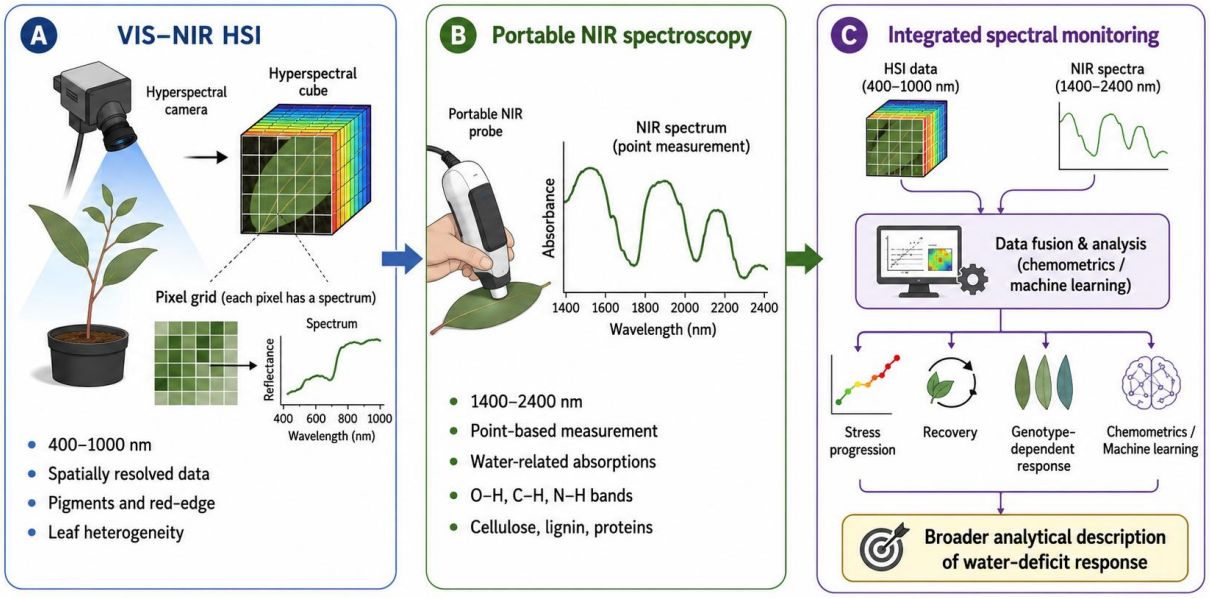

Figure 1.2 Complementarity between VIS–NIR hyperspectral imaging and portable NIR spectroscopy for water-deficit monitoring in *Eucalyptus* spp.

1.5. Chemometrics and machine learning for spectral plant phenotyping

One of the main analytical challenges of spectral sensing is not only the acquisition of spectral data, but also their transformation into reliable and biologically interpretable information. VIS–NIR HSI and portable NIR spectroscopy generate high-dimensional, strongly collinear, and highly structured datasets because adjacent wavelengths frequently contain partially redundant information. Direct visual inspection of spectral profiles is generally insufficient, as relevant

information may be distributed across multiple wavelengths and influenced by light scattering, baseline shifts, sample geometry, instrumental conditions, genotype, and measurement-related variability.

Signal preprocessing and data pretreatment therefore often constitute critical steps before multivariate modelling. Methods such as standard normal variate transformation (SNV) and multiplicative scatter correction (MSC) are commonly used to reduce scattering-related variability, whereas smoothing and spectral derivatives can attenuate noise, correct baseline effects, and enhance partially overlapping spectral features. Mean centering is generally applied subsequently to express each variable relative to its average value before latent-variable modelling. However, preprocessing must be selected and justified carefully, because each transformation modifies the original signal and may attenuate biologically relevant information or exaggerate apparent differences among samples (Oliveri et al., 2019; Rinnan et al., 2009).

Chemometric and machine-learning methods can subsequently be used to extract structured information from spectral matrices. Principal component analysis (PCA) is commonly applied as an unsupervised exploratory method to summarize dominant directions of variance, examine sample distributions, identify anomalous observations, and investigate the variables contributing to spectral patterns (Jollife & Cadima, 2016). Supervised discriminant methods such as partial least squares discriminant analysis (PLS-DA), k-nearest neighbours (k-NN), support vector machine classification (SVM-C), random forest (RF), and Extreme Gradient Boosting (XGBoost) can be used to discriminate control and water-deficit plants or to differentiate progressive stress stages. These approaches represent different modelling assumptions, ranging from linear latent-variable models to distance-based, kernel-based, and tree-ensemble algorithms (Barker & Rayens, 2003; Breiman, 2001; Chen & Guestrin, 2016; Cortes et al., 1995; Cover & Hart, 1952).

Soft independent modelling of class analogy (SIMCA) should be distinguished from conventional discriminant classification. Rather than directly separating two or more predefined classes, SIMCA constructs an independent multivariate model for each target class and evaluates whether an unknown sample is sufficiently similar to belong to that class. It is therefore more accurately described as a supervised class-modelling approach (De Angelis et al., 2024).

Regression methods such as partial least squares regression (PLS-R) and support vector machine regression (SVM-R) can be used to relate spectral information to quantitative reference variables, including physiological traits associated with plant water status, photosynthetic performance, thermal regulation, and growth. PLS-R represents the predictor and response matrices through latent variables, whereas SVR can describe linear or nonlinear relationships depending on the selected kernel. These approaches allow spectral modelling to move beyond categorical stress discrimination and provide continuous estimates of biological responses (Smola et al., 2004).

Nevertheless, high classification accuracy alone does not demonstrate that a spectral model is biologically meaningful, robust, or transferable. Predictive performance should be assessed using appropriate class-specific metrics and samples that are independent of those used for model optimization. This is particularly important when datasets contain repeated measurements, multiple pixels from the same hyperspectral image, or several observations from the same biological individual. Randomly distributing dependent observations between calibration and validation sets may result in optimistic performance estimates because the model can exploit sample-specific information rather than the intended biological effect (Rodionova et al., 2024; Sokolova & Lapalme, 2009).

In factorial biological experiments, spectral differences may also be driven by genotype, sampling day, replicate-to-replicate variability, treatment condition, or interactions among these factors. If these effects are not explicitly evaluated, an apparently successful classifier may partly exploit confounded or unintended sources of variation. This issue is particularly relevant in *Eucalyptus* spp., where species, hybrid origin, genotype, and leaf developmental stage can produce spectral differences that overlap with treatment-related responses (Humphreys et al., 2008; Migacz et al., 2022). Apparent discrimination among water-status conditions may therefore reflect genetic structure, temporal dynamics, or individual heterogeneity rather than the water-deficit effect alone.

For this reason, design-aware methods such as Analysis of Variance–Simultaneous Component Analysis (ASCA) are particularly relevant. ASCA integrates the factorial decomposition principles of ANOVA with component analysis, allowing a multivariate matrix to be partitioned into effect matrices associated with experimental factors and their interactions. The resulting

score and loading structures can be used to evaluate the magnitude and spectral pattern of each modelled effect, while permutation procedures can support the statistical assessment of their significance (Bertinetto et al., 2020; Jansen et al., 2005). Nevertheless, ASCA does not compensate for an inadequately designed experiment; its validity depends on the appropriate definition of experimental factors, interactions, replication, and dependence among observations.

Beyond its interpretative role, the variance structure identified through ASCA can provide a rational basis for constructing hierarchical classification workflows. Hierarchical classification divides a complex multiclass problem into sequential decision levels, potentially reducing overlap between classes that are difficult to separate simultaneously (Silla & Freitas, 2011). When the sequence of decisions is informed by experimentally attributable sources of spectral variation, the resulting workflow can connect experimental design, variance decomposition, and supervised modelling. This strategy moves the analysis from direct classification toward more interpretable spectral decision-making, although its predictive advantage must still be demonstrated through independent validation rather than assumed from the hierarchical structure alone.

1.6. State of the art: spectral and chemometric approaches for plant water-deficit monitoring

Spectral sensing has been increasingly investigated as a non-destructive strategy for detecting and monitoring plant responses to water deficit. Early studies demonstrated that changes in tissue water content, pigment composition, cellular structure, and physiological performance can modify plant reflectance across the visible, near-infrared, and short-wave infrared regions. These findings supported the development of spectral indices, hyperspectral imaging systems, and full-spectrum predictive models for detecting stress before severe visual symptoms become evident (Behmann et al., 2014a; Li et al., 2021; Ryckewaert et al., 2021).

A considerable proportion of the literature has focused on the estimation of plant water-related traits. Water absorption features located near 1450 and 1940 nm have been associated with changes in leaf and canopy water content, supporting the use of NIR and SWIR spectroscopy for quantitative assessment (J. Wang et al., 2009b). Subsequent investigations have proposed

spectral indices and multivariate models for estimating leaf water content across different plant species and experimental conditions (Li et al., 2021; Peguero-Pina et al., 2023). In eucalypt leaves, handheld NIR spectroscopy has also shown potential for rapid prediction of leaf water content, illustrating the feasibility of portable measurements for forest-plant assessment (Johnson, 2023b).

Hyperspectral imaging extends these applications by combining spectral and spatial information. This approach has been used to identify localized plant responses, characterize spatial heterogeneity, and monitor the temporal development of stress. Behmann et al. (2014) demonstrated the potential of hyperspectral imaging for detecting early plant stress responses, whereas Asaari et al. (2019) applied hyperspectral analysis to distinguish drought stress and subsequent recovery in maize within a high-throughput phenotyping platform. Field-oriented studies have further shown that high spectral resolution can support the phenotyping of physiological and structural traits associated with plant water status (Cotrozzi et al., 2020; Ryckewaert et al., 2021).

In forest species, the number of studies remains comparatively limited. Spectral reflectance has been used to examine water-stress responses in *Eucalyptus saligna* (Moura Melo et al., 2019), while portable NIR and high-resolution VIS–SWIR spectroscopy have been investigated for predicting leaf water content and physiological water-stress indicators in eucalypts (Haynes et al., 2024b; Johnson, 2023b). Hyperspectral imaging has also been applied to discriminate experimentally induced drought and thermal stress in coniferous trees, demonstrating its potential to distinguish partially overlapping abiotic stress responses (Pivovar et al., 2025).

A further analytical challenge is that spectral variability in forest plants may be strongly influenced by species, genotype, hybrid origin, and leaf developmental stage. NIR spectroscopy has been used to discriminate *Eucalyptus globulus*, *Eucalyptus nitens*, and their hybrids (Humphreys et al., 2008), while later studies have shown that leaf age and species identity can influence VIS–NIR classification patterns in *Eucalyptus* material (Migacz et al., 2022). These findings indicate that genotype-related spectral differences may overlap with water-deficit effects and should therefore be explicitly considered when developing stress-classification models.

Recovery after re-irrigation has received less attention than active water deficit. Hyperspectral monitoring has shown that recovering plants may retain spectral characteristics that differ from both continuously irrigated controls and actively stressed plants (Asaari et al., 2019). In *Eucalyptus globulus*, physiological and biochemical recovery has also been shown to vary between clones, indicating that drought resistance, recovery capacity, and growth performance are not necessarily controlled by the same mechanisms (Ammitzboll et al., 2020; Correia et al., 2014a). These results support the inclusion of recovery as a distinct temporal and biological condition rather than treating it as an automatic return to the control state.

Overall, previous studies demonstrate that spectral technologies can detect plant water deficit, estimate water-related traits, and capture temporal and genotype-dependent variability. Nevertheless, most investigations have used either a single spectral modality, selected vegetation indices, or direct predictive modelling. Fewer studies have integrated spatially resolved VIS–NIR hyperspectral imaging, portable NIR spectroscopy, physiological reference measurements, recovery stages, and experimental-design-aware multivariate analysis within the same analytical framework. Table 1.2 summarizes representative studies and highlights their main contributions and remaining methodological limitations.

Table 1.2 Representative studies applying spectral sensing and multivariate analysis to plant water-deficit assessment, recovery monitoring, and the evaluation of related biological variability.

Reference	*Plant material*	*Stress/condition*	*Spectral technique*	*Data analysis*	*Main contribution*	*Limitation/gap*
Behmann et al. (2014)	Crop plants monitored during progressive stress development	Progressive plant stress before visible symptoms	Close-range hyperspectral imaging	Combination of unsupervised and supervised methods for temporal stress-stage identification	Demonstrated that hyperspectral imaging can detect progressive plant responses before they become visually evident	General plant-stress framework; limited biological interpretation of the spectral variation and no explicit separation of genotype, time, and treatment effects
Asaari et al. (2019)	Maize plants in a high-throughput phenotyping platform	Water deficit followed by rewatering and recovery	Close-range hyperspectral imaging	SNV normalization, supervised pixel filtering, discriminant-band selection, and spectral-similarity analysis	Demonstrated early detection of drought responses and rapid identification of recovery effects after rewatering	Evaluated one crop species and one spectral modality; recovery was assessed mainly through spectral similarity to well-watered controls
Melo et al. (2019)	Twenty-four-month-old *Eucalyptus saligna* plants	Five simulated drought cycles compared with well-watered controls	FieldSpec spectroradiometry, 400–1700 nm	Spectral-profile and wavelength-wise comparison across water-stress cycles	Provided one of the few direct evaluations of the spectral response of *Eucalyptus* under repeated water-deficit conditions	Only small spectral differences were observed; no multivariate predictive model, independent validation, or explicit evaluation of genotype and recovery
Cotrozzi et al. (2020)	Six maize hybrids with contrasting yield stability	Different water-availability conditions in greenhouse and field environments	Leaf hyperspectral reflectance spectroscopy	PLS-R with independent external validation; association among physiological, anatomical, and spectral traits	Showed that physiological and anatomical traits related to water status can be estimated non-destructively from full-spectrum measurements	Focused on trait prediction from individual leaves rather than whole-plant imaging or classification of progressive stress and recovery stages

Li et al. (2021)	Leaves from three tree species	Variation in equivalent water thickness and fuel moisture content	Leaf hyperspectral reflectance	Development of spectral absorption indices at 970, 1200, and 1660 nm; regression and cross-validation	Developed water-sensitive indices that accounted for variation in leaf absorption features among species	Index-based approach compresses the spectral information into selected bands; evaluated detached leaves rather than dynamic whole-plant stress responses
Ryckewaert et al. (2021)	Maize genotypes under field conditions	Field water stress	High-spectral-resolution field spectroscopy	Full-spectrum modelling and selection of informative spectral regions	Demonstrated the potential of high-resolution spectroscopy for field phenotyping and genotype screening under water stress	Field variability increases model complexity; the study did not combine spatial HSI with portable NIR or explicitly monitor post-stress recovery
Migacz et al. (2022)	Six *Eucalyptus* species sampled at different leaf ages	Species and leaf-age variability rather than experimentally imposed drought	VIS spectroscopy, 360–740 nm, and NIR spectroscopy, 1000–2500 nm	PCA, spectral derivatives, and linear discriminant analysis	Demonstrated that species identity and leaf developmental stage influence VIS–NIR spectral classification in *Eucalyptus*	Did not evaluate water deficit; nevertheless, it reveals a major potential confounding effect for stress-classification models
Johnson (2023)	Eucalypt leaves	Variation in leaf water content	Handheld NIR spectroscopy	Spectral preprocessing and PLS regression	Demonstrated the feasibility of portable NIR instruments for rapid prediction of water-related properties in eucalypt leaves	Based on leaf-level water-content prediction; did not assess intact plants, progressive stress, recovery, or genotype-by-treatment interactions
Peguero-Pina et al. (2023)	Mature leaves of *Quercus ilex* subsp. *rotundifolia*	Progressive leaf dehydration and variation in relative water content	Contact NIR reflectance at water-sensitive bands near 1450, 1599, and 1940 nm	Linear, sigmoidal, and polynomial regression; reflectance ratios and leaf water content indices	Demonstrated strong relationships between NIR water bands and relative water content and evaluated the effect of reference wavelengths	Contact measurements and controlled leaf dehydration limit direct field transfer; some indices require reflectance at full turgor as a reference

Haynes et al. (2024)	*Eucalyptus viminalis* and *Callitris rhomboidea* foliage	Progressive dehydration and variation in physiological water-stress indicators	High-resolution leaf-level VIS–SWIR spectroscopy	Normalized ratio indices, regression, and breakpoint/segmented analyses	Identified spectral features associated with leaf water potential and other key water-stress indicators in two forest species	Conducted at leaf level under controlled measurement conditions; did not evaluate whole-plant spatial heterogeneity, recovery, or multiclass stress trajectories
Pivovar et al. (2025)	Mature Norway spruce trees	Chronic drought, acute thermal stress, and control conditions	Airborne VIS–NIR–SWIR hyperspectral imaging, 380–2500 nm	Spectral and derivative analysis, stress discrimination, and identification of informative wavebands	Demonstrated that airborne HSI can distinguish drought, thermal stress, and non-stressed trees and identify stress-sensitive bands	Stress responses varied seasonally; species, plant scale, sensor platform, and environmental conditions differ substantially from juvenile *Eucalyptus* screening

Overall, the reviewed studies demonstrate the potential of spectral technologies for detecting plant water deficit and estimating stress-related variables. However, important gaps remain regarding the integration of spatially resolved VIS–NIR information with portable NIR measurements, the explicit partitioning of genotype and temporal effects, the use of independent external validation, and the monitoring of post-stress recovery. These limitations support the development of more integrative and design-aware spectral strategies for water-deficit assessment in *Eucalyptus* spp.

1.7. Physiological, molecular, and spectral dynamics during post-stress recovery

The assessment of plant recovery after water-deficit stress is essential because the disappearance of visible symptoms following re-irrigation does not necessarily indicate complete functional restoration. Plants may rapidly recover tissue hydration and visual appearance while maintaining alterations in stomatal regulation, photosynthetic performance, photochemical efficiency, thermal balance, biochemical status, or growth. Recovery should therefore be understood as a dynamic and multidimensional process rather than as an immediate return to the pre-stress or continuously irrigated condition.

Physiological recovery may occur at different rates depending on the variable being evaluated. Leaf water status and tissue turgor may be restored relatively rapidly after re-irrigation, whereas stomatal conductance, carbon assimilation, photochemical regulation, antioxidant metabolism, and biomass accumulation may require longer periods or remain partially impaired. In *Eucalyptus globulus*, clone-dependent differences in physiological and biochemical performance have been observed during both water stress and subsequent recovery, indicating that the capacity to withstand water deficit does not necessarily imply an equivalent capacity to restore normal functioning after rewatering (Correia et al., 2014).

Recovery capacity is also strongly influenced by genetic background. Genotypes may differ not only in the intensity of their initial response to water deficit, but also in the rate and completeness with which physiological functions are restored. Genetic analyses of *Eucalyptus globulus* seedlings have indicated that drought resistance, recovery capacity, and growth may be at least partially controlled by different genetic components (Ammitzboll et al., 2020). Consequently, genotypes that maintain higher performance during water limitation are not necessarily the same genotypes that recover most rapidly after re-irrigation. This distinction is particularly important for breeding and screening programs, where both stress resistance and post-stress resilience should be considered.

At the molecular level, water deficit activates genotype-dependent transcriptional responses associated with osmotic adjustment, cellular protection, redox regulation, and stress signalling in

Eucalyptus spp. (Spokevicius et al., 2017; Ulloa et al., 2022; Villar et al., 2011). After re-irrigation, the expression of stress-responsive genes may decrease, remain elevated, or follow gene- and genotype-specific trajectories. However, compared with the extensive literature describing molecular responses during active drought, post-rewatering transcriptional dynamics in *Eucalyptus* remain comparatively less studied. Evaluating drought-responsive genes during recovery can therefore help determine whether physiological improvement is accompanied by molecular restoration or whether protective mechanisms remain active after water availability has been re-established.

From an analytical perspective, recovery introduces an additional level of complexity. Spectral signatures acquired after re-irrigation may reflect a combination of restored tissue water content, persistent pigment or structural changes, residual physiological impairment, and genotype-dependent recovery strategies. Recovery spectra may therefore differ from both continuously irrigated controls and actively stressed plants. Hyperspectral imaging has demonstrated the potential to detect spectral changes associated with drought recovery in high-throughput plant phenotyping systems (Asaari et al., 2019), but recovery-oriented spectral studies remain less common than models focused exclusively on the discrimination of irrigated and water-deficit conditions.

Consequently, models trained only to distinguish control and actively stressed plants may be insufficient to characterize intermediate and post-stress states. A recovering plant could be classified as control because its water content has been restored, despite maintaining altered photosynthetic or molecular responses. Conversely, persistent spectral differences may indicate structural or biochemical effects of previous stress rather than continued water limitation. Recovery assessment therefore requires a temporal framework in which spectral trajectories are interpreted together with physiological and molecular reference measurements.

The integration of spectral, physiological, and gene-expression information provides a broader framework for distinguishing immediate rehydration from functional recovery and persistent post-stress effects. Such a multidomain approach can improve the biological interpretation of non-destructive spectral measurements, reveal genotype-dependent recovery strategies, and

support the identification of plant material combining water-deficit tolerance with effective post-stress resilience.

Taken together, these findings indicate that post-stress recovery cannot be inferred solely from the restoration of tissue hydration or the disappearance of visible symptoms. Physiological functions, molecular responses, and spectral properties may follow different temporal trajectories, and their recovery may vary among genotype.

The joint interpretation of spectral measurements, physiological variables, and drought-responsive gene expression therefore provides a suitable framework for distinguishing immediate rehydration from functional recovery and persistent post-stress effects. Such an approach may improve the biological interpretation of non-destructive measurements and support the characterization of genotype-dependent resilience in juvenile *Eucalyptus* plants.

1.8. References

Abdelaali, B., Taha, D., Hannou, Z., Ayoub, E. H., El Menyiy, N., Bouyahya, A., & Mubarak, M. S. (2023). Bioactive Compounds and Antidiabetic and Other Health Benefits of Eucalyptus globulus. In *Antidiabetic Medicinal Plants and Herbal Treatments* (pp. 469–480). CRC Press. https://doi.org/10.1201/b23347-31

Ahmad, R. S., Imran, M., Ahmad, M. H., Khan, M. K., Yasmin, A., Saima, H., Abbas, K., Chaudhary, R., & Rahim, M. A. (2023). Eucalyptus essential oils. In *Essential Oils* (pp. 217–239). Elsevier. https://doi.org/10.1016/B978-0-323-91740-7.00005-0

Allen, C. D., Macalady, A. K., Chenchouni, H., Bachelet, D., McDowell, N., Vennetier, M., Kitzberger, T., Rigling, A., Breshears, D. D., Hogg, E. H. (Ted), Gonzalez, P., Fensham, R., Zhang, Z., Castro, J., Demidova, N., Lim, J. H., Allard, G., Running, S. W., Semerci, A., & Cobb, N. (2010). A global overview of drought and heat-induced tree mortality reveals emerging climate change risks for forests. *Forest Ecology and Management*, *259*(4), 660–684. https://doi.org/10.1016/j.foreco.2009.09.001

Ammitzboll, H., Vaillancourt, R. E., Potts, B. M., Harrison, P. A., Brodribb, T., Sussmilch, F. C., & Freeman, J. S. (2020). Independent genetic control of drought resistance, recovery, and growth of Eucalyptus globulus seedlings. *Plant Cell and Environment*, *43*(1), 103–115. https://doi.org/10.1111/pce.13649

Amrutha, S., Parveen, A. B. M., Muthupandi, M., Sivakumar, V., Nautiyal, R., & Ghosh Dasgupta, M. (2019). Variation in morpho-physiological, biochemical and molecular responses of two Eucalyptus species under short-term water stress. *Acta Botanica Croatica*, *78*(2), 125–134. https://doi.org/10.2478/botcro-2019-0021

Angel Prieto Lage, M., Barral Martínez, M., Seyyedimansour, S., Manikantan, M. R., Trif, M., & Khaneghah, M. A. (2022). *Recent advancements in NIR spectroscopy for assessing the quality and safety of horticultural products: A comprehensive review*.

Aranjuelo, I., Molero, G., Erice, G., Avice, J. C., & Nogués, S. (2011). Plant physiology and proteomics reveals the leaf response to drought in alfalfa (Medicago sativa L.). *Journal of Experimental Botany*, *62*(1), 111–123. https://doi.org/10.1093/jxb/erq249

Asaari, M. S. M., Mertens, S., Dhondt, S., Inzé, D., Wuyts, N., & Scheunders, P. (2019). Analysis of hyperspectral images for detection of drought stress and recovery in maize plants in a high-throughput phenotyping platform. *Computers and Electronics in Agriculture*, *162*, 749–758. https://doi.org/10.1016/j.compag.2019.05.018

Ballabio, D., & Consonni, V. (2013). Classification tools in chemistry. Part 1: linear models. PLS-DA. *Analytical Methods*, *5*(16), 3790. https://doi.org/10.1039/c3ay40582f

Ballester, C., Zarco-Tejada, P. J., Nicolás, E., Alarcón, J. J., Fereres, E., Intrigliolo, D. S., & Gonzalez-Dugo, V. (2018). Evaluating the performance of xanthophyll, chlorophyll and structure-sensitive spectral indices to detect water stress in five fruit tree species. *Precision Agriculture*, *19*(1), 178–193. https://doi.org/10.1007/s11119-017-9512-y

Barker, M., & Rayens, W. (2003). Partial least squares for discrimination. *Journal of Chemometrics*, *17*(3), 166–173. https://doi.org/10.1002/cem.785

Bayat, B., van der Tol, C., & Verhoef, W. (2016). Remote sensing of grass response to drought stress using spectroscopic techniques and canopy reflectance model inversion. *Remote Sensing*, *8*(7). https://doi.org/10.3390/rs8070557

Beć, K. B., Grabska, J., & Huck, C. W. (2020a). Near-infrared spectroscopy in bio-applications. In *Molecules* (Vol. 25, Number 12). MDPI AG. https://doi.org/10.3390/molecules25122948

Beć, K. B., Grabska, J., & Huck, C. W. (2020b). Near-infrared spectroscopy in bio-applications. In *Molecules* (Vol. 25, Number 12). MDPI AG. https://doi.org/10.3390/molecules25122948

Beć, K. B., Grabska, J., & Huck, C. W. (2020c). Near-infrared spectroscopy in bio-applications. In *Molecules* (Vol. 25, Number 12). MDPI AG. https://doi.org/10.3390/molecules25122948

Behmann, J., Steinrücken, J., & Plümer, L. (2014a). Detection of early plant stress responses in hyperspectral images. *ISPRS Journal of Photogrammetry and Remote Sensing*, *93*, 98–111. https://doi.org/10.1016/j.isprsjprs.2014.03.016

Behmann, J., Steinrücken, J., & Plümer, L. (2014b). Detection of early plant stress responses in hyperspectral images. *ISPRS Journal of Photogrammetry and Remote Sensing*, *93*, 98–111. https://doi.org/10.1016/j.isprsjprs.2014.03.016

Belgiu, M., & Drăgu, L. (2016). Random forest in remote sensing: A review of applications and future directions. In *ISPRS Journal of Photogrammetry and Remote Sensing* (Vol. 114, pp. 24–31). Elsevier B.V. https://doi.org/10.1016/j.isprsjprs.2016.01.011

Benhizia, R., Phinzi, K., Hateffard, F., Aib, H., & Szabó, G. (2024). Drought Monitoring Using Moderate Resolution Imaging Spectroradiometer-Derived NDVI Anomalies in Northern Algeria from 2011 to 2022. *Environments - MDPI*, *11*(5). https://doi.org/10.3390/environments11050095

Berenguer, H. D. P., Alves, A., Amaral, J., Leal, L., Monteiro, P., de Jesus, C., & Pinto, G. (2018). Differential physiological performance of two Eucalyptus species and one hybrid under different imposed water availability scenarios. *Trees - Structure and Function*, *32*(2), 415–427. https://doi.org/10.1007/s00468-017-1639-y

Bertinetto, C., Engel, J., & Jansen, J. (2020). ANOVA simultaneous component analysis: A tutorial review. In *Analytica Chimica Acta: X* (Vol. 6). Elsevier B.V. https://doi.org/10.1016/j.acax.2020.100061

Blackburn, G. A. (2007a). Hyperspectral remote sensing of plant pigments. *Journal of Experimental Botany*, *58*(4), 855–867. https://doi.org/10.1093/jxb/erl123

Blackburn, G. A. (2007b). Hyperspectral remote sensing of plant pigments. *Journal of Experimental Botany*, *58*(4), 855–867. https://doi.org/10.1093/jxb/erl123

Breiman, L. (2001). *Random Forests* (Vol. 45).

Brockerhoff, E. G., Jactel, H., Parrotta, J. A., & Ferraz, S. F. B. (2013). Role of eucalypt and other planted forests in biodiversity conservation and the provision of biodiversity-related ecosystem services. *Forest Ecology and Management*, *301*, 43–50. https://doi.org/10.1016/j.foreco.2012.09.018

Bustin, S. A., Benes, V., Garson, J. A., Hellemans, J., Huggett, J., Kubista, M., Mueller, R., Nolan, T., Pfaffl, M. W., Shipley, G. L., Vandesompele, J., & Wittwer, C. T. (2009). The MIQE guidelines: Minimum information for publication of quantitative real-time PCR experiments. *Clinical Chemistry*, *55*(4), 611–622. https://doi.org/10.1373/clinchem.2008.112797

Bustin, S. A., Ruijter, J. M., Van den Hoff, M. J. B., Kubista, M., Pfaffl, M. W., Shipley, G. L., Tran, N., Rödiger, S., Untergasser, A., Mueller, R., Nolan, T., Milavec, M., Burns, M. J., Huggett, J. F., Vandesompele, J., & Wittwer, C. T. (2025). MIQE 2.0: Revision of the Minimum Information for Publication of Quantitative Real-Time PCR Experiments Guidelines. In *Clinical Chemistry* (Vol. 71, Number 6, pp. 634–651). Oxford University Press. https://doi.org/10.1093/clinchem/hvaf043

Cen, H., & He, Y. (2007). Theory and application of near infrared reflectance spectroscopy in determination of food quality. *Trends in Food Science and Technology*, *18*(2), 72–83. https://doi.org/10.1016/j.tifs.2006.09.003

Chen, T., & Guestrin, C. (2016). XGBoost: A scalable tree boosting system. *Proceedings of the ACM SIGKDD International Conference on Knowledge Discovery and Data Mining*, *13-17-August-2016*, 785–794. https://doi.org/10.1145/2939672.2939785

Correia, B., Hancock, R. D., Amaral, J., Gomez-Cadenas, A., Valledor, L., & Pinto, G. (2018). Combined Drought and Heat Activates Protective Responses in Eucalyptus globulus That Are Not Activated When Subjected to Drought or Heat Stress Alone. *Frontiers in Plant Science*, *9*. https://doi.org/10.3389/fpls.2018.00819

Correia, B., Pintó-Marijuan, M., Neves, L., Brossa, R., Dias, M. C., Costa, A., Castro, B. B., Araújo, C., Santos, C., Chaves, M. M., & Pinto, G. (2014a). Water stress and recovery in the performance of two Eucalyptus globulus clones: Physiological and biochemical profiles. *Physiologia Plantarum*, *150*(4), 580–592. https://doi.org/10.1111/ppl.12110

Correia, B., Pintó-Marijuan, M., Neves, L., Brossa, R., Dias, M. C., Costa, A., Castro, B. B., Araújo, C., Santos, C., Chaves, M. M., & Pinto, G. (2014b). Water stress and recovery in the performance of two Eucalyptus globulus clones: Physiological and biochemical profiles. *Physiologia Plantarum*, *150*(4), 580–592. https://doi.org/10.1111/ppl.12110

Correia, B., Valledor, L., Hancock, R. D., Jesus, C., Amaral, J., Meijón, M., & Pinto, G. (2016). Depicting how Eucalyptus globulus survives drought: involvement of redox and DNA methylation events. *Functional Plant Biology*, *43*(9), 838. https://doi.org/10.1071/FP16064

Cortes, C., Vapnik, V., & Saitta, L. (1995). Support-Vector Networks Editor. In *Machine Leaming* (Vol. 20). Kluwer Academic Publishers.

Cotrozzi, L., Peron, R., Tuinstra, M. R., Mickelbart, M. V., & Couture, J. J. (2020). Spectral phenotyping of physiological and anatomical leaf traits related with maize water status1[open]. *Plant Physiology*, *184*(3), 1363–1377. https://doi.org/10.1104/pp.20.00577

Cover, T. M., & Hart, P. E. (1952). Approximate formulas for the information transmitted bv a discrete communication channel. In *IEEE TRANSACTIONS ON INFORMATION THEORY* (Vol. 24, Number 1).

Cursi, A. G., Oliveira, F. S., Gouveia, D. G., Oder, J. C., Barrios, W. E. B., Ferreira, G. V., Martins, A. O., Peterle, G., Nunes-Nesi, A., & Araújo, W. L. (2024). Deciphering the importance of morphological aspects in drought tolerance in eucalyptus progenies. *Forest Ecology and Management*, *569*. https://doi.org/10.1016/j.foreco.2024.122198

Cvetković, D., Marković, D., Cvetković, D., & Radovanović, B. (2011). Effects of continuous UV-irradiation on the antioxidant activities of quercetin and rutin in solution in the presence of lecithin as the protective target. *Journal of the Serbian Chemical Society*, *76*(7), 973–985. https://doi.org/10.2298/JSC101123089C

Da Fonseca-Pereira, P., Daloso, D. M., Gago, J., De Oliveira Silva, F. M., Condori-Apfata, J. A., Florez-Sarasa, I., Tohge, T., Reichheld, J. P., Nunes-Nesi, A., Fernie, A. R., & Arajo, W. L. (2019). The Mitochondrial Thioredoxin System Contributes to the Metabolic Responses under Drought Episodes in Arabidopsis. *Plant and Cell Physiology*, *60*(1), 213–229. https://doi.org/10.1093/pcp/pcy194

Datt, B. (1993). Remote Sensing of Chlorophyll a, Chlorophyll b, Chlorophyll ab, and Total Carotenoid Content in Eucalyptus Leaves Recent studies have devel-oped several new vegetation indices based on other visi. In *REMOTE SENS. ENVIRON* (Vol. 66).

Datt, B. (1999). A New Reflectance Index for Remote Sensing of Chlorophyll Content in Higher Plants: Tests using Eucalyptus Leaves. *Journal of Plant Physiology*.

De Angelis, D., Summo, C., Pasqualone, A., Faccia, M., & Squeo, G. (2024). Advancements in food authentication using soft independent modelling of class analogy (SIMCA): a review. *Food Quality and Safety*, *8*. https://doi.org/10.1093/fqsafe/fyae032

Deribe, H. (2025). Review on Effects of Drought Stress on Maize Growth, Yield and Its Management Strategies. *Communications in Soil Science and Plant Analysis*, *56*(1), 123–143. https://doi.org/10.1080/00103624.2024.2404663

Dmitriev, P., Kozlovsky, B., Dmitrieva, A., Lysenko, V., Chokheli, V., Minkina, T., Mandzhieva, S., Sushkova, S., & Varduni, T. (2023). Identification of species of the genus Quercus L. with different responses to soil and climatic conditions according to hyperspectral survey data. *Eurasian Journal of Soil Science*, *12*(1), 37–62. https://doi.org/10.18393/ejss.1183524

Ejaz, I., Li, W., Naseer, M. A., Li, Y., Qin, W., Farooq, M., Li, F., Huang, S., Zhang, Y., Wang, Z., Sun, Z., & Yu, K. (2023). Detection of combined frost and drought stress in wheat using hyperspectral and chlorophyll fluorescence imaging. *Environmental Technology & Innovation*, *30*, 103051. https://doi.org/10.1016/j.eti.2023.103051

El Azizi, S., Amharref, M., Es-Saouini, H., Bernoussi, A. S., & El Abdellaoui, J. E. (2024). Towards a Spectral Library of Medicinal and Aromatic Plant species (MAPs): Plant Discrimination and Wavelength Selection. *Microchemical Journal*, *207*. https://doi.org/10.1016/j.microc.2024.111854

Ezenarro, J., Saouabi, I., García-Pizarro, Á., Schorn-García, D., Mestres, M., Amigo, J. M., Busto, O., & Boqué, R. (2025). NIR-HSI for the non-destructive monitoring of in-bag hazelnut oxidation. *Spectrochimica Acta - Part A: Molecular and Biomolecular Spectroscopy*, *333*. https://doi.org/10.1016/j.saa.2025.125906

Eziz, A., Yan, Z., Tian, D., Han, W., Tang, Z., & Fang, J. (2017). Drought effect on plant biomass allocation: A meta-analysis. *Ecology and Evolution*, *7*(24), 11002–11010. https://doi.org/10.1002/ece3.3630

Farooq, M., Wahid, A., Kobayashi, N., Fujita, D., & Basra, S. M. A. (2009). Plant drought stress: Effects, mechanisms and management. In *Agronomy for Sustainable Development* (Vol. 29, Number 1, pp. 185–212). https://doi.org/10.1051/agro:2008021

Fernández, M., Valenzuela, S., Barraza, H., Latorre, J., & Neira, V. (2012). Photoperiod, temperature and water deficit differentially regulate the expression of four dehydrin genes from Eucalyptus globulus. *Trees - Structure and Function*, *26*(5), 1483–1493. https://doi.org/10.1007/s00468-012-0722-7

Fernández, M., Villarroel, C., Balbontín, C., & Valenzuela, S. (2010). Validation of reference genes for real-time qRT-PCR normalization during cold acclimation in Eucalyptus globulus. *Trees - Structure and Function*, *24*(6), 1109–1116. https://doi.org/10.1007/s00468-010-0483-0

Freitag, S., Anlanger, M., Lippl, M., Mechtler, K., Reiter, E., Grausgruber, H., & Krska, R. (2024). Simplifying Wheat Quality Assessment: Using Near-Infrared Spectroscopy and Analysis of Variance Simultaneous Component Analysis to Study Regional and Annual Effects. *ACS Measurement Science Au*. https://doi.org/10.1021/acsmeasuresciau.4c00044

Gamon, A., Pe uelas, J., & Field, C. B. (1992). *A Narrow-Waveband Spectral Index That Tracks Diurnal Changes in Photosynthetic Efficiency** (Vol. 41).

Ge, S., Carruthers, R. I., Spencer, D. F., & Yu, Q. (2008). Canopy assessment of biochemical features by ground-based hyperspectral data for an invasive species, giant reed (Arundo donax). *Environmental Monitoring and Assessment*, *147*(1–3), 271–278. https://doi.org/10.1007/s10661-007-0119-z

Gitelson, A. A., Gritz, Y., & Merzlyak, M. N. (2003). Relationships between leaf chlorophyll content and spectral reflectance and algorithms for non-destructive chlorophyll assessment in higher plant leaves. In *J. Plant Physiol* (Vol. 160). http://www.urbanfischer.de/journals/jpp

Gitelson, A. A., Keydan, G. P., & Merzlyak, M. N. (2006). Three-band model for noninvasive estimation of chlorophyll, carotenoids, and anthocyanin contents in higher plant leaves. *Geophysical Research Letters*, *33*(11). https://doi.org/10.1029/2006GL026457

Guigou, M., Moure, S., Bermúdez, F., Clavijo, L., Cabrera, M. N., Xavier, L., Ferrari, M. D., & Lareo, C. (2023). Ethanol Production from Eucalyptus Sawdust Following Sequential Alkaline Thermochemical Pretreatment with Recovery of Extractives. *Bioenergy Research*, *16*(4), 2012–2021. https://doi.org/10.1007/s12155-023-10619-1

Ha, S., Vankova, R., Yamaguchi-Shinozaki, K., Shinozaki, K., & Tran, L. S. P. (2012). Cytokinins: Metabolism and function in plant adaptation to environmental stresses. In *Trends in Plant Science* (Vol. 17, Number 3, pp. 172–179). https://doi.org/10.1016/j.tplants.2011.12.005

Hanin, M., Brini, F., Ebel, C., Toda, Y., Takeda, S., & Masmoudi, K. (2011). Plant dehydrins and stress tolerance: Versatile proteins for complex mechanisms. In *Plant Signaling and Behavior* (Vol. 6, Number 10, pp. 1503–1509). https://doi.org/10.4161/psb.6.10.17088

Hartmann, H., Bastos, A., Das, A. J., Esquivel-Muelbert, A., Hammond, W. M., Martínez-Vilalta, J., Mcdowell, N. G., Powers, J. S., Pugh, T. A. M., Ruthrof, K. X., & Allen, C. D. (2025). Climate Change Risks to Global Forest Health: Emergence of Unexpected Events of Elevated Tree Mortality Worldwide. *Annual Review of Plant Biology*. https://doi.org/10.1146/annurev-arplant-102820

Haynes, R. S., Lucieer, A., Brodribb, T. J., Tonet, V., & Cimoli, E. (2024a). Predicting key water stress indicators of Eucalyptus viminalis and Callitris rhomboidea using high-resolution visible to short-wave infrared spectroscopy. *Plant Cell and Environment*, *47*(12), 4992–5006. https://doi.org/10.1111/pce.15083

Haynes, R. S., Lucieer, A., Brodribb, T. J., Tonet, V., & Cimoli, E. (2024b). Predicting key water stress indicators of Eucalyptus viminalis and Callitris rhomboidea using high-resolution visible to short-wave infrared spectroscopy. *Plant Cell and Environment*, *47*(12), 4992–5006. https://doi.org/10.1111/pce.15083

Humphreys, J. R., O'Reilly-Wapstra, J. M., Harbard, J. L., Davies, N. W., Griffin, A. R., Jordan, G. J., & Potts, B. M. (2008). Discrimination between seedlings of Eucalyptus globulus, E. nitens and their F1 hybrid using near-infrared reflectance spectroscopy and foliar oil content. *Silvae Genetica*, *57*(4–5), 262–269. https://doi.org/10.1515/sg-2008-0040

Hussain, S., Hussain, S., Qadir, T., Khaliq, A., Ashraf, U., Parveen, A., Saqib, M., & Rafiq, M. (2019). Drought stress in plants: An overview on implications, tolerance mechanisms and agronomic mitigation strategies. *Plant Science Today*, *6*(4), 389–402. https://doi.org/10.14719/pst.2019.6.4.578

Ibarra, L., Hodge, G., & Acosta, J. J. (2023). Quantitative Genetics of a Hybrid Population of Eucalyptus nitens × Eucalyptus globulus: Estimation of Genetic Parameters and Implications for Breeding Strategies. *Forests*, *14*(2). https://doi.org/10.3390/f14020381

Jansen, J. J., Hoefsloot, H. C. J., Van Der Greef, J., Timmerman, M. E., Westerhuis, J. A., & Smilde, A. K. (2005). ASCA: Analysis of multivariate data obtained from an experimental design. *Journal of Chemometrics*, *19*(9), 469–481. https://doi.org/10.1002/cem.952

Johnson, J. B. (2023a). Rapid Prediction of Leaf Water Content in Eucalypt Leaves Using a Handheld NIRS Instrument. *Eng*, *4*(2), 1198–1209. https://doi.org/10.3390/eng4020070

Johnson, J. B. (2023b). Rapid Prediction of Leaf Water Content in Eucalypt Leaves Using a Handheld NIRS Instrument. *Eng*, *4*(2), 1198–1209. https://doi.org/10.3390/eng4020070

Jollife, I. T., & Cadima, J. (2016). Principal component analysis: A review and recent developments. In *Philosophical Transactions of the Royal Society A: Mathematical, Physical and Engineering Sciences* (Vol. 374, Number 2065). Royal Society of London. https://doi.org/10.1098/rsta.2015.0202

Jones, H. G. (2007). Monitoring plant and soil water status: Established and novel methods revisited and their relevance to studies of drought tolerance. *Journal of Experimental Botany*, *58*(2), 119–130. https://doi.org/10.1093/jxb/erl118

Josep Peñuelas, I. F. (1998). *Visible and near-infrared reflectance techniques for diagnosing plant physiological status*.

Kawamura, K., Watanabe, N., Sakanoue, S., & Inoue, Y. (2008). Estimating forage biomass and quality in a mixed sown pasture based on partial least squares regression with waveband selection. *Grassland Science*, *54*(3), 131–145. https://doi.org/10.1111/j.1744-697x.2008.00116.x

Kim, Y., Glenn, D. M., Park, J., Ngugi, H. K., & Lehman, B. L. (2011a). Hyperspectral image analysis for water stress detection of apple trees. *Computers and Electronics in Agriculture*, *77*(2), 155–160. https://doi.org/10.1016/j.compag.2011.04.008

Kim, Y., Glenn, D. M., Park, J., Ngugi, H. K., & Lehman, B. L. (2011b). Hyperspectral image analysis for water stress detection of apple trees. *Computers and Electronics in Agriculture*, *77*(2), 155–160. https://doi.org/10.1016/j.compag.2011.04.008

Koag, M. C., Fenton, R. D., Wilkens, S., & Close, T. J. (2003). The binding of maize DHN1 to lipid vesicles. Gain of structure and lipid specificity. *Plant Physiology*, *131*(1), 309–316. https://doi.org/10.1104/pp.011171

Kohzuma, K., Tamaki, M., & Hikosaka, K. (2021). Corrected photochemical reflectance index (PRI) is an effective tool for detecting environmental stresses in agricultural crops under light conditions. *Journal of Plant Research*, *134*(4), 683–694. https://doi.org/10.1007/s10265-021-01316-1

Korek, M., & Marzec, M. (2023). Strigolactones and abscisic acid interactions affect plant development and response to abiotic stresses. In *BMC Plant Biology* (Vol. 23, Number 1). BioMed Central Ltd. https://doi.org/10.1186/s12870-023-04332-6

Kuang, X., Cheng, Q., Chen, D., Fu, W., Li, H., & Chen, Z. (2026). Intelligent Diagnosis of Winter Wheat Water Stress Based on UAV Multi-Modal Remote Sensing. *Smart Agricultural Technology*, 101781. https://doi.org/10.1016/j.atech.2026.101781

Lee, S. C., & Luan, S. (2012). ABA signal transduction at the crossroad of biotic and abiotic stress responses. In *Plant, Cell and Environment* (Vol. 35, Number 1, pp. 53–60). https://doi.org/10.1111/j.1365-3040.2011.02426.x

Li, H., Yang, W., Lei, J., She, J., & Zhou, X. (2021). Estimation of leaf water content from hyperspectral data of different plant species by using three new spectral absorption indices. *PLoS ONE*, *16*(3 March). https://doi.org/10.1371/journal.pone.0249351

M. N. Merzlyak*, A. A. G. O. B. C. A. E. S. and S. I. P. (2003). *Application of Reflectance Spectroscopy for Analysis of Higher Plant Pigments*.

Manley, M. (2014). Near-infrared spectroscopy and hyperspectral imaging: Non-destructive analysis of biological materials. In *Chemical Society Reviews* (Vol. 43, Number 24, pp. 8200–8214). Royal Society of Chemistry. https://doi.org/10.1039/c4cs00062e

Martins, G. S., Freitas, N. C., Máximo, W. P. F., & Paiva, L. V. (2018). Gene expression in two contrasting hybrid clones of Eucalyptus camaldulensis x Eucalyptus urophylla grown under water deficit conditions. *Journal of Plant Physiology*, *229*, 122–131. https://doi.org/10.1016/j.jplph.2018.07.007

McFeeters, S. K. (1996). The use of the Normalized Difference Water Index (NDWI) in the delineation of open water features. *International Journal of Remote Sensing*, *17*(7), 1425–1432. https://doi.org/10.1080/01431169608948714

Merchant, A., Callister, A., Arndt, S., Tausz, M., & Adams, M. (2007). Contrasting physiological responses of six Eucalyptus species to water deficit. *Annals of Botany*, *100*(7), 1507–1515. https://doi.org/10.1093/aob/mcm234

Migacz, I. P., Manfron, J., Farago, P. V., Raman, V., de Muñiz, G. I. B., & Nisgoski, S. (2022). VIS/NIR spectra and color parameters according to leaf age of some Eucalyptus species: influence on their classification and discrimination. *Forest Systems*, *31*(2). https://doi.org/10.5424/fs/2022312-19242

Mobaraki, N., & Amigo, J. M. (2018). HYPER-Tools. A graphical user-friendly interface for hyperspectral image analysis. *Chemometrics and Intelligent Laboratory Systems*, *172*, 174–187. https://doi.org/10.1016/j.chemolab.2017.11.003

Mondal, M., Edida, M., Sharma, N., Lall, B., & Raju, D. (2019). Plants Stress Response Detection by Selecting Minimal Bands of Hyperspectral Images. *2019 9th International Conference on Advances in Computing and Communication (ICACC)*, 230–233. https://doi.org/10.1109/ICACC48162.2019.8986161

Mountrakis, G., Im, J., & Ogole, C. (2011). Support vector machines in remote sensing: A review. In *ISPRS Journal of Photogrammetry and Remote Sensing* (Vol. 66, Number 3, pp. 247–259). https://doi.org/10.1016/j.isprsjprs.2010.11.001

Moura, J. C. M. S., Araújo, P., Brito, M. D. S., Souza, U. R., Viana, J. O. F., & Mazzafera, P. (2012). Validation of reference genes from Eucalyptus spp. under different stress conditions. *BMC Research Notes*, *5*. https://doi.org/10.1186/1756-0500-5-634

Moura Melo, L. de, Dos Santos, A. C., Arteiro da Silva, K., Barbosa, U. do N., De Sena Oliveira, G. F., Alba, E., André Bellé, P., Monteiro Junior, J. J., & Araújo Silva, E. (2019). Spectral Response of Eucalyptus saligna under Water Stress in Southern Brazil. *Journal of Experimental Agriculture International*, 1–8. https://doi.org/10.9734/jeai/2019/v41i430405

Moussa Kourouma, J., Eze, E., Negash, E., Phiri, D., Vinya, R., Girma, A., & Zenebe, A. (2021). Assessing the spatio-temporal variability of NDVI and VCI as indices of crops productivity in Ethiopia: a remote sensing approach. *Geomatics, Natural Hazards and Risk*, *12*(1), 2880–2903. https://doi.org/10.1080/19475705.2021.1976849

Munera, S., Amigo, J. M., Aleixos, N., Talens, P., Cubero, S., & Blasco, J. (2018). Potential of VIS-NIR hyperspectral imaging and chemometric methods to identify similar cultivars of nectarine. *Food Control*, *86*, 1–10. https://doi.org/10.1016/j.foodcont.2017.10.037

Munns, R., James, R. A., Sirault, X. R. R., Furbank, R. T., & Jones, H. G. (2010). New phenotyping methods for screening wheat and barley for beneficial responses to water deficit. In *Journal of Experimental Botany* (Vol. 61, Number 13, pp. 3499–3507). https://doi.org/10.1093/jxb/erq199

Murchie, E. H., & Lawson, T. (2013). Chlorophyll fluorescence analysis: A guide to good practice and understanding some new applications. In *Journal of Experimental Botany* (Vol. 64, Number 13, pp. 3983–3998). https://doi.org/10.1093/jxb/ert208

Okyere, F. G., Cudjoe, D. K., Virlet, N., Castle, M., Riche, A. B., Greche, L., Mohareb, F., Simms, D., Mhada, M., & Hawkesford, M. J. (2024). Hyperspectral Imaging for Phenotyping Plant Drought Stress and Nitrogen Interactions Using Multivariate Modeling and Machine Learning Techniques in Wheat. *Remote Sensing*, *16*(18), 3446. https://doi.org/10.3390/rs16183446

Oliveira, L. A., Cardoso, A. A., Andrade, M. T., Pereira, T. S., Araújo, W. L., Santos, G. A., Damatta, F. M., & Martins, S. C. V. (2022). Exploring leaf hydraulic traits to predict drought tolerance of *Eucalyptus* clones. *Tree Physiology*, *42*(9), 1750–1761. https://doi.org/10.1093/treephys/tpac040

Oliveri, P., Malegori, C., Simonetti, R., & Casale, M. (2019). The impact of signal pre-processing on the final interpretation of analytical outcomes – A tutorial. In *Analytica Chimica Acta* (Vol. 1058, pp. 9–17). Elsevier B.V. https://doi.org/10.1016/j.aca.2018.10.055

Olvera-Carrillo, Y., Campos, F., Reyes, J. L., Garciarrubio, A., & Covarrubias, A. A. (2010). Functional analysis of the group 4 late embryogenesis abundant proteins reveals their relevance in the adaptive response during water deficit in arabidopsis. *Plant Physiology*, *154*(1), 373–390. https://doi.org/10.1104/pp.110.158964

Olvera-Carrillo, Y., Reyes, J. L., & Covarrubias, A. A. (2011). Late embryogenesis abundant proteins: Versatile players in the plant adaptation to water limiting environments. *Plant Signaling and Behavior*, *6*(4), 586–589. https://doi.org/10.4161/psb.6.4.15042

Peerbhay, K. Y., Mutanga, O., & Ismail, R. (2013). Commercial tree species discrimination using airborne AISA Eagle hyperspectral imagery and partial least squares discriminant analysis (PLS-DA) in KwaZulu-Natal, South Africa. *ISPRS Journal of Photogrammetry and Remote Sensing*, *79*, 19–28. https://doi.org/10.1016/j.isprsjprs.2013.01.013

Peguero-Pina, J. J., Sancho-Knapik, D., Ferrio, J. P., López-Ballesteros, A., Ruiz-Llata, M., & Gil-Pelegrín, E. (2023). Reevaluating Near-Infrared Reflectance as a Tool for the Study of Plant Water Status in Holm Oak (Quercus ilex subsp. rotundifolia). *Forests*, *14*(9). https://doi.org/10.3390/f14091825

Peng, Y., Zhang, M., Xu, Z., Yang, T., Su, Y., Zhou, T., Wang, H., Wang, Y., & Lin, Y. (2020). Estimation of leaf nutrition status in degraded vegetation based on field survey and hyperspectral data. *Scientific Reports*, *10*(1). https://doi.org/10.1038/s41598-020-61294-7

Penuelas, J., Pinol, J., Ogaya, R., & Filella, I. (1997). Estimation of plant water concentration by the reflectance Water Index WI (R900/R970). *International Journal of Remote Sensing*, *18*(13), 2869–2875. https://doi.org/10.1080/014311697217396

Peñuelas Josep, & Filella Iolanda. (1998). *Visible and near-infrared reflectance techniques for diagnosing plant physiological status*.

Pita, P., & Pardos, J. A. (2001). Growth, leaf morphology, water use and tissue water relations of Eucalyptus globulus clones in response to water deficit. *Tree Physiology*, *21*(9), 599–607. https://doi.org/10.1093/treephys/21.9.599

Pivovar, M., Näsi, R., Honkavaara, E., Blaženec, M., Škvarenina, J., Modlinger, R., Rožnovský, J., & Jakuš, R. (2025). Spectral signatures discrimination of Norway spruce trees under experimentally induced drought and acute thermal stress using hyperspectral imaging. *Forest Ecology and Management*, *586*. https://doi.org/10.1016/j.foreco.2025.122692

Poblete Hernández, P., Carlos, J., Munita, B., Caselli, J. G., Kahler González, C., Pardo Velásquez, E., Rocha, D. B., Catelicán Vera, L., Pineda, J. H., Celis Cantillana, B., & Recabarren, H. T. (2025). *ANUARIO FORESTAL CHILEAN STATISTICAL YEARBOOK OF FORESTRY 2025*. www.infor.cl

Ram, B. G., Oduor, P., Igathinathane, C., Howatt, K., & Sun, X. (2024). A systematic review of hyperspectral imaging in precision agriculture: Analysis of its current state and future prospects. In *Computers and Electronics in Agriculture* (Vol. 222). Elsevier B.V. https://doi.org/10.1016/j.compag.2024.109037

Raymond Hunt, E., & Rock, B. N. (1989). *Detection of Changes in Leaf Water Content Using Near-and Middle-Infrared Reflectances* (Vol. 30).

Rinnan, Å., Berg, F. van den, & Engelsen, S. B. (2009). Review of the most common pre-processing techniques for near-infrared spectra. In *TrAC - Trends in Analytical Chemistry* (Vol. 28, Number 10, pp. 1201–1222). https://doi.org/10.1016/j.trac.2009.07.007

Rodionova, O. Ye., Oliveri, P., Malegori, C., & Pomerantsev, A. L. (2024). Chemometrics as an efficient tool for food authentication: Golden pillars for building reliable models. *Trends in Food Science & Technology*, *147*, 104429. https://doi.org/10.1016/j.tifs.2024.104429

Rojas-Rioseco, M., Castillo, R. del P., González-Campos, J., Ipinza, R., Sanhueza, M. I., & Hasbún, R. (2022). Phylogeographic origin authentication of Araucaria araucana (Mol.) K Koch seedlings through the application of spectroscopy techniques in different infrared ranges and chemometric methods. *New Forests*. https://doi.org/10.1007/s11056-022-09933-x

Rojek, L., Möller, M., Richter, M., Bischoff-Schaefer, M., & Hehl, K. (2023). PLANTSENS: A rail-based multi-sensor imaging system for redundant water stress detection in greenhouses. In *Smart Agricultural Technology* (Vol. 4). Elsevier B.V. https://doi.org/10.1016/j.atech.2023.100223

Ryckewaert, M., Gorretta, N., Henriot, F., Gobrecht, A., Héran, D., Moura, D., Bendoula, R., & Roger, J. M. (2021). Potential of high-spectral resolution for field phenotyping in plant breeding: Application to maize under water stress. *Computers and Electronics in Agriculture*, *189*. https://doi.org/10.1016/j.compag.2021.106385

Saadaoui, E., Ben Yahia, K., Dhahri, S., Ben Jamaa, M. L., & Khouja, M. L. (2017). An overview of adaptative responses to drought stress in Eucalyptus spp. *Forestry Studies*, *67*(1), 86–96. https://doi.org/10.1515/fsmu-2017-0014

Saddiq, M. S., Wang, X., Iqbal, S., Bilal Hafeez, M., Khan, S., Raza, A., Iqbal, J., Maqbool, M. M., Fiaz, S., Qazi, M. A., Bakhsh, A., 10, J., Gulshan, A. B., & Yang, S. H. (1934). *Effect of Water Stress on Grain Yield and Physiological Characters of Quinoa Genotypes*. *11*. https://doi.org/10.3390/agronomy

Salazar, C., Hernández, C., & Pino, M. T. (2015). Plant water stress: Associations between ethylene and abscisic acid response. In *Chilean Journal of Agricultural Research* (Vol. 75, pp. 71–79). Instituto de Investigaciones Agropecuarias, INIA. https://doi.org/10.4067/S0718-58392015000300008

Sánchez, J. C. M., Mesa, H. G. A., Espinosa, A. T., Castilla, S. R., & Lamont, F. G. (2025). Improving wheat yield prediction through variable selection using Support Vector Regression, Random Forest, and Extreme Gradient Boosting. In *Smart Agricultural Technology* (Vol. 10). Elsevier B.V. https://doi.org/10.1016/j.atech.2025.100791

Sanhueza-Novoa, P., Fernández, M., Hernández-Fuentes, C., Valenzuela, S., Hayat, M. Q., Ricardo Ramírez, H., & Castillo, R. del P. (2026). Detection of water deficit stress in Eucalyptus spp. through VIS-NIR hyperspectral imaging and chemometric methods. *Spectrochimica Acta Part A: Molecular and Biomolecular Spectroscopy*, *344*, 126675. https://doi.org/10.1016/j.saa.2025.126675

Santana, D. C., Baio, F. H. R., Oliveira, I. C. de, Araújo, F. C. de, Azevedo, G. B. de, Silva, E. V. M., Silva Junior, C. A. da, Teodoro, P. E., & Teodoro, L. P. R. (2025). From spectral data to species identity: Machine learning and VIS/NIR reflectance in eucalyptus classification. *Remote Sensing Applications: Society and Environment*, *39*. https://doi.org/10.1016/j.rsase.2025.101686

Schwanninger, M., Rodrigues, J. C., & Fackler, K. (2011). A review of band assignments in near infrared spectra of wood and wood components. In *Journal of Near Infrared Spectroscopy* (Vol. 19, Number 5, pp. 287–308). https://doi.org/10.1255/jnirs.955

Shi, Y., Liu, X., Zhao, S., & Guo, Y. (2022). The PYR-PP2C-CKL2 module regulates ABA-mediated actin reorganization during stomatal closure. *New Phytologist*, *233*(5), 2168–2184. https://doi.org/10.1111/nph.17933

Silla, C. N., & Freitas, A. A. (2011). A survey of hierarchical classification across different application domains. In *Data Mining and Knowledge Discovery* (Vol. 22, Numbers 1–2, pp. 31–72). https://doi.org/10.1007/s10618-010-0175-9

Singh, D., Singh, C. K., Taunk, J., Tomar, R. S. S., Chaturvedi, A. K., Gaikwad, K., & Pal, M. (2017). Transcriptome analysis of lentil (Lens culinaris Medikus) in response to seedling drought stress. *BMC Genomics*, *18*(1). https://doi.org/10.1186/s12864-017-3596-7

Smola, A. J., Sch¨olkopf, B., & Sch¨olkopf, S. (2004). A tutorial on support vector regression *. In *Statistics and Computing* (Vol. 14). Kluwer Academic Publishers.

Sobejano-Paz, V., Mikkelsen, T. N., Baum, A., Mo, X., Liu, S., Köppl, C. J., Johnson, M. S., Gulyas, L., & García, M. (2020). Hyperspectral and Thermal Sensing of Stomatal Conductance, Transpiration, and Photosynthesis for Soybean and Maize under Drought. *Remote Sensing*, *12*(19), 3182. https://doi.org/10.3390/rs12193182

Sokolova, M., & Lapalme, G. (2009). A systematic analysis of performance measures for classification tasks. *Information Processing and Management*, *45*(4), 427–437. https://doi.org/10.1016/j.ipm.2009.03.002

Spokevicius, A. V., Tibbits, J., Rigault, P., Nolin, M. A., Müller, C., & Merchant, A. (2017). Medium term water deficit elicits distinct transcriptome responses in Eucalyptus species of contrasting environmental origin. *BMC Genomics*, *18*(1). https://doi.org/10.1186/s12864-017-3664-z

Steidle Neto, A. J., Lopes, D. de C., Silva, T. G. F. da, Ferreira, S. O., & Grossi, J. A. S. (2017). Estimation of leaf water content in sunflower under drought conditions by means of spectral reflectance. *Engineering in Agriculture, Environment and Food*, *10*(2), 104–108. https://doi.org/10.1016/j.eaef.2016.11.006

Stellacci, A. M., Castrignanò, A., Diacono, M., Troccoli, A., Ciccarese, A., Armenise, E., Gallo, A., De Vita, P., Lonigro, A., Mastro, M. A., & Rubino, P. (2012). Combined approach based on principal component analysis and canonical discriminant analysis for investigating hyperspectral plant response. *Italian Journal of Agronomy*, *7*(3), 247–253. https://doi.org/10.4081/ija.2012.e34

T Daughtry, C. S., Walthall, C. L., Kim, M. S., Brown de Colstoun, E., & McMurtrey III, J. E. (1999). Estimating Corn Leaf Chlorophyll Concentration from Leaf and Canopy Reflectance. In *REMOTE SENS. ENVIRON* (Vol. 74).

Taniguchi, M., LaRocca, C. A., Bernat, J. D., & Lindsey, J. S. (2023). Digital Database of Absorption Spectra of Diverse Flavonoids Enables Structural Comparisons and Quantitative Evaluations. *Journal of Natural Products*, *86*(4), 1087–1119. https://doi.org/10.1021/acs.jnatprod.2c00720

Torrion, J. A., Maas, S. J., Guo, W., Bordovsky, J. P., & Cranmer, A. M. (2014). A three-dimensional index for characterizing crop water stress. *Remote Sensing*, *6*(5), 4025–4042. https://doi.org/10.3390/rs6054025

Türker-Kaya, S., & Huck, C. W. (2017a). A review of mid-infrared and near-infrared imaging: Principles, concepts and applications in plant tissue analysis. In *Molecules* (Vol. 22, Number 1). MDPI AG. https://doi.org/10.3390/molecules22010168

Türker-Kaya, S., & Huck, C. W. (2017b). A review of mid-infrared and near-infrared imaging: Principles, concepts and applications in plant tissue analysis. In *Molecules* (Vol. 22, Number 1). MDPI AG. https://doi.org/10.3390/molecules22010168

Ulloa, J. L., Aguayo, P., Conejera, D., Rubilar, R., Balocchi, C., & Valenzuela, S. (2022). Transcriptomic response in foliar and root tissues of a drought-tolerant Eucalyptus globulus genotype under drought stress. *Trees - Structure and Function*, *36*(2), 697–709. https://doi.org/10.1007/s00468-021-02241-5

Umami, M., Parker, L. M., & Arndt, S. K. (2021). The impacts of drought stress and phytophthora cinnamomi infection on short-term water relations in two year-old eucalyptus obliqua. *Forests*, *12*(2), 1–14. https://doi.org/10.3390/f12020109

Valdés, A. E., Irar, S., Majada, J. P., Rodríguez, A., Fernández, B., & Pagès, M. (2013). Drought tolerance acquisition in Eucalyptus globulus (Labill.): A research on plant morphology, physiology and proteomics. *Journal of Proteomics*, *79*, 263–276. https://doi.org/10.1016/j.jprot.2012.12.019

Valverde, J. C., Rubilar, R. A., Medina, A., Pincheira, M., Emhart, V., Espinoza, Y., Bozo, D., & Campoe, O. C. (2025). Transpiration and Water Use Efficiency of Mediterranean Eucalyptus Genotypes Under Contrasting Irrigation Regimes. *Plants*, *14*(14). https://doi.org/10.3390/plants14142232

Vicente-Serrano, S. M., Quiring, S. M., Peña-Gallardo, M., Yuan, S., & Domínguez-Castro, F. (2020). A review of environmental droughts: Increased risk under global warming? In *Earth-Science Reviews* (Vol. 201). Elsevier B.V. https://doi.org/10.1016/j.earscirev.2019.102953

Vieira Dos Santos, C., & Rey, P. (2006). Plant thioredoxins are key actors in the oxidative stress response. *Trends in Plant Science*, *11*(7), 329–334. https://doi.org/10.1016/j.tplants.2006.05.005

Villar, E., Klopp, C., Noirot, C., Novaes, E., Kirst, M., Plomion, C., & Gion, J. M. (2011). RNA-Seq reveals genotype-specific molecular responses to water deficit in eucalyptus. *BMC Genomics*, *12*. https://doi.org/10.1186/1471-2164-12-538

Virtuoso, M. C. S., Souza, J. V. O., Zanatto, B., Valente, T. S., Silva, E. H. C., & de Paula, R. C. (2022). Germinative and physiological performance of eucalyptus species under abiotic stress. *Trees, Forests and People*, *10*. https://doi.org/10.1016/j.tfp.2022.100348

Wang, J., Xu, R., & Yang, S. (2009a). Estimation of plant water content by spectral absorption features centered at 1,450 nm and 1,940 nm regions. *Environmental Monitoring and Assessment*, *157*(1–4), 459–469. https://doi.org/10.1007/s10661-008-0548-3

Wang, J., Xu, R., & Yang, S. (2009b). Estimation of plant water content by spectral absorption features centered at 1,450 nm and 1,940 nm regions. *Environmental Monitoring and Assessment*, *157*(1–4), 459–469. https://doi.org/10.1007/s10661-008-0548-3

Wang, L., Hunt, E. R., Qu, J. J., Hao, X., & Daughtry, C. S. T. (2011). Estimating dry matter content of fresh leaves from the residuals between leaf and water reflectance. *Remote Sensing Letters*, *2*(2), 137–145. https://doi.org/10.1080/01431161.2010.503973

Warren, C. R., Aranda, I., & Cano, F. J. (2011a). Responses to water stress of gas exchange and metabolites in Eucalyptus and Acacia spp. *Plant, Cell and Environment*, *34*(10), 1609–1629. https://doi.org/10.1111/j.1365-3040.2011.02357.x

Warren, C. R., Aranda, I., & Cano, F. J. (2011b). Responses to water stress of gas exchange and metabolites in Eucalyptus and Acacia spp. *Plant, Cell and Environment*, *34*(10), 1609–1629. https://doi.org/10.1111/j.1365-3040.2011.02357.x

Wold, S., Esbensen, K., & Geladi, P. (n.d.). *Principal Component Analysis*.

Workman, Jerry., & Weyer, Lois. (2012). *Practical guide and spectral atlas for interpretive near-infrared spectroscopy*. CRC Press.

Xie, Y., Plett, D., & Liu, H. (2021). The Promise of Hyperspectral Imaging for the Early Detection of Crown Rot in Wheat. *AgriEngineering*, *3*(4), 924–941. https://doi.org/10.3390/agriengineering3040058

Ye, N., Zhong, S., Fang, Z., Gao, H., Du, Z., Chen, H., Yuan, L., & Pan, T. (2022). Performance Improvement of NIR Spectral Pattern Recognition from Three Compensation Models' Voting and Multi-Modal Fusion. *Molecules*, *27*(14). https://doi.org/10.3390/molecules27144485

Zade, S. V., & Abdollahi, H. (2024). Evaluation of Classical Least Squares Discriminant Analysis (CLS-DA) as a Novel Supervised Pattern Recognition Technique. *Journal of Chemometrics*. https://doi.org/10.1002/cem.3609

Zahir, S. A. D. M., Omar, A. F., Jamlos, M. F., Azmi, M. A. M., & Muncan, J. (2022). A review of visible and near-infrared (Vis-NIR) spectroscopy application in plant stress detection. In *Sensors and Actuators A: Physical* (Vol. 338). Elsevier B.V. https://doi.org/10.1016/j.sna.2022.113468

Zahra, N., Hafeez, M. B., Kausar, A., Al Zeidi, M., Asekova, S., Siddique, K. H. M., & Farooq, M. (2023a). Plant photosynthetic responses under drought stress: Effects and management. In *Journal of Agronomy and Crop Science*. John Wiley and Sons Inc. https://doi.org/10.1111/jac.12652

Zahra, N., Hafeez, M. B., Kausar, A., Al Zeidi, M., Asekova, S., Siddique, K. H. M., & Farooq, M. (2023b). Plant photosynthetic responses under drought stress: Effects and management. In *Journal of Agronomy and Crop Science*. John Wiley and Sons Inc. https://doi.org/10.1111/jac.12652

Zhu, J. K. (2016). Abiotic Stress Signaling and Responses in Plants. In *Cell* (Vol. 167, Number 2, pp. 313–324). Cell Press. https://doi.org/10.1016/j.cell.2016.08.029

Zhuang, J., Wang, Y., Chi, Y., Zhou, L., Chen, J., Zhou, W., Song, J., Zhao, N., & Ding, J. (2020). Drought stress strengthens the link between chlorophyll fluorescence parameters and photosynthetic traits. *PeerJ*, *8*. https://doi.org/10.7717/peerj.10046

Chapter 2
Hypothesis and Objectives

2.1. Hypothesis

The combined use of VIS–NIR spectroscopy and computer vision through hyperspectral imaging (HSI), together with multivariate analysis, will enable the early and selective detection of water-deficit stress in *Eucalyptus* spp. through predictive models capable of estimating stress levels during both the response and recovery phases, before the appearance of visible symptoms.

2.2. General objective

To develop and validate a spectroscopic prediction tool based on chemometric techniques for the effective detection of water-deficit stress in *Eucalyptus* spp. plants before the appearance of visible symptoms. Additionally, this tool will support the identification of genotypes exhibiting more favorable responses under water-deficit conditions.

2.3. Specific objectives

1. To establish an optimal experimental design for the analysis of water-deficit stress in *Eucalyptus* spp. plants.
2. To obtain and evaluate spectral information from the samples using NIR spectroscopy and hyperspectral imaging (HSI), and to compare it with the vegetation indices that contribute most to water-deficit stress analysis, based on physiological measurements and the assessment of water-deficit-responsive gene expression in the plant material.
3. To develop and validate a predictive tool for the identification of early water-deficit stress using the acquired spectroscopic data and supervised pattern-recognition techniques, including SIMCA, PLS-DA, SVM, among others.
4. To evaluate the progression of plant recovery after the stress period using spectral tools and complementary techniques.
5. To select, from among the evaluated genotypes, the plant material exhibiting superior performance under induced water-deficit stress using the developed predictive tools.

Chapter 3
General Analytical Strategy

3. Analytical strategy

An integrated analytical strategy was developed to characterize, detect, and monitor water-deficit stress in young *Eucalyptus* spp. plants using complementary spectral, physiological, and molecular information. The strategy was structured according to the five specific objectives of this Ph.D. thesis and comprised: (i) optimization of a controlled and reproducible experimental and analytical design; (ii) acquisition and biological interpretation of VIS–NIR hyperspectral imaging and portable NIR data; (iii) development and validation of supervised classification models for early water-deficit detection; (iv) spectral and physiological monitoring of plant recovery after rewatering; and (v) integration of the generated information to identify genotypes exhibiting superior performance under water-deficit conditions.

The experimental work was conducted through sequential assays under controlled environmental conditions. An initial assay was used to assess the feasibility of the spectral methodology and refine the sampling and image-acquisition procedures. A subsequent expanded assay incorporated six genotypes, control and water-deficit conditions, repeated measurements during stress development, and a post-stress recovery period. This sequential approach allowed the analytical workflow to be refined before its application to a more complex factorial structure involving genotype, irrigation condition, sampling day, and biological variability.

The general analytical strategy is summarized in Figure 3.1. Two sequential controlled-environment assays were conducted. In Assay I, four genotypes were monitored at T0 and at three subsequent sampling times (T1-T3) during progressive water deficit, without a subsequent recovery phase. Assay II included six genotypes and extended the monitoring T0 through three water-deficit stages (T1-T3), followed by two sampling times after rewatering to assess recovery (R1:T4 and R2:T5). In addition to spectral acquisition, complementary measurements included fresh mass and plant height in Assay I, while Assay II incorporated plant water potential, gas-exchange and chlorophyll-fluorescence parameters, leaf temperature, fresh mass, and height, together with candidate gene-expression analysis. Spectral data were analyzed using exploratory and supervised multivariate methods, and classification models were developed from mean plant spectra, while HSI data were also evaluated at the pixel level to visualize the spatial distribution of water-deficit responses.

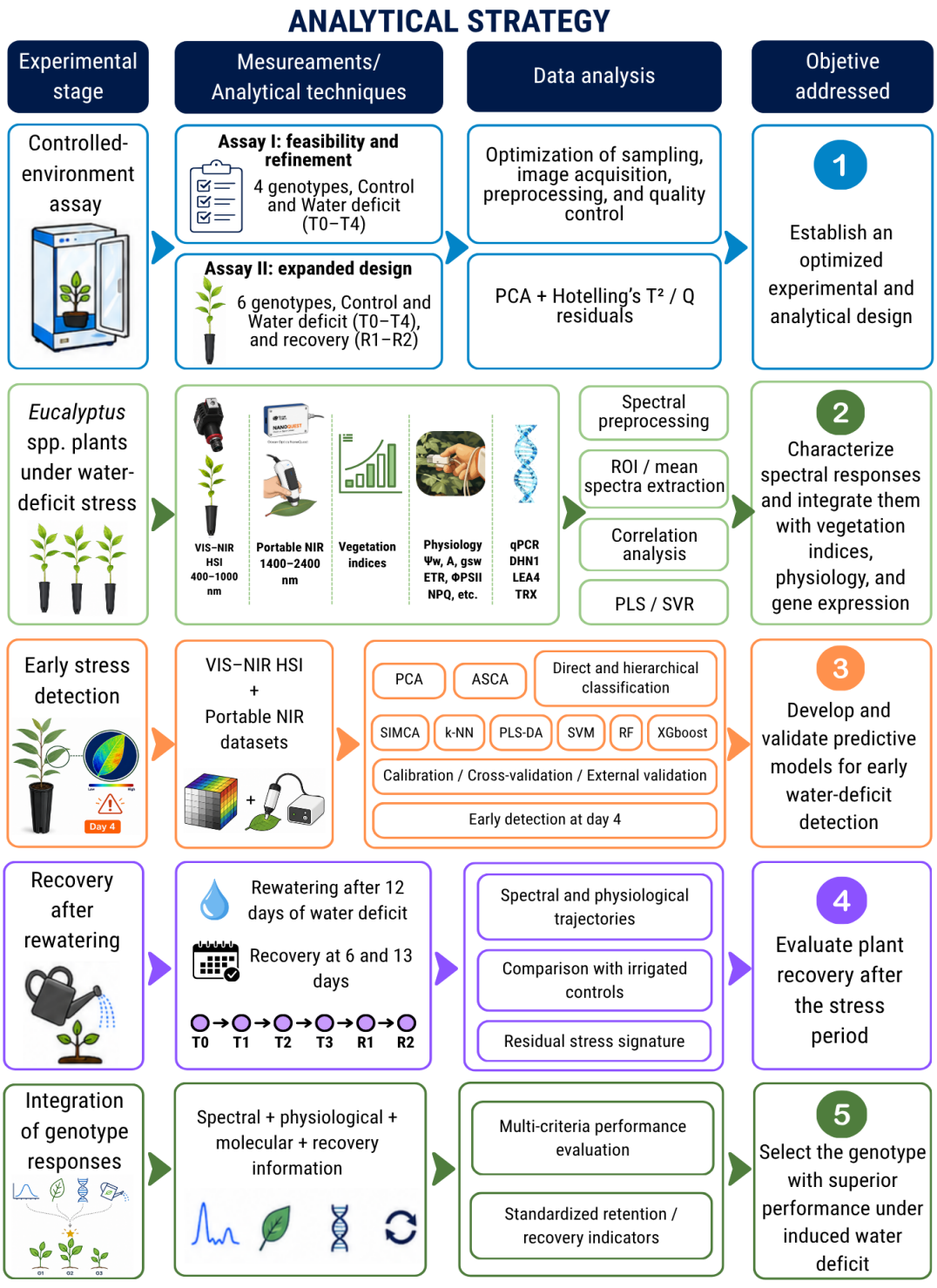

Figure 3.1 Schematic representation of the analytical strategy developed to address the proposed objectives, integrating spectral, physiological, molecular, and multivariate analyses.

3.1. Analytical strategy to address specific objective 1: optimization of the experimental and analytical design

To establish an optimized design for the analysis of water-deficit stress in *Eucalyptus* spp., the biological experiment and the spectral–chemometric workflow were considered as components of an integrated analytical system. In this thesis, the term "optimized design" refers to the combination of experimental, acquisition, processing, and modelling conditions that provided reproducible spectral measurements, adequate representation of genotype and stress progression, reliable discrimination of early water deficit, and the best predictive performance among the alternatives evaluated.

Two sequential controlled-environment assays were conducted. The first assay was used to assess the feasibility of VIS–NIR hyperspectral imaging for monitoring water-deficit responses and to refine the sampling, image-acquisition, and analytical procedures. The second assay expanded the experimental design to include six genotypes, control and water-deficit conditions, multiple sampling times during stress progression, portable NIR spectroscopy, VIS–NIR hyperspectral imaging, physiological measurements, and a subsequent recovery period.

The second assay initially comprised 126 plants. Before multivariate modelling, the spectral matrices were subjected to exploratory quality assessment using principal component analysis. Hotelling's T^2 and Q-residual statistics, evaluated at a 95% confidence level, were used to identify anomalous spectral observations. Observations showing abnormal behaviour associated with acquisition problems or visibly deteriorated plant material were excluded from the corresponding analytical matrix. Therefore, the final number of observations used for modelling depended on the spectral technique and the quality-control criteria applied. The exclusion of a spectral observation did not necessarily imply the exclusion of the entire plant unless all measurements associated with that biological unit failed to meet the predefined quality criteria.

Optimization of the analytical workflow included the definition of acquisition conditions, selection of representative plant regions, extraction of spectral information, evaluation of spectral preprocessing methods, detection of anomalous observations, exploratory assessment of the main sources of variability, selection of supervised classification algorithms, and validation of the

resulting predictive models. This sequential strategy allowed the experimental and analytical procedures to be adjusted according to both biological response and analytical performance.

3.2. Analytical strategy to address specific objective 2: spectral characterization and integration with vegetation indices, physiology, and gene expression

To obtain complementary spectral information from plants subjected to water deficit, two non-destructive analytical techniques were employed. VIS–NIR hyperspectral images were acquired using a Resonon Pika-L system covering approximately 400–1000 nm, providing information associated mainly with foliar pigments, visible colour changes, red-edge behaviour, and tissue structure. Portable NIR spectra were acquired directly from juvenile leaves in the 1400–2400 nm range, which is particularly sensitive to water-related absorption bands and variations in O–H, C–H, and C–O-containing constituents. These spectral domains therefore provided complementary information regarding pigment-related, structural, biochemical, and hydration changes.

For the hyperspectral images, the background was removed and representative regions of plant tissue were selected. Mean spectra were extracted from the selected regions, while the complete spatial information was retained for analyses requiring pixel-level interpretation. Several preprocessing approaches, including smoothing, standard normal variate transformation, multiplicative scatter correction, derivatives, normalization, and mean centering, were evaluated to reduce physical and instrumental variation without eliminating biologically relevant information.

Vegetation indices associated with chlorophyll, carotenoids, photosynthetic activity, water status, and red-edge changes were calculated from the hyperspectral images. Their responses were compared across genotypes, irrigation treatments, and sampling days. The analytical relevance of each index was not determined exclusively from statistical significance, because an index could show significant differences at an isolated sampling point without presenting a consistent response across genotypes or throughout stress progression. Consequently, index relevance was

evaluated according to temporal consistency, effect magnitude, relationship with water-deficit progression, and association with independent physiological measurements.

Physiological measurements were used to provide independent biological information on plant water status and functional performance. These measurements included water potential, net CO_2 assimilation, stomatal conductance, electron transport rate, quantum yields associated with photosynthesis and photosystem II, non-photochemical quenching, leaf energy balance, and complementary growth or biomass-related measurements. Relationships between spectral and physiological information were evaluated using correlation analysis and multivariate regression methods, including partial least squares regression and support vector machine regression, as applicable to each dataset.

At the molecular level, the relative expression of water-deficit-responsive genes associated with complementary protective mechanisms was assessed by qPCR. These genes were DHN1, associated with membrane and macromolecule protection during dehydration**;** LEA4, associated with protein and cellular-structure stabilization; and TRDX**,** involved in redox regulation and protection against oxidative stress.

Gene-expression analysis was performed using the subset of plant material from which RNA of sufficient concentration, purity, and integrity could be obtained. Although RNA extraction was initially attempted for all available samples, the final molecular dataset was reduced and unbalanced because several samples yielded insufficient RNA for cDNA synthesis and qPCR analysis.

In the first experiment, gene expression analysis allowed for a comparison between control plants and those subjected to water deficit at the same sampling time, corresponding to a condition of moderate stress. In the second experiment, the molecular analysis focused on characterizing the gene response at the final stage of severe stress by comparing the initial baseline condition with plants subjected to 12 days of withheld irrigation. Both experiments provided complementary information: the first allowed for the evaluation of the treatment-associated response at an intermediate stage, while the second expanded the range of observation to include a condition of greater stress intensity.

Because the comparison in the second experiment involved two experimentally distinct states separated in time, its results were interpreted as an integrated molecular response spanning the baseline condition and the final state of severe stress, without attributing all observed differences exclusively to water deficit. For this reason, the expression of DHN1, LEA4, and TRDX was used to characterize the relative activation of mechanisms associated with structural protection, protein stabilization, and redox regulation, rather than as a quantitative reference variable for constructing or validating spectral models.

The molecular data were integrated with physiological responses, spectral profiles, and vegetation indices. This triangulation made it possible to assess whether the changes detected using HSI and NIR were consistent with functional alterations in the plant and with the activation of recognized molecular mechanisms in response to water deficit. Furthermore, elevated gene expression was not considered in and of itself as evidence of tolerance, but was interpreted in terms of the maintenance or deterioration of physiological performance and the recovery capacity of each genotype.

3.3. Analytical strategy to address specific objective 3: development and validation of predictive models for early water-deficit detection

To develop a predictive tool for early water-deficit identification, the processed VIS–NIR HSI and portable NIR datasets were initially evaluated through exploratory analysis. Principal component analysis was used to identify spectral trends, anomalous observations, and wavelengths contributing to the main sources of sample variability.

Because the spectral response could be simultaneously influenced by genotype, irrigation condition, sampling day, and their interactions, ANOVA–simultaneous component analysis was applied to partition the spectral variability according to the experimental design. ASCA was used to estimate the relative contribution of the experimental factors and to determine whether the predictive problem should be addressed using direct or hierarchical classification strategies. The factor structure evaluated through ASCA was subsequently considered when defining the sequence of the supervised models.

Supervised pattern-recognition methods with different mathematical foundations were evaluated, including soft independent modelling of class analogy (SIMCA), k-nearest neighbours (k-NN), partial least squares discriminant analysis (PLS-DA), support vector machines (SVM), random forest (RF), and extreme gradient boosting (XGBoost). SIMCA was included as a class-modelling approach, whereas k-NN, PLS-DA, SVM, RF, and XGBoost were evaluated as discriminant classification methods. This methodological diversity allowed linear and nonlinear algorithms, local and global models, and class-modelling and discriminant approaches to be compared under a common validation framework.

Two classification structures were evaluated. The first comprised direct binary and multiclass models designed to discriminate control from water-deficit plants and to classify stress progression. The second comprised hierarchical models in which the prediction problem was divided into sequential classification stages according to the experimental sources of variability. For the VIS–NIR HSI dataset, the hierarchical workflow initially considered genetic variability, followed by classification according to water status and stress progression. For the portable NIR dataset, the hierarchical workflow prioritized the discrimination between control and water-deficit plants, followed by classification of the progressive stress stages. These structures describe the sequence of the modelling strategy; their comparative performance was evaluated in the corresponding results chapter.

Calibration, cross-validation, and independent validation sets were generated at the level of the biological unit. Spectra or pixels obtained from the same plant were not distributed simultaneously between calibration and validation sets, because this would introduce information leakage and artificially inflate predictive performance.

Model performance was assessed using confusion matrices and classification figures of merit, including accuracy, sensitivity, specificity, F1-score, and classification error. The optimal model complexity and model parameters were selected using the calibration and cross-validation datasets, whereas final predictive performance was assessed using observations not employed during model construction.

Early detection was evaluated specifically at the first water-deficit sampling point, corresponding to four days after irrigation withdrawal. Overall classification accuracy was not considered

sufficient evidence of early detection unless the model also correctly classified plants at this initial stage of stress development.

The final predictive workflow was selected by comparing the performance of all evaluated methods using calibration, cross-validation, and independent-validation results. Model selection considered not only classification accuracy, but also sensitivity, specificity, F1-score, classification error, stability, interpretability, and practical applicability.

3.4. Analytical strategy to address specific objective 4: evaluation of plant recovery after rewatering

To evaluate the progression of plant recovery after the water-deficit period, irrigation was restored after 12 days of water withholding. Plants were subsequently evaluated after 6 and 13 days of recovery using the same spectral acquisition protocols applied during the stress period. Portable NIR, VIS–NIR HSI, and complementary physiological measurements were therefore used to construct continuous trajectories from the initial control condition through stress development and subsequent recovery.

Recovery was evaluated by comparing previously stressed plants with continuously irrigated controls at equivalent sampling points. Changes in spectral profiles, vegetation indices, water potential, gas exchange, chlorophyll-fluorescence parameters, and growth-related variables were examined to determine whether each genotype returned toward its initial or control-associated condition.

Exploratory score trajectories were used to visualize the movement of stressed samples toward or away from the control spectral space after rewatering. ASCA or repeated-measures statistical approaches were used to separate the effects of genotype, experimental phase, sampling time, and irrigation history. Supervised models were additionally evaluated to determine whether recovered plants continued to exhibit a residual spectral signature distinguishable from continuously irrigated controls.

Recovery was not defined exclusively as the disappearance of spectral classification as stressed. Instead, it was considered a multidimensional process involving restoration of plant water status,

photosynthetic function, and spectral characteristics. A plant could therefore recover its water-related NIR response while retaining pigment, structural, or physiological alterations detectable in VIS–NIR HSI or complementary measurements.

Recovery performance was compared among genotypes using direction-adjusted changes relative to the maximum-stress and corresponding control conditions. This approach allowed recovery rate and recovery completeness to be compared among variables with different units and response directions.

3.5. Analytical strategy to address specific objective 5: selection of superior plant material under water-deficit stress

To address specific objective 5, genotype performance was comparatively evaluated using the results obtained during water-deficit development and after rewatering. The comparison was based primarily on physiological and whole-plant responses, because these measurements were available across all genotypes and directly described functional impairment during stress and subsequent recovery.

Four complementary aspects of genotype performance were considered: functional maintenance during water deficit, recovery of plant water status, recovery of photosynthetic function, and recovery of overall plant condition. Functional maintenance was examined from the behaviour of water potential, stomatal conductance, net CO_2 assimilation, electron transport rate, and photosystem II performance during water withholding. Recovery was evaluated by comparing previously stressed plants with their corresponding continuously irrigated controls at equivalent sampling times after irrigation was restored.

Water-status recovery was assessed from the restoration of plant water potential. Recovery of photosynthetic function was evaluated jointly from gas-exchange and chlorophyll-fluorescence variables, particularly net CO_2 assimilation, stomatal conductance, electron transport rate, and the effective quantum yield of photosystem II. Recovery of overall plant condition was examined from changes in whole-plant fresh mass and the general physiological condition of the plants, considering that increased fresh mass after rewatering could reflect tissue rehydration without complete functional restoration.

Based on the observed trajectories, each response dimension was qualitatively described as favourable, partial or intermediate, or limited. The resulting comparison was used to identify genotypes showing the most consistent maintenance or restoration of physiological function under the evaluated experimental conditions.

The spectral analyses developed in the preceding objectives provided complementary information on the detectability of water-deficit responses and on the influence of genotype, treatment, and sampling time on plant spectral behaviour. However, spectral model outputs were not used as independent criteria for genotype selection because the classification models were developed to identify water-deficit condition and progression rather than to predict superior genotype performance.

The expression patterns of DHN1, LEA4, and TRDX were also considered as complementary biological evidence for the genotypes included in the molecular analysis. Because molecular information was not equally available for all genotypes, it was interpreted separately and used to support the discussion of contrasting response mechanisms rather than the comparative table itself.

Overall, plant material with favourable performance was identified from the consistency of physiological maintenance during water deficit and the restoration of water status, photosynthetic function, and whole-plant condition after rewatering. This approach allowed genotype performance to be compared as a multidimensional biological response while retaining the spectral and molecular results as complementary evidence generated by the analytical framework.

Chapter 4
Detection of water-deficit stress in *Eucalyptus* spp. through VIS-NIR hyperspectral imaging and chemometric methods

This chapter contributes primarily to Specific Objective 3 and provides partial contributions to Specific Objectives 1 and 2. The first experimental assay was used to establish and refine the VIS–NIR HSI acquisition and analytical workflow for monitoring water-deficit responses in *Eucalyptus* spp. (Specific Objective 1), to evaluate hyperspectral information in comparison with conventional vegetation indices and complementary plant measurements (Specific Objective 2), and to develop and validate supervised classification models for the detection and discrimination of progressive water-deficit conditions using both mean spectra and pixel-level information (Specific Objective 3).

This section presents and discusses the results that led to the publication of the article *"Detection of water-deficit stress in Eucalyptus spp. through VIS-NIR hyperspectral imaging and chemometric methods",* published in Spectrochimica Acta Part A: Molecular and Biomolecular Spectroscopy 344 (2026) 126675. https://doi.org/10.1016/j.saa.2025.126675

These results were presented at the following conferences:

"Detection of water deficit stress in *Eucalyptus* spp. through VIS-NIR hyperspectral imaging technologies and multivariate analysis." XIX Chemometrics in Analytical Chemistry (CAC 2024), 9–12 September 2024, Santa Fe, Argentina. Poster presentation.

"Early detection of water deficit stress in *Eucalyptus* spp. through VIS-NIR hyperspectral imaging technologies and multivariate analysis." Ninth International Conference in Spectral Imaging (IASIM 2024), 6–10 July 2024, Bilbao, Spain. Oral presentation.

"Detección temprana de estrés hídrico en *Eucalyptus* spp. a través de tecnologías de imágenes hiperespectrales VIS-NIR y análisis multivariado." XXXIV Jornadas Chilenas de Química, 9–12 January 2024, Puerto Varas, Chile. Poster presentation.

Detection of water deficit stress in *Eucalyptus spp.* through VIS-NIR hyperspectral imaging and chemometric methods

Pamela Sanhueza-Novoa[1], Marta Fernández[2], Carolina Hernández-Fuentes[3], Sofía Valenzuela[2], Muhammad Qasim Hayat[4], Ricardo Ramírez H.[1] and Rosario del P. Castillo[1*]

[1] Laboratory of Biospectroscopy and Chemometrics, Biotechnology Center & Faculty of Pharmacy, University of Concepción, Chile.

[2] Laboratory of Forest Genomics, Biotechnology Center & Faculty of Forestry Sciences, University of Concepción, Chile.

[3] Bioforest S.A., km 15 road to Coronel, Chile.

[4] Medicinal Plants Research Laboratory (MPRL), Department of Agricultural Sciences and Technology, Atta-11 Ur-Rahman School of Applied Biosciences (ASAB), National University of Sciences and Technology, 12 (NUST), H-12, Islamabad 44000, Pakistan.

*Corresponding author: rosariocastillo@udec.cl

4.1. Abstract

Water deficit stress (WDS) can negatively affect the development, productivity and quality of *Eucalyptus* spp. To minimize this impact, the development of high throughput techniques for early and accurate WDS detection is necessary. This study focuses in the use of visible-near infrared hyperspectral imaging (VIS-NIR HSI) and chemometric methods to detect water deficit spectral patterns of these species and to develop predictive models for early detection of water deficit level in juvenile plants. The research included the analysis of four *Eucalyptus* genotypes, two *Eucalyptus globulus* and two *Eucalyptus* GloNi (hybrid of *E. nitens* and *E. globulus*). Forty ramets of each genotype were submitted to WDS conditions associated with different stress levels and compared with control samples using conventional physical characterization and common vegetative indices of plants, besides VIS-NIR HSI. The HSI data were analyzed using principal component analysis (PCA) and supervised pattern recognition methods to classify the samples by WDS level using as validation set the mean spectra of images (bulk prediction) and all the pixels of whole plant (single pixel prediction). The results of PCA showed a differentiated response on the different WDS conditions, especially at day 10 of water deficit. Conventional vegetation indices, such as NDVI, PRI and MCARI, did not detect indications of an early WDS response, while pattern recognition methods including partial least squares (PLS-DA), discriminant support vector machine (SVM-DA) and k-nearest neighbor (KNN) showed a remarkable predictive ability for WDS level with a prediction error (Err) of 2% in external validation sets. Supervised models were applied also to reconstruct the stress level in all the pixels of whole plants. The superior effectiveness of the SVM-DA and KNN models to predict stress level in images of *Eucalyptus spp.* provided valuable information on spatial distribution of stress in the plant.

Keywords: Water deficit stress, Hyperspectral imaging, *Eucalyptus* spp., phenotyping, vegetation indices.

4.2. Introduction

Eucalypts spp. are a widely cultivated species in the world due to their rapid growth, resistance and and industrial applications such as pulp and paper production, wood production, essential oils and biofuels (Abdelaali et al., 2023; Ahmad et al., 2023; Brockerhoff et al., 2013; Guigou et al., 2023). However, water scarcity shortage can negatively affect their development, productivity and quality (Saddiq et al., 1934; Zahra et al., 2023b). Therefore, it is crucial to understand the effects of water deficit stress (WDS) on these species and find ways to mitigate its impacts to ensure their sustainability and optimize their performance. When a plant experiences WDS, a series of physiological and morphological responses are triggered to try to survive under conditions of water shortage (Salazar et al., 2015). Some of the most common behaviors that plants experiment under WDS include the stomata closure that is responsible for regulating gas exchange and water loss through transpiration (Warren et al., 2011b). Under drought conditions, plants tend to close stomata to reduce transpiration and conserve water inside. In addition, in response to WDS, plants may decrease their growth rate, both in height and in the development of new leaves and branches (Aranjuelo et al., 2011), which allows them to conserve energy and resources to survive in adverse conditions. When the plant does not receive enough water, its tissues can lose turgor, resulting in wilting; this is a common symptom of WDS and can be reversible if the water supply to the plant is restored in time (Correia et al., 2014b). Physiological information plays an essential role in understanding how water affects the development and performance of these species (Ejaz et al., 2023).

WDS induces significant molecular changes in plants, triggering a cascade of transcriptional, translational, and metabolic responses aimed at adapting to water-limited conditions. At the molecular level, the expression of genes involved in the synthesis of osmoprotectants, such as proline, glycine betaine, and sugars, is upregulated to maintain cellular osmotic balance and protect macromolecules from damage (Singh et al., 2017). Reactive oxygen species (ROS) accumulation is another hallmark of drought stress, which can cause oxidative damage to lipids, proteins, and nucleic acids. To mitigate this, plants enhance the activity of antioxidant enzymes, including superoxide dismutase (SOD), catalase (CAT), and ascorbate peroxidase (APX), as part of their defense mechanisms (Deribe, 2025). Furthermore, the regulation of abscisic acid (ABA) signaling pathways plays a central role in orchestrating drought tolerance by modulating stomatal

closure and inducing stress-responsive gene expression, including those encoding late embryogenesis abundant (LEA) proteins and dehydrins (Lee & Luan, 2012; Shi et al., 2022). These molecular adjustments are critical for improving drought resilience and highlight potential targets for genetic or biotechnological interventions in *Eucalyptus spp*. and other crop species.

Biomass is a direct indicator of yield and overall plant health (Umami et al., 2021). During periods of WDS, it is common for plants to experience a decrease in biomass due to reduced water and nutrient availability. Thus, physiological parameters provide an overview of how plants respond to various types of stress; however, they mostly require advanced symptoms for the detection of stress-related changes, which may irreversibly affect the plant and may not be suitable for early detection of stress. Another limitation is the low specificity, because physiological changes may not be due specifically to the WDS response, but also to other types of abiotic stresses (Ha et al., 2012; Korek & Marzec, 2023; Virtuoso et al., 2022). To address these limitations, multispectral analysis, including the calculation of vegetative indices, has emerged as a widely used tool for assessing plant health and response to WDS (McFeeters, 1996; Penuelas et al., 1997; Torrion et al., 2014). Photosynthetic pigments, mainly chlorophyll, carotenoids and anthocyanins (Ballester et al., 2018), are crucial for plant survival because they play a fundamental role in photosynthesis, photoprotection and plant-environment interactions (Gamon et al., 1992). Some of the most common vegetative indices used in stress assessment include the normalized difference vegetation index (NDVI), modified chlorophyll absorption reflectance index (MCARI), and photochemical reflectance index (PRI). NDVI, for example, is an index that uses the difference between near infrared (NIR) and red light to determine vegetation health. This index is sensitive to the chlorophyll content in plants (Hussain et al., 2019), which is responsible for photosynthesis, and is often used as an indicator of plant health. NDVI has been used extensively in studies related to vegetation health, crop yields and drought monitoring (Benhizia et al., 2024; Moussa Kourouma et al., 2021). The PRI is sensitive to changes in the xanthophyll cycle pigments (Kohzuma et al., 2021), which are involved in the regulation of light energy absorption in plants. Changes in the PRI can indicate changes in the photosynthetic activity of plants under stress conditions. MCARI is an index designed to maximize sensitivity to leaf chlorophyll content by minimizing the influence of leaf area index (LAI) and soil background. These indices provide an effective tool for identifying stressed areas in *Eucalyptus* plantations; however, they may not be accurate for detecting stress caused by water

deficit (WD) because they are based on spectral bands that include chemical compounds that can also be influenced by other types of abiotic stresses (Zhu, 2016).

However, recent advances in remote sensing techniques, particularly visible-near infrared hyperspectral imaging (VIS-NIR HSI), have opened new possibilities for improving early detection of WDS. Unlike traditional vegetation indices, hyperspectral imaging captures detailed spectral information across a continuous range of wavelengths, allowing the identification of subtle changes in plant physiology before visible symptoms appear (Peñuelas Josep & Filella Iolanda, 1998). HSI has been successfully applied in various agricultural and forestry studies to detect abiotic stress, including water stress, with higher accuracy than conventional indices (Ejaz et al., 2023; Kim et al., 2011a).

Although some studies have used HSI to assess plant stress responses, there is limited research on its application to detect early WDS in *Eucalyptus* spp. The ability of VIS-NIR HSI to detect spectral variations associated with water stress in a non-invasive manner could offer a more effective tool for stress monitoring in forestry plantations. Previous studies have demonstrated that hyperspectral data combined with multivariate statistical methods, such as Principal Component Analysis (PCA) and machine learning models, can successfully classify different stress levels in plants (Mondal et al., 2019; Okyere et al., 2024; Stellacci et al., 2012; Xie et al., 2021). Nevertheless, its potential for early detection in *Eucalyptus* spp. remains unexplored.

To address this gap, this study aims to apply VIS-NIR HSI to identify spectral patterns associated with WDS in four *Eucalyptus* genotypes, two *Eucalyptus globulus* and two *Eucalyptus* gloni hybrids. The spectral data will be compared with physiological measurements and conventional vegetation indices (NDVI, PRI, MCARI) to evaluate the capability of HSI for early and accurate stress detection. In addition, supervised classification models such as Partial Least Squares Discriminant Analysis (PLS-DA), Support Vector Machine Discriminant Analysis (SVM-DA), and k-Nearest Neighbors (KNN) will be used to develop predictive models that classify plant samples according to their stress levels. This approach will provide valuable insights into the spatial distribution of water stress in *Eucalyptus* spp. and its potential for improving precision forestry management.

4.3. Methodology

4.3.1. Plant material and WD assay

The experiment was conducted with 160 six-month-old, rooted plants donated by BIOFOREST S.A. Arauco (Chile). Two genotypes correspond to *Eucalyptus globulus* species, G1 and G2, and two *Eucalyptus* GloNi hybrid (*E. nitens* x *E. globulus*), G3 and G4. Each genotype was represented by forty ramets that were randomly placed in an aislapool box. Genotypes underwent controlled conditions in a growth chamber, following the parameters evaluated by Fernández et al., (2012), corresponding to a summer photoperiod of 14 hours of light (>150 umol photons $m^{-2}s^{-1}$) and 10 hours of darkness, day temperature of 22±1°C, night temperature of 16±1 °C and humidity of 60-70%. The plants were subjected to a 3-day sanitization period, then a 10-day acclimatization period in which water supply was constantly maintained. Subsequently the samples were divided into two groups: 36 control plants (C), with constant irrigation, and a group, of 36 plants, that underwent 10 days of WD (no water supply), as shown in Figure 4.1. Days 16, 20 and 23 of the experimental periods, corresponding to day 3 (D3), day 7 (D7) and day 10 (D10) of WD and will be referred to as such throughout the text, were associated with mild, moderate and severe stress levels, respectively. On each of these days, physiological analyses, multispectral studies and image acquisition were carried out, evaluating three ramets for each genotype at each sampling point.

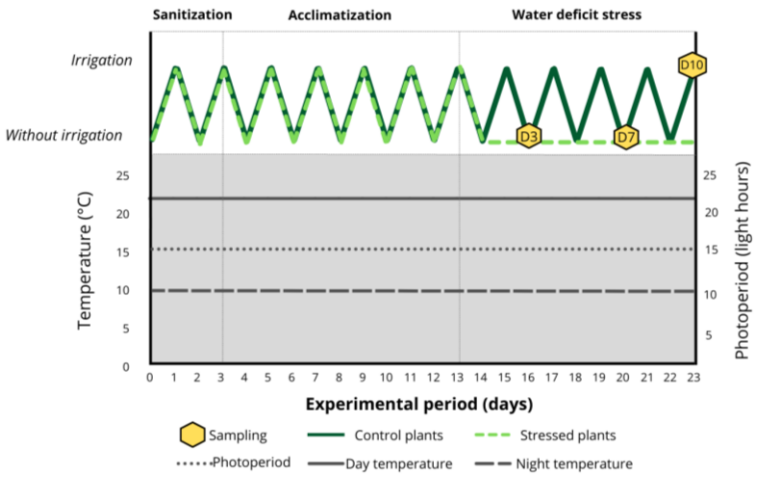

Figure 4.1 Sanitization, acclimatization, irrigation, non-irrigation and sampling stages of control and stressed plants throughout the experimental period.

4.3.2. Physiological response under WD treatments

To identify differences in fresh biomass (g) and height (cm) of genotypes G1, G2, G3 and G4 exposed to WD and their control samples, a methodological monitoring was implemented that included measurements on days D3, D7 and D10, allowing the analysis of their growth and development during this period. A two-way analysis of variance (ANOVA) was performed, establishing a significance level of $p < 0.05$, to evaluate the statistical significance of the differences between genotypes, treatment conditions and the interaction between both factors. Subsequently, post hoc tests were applied to identify which specific groups showed significant differences in biomass and height. In total, 72 plants were evaluated throughout the experiment according to the Table S4.1 (supplementary material). This statistical analysis not only allows us to identify significant differences between WD and C plants, but also to detect whether certain genotypes show differences in biomass under WDS.

$$\mathrm{NDVI} = (\mathrm{R800} - \mathrm{R680})/(\mathrm{R800} + \mathrm{R680}) \quad (1)$$

$$\mathrm{PRI} = (\mathrm{R530} - \mathrm{R570})/(\mathrm{R530} + \mathrm{R570}) \quad (2)$$

$$\mathrm{MCARI} = [(\mathrm{R700} - \mathrm{R670}) - 0{,}2(\mathrm{R700} - \mathrm{R550})](\mathrm{R700}/\mathrm{R670}) \quad (3)$$

To analyze variations in vegetation index values between genotypes and between C and WD plants, a two-way ANOVA analysis was used with a significance level of $p < 0.05$. This analysis allows us to evaluate the statistical significance of both the individual effects of treatments and genotypes and their interaction on each index, which is fundamental to determine if these indices can reliably identify water stress in *Eucalyptus* spp. and how it differentially affects according to genotype. Subsequently, post hoc tests were performed to identify the specific groups with significant differences in each index.

4.3.3. HIS data acquisition and array

A Pika-L Resonon hyperspectral camera operating in a spectral range of 385 – 1010 nm, a spectral interval of 2.1 nm, spectral resolution of 3.3 nm and 900 spatial pixels per line, was used in a benchtop system to acquire reflectance spectra using Spectronon PRO software (Resonon Inc). Independent images of the whole plant, the apex, the leaves of the fourth whorl and part of

the stem were captured, as it is shown in the Figure 2A, obtaining a total of 288 hyperspectral images, considering four genotypes under study (G1, G2, G3 and G4), three ramets per sample, three sampling days (D3, D7 and D10), four zones of plants (whole plant, apex, leaves and stems) and two conditions (control and stressed). K-means algorithm was used to remove the background of the images using the Hyper-Tools v.3.0 graphical user interface (GUI) developed by Mobaraki & Amigo (2018). Once the zones of interest were defined, the mean spectrum of each image was obtained and used to construct a data matrix (M1) that provided representative information on the levels of mild, moderate and severe stress associated with D3, D7 and D10, respectively.

4.3.4. Chemometric analysis: PCA and supervised analysis

Figure 4.2.B shows the sequence of chemometric analysis followed in this study. The total matrix (M1), of dimensions 288 × 300, was transformed from the reflectance to pseudo absorbance according to pA = -log10(R). Several preprocessing techniques were compared for both exploratory analysis and supervised model development, including standard normal variation (SNV), multiplicative dispersion correction (MSC), first derivative, second derivative and mean-centered. All these corrections were applied with the MATLAB 2021a using the PLS_Toolbox 8.9.2 version from Eigenvector Research Inc. The mean spectra of whole plants were extracted from matrix M1 for PCA, resulting in a second matrix (M2) of dimensions 72 × 300, corresponding to 36 controls and 36 water deficit plants (4 genotypes x 3 days sampling x 3 replicates). Subsequently, supervised pattern recognition methods such as SIMCA, PLS-DA, SVM-DA and KNN were applied. The complexity of each model was determined as follows: for PLS-DA, the optimal number of latent variables (LVs) was selected via venetian blinds cross-validation on the calibration set, minimizing the classification error without overfitting; for KNN, the number of neighbors (K) was optimized using leave-one-out cross-validation within the calibration set, selecting the K with the lowest error rate; and for For the SVM-DA model, a radial basis function (RBF) kernel with optimized hyperparameters was used.

The model performance was evaluated using 10-fold venetian blinds cross-validation with a blind thickness of 1. Although the SIMCA method was included and initially explored, its performance metrics, especially for classes D3 and D7, were notably lower compared to PLS-DA, SVM-DA

and KNN. As a result, its results were not presented in the main results section to maintain clarity and focus on the most effective models. However, full performance metrics for all models and preprocessing combinations, including SIMCA, are provided in Table S4.5 of the supplementary material.

For which the mean spectra of the whole plant, apex, leaves and stem of the plants subjected to water deficit were taken, generating a third matrix (M3) of dimensions 144 x 300. This M3 matrix was divided into a 70:30 proportion, with 96 spectra destined to the calibration set and 48 to the validation set (Fig. 2B). The obtained classification models were evaluated using their confusion matrix, sensitivity *(Sn)*, specificity *(Sp),* class errors *(Er)* and accuracy *(Ac),* according to equations 4, 5, 6 and 7 respectively, described by Ballabio & Consonni, (2013) and Zade & Abdollahi, (2024).

$$Sn = \frac{\mathrm{TP}}{\mathrm{TP+FN}} \tag{4}$$

$$Sp = \frac{\mathrm{TN}}{\mathrm{FP+TN}} \tag{5}$$

$$Er = 1 - \frac{(\mathrm{Sn+Sp})}{2} \tag{6}$$

$$Ac = \frac{(\mathrm{TP+TN})}{(\mathrm{TP+TN+FP+FN})} \tag{7}$$

Where true positive (TP) and true negative (TN) represent samples correctly assigned as belonging or not belonging, to a specific class, respectively. False positive (FP) and false negative (FN) represent samples erroneously assigned as belonging or not belonging, respectively, to a specific class (Munera et al., 2018). Two types of predictions were carried out for external validation. The first one was applied directly on the mean spectra of the different plant zones (bulk prediction), while the second used all the pixels of whole plant images (pixel-by-pixel prediction), coloring each pixel according to its predicted class. This meant that the stress level of each pixel in the image was assessed individually, allowing a detailed visualization of how the water deficit affects different parts of the plant.

To facilitate the processing and reconstruction of the images, which have an average size of 1140 x 860 pixels, spatial binning was performed. This process consists of averaging ten pixels in the *x* and *y* directions, thus reducing the data dimension to 114 × 86 pixels on average. This simplifies the analysis and maintains a sufficient level of detail without loss of spectral information.

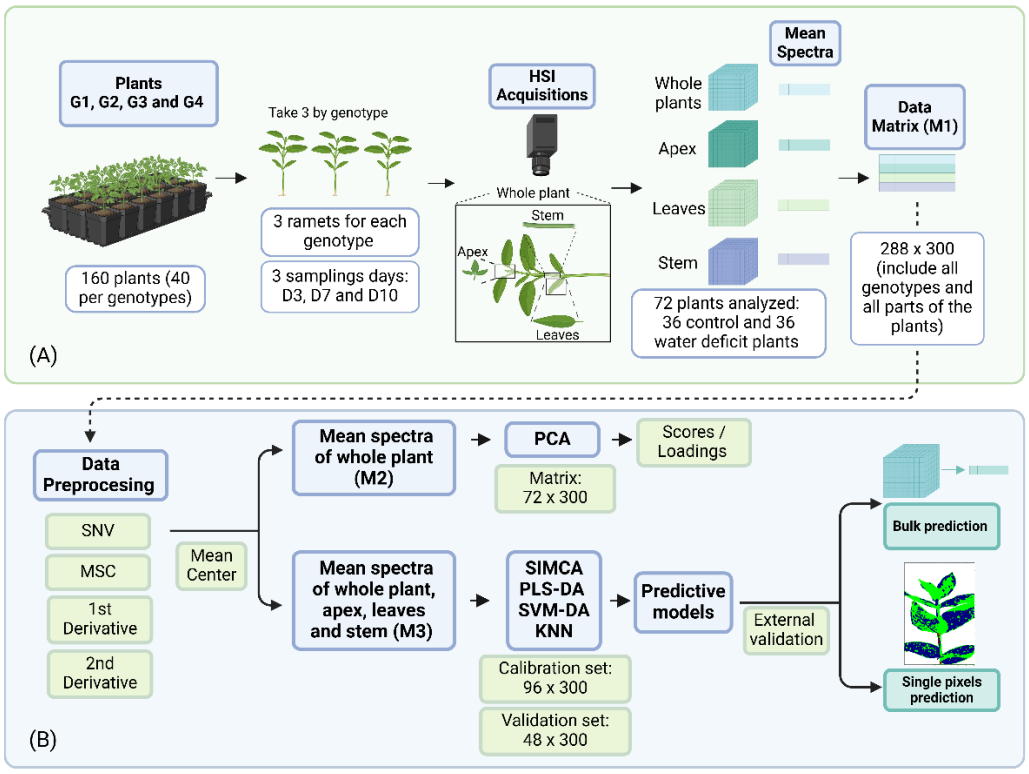

Figure 4.2 Samples and HSI data acquisition (A) and chemometric analysis of HSI data (B)

4.4. Results and discussion

4.4.1. Physiological response under WD treatments

Variations in physiological characteristics were detected by comparing mean biomasses and mean heights by ANOVA. Results are shown in Table S4.2 and Figure S4.1 of supplementary material. These comparisons indicated that on the three days, D3, D7 and D10, there were significant ($p<0.05$) discrepancies in biomass between control and WD plants. Height analysis indicated that no significant differences ($p>0.05$) were observed in G1, G2 and G3 genotypes between control and WD plants on D3, D7 and D10. However, differences ($p<0.05$) were found

between plant heights of genotype G4 plants in D3 (Figure S4.1). This discrepancy between biomass and height measurements could be attributed to genotype-specific responses to WDS (Amrutha et al., 2019). It is plausible that some plant varieties reduce their biomass as an immediate response to stress, while others maintain their height, suggesting the existence of compensatory mechanisms that protect vertical growth even under adverse conditions (Peng et al., 2020). These results emphasize the importance of considering both biomass and height as complementary indicators to assess the physiological response of plants to WDS, underscoring the need for further research to better understand the mechanisms underlying these responses.

4.4.2. Vegetation indices

The results obtained from the spectral information for NDVI, PRI and MCARI are shown in Table 4.1. The vegetation indices show that NDVI presented a decrease under WD conditions compared to C, especially on D10 in G3 and G4, indicating a reduction in photosynthetic activity (Benhizia et al., 2024; Hussain et al., 2019). PRI reflected lower photochemical efficiency in plants subjected to WD, with more marked differences in G2 and G3 at D10, suggesting alterations in xanthophyll pigment cycling (Kohzuma et al., 2021). MCARI showed the greatest sensitivity to advanced water stress, with significant increases in WD on D10, particularly in G3 and G4, evidencing alterations in chlorophyll uptake (Ballester et al., 2018). However, at early stages of stress (D3 and D7), differences between C and WD were less evident in these indices.

To statistically validate these differences, an ANOVA and a Tukey test were performed. The ANOVA results indicated that NDVI showed no significant differences ($p>0.05$) between the C and WD groups in all genotypes (Table S4.3). However, Tukey's post hoc test revealed that on D10 significant differences ($p<0.05$) emerged between C and WD specifically in genotype G3 (Table S4.4, Figure S4.2). For PRI, ANOVA revealed significant differences ($p<0.05$) between C and WD in G1 and G4 (Table S4.3). Tukey's test further identified that these differences in G4 were specifically observed in D10 (Table S4, Figure S4.2). As for MCARI, ANOVA detected significant differences ($p<0.05$) in G1, G2 and G3 (Table S4.3). However, Tukey's test indicated that significant differences in C vs. WD comparisons were found mainly in G3 at D10 (Table S4.4, Figure S4.2).

These results suggest that while vegetation indices such as NDVI, PRI, and MCARI can reflect changes associated with WDS, their sensitivity varies across genotypes and stress conditions. The inconsistencies between ANOVA and Tukey's test emphasize the importance of considering both global and pairwise statistical approaches, as significant differences may not always be detected at the overall level but can emerge in specific time points or genotypes. Furthermore, the disparities observed across the indices indicate that a single vegetation index may not be a fully reliable indicator of WDS status, as each responds differently to stress progression.

Table 4.1 NDVI, PRI and MCARI calculated on genotypes G1, G2, G3 and G4 for D3, D7 and D10. Each genotype was measured in triplicate, where C and WD represent the mean of the replicates and their respective standard deviations (SD).

			Sampling days								
Vegetative Indices	***Genotypes***	***Condition***	**D3**			**D7**			**D10**		
NDVI	G1	C ± *DS*	0,244	±	*0,039*	0,250	±	*0,004*	0,259	±	*0,020*
		WD ± *DS*	0,230	±	*0,028*	0,259	±	*0,013*	0,234	±	*0,009*
	G2	C ± *DS*	0,262	±	*0,021*	0,287	±	*0,018*	0,297	±	*0,026*
		WD ± *DS*	0,299	±	*0,030*	0,278	±	*0,044*	0,292	±	*0,031*
	G3	C ± *DS*	0,269	±	*0,029*	0,299	±	*0,020*	0,340	±	*0,017*
		WD ± *DS*	0,307	±	*0,010*	0,316	±	*0,009*	0,271	±	*0,021*
	G4	C ± *DS*	0,253	±	*0,029*	0,271	±	*0,016*	0,269	±	*0,029*
		WD ± *DS*	0,237	±	*0,025*	0,317	±	*0,023*	0,260	±	*0,027*
PRI	G1	C ± *DS*	0,053	±	*0,006*	0,058	±	*0,004*	0,063	±	*0,004*
		WD ± *DS*	0,052	±	*0,008*	0,053	±	*0,005*	0,049	±	*0,005*
	G2	C ± *DS*	0,036	±	*0,013*	0,032	±	*0,006*	0,039	±	*0,011*
		WD ± *DS*	0,028	±	*0,010*	0,023	±	*0,009*	0,020	±	*0,020*
	G3	C ± *DS*	0,056	±	*0,003*	0,060	±	*0,005*	0,072	±	*0,001*
		WD ± *DS*	0,042	±	*0,010*	0,049	±	*0,004*	0,042	±	*0,008*
	G4	C ± *DS*	0,051	±	*0,005*	0,057	±	*0,008*	0,044	±	*0,012*
		WD ± *DS*	0,042	±	*0,010*	0,049	±	*0,004*	0,042	±	*0,008*
MCARI	G1	C ± *DS*	0,306	±	*0,039*	0,312	±	*0,070*	0,304	±	*0,035*
		WD ± *DS*	0,352	±	*0,054*	0,325	±	*0,083*	0,439	±	*0,013*
	G2	C ± *DS*	0,267	±	*0,032*	0,289	±	*0,053*	0,259	±	*0,027*
		WD ± *DS*	0,403	±	*0,067*	0,426	±	*0,054*	0,385	±	*0,042*
	G3	C ± *DS*	0,364	±	*0,038*	0,309	±	*0,026*	0,285	±	*0,028*
		WD ± *DS*	0,420	±	*0,051*	0,439	±	*0,061*	0,560	±	*0,047*
	G4	C ± *DS*	0,379	±	*0,044*	0,347	±	*0,029*	0,321	±	*0,099*
		WD ± *DS*	0,420	±	*0,051*	0,439	±	*0,061*	0,560	±	*0,047*

4.4.3. Spectral information

Whole plant spectral signatures of stressed and unstressed samples are shown in Figures 4.3 (A-C). The spectra show high reflectance above 700 nm in the near infrared region which may be

related to biochemical changes in plants in response to drought stress (Kim et al., 2011a; Peñuelas Josep & Filella Iolanda, 1998). Besides, a band in the green region around 550 nm is observed, which is consistent with previous studies that have shown maxima reflectance in this region due to chlorophyll and carotenoid absorption (Datt, 1993) (Fig 4.3A). A decreasing in absorbance in the red region is observed at 675 nm for most of samples at D7 and D10 conditions (Fig 4.3.B-C), which is consistent with the reduction of chlorophyll observed in stressed plants. In addition, a reduction in reflectance near 385 nm is observed in the D10 stress condition (Fig. 4.3.A), which may be indicative of a decrease in chlorophyll content or the accumulation of secondary metabolites such as flavonoids, as suggested in previous studies (Cvetković et al., 2011). This spectral feature is supported by corresponding changes in the absorbance spectra (Fig. 4.3B). Although a prominent signal is also observed around 385 nm in the second derivative spectra (Fig. 4.3C), it is known that the use of derivatives can introduce spectral distortions or shifts (Oliveri et al., 2019). Therefore, this region was interpreted by jointly considering the raw reflectance and absorbance spectra, avoiding attribution based solely on the derivative profile.

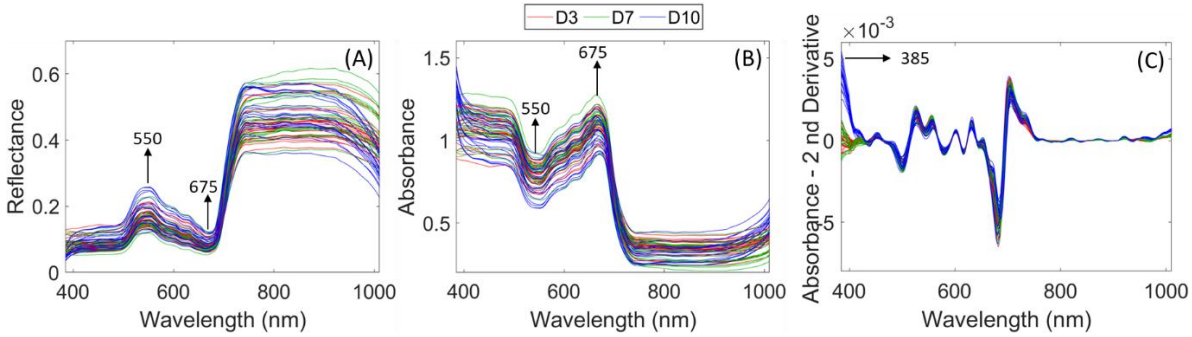

Figure 4.3 Seventy-two mean spectra corresponding to M2 matrix, where (A) Mean spectra in reflectance, (B) Mean spectra in pseudo absorbance and (C) Mean spectra in pseudo absorbance with second derivative and integration window of 15 points.

4.4.4. Exploratory analysis: PCA

PCA was performed on the M2 matrix to identify possible differences between the mean spectra of C and WD plants on D3, D7 and D10 of whole plants. Several pretreatments were applied, but the best result was obtained with second derivative, smoothed with a 15-point window and mean centered pretreatment. Fig. 4.4.A shows the distribution of scores according to sampling days (D3, D7 and D10), where a clear clustering of the samples corresponding to D10 (green circles

and triangles) can be seen. This grouping includes both C and WD samples, suggesting the presence of an additional factor, besides the WD, that is influencing the response of the plants, causing the C to experiment changes.

The D10 group is separated from the D3 and D7 samples by the first principal component (PC 1), which has a high influence of the band at 385 nm according to the loading plot of Fig. 4.4.B, possibly associated with flavonoids (Taniguchi et al., 2023). On the other hand, PC 2 reveals a separation between control and WD samples in D10, which according to the loadings plot in Fig. 4.4.B is principally attributed to the bands at 676 and 695 nm, which could be associated with changes in chlorophyll absorption (Gitelson et al., 2003).

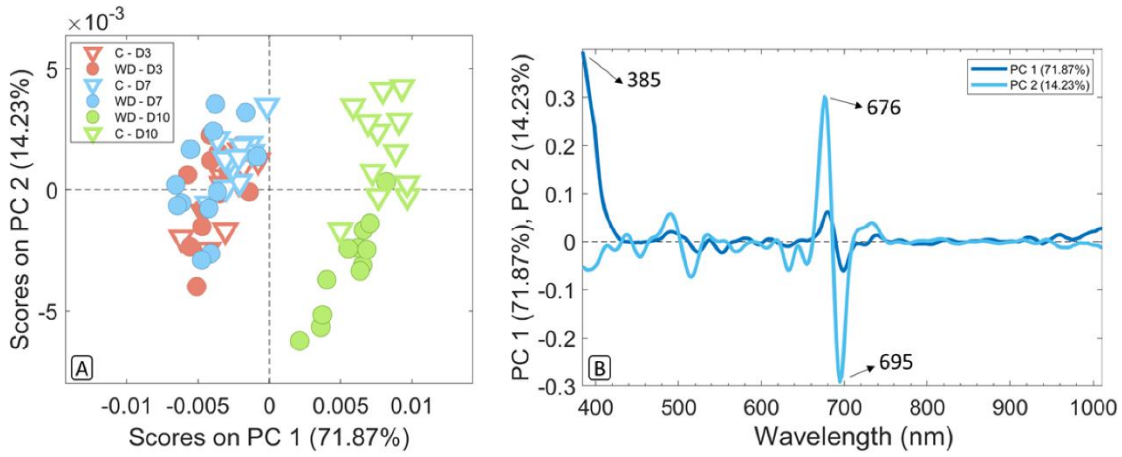

Figure 4.4 Plots of scores (A) and loadings (B) for all samples (G1, G2, G3 and G4) including c: Control samples and WD: water deficit samples on days D3, D7 and D10.

Results of PCA performed for each genotype using matrices of dimension 12 × 300 are shown in Figure 4.5. In these analyses, the same separation of samples corresponding to D10 that had been previously identified in the pooled PCA of all genotypes is observed. However, in genotypes G1 and G3, a better separation between the WD samples on D3 and D7 is observed, according to the contribution of their PC4 and PC3, respectively. Although these components explain a lower percentage of total variance, they were selected because they provide a clearer discrimination between early stress levels that is not evident in PC1 or PC2. To support this observation, Figure S4 in the supplementary material shows the score and loading plots of PC1 versus PC2 for genotypes G1 and G3, where it can be seen that these two components do not

allow for a satisfactory separation of the D3 and D7 samples, neither between them nor with respect to their corresponding daily controls. Besides, G4 shows a better separation between control and stressed samples, especially at the D10 condition and even at mild stress (D3). These slight variations in the results indicate that WD impacts the physiological response differently among genotypes (Berenguer et al., 2018; Merchant et al., 2007; Villar et al., 2011), which is a significant finding for high throughput phenotyping of WDS in *Eucalyptus spp.*, detecting differences in the responses of adaptation to water stress. Loadings plots confirm for all the genotypes the importance of the band at 385 nm to differentiate the advanced WD level at D10 from the D3 and D7 conditions, as well as the relevance of the bands at 676–696 nm and 711–735 nm for separation of the control and stressed samples, found in the loadings of second, third or fourth PC in the analysis of genotypes. To evaluate the relevance of the band observed around 385 nm, we performed an additional PCA excluding the spectral region between 385 and 420 nm. However, the separation of samples according to stress condition did not improve compared to the results obtained using the full spectral range. These additional PCA results are presented in the supplementary material as Figure S4.5.

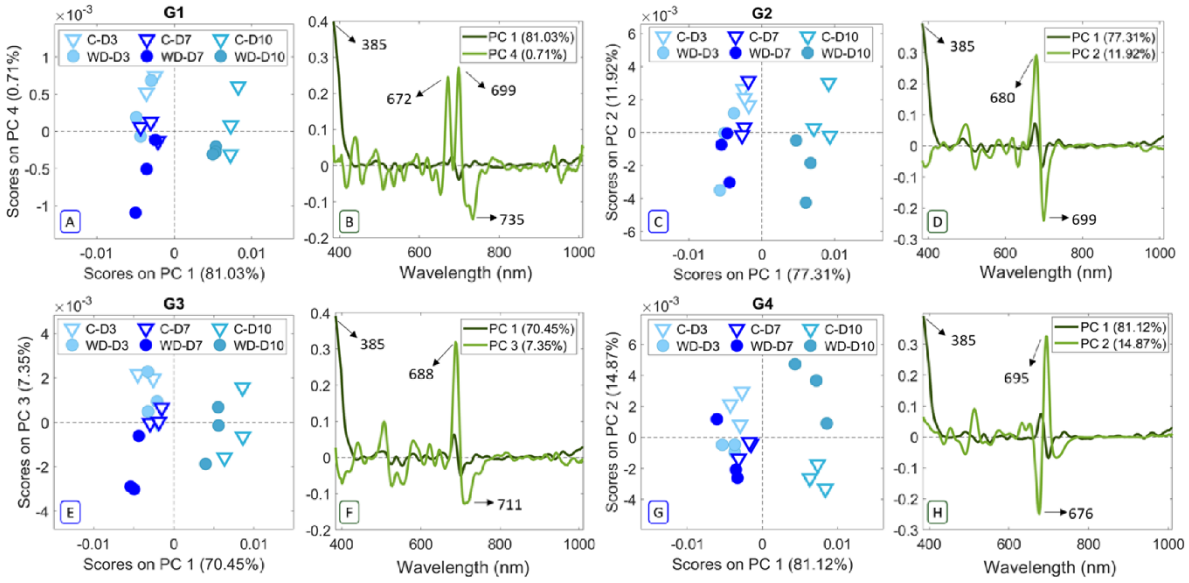

Figure 4.5 Plots of scores and loadings for the PCA, pretreated with the second derivative of absorbance, smoothed with a 15-point window and mean center, that best explain the differentiation according to stress level of Eucalyptus spp. plants: A) G1 scores plot

4.5. Supervised pattern recognition analysis

4.5.1. Prediction by mean spectra (bulk prediction)

The SIMCA, PLS-DA, SVM-DA and KNN models for predicting the WDS level using the mean spectra of the different plant zones were optimized using various preprocessing techniques and their figures of merit for calibration and validation are shown in Table 4.2. According to the results obtained in the figures of merit, PLS-DA and SVM-DA with second derivative and mean-centered preprocessing were chosen as the best models, with Ac equal to 1.00 in calibration and external validation for the "bulk prediction" data set. In addition, KNN with second derivative and mean-centered obtained a prediction Er of only 0.02 in external validation and 0.00 in calibration. It is worth noting that Table S4.5 of the supplementary material also includes the confusion matrix corresponding to the best models, which allows us to visualize in detail their performance by class and to confirm the consistency of the results. In contrast to the analysis of vegetative indices, PLS-DA, SVM-DA and KNN models applied to hyperspectral images seem to be able to better capture the complexity of the plant response to WDS, detecting even early plant stress, before the appearance of visible signs and distinguishing between different stress conditions in plants.

Table 4.2 Performance metrics for SIMCA, PLS-DA, SVM-DA, and KNN models applied to *Eucalyptus* spp.

		Class 1 – D3							Class 2 – D7				Class 3 – D10			
Model	***Preprocessing***	***LVs***	***SVs***	***PCs***	***K***	***Sn***	***Sp***	***Er***	***PCs***	***Sn***	***Sp***	***Er***	***PCs***	***Sn***	***Sp***	***Er***
							Calibration set									
SIMCA	SNV	---	---	3	---	0.94	0.59	0.29	3	0.16	0.98	0.29	3	1.00	0.97	0.02
	SNV-MC	---	---	5	---	0.97	0.59	0.26	4	0.19	1.00	0.29	4	1.00	0.97	0.02
	2nd Deriv.	---	---	3	---	1.00	0.95	0.03	5	0.91	1.00	0.03	4	1.00	1.00	0.00
	2nd Deriv. - MC	---	---	4	---	1.00	1.00	0.00	4	1.00	1.00	0.00	4	1.00	1.00	0.00
	MC	---	---	3	---	0.97	0.59	0.28	4	0.19	0.98	0.28	4	1.00	1.00	0.00
PLS-DA	SNV	5	---	---	---	0.71	0.92	0.14	---	0.85	0.88	0.15	---	1.00	0.98	0.01
	SNV-MC	5	---	---	---	0.78	0.94	0.11	---	0.88	0.89	0.12	---	1.00	0.98	0.01
	2nd Deriv.	5	---	---	---	1.00	1.00	0.00	---	1.00	1.00	0.00	---	1.00	1.00	0.00
	2nd Deriv. - MC	**4**	**---**	**---**	**---**	**1.00**	**1.00**	**0.00**	**---**	**1.00**	**1.00**	**0.00**	**---**	**1.00**	**1.00**	**0.00**
	MC	5	---	---	---	0.75	0.88	0.17	---	0.75	0.88	0.17	---	1.00	1.00	0.00
SVM-DA	SNV	---	43	---	---	1.00	0.98	0.01	---	0.97	1.00	0.01	---	1.00	1.00	0.00
	SNV-MC	---	43	---	---	1.00	0.98	0.01	---	0.97	1.00	0.01	---	1.00	1.00	0.00
	2nd Deriv.	---	35	---	---	1.00	1.00	0.00	---	1.00	1.00	0.00	---	1.00	1.00	0.00
	2nd Deriv. - MC	**---**	**35**	**---**	**---**	**1.00**	**1.00**	**0.00**	**---**	**1.00**	**1.00**	**0.00**	**---**	**1.00**	**1.00**	**0.00**
	MC	---	96	---	---	1.00	1.00	0.00	---	1.00	1.00	0.00	---	1.00	1.00	0.00
KNN	SNV	---	---	---	5	0.69	0.83	0.22	---	0.62	0.84	0.23	---	1.00	0.98	0.01

	SNV-MC	---	---	---	5	0.69	0.83	0.22	---	0.62	0.84	0.23	---	1.00	0.98	0.01
	2nd Deriv.	---	---	---	3	1.00	0.94	0.02	---	0.97	1.00	0.00	---	1.00	1.00	0.02
	2nd Deriv. - MC	---	---	---	3	1.00	1.00	0.00	---	0.97	1.00	0.01	---	1.00	0.98	0.01
	MC	---	---	---	3	0.72	0.66	0.32	---	0.56	0.88	0.23	---	0.62	0.82	0.18
	External validation set															
SIMCA	SNV	---	---	---	---	0.94	0.50	0.35	---	0.12	1.00	0.29	---	0.88	0.97	0.06
	SNV-MC	---	---	---	---	1.00	0.59	0.27	---	0.12	1.00	0.29	---	1.00	0.97	0.02
	2nd Deriv.	---	---	---	---	1.00	0.88	0.08	---	0.75	1.00	0.08	---	1.00	1.00	0.00
	2nd Deriv. - MC	---	---	---	---	1.00	0.94	0.04	---	0.88	1.00	0.04	---	1.00	1.00	0.00
	MC	---	---	---	---	1.00	0.59	0.27	---	0.19	1.00	0.27	---	1.00	1.00	0.00
PLS-DA	SNV	---	---	---	---	0.62	0.78	0.27	---	0.62	0.78	0.27	---	0.88	1.00	0.04
	SNV-MC	---	---	---	---	0.88	0.78	0.19	---	0.62	0.94	0.17	---	0.94	1.00	0.02
	2nd Deriv.	---	---	---	---	0.94	1.00	0.02	---	1.00	1.00	0.00	---	1.00	0.97	0.02
	2nd Deriv. - MC	**---**	**---**	**---**	**---**	**1.00**	**1.00**	**0.00**	**---**	**1.00**	**1.00**	**0.00**	**---**	**1.00**	**1.00**	**0.00**
	MC	---	---	---	---	0.62	0.81	0.25	---	0.62	0.81	0.25	---	1.00	1.00	0.00
SVM-DA	SNV	---	---	---	---	0.88	0.84	0.15	---	0.69	0.94	0.15	---	1.00	1.00	0.00
	SNV-MC	---	---	---	---	0.88	0.94	0.08	---	0.88	0.94	0.08	---	1.00	1.00	0.00
	2nd Deriv.	---	---	---	---	1.00	1.00	0.00	---	1.00	1.00	0.00	---	1.00	1.00	0.00
	2nd Deriv. - MC	**---**	**---**	**---**	**---**	**1.00**	**1.00**	**0.00**	**---**	**1.00**	**1.00**	**0.00**	**---**	**1.00**	**1.00**	**0.00**
	MC	---	---	---	---	0.44	0.84	0.29	---	0.25	0.88	0.33	---	1.00	0.62	0.25
KNN	SNV	---	---	---	---	0.62	0.72	0.31	---	0.44	0.81	0.31	---	1.00	1.00	0.00
	SNV-MC	---	---	---	---	0.62	0.72	0.31	---	0.44	0.81	0.31	---	1.00	1.00	0.00
	2nd Deriv.	---	---	---	---	0.94	1.00	0.02	---	1.00	1.00	0.00	---	1.00	0.97	0.02
	2nd Deriv. - MC	---	---	---	---	0.94	1.00	0.02	---	1.00	1.00	0.00	---	1.00	0.97	0.02
	MC	---	---	---	---	0.62	0.62	0.38	---	0.56	0.81	0.27	---	0.62	0.97	0.15

4.5.2. Single pixel prediction

To approximate the spatial distribution of WDS in plants and to understand how the response varies among species, a pixel-by-pixel image reconstruction was performed using the validation set, which included one representative plant per genotype and sampling day. Since these plants are ramets, they are genetically identical replicates within each genotype, ensuring that the selected individuals are representative of their respective experimental groups. The reconstruction was carried out by applying the three best-performing models, PLS-DA, SVM-DA and KNN, trained using mean spectra from different plant zones, directly to each pixel of the validation images. It is important to note that these models were not specifically optimized for individual pixel classification, but rather projected onto the pixel level to explore spatial patterns of stress response across the whole plant. Figure 4.6 shows the single pixel reconstruction of the original images. In this figure, colors represent the predicted class while real class of samples is explicated in text in each row. SVM-DA and KNN exhibited a strong agreement between predicted and actual stress levels across the whole plant, with some pixels classified in other

levels but maintaining a consistent and interpretable pattern. Table 4.3 shows the percentage of pixels correctly classified by the supervised models. Although the PLS-DA and KNN models achieved high accuracy in predicting unknown samples based on mean spectra, reaching 0.98-1 *Ac*, their per-pixel classification performance was lower. For the PLS-DA model, the percentages of correct classification per pixel were 45 - 48% in D3, 30 - 44% in D7 and 30 - 38% in D10. For KNN, the per-pixel results ranged from 34-49% for D3, 29-56% for D7 and 53-71% for D10. In contrast, the SVM-DA model showed higher per-pixel prediction accuracy, with percentages ranging from 55-70% for D3, 51-90% for D7 and 84-89% for D10, which is consistent with the images of Although these pixel-level classification rates may seem modest, especially when compared to the mean-spectrum performance, they consistently exceed the chance level for three-class classification (33%), and, more importantly, produce spatially coherent and biologically interpretable patterns. Misclassified pixels tend to be adjacent to the correct class and follow morpho-anatomical gradients, suggesting that the models capture subtle local variations in stress progression. This capability is particularly valuable for identifying heterogeneous stress responses within a single plant, thus providing detailed insights into the dynamics of WDS. Therefore, this approach supports high-resolution phenotyping and can contribute to the selection of more drought-resistant genotypes.

The superior performance of the SVM-DA model is attributed to its ability to capture nonlinear relationships in the spectral data through the use of a radial basis function (RBF) kernel. This enables more accurate modeling of the complex and gradual physiological changes caused by water stress, which often do not follow linear patterns. Such capacity is especially important when predicting pixel-level variation across plant structures, where stress responses can be subtle and spatially heterogeneous.

Table 4.3 Number and percentage of pixels correctly classified by PLS-DA, SVM-DA, and KNN according to sampling day in images of genotypes G1, G2, G3 and G4. Class 1: D3, Class 2: D7 and Class 3: D10. Highest percentages are highlighted in bold.

Genotype - Sampling day	***Single pixel prediction per class***									
	D3		*D7*		*D10*		*Unassigned*		*Total pixels*	
PLS-DA										
G1 – D3	**1740**	**48%**	483	13%	198	5%	1190	33%	3611	100%
G2 - D3	**2031**	**46%**	537	12%	248	6%	1554	36%	4370	100%
G3 - D3	**2092**	**47%**	505	11%	276	6%	1585	36%	4458	100%
G4 - D3	**1743**	**45%**	586	15%	227	6%	1292	34%	3848	100%

G1 – D7	590	20%	**1159**	**38%**	340	11%	929	31%	3018	100%
G2 - D7	629	12%	**1535**	**30%**	567	11%	2470	47%	5201	100%
G3 - D7	1037	19%	**2050**	**38%**	647	12%	1709	31%	5443	100%
G4 - D7	598	16%	**1665**	**44%**	432	11%	1120	29%	3815	100%
G1 – D10	632	11%	712	13%	**2146**	**38%**	2166	38%	5656	100%
G2 - D10	499	14%	794	22%	**1112**	**30%**	1278	35%	3683	100%
G3 - D10	474	11%	486	12%	**1609**	**38%**	1649	39%	4218	100%
G4 - D10	351	14%	485	20%	**781**	**32%**	838	34%	2455	100%
SVM-DA										
G1 – D3	**2536**	**70%**	1054	29%	21	1%	0	0%	3611	100%
G2 - D3	**2526**	**58%**	1838	42%	6	0%	0	0%	4370	100%
G3 - D3	**3283**	**74%**	1163	26%	12	0%	0	0%	4458	100%
G4 - D3	**2120**	**55%**	1693	44%	35	1%	0	0%	3848	100%
G1 – D7	1293	43%	**1707**	**57%**	18	1%	0	0%	3018	100%
G2 - D7	412	10%	**3788**	**90%**	1	0%	0	0%	4201	100%
G3 - D7	2637	48%	**2772**	**51%**	34	1%	0	0%	5443	100%
G4 - D7	1211	32%	**2562**	**67%**	42	1%	0	0%	3815	100%
G1 – D10	139	2%	466	8%	**5051**	**89%**	0	0%	5656	100%
G2 - D10	60	2%	528	14%	**3195**	**84%**	0	0%	3783	100%
G3 - D10	28	1%	447	11%	**3743**	**89%**	0	0%	4218	100%
G4 - D10	0	0%	352	14%	**2103**	**86%**	0	0%	2455	100%
KNN										
G1 – D3	**1241**	**34%**	1725	48%	645	18%	0	0%	3611	100%
G2 - D3	**2155**	**49%**	1923	44%	292	7%	0	0%	4370	100%
G3 - D3	**2045**	**46%**	1834	41%	579	13%	0	0%	4458	100%
G4 - D3	**1547**	**40%**	1560	41%	741	19%	0	0%	3848	100%
G1 – D7	1020	34%	**1270**	**42%**	728	24%	0	0%	3018	100%
G2 - D7	2793	66%	**1226**	**29%**	182	4%	0	0%	4201	100%
G3 - D7	2055	38%	**2480**	**46%**	908	17%	0	0%	5443	100%
G4 - D7	1077	28%	**2128**	**56%**	610	16%	0	0%	3815	100%
G1 – D10	1469	26%	1215	21%	**2972**	**53%**	0	0%	5656	100%
G2 - D10	540	14%	869	23%	**2374**	**63%**	0	0%	3783	100%
G3 - D10	867	21%	469	11%	**2882**	**68%**	0	0%	4218	100%
G4 - D10	218	9%	485	20%	**1752**	**71%**	0	0%	2455	100%

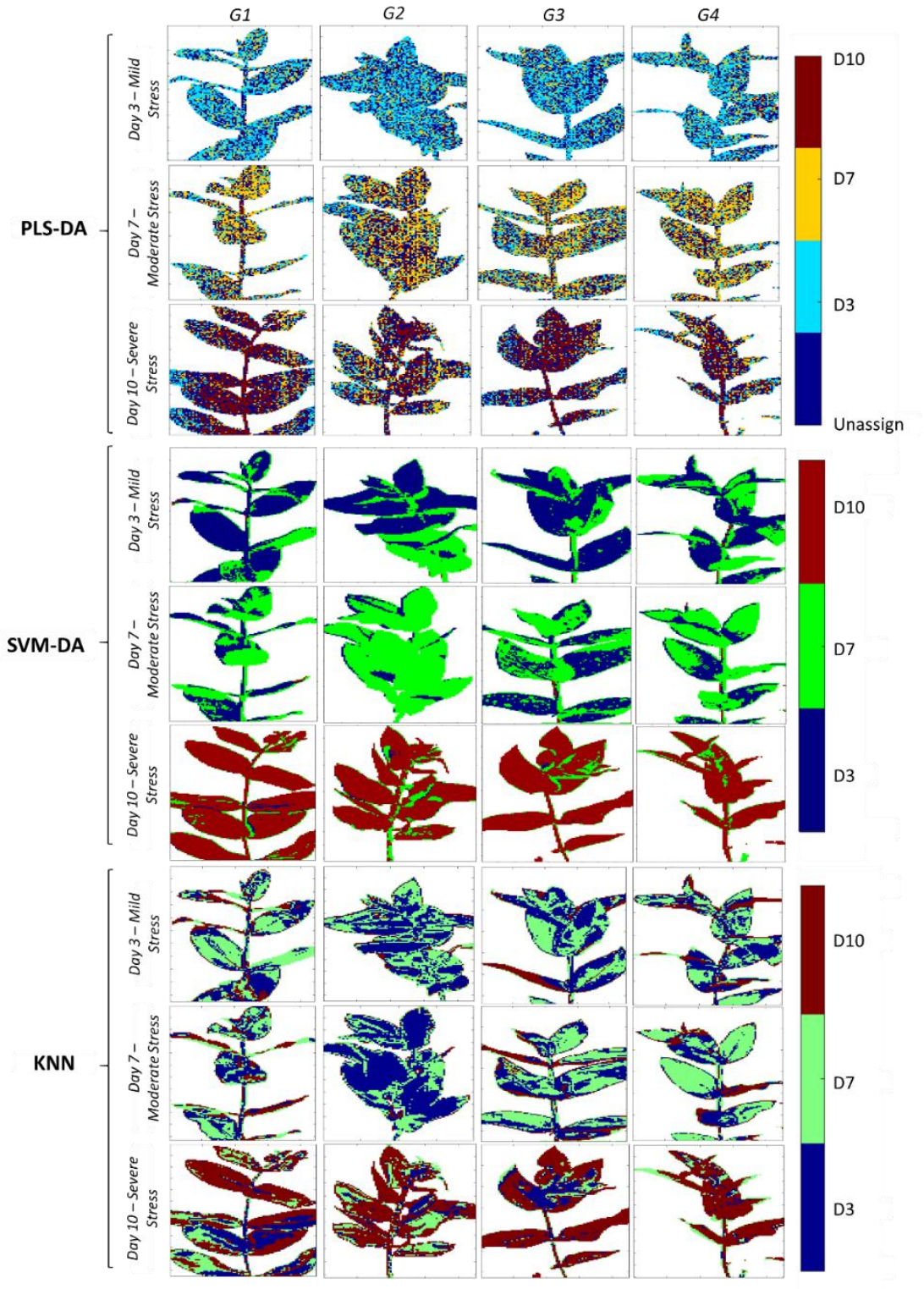

Figure 4.6 Pixel-by-pixel image reconstruction for D3, D7 and D10 of WD, corresponding to plants from the validation set of genotypes G1, G2, G3 and G4, using PLS-DA, KNN and SVM-DA models.

4.6. Conclusions

VIS-NIR HSI identified spectral differences that effectively distinguish between mild, moderate, and severe stress in *Eucalyptus spp.*, particularly differentiating plants after 10 days of water deficit, which were clearly distinguishable from control samples, and to a lesser extent, after 3 and 7 days. The bands associated with chlorophyll, flavonoids, and carotenoids appear to be responsible for differentiating between control and stressed plants in the visible region. Although slight differences were observed in the response of genotypes to distinguish between control and water deficit conditions, HSI has the potential to improve these distinctions by incorporating a larger sample size in future studies. When combined with supervised pattern recognition techniques, HSI demonstrated an impressive ability to predict stress induced by water deficit, with error rates ranging from 0 to 2% for validation samples. These results outperformed traditional physical characterization and vegetative index analysis, which were insufficient to differentiate between control, mild, moderate, and severe water deficit conditions in the plants. The SVM-DA model demonstrated high accuracy in bulk predictions of water deficit stress (WDS) and excelled in reconstructing images of whole *Eucalyptus spp.* plants to detect stress at a pixel level. This robust performance is explained by the model's ability to handle complex, nonlinear data structures through the RBF kernel, making it particularly suitable for modeling the subtle and progressive nature of plant stress responses. This approach provides valuable insights into the WDS process and could facilitate high-throughput phenotyping in breeding programs in a rapid, non-destructive manner.

4.7. Acknowledgments

Authors thanks the financial support of the projects FONDEQUIP EQM230094 and FONDECYT 1251201 of the "Agencia Chilena de Investigación y Desarrollo (ANID)", Chile. Pamela Sanhueza thanks the National Grant Number 21221771 from ANID Chile.

4.8. References

Abdelaali, B., Taha, D., Hannou, Z., Ayoub, E. H., El Menyiy, N., Bouyahya, A., & Mubarak, M. S. (2023). Bioactive Compounds and Antidiabetic and Other Health Benefits of Eucalyptus globulus. In *Antidiabetic Medicinal Plants and Herbal Treatments* (pp. 469–480). CRC Press. https://doi.org/10.1201/b23347-31

Ahmad, R. S., Imran, M., Ahmad, M. H., Khan, M. K., Yasmin, A., Saima, H., Abbas, K., Chaudhary, R., & Rahim, M. A. (2023). Eucalyptus essential oils. In *Essential Oils* (pp. 217–239). Elsevier. https://doi.org/10.1016/B978-0-323-91740-7.00005-0

Allen, C. D., Macalady, A. K., Chenchouni, H., Bachelet, D., McDowell, N., Vennetier, M., Kitzberger, T., Rigling, A., Breshears, D. D., Hogg, E. H. (Ted), Gonzalez, P., Fensham, R., Zhang, Z., Castro, J., Demidova, N., Lim, J. H., Allard, G., Running, S. W., Semerci, A., & Cobb, N. (2010). A global overview of drought and heat-induced tree mortality reveals emerging climate change risks for forests. *Forest Ecology and Management*, *259*(4), 660–684. https://doi.org/10.1016/j.foreco.2009.09.001

Ammitzboll, H., Vaillancourt, R. E., Potts, B. M., Harrison, P. A., Brodribb, T., Sussmilch, F. C., & Freeman, J. S. (2020). Independent genetic control of drought resistance, recovery, and growth of Eucalyptus globulus seedlings. *Plant Cell and Environment*, *43*(1), 103–115. https://doi.org/10.1111/pce.13649

Amrutha, S., Parveen, A. B. M., Muthupandi, M., Sivakumar, V., Nautiyal, R., & Ghosh Dasgupta, M. (2019). Variation in morpho-physiological, biochemical and molecular responses of two Eucalyptus species under short-term water stress. *Acta Botanica Croatica*, *78*(2), 125–134. https://doi.org/10.2478/botcro-2019-0021

Angel Prieto Lage, M., Barral Martínez, M., Seyyedimansour, S., Manikantan, M. R., Trif, M., & Khaneghah, M. A. (2022). *Recent advancements in NIR spectroscopy for assessing the quality and safety of horticultural products: A comprehensive review*.

Aranjuelo, I., Molero, G., Erice, G., Avice, J. C., & Nogués, S. (2011). Plant physiology and proteomics reveals the leaf response to drought in alfalfa (Medicago sativa L.). *Journal of Experimental Botany*, *62*(1), 111–123. https://doi.org/10.1093/jxb/erq249

Asaari, M. S. M., Mertens, S., Dhondt, S., Inzé, D., Wuyts, N., & Scheunders, P. (2019). Analysis of hyperspectral images for detection of drought stress and recovery in maize plants in a high-throughput phenotyping platform. *Computers and Electronics in Agriculture*, *162*, 749–758. https://doi.org/10.1016/j.compag.2019.05.018

Ballabio, D., & Consonni, V. (2013). Classification tools in chemistry. Part 1: linear models. PLS-DA. *Analytical Methods*, *5*(16), 3790. https://doi.org/10.1039/c3ay40582f

Ballester, C., Zarco-Tejada, P. J., Nicolás, E., Alarcón, J. J., Fereres, E., Intrigliolo, D. S., & Gonzalez-Dugo, V. (2018). Evaluating the performance of xanthophyll, chlorophyll and structure-sensitive spectral indices to detect water stress in five fruit tree species. *Precision Agriculture*, *19*(1), 178–193. https://doi.org/10.1007/s11119-017-9512-y

Barker, M., & Rayens, W. (2003). Partial least squares for discrimination. *Journal of Chemometrics*, *17*(3), 166–173. https://doi.org/10.1002/cem.785

Bayat, B., van der Tol, C., & Verhoef, W. (2016). Remote sensing of grass response to drought stress using spectroscopic techniques and canopy reflectance model inversion. *Remote Sensing*, *8*(7). https://doi.org/10.3390/rs8070557

Beć, K. B., Grabska, J., & Huck, C. W. (2020a). Near-infrared spectroscopy in bio-applications. In *Molecules* (Vol. 25, Number 12). MDPI AG. https://doi.org/10.3390/molecules25122948

Beć, K. B., Grabska, J., & Huck, C. W. (2020b). Near-infrared spectroscopy in bio-applications. In *Molecules* (Vol. 25, Number 12). MDPI AG. https://doi.org/10.3390/molecules25122948

Beć, K. B., Grabska, J., & Huck, C. W. (2020c). Near-infrared spectroscopy in bio-applications. In *Molecules* (Vol. 25, Number 12). MDPI AG. https://doi.org/10.3390/molecules25122948

Behmann, J., Steinrücken, J., & Plümer, L. (2014a). Detection of early plant stress responses in hyperspectral images. *ISPRS Journal of Photogrammetry and Remote Sensing*, *93*, 98–111. https://doi.org/10.1016/j.isprsjprs.2014.03.016

Behmann, J., Steinrücken, J., & Plümer, L. (2014b). Detection of early plant stress responses in hyperspectral images. *ISPRS Journal of Photogrammetry and Remote Sensing*, *93*, 98–111. https://doi.org/10.1016/j.isprsjprs.2014.03.016

Belgiu, M., & Drăgu, L. (2016). Random forest in remote sensing: A review of applications and future directions. In *ISPRS Journal of Photogrammetry and Remote Sensing* (Vol. 114, pp. 24–31). Elsevier B.V. https://doi.org/10.1016/j.isprsjprs.2016.01.011

Benhizia, R., Phinzi, K., Hateffard, F., Aib, H., & Szabó, G. (2024). Drought Monitoring Using Moderate Resolution Imaging Spectroradiometer-Derived NDVI Anomalies in Northern Algeria from 2011 to 2022. *Environments - MDPI*, *11*(5). https://doi.org/10.3390/environments11050095

Berenguer, H. D. P., Alves, A., Amaral, J., Leal, L., Monteiro, P., de Jesus, C., & Pinto, G. (2018). Differential physiological performance of two Eucalyptus species and one hybrid under different imposed water availability scenarios. *Trees - Structure and Function*, *32*(2), 415–427. https://doi.org/10.1007/s00468-017-1639-y

Bertinetto, C., Engel, J., & Jansen, J. (2020). ANOVA simultaneous component analysis: A tutorial review. In *Analytica Chimica Acta: X* (Vol. 6). Elsevier B.V. https://doi.org/10.1016/j.acax.2020.100061

Blackburn, G. A. (2007a). Hyperspectral remote sensing of plant pigments. *Journal of Experimental Botany*, *58*(4), 855–867. https://doi.org/10.1093/jxb/erl123

Blackburn, G. A. (2007b). Hyperspectral remote sensing of plant pigments. *Journal of Experimental Botany*, *58*(4), 855–867. https://doi.org/10.1093/jxb/erl123

Breiman, L. (2001). *Random Forests* (Vol. 45).

Brockerhoff, E. G., Jactel, H., Parrotta, J. A., & Ferraz, S. F. B. (2013). Role of eucalypt and other planted forests in biodiversity conservation and the provision of biodiversity-related ecosystem services. *Forest Ecology and Management*, *301*, 43–50. https://doi.org/10.1016/j.foreco.2012.09.018

Bustin, S. A., Benes, V., Garson, J. A., Hellemans, J., Huggett, J., Kubista, M., Mueller, R., Nolan, T., Pfaffl, M. W., Shipley, G. L., Vandesompele, J., & Wittwer, C. T. (2009). The MIQE guidelines:

Minimum information for publication of quantitative real-time PCR experiments. *Clinical Chemistry*, *55*(4), 611–622. https://doi.org/10.1373/clinchem.2008.112797

Bustin, S. A., Ruijter, J. M., Van den Hoff, M. J. B., Kubista, M., Pfaffl, M. W., Shipley, G. L., Tran, N., Rödiger, S., Untergasser, A., Mueller, R., Nolan, T., Milavec, M., Burns, M. J., Huggett, J. F., Vandesompele, J., & Wittwer, C. T. (2025). MIQE 2.0: Revision of the Minimum Information for Publication of Quantitative Real-Time PCR Experiments Guidelines. In *Clinical Chemistry* (Vol. 71, Number 6, pp. 634–651). Oxford University Press. https://doi.org/10.1093/clinchem/hvaf043

Cen, H., & He, Y. (2007). Theory and application of near infrared reflectance spectroscopy in determination of food quality. *Trends in Food Science and Technology*, *18*(2), 72–83. https://doi.org/10.1016/j.tifs.2006.09.003

Chen, T., & Guestrin, C. (2016). XGBoost: A scalable tree boosting system. *Proceedings of the ACM SIGKDD International Conference on Knowledge Discovery and Data Mining*, *13-17-August-2016*, 785–794. https://doi.org/10.1145/2939672.2939785

Correia, B., Hancock, R. D., Amaral, J., Gomez-Cadenas, A., Valledor, L., & Pinto, G. (2018). Combined Drought and Heat Activates Protective Responses in Eucalyptus globulus That Are Not Activated When Subjected to Drought or Heat Stress Alone. *Frontiers in Plant Science*, *9*. https://doi.org/10.3389/fpls.2018.00819

Correia, B., Pintó-Marijuan, M., Neves, L., Brossa, R., Dias, M. C., Costa, A., Castro, B. B., Araújo, C., Santos, C., Chaves, M. M., & Pinto, G. (2014a). Water stress and recovery in the performance of two Eucalyptus globulus clones: Physiological and biochemical profiles. *Physiologia Plantarum*, *150*(4), 580–592. https://doi.org/10.1111/ppl.12110

Correia, B., Pintó-Marijuan, M., Neves, L., Brossa, R., Dias, M. C., Costa, A., Castro, B. B., Araújo, C., Santos, C., Chaves, M. M., & Pinto, G. (2014b). Water stress and recovery in the performance of two Eucalyptus globulus clones: Physiological and biochemical profiles. *Physiologia Plantarum*, *150*(4), 580–592. https://doi.org/10.1111/ppl.12110

Correia, B., Valledor, L., Hancock, R. D., Jesus, C., Amaral, J., Meijón, M., & Pinto, G. (2016). Depicting how Eucalyptus globulus survives drought: involvement of redox and DNA methylation events. *Functional Plant Biology*, *43*(9), 838. https://doi.org/10.1071/FP16064

Cortes, C., Vapnik, V., & Saitta, L. (1995). Support-Vector Networks Editor. In *Machine Leaming* (Vol. 20). Kluwer Academic Publishers.

Cotrozzi, L., Peron, R., Tuinstra, M. R., Mickelbart, M. V., & Couture, J. J. (2020). Spectral phenotyping of physiological and anatomical leaf traits related with maize water status1[open]. *Plant Physiology*, *184*(3), 1363–1377. https://doi.org/10.1104/pp.20.00577

Cover, T. M., & Hart, P. E. (1952). Approximate formulas for the information transmitted bv a discrete communication channel. In *IEEE TRANSACTIONS ON INFORMATION THEORY* (Vol. 24, Number 1).

Cursi, A. G., Oliveira, F. S., Gouveia, D. G., Oder, J. C., Barrios, W. E. B., Ferreira, G. V., Martins, A. O., Peterle, G., Nunes-Nesi, A., & Araújo, W. L. (2024). Deciphering the importance of morphological aspects in drought tolerance in eucalyptus progenies. *Forest Ecology and Management*, *569*. https://doi.org/10.1016/j.foreco.2024.122198

Cvetković, D., Marković, D., Cvetković, D., & Radovanović, B. (2011). Effects of continuous UV-irradiation on the antioxidant activities of quercetin and rutin in solution in the presence of lecithin as the protective target. *Journal of the Serbian Chemical Society*, *76*(7), 973–985. https://doi.org/10.2298/JSC101123089C

Da Fonseca-Pereira, P., Daloso, D. M., Gago, J., De Oliveira Silva, F. M., Condori-Apfata, J. A., Florez-Sarasa, I., Tohge, T., Reichheld, J. P., Nunes-Nesi, A., Fernie, A. R., & Arajo, W. L. (2019). The Mitochondrial Thioredoxin System Contributes to the Metabolic Responses under Drought Episodes in Arabidopsis. *Plant and Cell Physiology*, *60*(1), 213–229. https://doi.org/10.1093/pcp/pcy194

Datt, B. (1993). Remote Sensing of Chlorophyll a, Chlorophyll b, Chlorophyll ab, and Total Carotenoid Content in Eucalyptus Leaves Recent studies have devel-oped several new vegetation indices based on other visi. In *REMOTE SENS. ENVIRON* (Vol. 66).

Datt, B. (1999). A New Reflectance Index for Remote Sensing of Chlorophyll Content in Higher Plants: Tests using Eucalyptus Leaves. *Journal of Plant Physiology*.

De Angelis, D., Summo, C., Pasqualone, A., Faccia, M., & Squeo, G. (2024). Advancements in food authentication using soft independent modelling of class analogy (SIMCA): a review. *Food Quality and Safety*, *8*. https://doi.org/10.1093/fqsafe/fyae032

Deribe, H. (2025). Review on Effects of Drought Stress on Maize Growth, Yield and Its Management Strategies. *Communications in Soil Science and Plant Analysis*, *56*(1), 123–143. https://doi.org/10.1080/00103624.2024.2404663

Dmitriev, P., Kozlovsky, B., Dmitrieva, A., Lysenko, V., Chokheli, V., Minkina, T., Mandzhieva, S., Sushkova, S., & Varduni, T. (2023). Identification of species of the genus Quercus L. with different responses to soil and climatic conditions according to hyperspectral survey data. *Eurasian Journal of Soil Science*, *12*(1), 37–62. https://doi.org/10.18393/ejss.1183524

Ejaz, I., Li, W., Naseer, M. A., Li, Y., Qin, W., Farooq, M., Li, F., Huang, S., Zhang, Y., Wang, Z., Sun, Z., & Yu, K. (2023). Detection of combined frost and drought stress in wheat using hyperspectral and chlorophyll fluorescence imaging. *Environmental Technology & Innovation*, *30*, 103051. https://doi.org/10.1016/j.eti.2023.103051

El Azizi, S., Amharref, M., Es-Saouini, H., Bernoussi, A. S., & El Abdellaoui, J. E. (2024). Towards a Spectral Library of Medicinal and Aromatic Plant species (MAPs): Plant Discrimination and Wavelength Selection. *Microchemical Journal*, *207*. https://doi.org/10.1016/j.microc.2024.111854

Ezenarro, J., Saouabi, I., García-Pizarro, Á., Schorn-García, D., Mestres, M., Amigo, J. M., Busto, O., & Boqué, R. (2025). NIR-HSI for the non-destructive monitoring of in-bag hazelnut oxidation. *Spectrochimica Acta - Part A: Molecular and Biomolecular Spectroscopy*, *333*. https://doi.org/10.1016/j.saa.2025.125906

Eziz, A., Yan, Z., Tian, D., Han, W., Tang, Z., & Fang, J. (2017). Drought effect on plant biomass allocation: A meta-analysis. *Ecology and Evolution*, *7*(24), 11002–11010. https://doi.org/10.1002/ece3.3630

Farooq, M., Wahid, A., Kobayashi, N., Fujita, D., & Basra, S. M. A. (2009). Plant drought stress: Effects, mechanisms and management. In *Agronomy for Sustainable Development* (Vol. 29, Number 1, pp. 185–212). https://doi.org/10.1051/agro:2008021

Fernández, M., Valenzuela, S., Barraza, H., Latorre, J., & Neira, V. (2012). Photoperiod, temperature and water deficit differentially regulate the expression of four dehydrin genes from Eucalyptus globulus. *Trees - Structure and Function*, *26*(5), 1483–1493. https://doi.org/10.1007/s00468-012-0722-7

Fernández, M., Villarroel, C., Balbontín, C., & Valenzuela, S. (2010). Validation of reference genes for real-time qRT-PCR normalization during cold acclimation in Eucalyptus globulus. *Trees - Structure and Function*, *24*(6), 1109–1116. https://doi.org/10.1007/s00468-010-0483-0

Freitag, S., Anlanger, M., Lippl, M., Mechtler, K., Reiter, E., Grausgruber, H., & Krska, R. (2024). Simplifying Wheat Quality Assessment: Using Near-Infrared Spectroscopy and Analysis of Variance Simultaneous Component Analysis to Study Regional and Annual Effects. *ACS Measurement Science Au*. https://doi.org/10.1021/acsmeasuresciau.4c00044

Gamon, A., Pe uelas, J., & Field, C. B. (1992). *A Narrow-Waveband Spectral Index That Tracks Diurnal Changes in Photosynthetic Efficiency** (Vol. 41).

Ge, S., Carruthers, R. I., Spencer, D. F., & Yu, Q. (2008). Canopy assessment of biochemical features by ground-based hyperspectral data for an invasive species, giant reed (Arundo donax). *Environmental Monitoring and Assessment*, *147*(1–3), 271–278. https://doi.org/10.1007/s10661-007-0119-z

Gitelson, A. A., Gritz, Y., & Merzlyak, M. N. (2003). Relationships between leaf chlorophyll content and spectral reflectance and algorithms for non-destructive chlorophyll assessment in higher plant leaves. In *J. Plant Physiol* (Vol. 160). http://www.urbanfischer.de/journals/jpp

Gitelson, A. A., Keydan, G. P., & Merzlyak, M. N. (2006). Three-band model for noninvasive estimation of chlorophyll, carotenoids, and anthocyanin contents in higher plant leaves. *Geophysical Research Letters*, *33*(11). https://doi.org/10.1029/2006GL026457

Guigou, M., Moure, S., Bermúdez, F., Clavijo, L., Cabrera, M. N., Xavier, L., Ferrari, M. D., & Lareo, C. (2023). Ethanol Production from Eucalyptus Sawdust Following Sequential Alkaline Thermochemical Pretreatment with Recovery of Extractives. *Bioenergy Research*, *16*(4), 2012–2021. https://doi.org/10.1007/s12155-023-10619-1

Ha, S., Vankova, R., Yamaguchi-Shinozaki, K., Shinozaki, K., & Tran, L. S. P. (2012). Cytokinins: Metabolism and function in plant adaptation to environmental stresses. In *Trends in Plant Science* (Vol. 17, Number 3, pp. 172–179). https://doi.org/10.1016/j.tplants.2011.12.005

Hanin, M., Brini, F., Ebel, C., Toda, Y., Takeda, S., & Masmoudi, K. (2011). Plant dehydrins and stress tolerance: Versatile proteins for complex mechanisms. In *Plant Signaling and Behavior* (Vol. 6, Number 10, pp. 1503–1509). https://doi.org/10.4161/psb.6.10.17088

Hartmann, H., Bastos, A., Das, A. J., Esquivel-Muelbert, A., Hammond, W. M., Martínez-Vilalta, J., Mcdowell, N. G., Powers, J. S., Pugh, T. A. M., Ruthrof, K. X., & Allen, C. D. (2025). Climate Change Risks to Global Forest Health: Emergence of Unexpected Events of Elevated Tree Mortality Worldwide. *Annual Review of Plant Biology*. https://doi.org/10.1146/annurev-arplant-102820

Haynes, R. S., Lucieer, A., Brodribb, T. J., Tonet, V., & Cimoli, E. (2024a). Predicting key water stress indicators of Eucalyptus viminalis and Callitris rhomboidea using high-resolution visible to short-

wave infrared spectroscopy. *Plant Cell and Environment*, *47*(12), 4992–5006. https://doi.org/10.1111/pce.15083

Haynes, R. S., Lucieer, A., Brodribb, T. J., Tonet, V., & Cimoli, E. (2024b). Predicting key water stress indicators of Eucalyptus viminalis and Callitris rhomboidea using high-resolution visible to short-wave infrared spectroscopy. *Plant Cell and Environment*, *47*(12), 4992–5006. https://doi.org/10.1111/pce.15083

Humphreys, J. R., O'Reilly-Wapstra, J. M., Harbard, J. L., Davies, N. W., Griffin, A. R., Jordan, G. J., & Potts, B. M. (2008). Discrimination between seedlings of Eucalyptus globulus, E. nitens and their F1 hybrid using near-infrared reflectance spectroscopy and foliar oil content. *Silvae Genetica*, *57*(4–5), 262–269. https://doi.org/10.1515/sg-2008-0040

Hussain, S., Hussain, S., Qadir, T., Khaliq, A., Ashraf, U., Parveen, A., Saqib, M., & Rafiq, M. (2019). Drought stress in plants: An overview on implications, tolerance mechanisms and agronomic mitigation strategies. *Plant Science Today*, *6*(4), 389–402. https://doi.org/10.14719/pst.2019.6.4.578

Ibarra, L., Hodge, G., & Acosta, J. J. (2023). Quantitative Genetics of a Hybrid Population of Eucalyptus nitens × Eucalyptus globulus: Estimation of Genetic Parameters and Implications for Breeding Strategies. *Forests*, *14*(2). https://doi.org/10.3390/f14020381

Jansen, J. J., Hoefsloot, H. C. J., Van Der Greef, J., Timmerman, M. E., Westerhuis, J. A., & Smilde, A. K. (2005). ASCA: Analysis of multivariate data obtained from an experimental design. *Journal of Chemometrics*, *19*(9), 469–481. https://doi.org/10.1002/cem.952

Johnson, J. B. (2023a). Rapid Prediction of Leaf Water Content in Eucalypt Leaves Using a Handheld NIRS Instrument. *Eng*, *4*(2), 1198–1209. https://doi.org/10.3390/eng4020070

Johnson, J. B. (2023b). Rapid Prediction of Leaf Water Content in Eucalypt Leaves Using a Handheld NIRS Instrument. *Eng*, *4*(2), 1198–1209. https://doi.org/10.3390/eng4020070

Jollife, I. T., & Cadima, J. (2016). Principal component analysis: A review and recent developments. In *Philosophical Transactions of the Royal Society A: Mathematical, Physical and Engineering Sciences* (Vol. 374, Number 2065). Royal Society of London. https://doi.org/10.1098/rsta.2015.0202

Jones, H. G. (2007). Monitoring plant and soil water status: Established and novel methods revisited and their relevance to studies of drought tolerance. *Journal of Experimental Botany*, *58*(2), 119–130. https://doi.org/10.1093/jxb/erl118

Josep Peñuelas, I. F. (1998). *Visible and near-infrared reflectance techniques for diagnosing plant physiological status*.

Kawamura, K., Watanabe, N., Sakanoue, S., & Inoue, Y. (2008). Estimating forage biomass and quality in a mixed sown pasture based on partial least squares regression with waveband selection. *Grassland Science*, *54*(3), 131–145. https://doi.org/10.1111/j.1744-697x.2008.00116.x

Kim, Y., Glenn, D. M., Park, J., Ngugi, H. K., & Lehman, B. L. (2011a). Hyperspectral image analysis for water stress detection of apple trees. *Computers and Electronics in Agriculture*, *77*(2), 155–160. https://doi.org/10.1016/j.compag.2011.04.008

Kim, Y., Glenn, D. M., Park, J., Ngugi, H. K., & Lehman, B. L. (2011b). Hyperspectral image analysis for water stress detection of apple trees. *Computers and Electronics in Agriculture*, *77*(2), 155–160. https://doi.org/10.1016/j.compag.2011.04.008

Koag, M. C., Fenton, R. D., Wilkens, S., & Close, T. J. (2003). The binding of maize DHN1 to lipid vesicles. Gain of structure and lipid specificity. *Plant Physiology*, *131*(1), 309–316. https://doi.org/10.1104/pp.011171

Kohzuma, K., Tamaki, M., & Hikosaka, K. (2021). Corrected photochemical reflectance index (PRI) is an effective tool for detecting environmental stresses in agricultural crops under light conditions. *Journal of Plant Research*, *134*(4), 683–694. https://doi.org/10.1007/s10265-021-01316-1

Korek, M., & Marzec, M. (2023). Strigolactones and abscisic acid interactions affect plant development and response to abiotic stresses. In *BMC Plant Biology* (Vol. 23, Number 1). BioMed Central Ltd. https://doi.org/10.1186/s12870-023-04332-6

Kuang, X., Cheng, Q., Chen, D., Fu, W., Li, H., & Chen, Z. (2026). Intelligent Diagnosis of Winter Wheat Water Stress Based on UAV Multi-Modal Remote Sensing. *Smart Agricultural Technology*, 101781. https://doi.org/10.1016/j.atech.2026.101781

Lee, S. C., & Luan, S. (2012). ABA signal transduction at the crossroad of biotic and abiotic stress responses. In *Plant, Cell and Environment* (Vol. 35, Number 1, pp. 53–60). https://doi.org/10.1111/j.1365-3040.2011.02426.x

Li, H., Yang, W., Lei, J., She, J., & Zhou, X. (2021). Estimation of leaf water content from hyperspectral data of different plant species by using three new spectral absorption indices. *PLoS ONE*, *16*(3 March). https://doi.org/10.1371/journal.pone.0249351

M. N. Merzlyak*, A. A. G. O. B. C. A. E. S. and S. I. P. (2003). *Application of Reflectance Spectroscopy for Analysis of Higher Plant Pigments*.

Manley, M. (2014). Near-infrared spectroscopy and hyperspectral imaging: Non-destructive analysis of biological materials. In *Chemical Society Reviews* (Vol. 43, Number 24, pp. 8200–8214). Royal Society of Chemistry. https://doi.org/10.1039/c4cs00062e

Martins, G. S., Freitas, N. C., Máximo, W. P. F., & Paiva, L. V. (2018). Gene expression in two contrasting hybrid clones of Eucalyptus camaldulensis x Eucalyptus urophylla grown under water deficit conditions. *Journal of Plant Physiology*, *229*, 122–131. https://doi.org/10.1016/j.jplph.2018.07.007

McFeeters, S. K. (1996). The use of the Normalized Difference Water Index (NDWI) in the delineation of open water features. *International Journal of Remote Sensing*, *17*(7), 1425–1432. https://doi.org/10.1080/01431169608948714

Merchant, A., Callister, A., Arndt, S., Tausz, M., & Adams, M. (2007). Contrasting physiological responses of six Eucalyptus species to water deficit. *Annals of Botany*, *100*(7), 1507–1515. https://doi.org/10.1093/aob/mcm234

Migacz, I. P., Manfron, J., Farago, P. V., Raman, V., de Muñiz, G. I. B., & Nisgoski, S. (2022). VIS/NIR spectra and color parameters according to leaf age of some Eucalyptus species: influence on their classification and discrimination. *Forest Systems*, *31*(2). https://doi.org/10.5424/fs/2022312-19242

Mobaraki, N., & Amigo, J. M. (2018). HYPER-Tools. A graphical user-friendly interface for hyperspectral image analysis. *Chemometrics and Intelligent Laboratory Systems*, *172*, 174–187. https://doi.org/10.1016/j.chemolab.2017.11.003

Mondal, M., Edida, M., Sharma, N., Lall, B., & Raju, D. (2019). Plants Stress Response Detection by Selecting Minimal Bands of Hyperspectral Images. *2019 9th International Conference on Advances in Computing and Communication (ICACC)*, 230–233. https://doi.org/10.1109/ICACC48162.2019.8986161

Mountrakis, G., Im, J., & Ogole, C. (2011). Support vector machines in remote sensing: A review. In *ISPRS Journal of Photogrammetry and Remote Sensing* (Vol. 66, Number 3, pp. 247–259). https://doi.org/10.1016/j.isprsjprs.2010.11.001

Moura, J. C. M. S., Araújo, P., Brito, M. D. S., Souza, U. R., Viana, J. O. F., & Mazzafera, P. (2012). Validation of reference genes from Eucalyptus spp. under different stress conditions. *BMC Research Notes*, *5*. https://doi.org/10.1186/1756-0500-5-634

Moura Melo, L. de, Dos Santos, A. C., Arteiro da Silva, K., Barbosa, U. do N., De Sena Oliveira, G. F., Alba, E., André Bellé, P., Monteiro Junior, J. J., & Araújo Silva, E. (2019). Spectral Response of Eucalyptus saligna under Water Stress in Southern Brazil. *Journal of Experimental Agriculture International*, 1–8. https://doi.org/10.9734/jeai/2019/v41i430405

Moussa Kourouma, J., Eze, E., Negash, E., Phiri, D., Vinya, R., Girma, A., & Zenebe, A. (2021). Assessing the spatio-temporal variability of NDVI and VCI as indices of crops productivity in Ethiopia: a remote sensing approach. *Geomatics, Natural Hazards and Risk*, *12*(1), 2880–2903. https://doi.org/10.1080/19475705.2021.1976849

Munera, S., Amigo, J. M., Aleixos, N., Talens, P., Cubero, S., & Blasco, J. (2018). Potential of VIS-NIR hyperspectral imaging and chemometric methods to identify similar cultivars of nectarine. *Food Control*, *86*, 1–10. https://doi.org/10.1016/j.foodcont.2017.10.037

Munns, R., James, R. A., Sirault, X. R. R., Furbank, R. T., & Jones, H. G. (2010). New phenotyping methods for screening wheat and barley for beneficial responses to water deficit. In *Journal of Experimental Botany* (Vol. 61, Number 13, pp. 3499–3507). https://doi.org/10.1093/jxb/erq199

Murchie, E. H., & Lawson, T. (2013). Chlorophyll fluorescence analysis: A guide to good practice and understanding some new applications. In *Journal of Experimental Botany* (Vol. 64, Number 13, pp. 3983–3998). https://doi.org/10.1093/jxb/ert208

Okyere, F. G., Cudjoe, D. K., Virlet, N., Castle, M., Riche, A. B., Greche, L., Mohareb, F., Simms, D., Mhada, M., & Hawkesford, M. J. (2024). Hyperspectral Imaging for Phenotyping Plant Drought Stress and Nitrogen Interactions Using Multivariate Modeling and Machine Learning Techniques in Wheat. *Remote Sensing*, *16*(18), 3446. https://doi.org/10.3390/rs16183446

Oliveira, L. A., Cardoso, A. A., Andrade, M. T., Pereira, T. S., Araújo, W. L., Santos, G. A., Damatta, F. M., & Martins, S. C. V. (2022). Exploring leaf hydraulic traits to predict drought tolerance of *Eucalyptus* clones. *Tree Physiology*, *42*(9), 1750–1761. https://doi.org/10.1093/treephys/tpac040

Oliveri, P., Malegori, C., Simonetti, R., & Casale, M. (2019). The impact of signal pre-processing on the final interpretation of analytical outcomes – A tutorial. In *Analytica Chimica Acta* (Vol. 1058, pp. 9–17). Elsevier B.V. https://doi.org/10.1016/j.aca.2018.10.055

Olvera-Carrillo, Y., Campos, F., Reyes, J. L., Garciarrubio, A., & Covarrubias, A. A. (2010). Functional analysis of the group 4 late embryogenesis abundant proteins reveals their relevance in the adaptive response during water deficit in arabidopsis. *Plant Physiology*, *154*(1), 373–390. https://doi.org/10.1104/pp.110.158964

Olvera-Carrillo, Y., Reyes, J. L., & Covarrubias, A. A. (2011). Late embryogenesis abundant proteins: Versatile players in the plant adaptation to water limiting environments. *Plant Signaling and Behavior*, *6*(4), 586–589. https://doi.org/10.4161/psb.6.4.15042

Peerbhay, K. Y., Mutanga, O., & Ismail, R. (2013). Commercial tree species discrimination using airborne AISA Eagle hyperspectral imagery and partial least squares discriminant analysis (PLS-DA) in KwaZulu-Natal, South Africa. *ISPRS Journal of Photogrammetry and Remote Sensing*, *79*, 19–28. https://doi.org/10.1016/j.isprsjprs.2013.01.013

Peguero-Pina, J. J., Sancho-Knapik, D., Ferrio, J. P., López-Ballesteros, A., Ruiz-Llata, M., & Gil-Pelegrín, E. (2023). Reevaluating Near-Infrared Reflectance as a Tool for the Study of Plant Water Status in Holm Oak (Quercus ilex subsp. rotundifolia). *Forests*, *14*(9). https://doi.org/10.3390/f14091825

Peng, Y., Zhang, M., Xu, Z., Yang, T., Su, Y., Zhou, T., Wang, H., Wang, Y., & Lin, Y. (2020). Estimation of leaf nutrition status in degraded vegetation based on field survey and hyperspectral data. *Scientific Reports*, *10*(1). https://doi.org/10.1038/s41598-020-61294-7

Penuelas, J., Pinol, J., Ogaya, R., & Filella, I. (1997). Estimation of plant water concentration by the reflectance Water Index WI (R900/R970). *International Journal of Remote Sensing*, *18*(13), 2869–2875. https://doi.org/10.1080/014311697217396

Peñuelas Josep, & Filella Iolanda. (1998). *Visible and near-infrared reflectance techniques for diagnosing plant physiological status*.

Pita, P., & Pardos, J. A. (2001). Growth, leaf morphology, water use and tissue water relations of Eucalyptus globulus clones in response to water deficit. *Tree Physiology*, *21*(9), 599–607. https://doi.org/10.1093/treephys/21.9.599

Pivovar, M., Näsi, R., Honkavaara, E., Blaženec, M., Škvarenina, J., Modlinger, R., Rožnovský, J., & Jakuš, R. (2025). Spectral signatures discrimination of Norway spruce trees under experimentally induced drought and acute thermal stress using hyperspectral imaging. *Forest Ecology and Management*, *586*. https://doi.org/10.1016/j.foreco.2025.122692

Poblete Hernández, P., Carlos, J., Munita, B., Caselli, J. G., Kahler González, C., Pardo Velásquez, E., Rocha, D. B., Catelicán Vera, L., Pineda, J. H., Celis Cantillana, B., & Recabarren, H. T. (2025). *ANUARIO FORESTAL CHILEAN STATISTICAL YEARBOOK OF FORESTRY 2025*. www.infor.cl

Ram, B. G., Oduor, P., Igathinathane, C., Howatt, K., & Sun, X. (2024). A systematic review of hyperspectral imaging in precision agriculture: Analysis of its current state and future prospects. In *Computers and Electronics in Agriculture* (Vol. 222). Elsevier B.V. https://doi.org/10.1016/j.compag.2024.109037

Raymond Hunt, E., & Rock, B. N. (1989). *Detection of Changes in Leaf Water Content Using Near-and Middle-Infrared Reflectances* (Vol. 30).

Rinnan, Å., Berg, F. van den, & Engelsen, S. B. (2009). Review of the most common pre-processing techniques for near-infrared spectra. In *TrAC - Trends in Analytical Chemistry* (Vol. 28, Number 10, pp. 1201–1222). https://doi.org/10.1016/j.trac.2009.07.007

Rodionova, O. Ye., Oliveri, P., Malegori, C., & Pomerantsev, A. L. (2024). Chemometrics as an efficient tool for food authentication: Golden pillars for building reliable models. *Trends in Food Science & Technology*, *147*, 104429. https://doi.org/10.1016/j.tifs.2024.104429

Rojas-Rioseco, M., Castillo, R. del P., González-Campos, J., Ipinza, R., Sanhueza, M. I., & Hasbún, R. (2022). Phylogeographic origin authentication of Araucaria araucana (Mol.) K Koch seedlings through the application of spectroscopy techniques in different infrared ranges and chemometric methods. *New Forests*. https://doi.org/10.1007/s11056-022-09933-x

Rojek, L., Möller, M., Richter, M., Bischoff-Schaefer, M., & Hehl, K. (2023). PLANTSENS: A rail-based multi-sensor imaging system for redundant water stress detection in greenhouses. In *Smart Agricultural Technology* (Vol. 4). Elsevier B.V. https://doi.org/10.1016/j.atech.2023.100223

Ryckewaert, M., Gorretta, N., Henriot, F., Gobrecht, A., Héran, D., Moura, D., Bendoula, R., & Roger, J. M. (2021). Potential of high-spectral resolution for field phenotyping in plant breeding: Application to maize under water stress. *Computers and Electronics in Agriculture*, *189*. https://doi.org/10.1016/j.compag.2021.106385

Saadaoui, E., Ben Yahia, K., Dhahri, S., Ben Jamaa, M. L., & Khouja, M. L. (2017). An overview of adaptative responses to drought stress in Eucalyptus spp. *Forestry Studies*, *67*(1), 86–96. https://doi.org/10.1515/fsmu-2017-0014

Saddiq, M. S., Wang, X., Iqbal, S., Bilal Hafeez, M., Khan, S., Raza, A., Iqbal, J., Maqbool, M. M., Fiaz, S., Qazi, M. A., Bakhsh, A., 10, J., Gulshan, A. B., & Yang, S. H. (1934). *Effect of Water Stress on Grain Yield and Physiological Characters of Quinoa Genotypes*. *11*. https://doi.org/10.3390/agronomy

Salazar, C., Hernández, C., & Pino, M. T. (2015). Plant water stress: Associations between ethylene and abscisic acid response. In *Chilean Journal of Agricultural Research* (Vol. 75, pp. 71–79). Instituto de Investigaciones Agropecuarias, INIA. https://doi.org/10.4067/S0718-58392015000300008

Sánchez, J. C. M., Mesa, H. G. A., Espinosa, A. T., Castilla, S. R., & Lamont, F. G. (2025). Improving wheat yield prediction through variable selection using Support Vector Regression, Random Forest, and Extreme Gradient Boosting. In *Smart Agricultural Technology* (Vol. 10). Elsevier B.V. https://doi.org/10.1016/j.atech.2025.100791

Sanhueza-Novoa, P., Fernández, M., Hernández-Fuentes, C., Valenzuela, S., Hayat, M. Q., Ricardo Ramírez, H., & Castillo, R. del P. (2026). Detection of water deficit stress in Eucalyptus spp. through VIS-NIR hyperspectral imaging and chemometric methods. *Spectrochimica Acta Part A: Molecular and Biomolecular Spectroscopy*, *344*, 126675. https://doi.org/10.1016/j.saa.2025.126675

Santana, D. C., Baio, F. H. R., Oliveira, I. C. de, Araújo, F. C. de, Azevedo, G. B. de, Silva, E. V. M., Silva Junior, C. A. da, Teodoro, P. E., & Teodoro, L. P. R. (2025). From spectral data to species identity: Machine learning and VIS/NIR reflectance in eucalyptus classification. *Remote Sensing Applications: Society and Environment*, *39*. https://doi.org/10.1016/j.rsase.2025.101686

Schwanninger, M., Rodrigues, J. C., & Fackler, K. (2011). A review of band assignments in near infrared spectra of wood and wood components. In *Journal of Near Infrared Spectroscopy* (Vol. 19, Number 5, pp. 287–308). https://doi.org/10.1255/jnirs.955

Shi, Y., Liu, X., Zhao, S., & Guo, Y. (2022). The PYR-PP2C-CKL2 module regulates ABA-mediated actin reorganization during stomatal closure. *New Phytologist*, *233*(5), 2168–2184. https://doi.org/10.1111/nph.17933

Silla, C. N., & Freitas, A. A. (2011). A survey of hierarchical classification across different application domains. In *Data Mining and Knowledge Discovery* (Vol. 22, Numbers 1–2, pp. 31–72). https://doi.org/10.1007/s10618-010-0175-9

Singh, D., Singh, C. K., Taunk, J., Tomar, R. S. S., Chaturvedi, A. K., Gaikwad, K., & Pal, M. (2017). Transcriptome analysis of lentil (Lens culinaris Medikus) in response to seedling drought stress. *BMC Genomics*, *18*(1). https://doi.org/10.1186/s12864-017-3596-7

Smola, A. J., Sch¨olkopf, B., & Sch¨olkopf, S. (2004). A tutorial on support vector regression *. In *Statistics and Computing* (Vol. 14). Kluwer Academic Publishers.

Sobejano-Paz, V., Mikkelsen, T. N., Baum, A., Mo, X., Liu, S., Köppl, C. J., Johnson, M. S., Gulyas, L., & García, M. (2020). Hyperspectral and Thermal Sensing of Stomatal Conductance, Transpiration, and Photosynthesis for Soybean and Maize under Drought. *Remote Sensing*, *12*(19), 3182. https://doi.org/10.3390/rs12193182

Sokolova, M., & Lapalme, G. (2009). A systematic analysis of performance measures for classification tasks. *Information Processing and Management*, *45*(4), 427–437. https://doi.org/10.1016/j.ipm.2009.03.002

Spokevicius, A. V., Tibbits, J., Rigault, P., Nolin, M. A., Müller, C., & Merchant, A. (2017). Medium term water deficit elicits distinct transcriptome responses in Eucalyptus species of contrasting environmental origin. *BMC Genomics*, *18*(1). https://doi.org/10.1186/s12864-017-3664-z

Steidle Neto, A. J., Lopes, D. de C., Silva, T. G. F. da, Ferreira, S. O., & Grossi, J. A. S. (2017). Estimation of leaf water content in sunflower under drought conditions by means of spectral reflectance. *Engineering in Agriculture, Environment and Food*, *10*(2), 104–108. https://doi.org/10.1016/j.eaef.2016.11.006

Stellacci, A. M., Castrignanò, A., Diacono, M., Troccoli, A., Ciccarese, A., Armenise, E., Gallo, A., De Vita, P., Lonigro, A., Mastro, M. A., & Rubino, P. (2012). Combined approach based on principal component analysis and canonical discriminant analysis for investigating hyperspectral plant response. *Italian Journal of Agronomy*, *7*(3), 247–253. https://doi.org/10.4081/ija.2012.e34

T Daughtry, C. S., Walthall, C. L., Kim, M. S., Brown de Colstoun, E., & McMurtrey III, J. E. (1999). Estimating Corn Leaf Chlorophyll Concentration from Leaf and Canopy Reflectance. In *REMOTE SENS. ENVIRON* (Vol. 74).

Taniguchi, M., LaRocca, C. A., Bernat, J. D., & Lindsey, J. S. (2023). Digital Database of Absorption Spectra of Diverse Flavonoids Enables Structural Comparisons and Quantitative Evaluations. *Journal of Natural Products*, *86*(4), 1087–1119. https://doi.org/10.1021/acs.jnatprod.2c00720

Torrion, J. A., Maas, S. J., Guo, W., Bordovsky, J. P., & Cranmer, A. M. (2014). A three-dimensional index for characterizing crop water stress. *Remote Sensing*, *6*(5), 4025–4042. https://doi.org/10.3390/rs6054025

Türker-Kaya, S., & Huck, C. W. (2017a). A review of mid-infrared and near-infrared imaging: Principles, concepts and applications in plant tissue analysis. In *Molecules* (Vol. 22, Number 1). MDPI AG. https://doi.org/10.3390/molecules22010168

Türker-Kaya, S., & Huck, C. W. (2017b). A review of mid-infrared and near-infrared imaging: Principles, concepts and applications in plant tissue analysis. In *Molecules* (Vol. 22, Number 1). MDPI AG. https://doi.org/10.3390/molecules22010168

Ulloa, J. L., Aguayo, P., Conejera, D., Rubilar, R., Balocchi, C., & Valenzuela, S. (2022). Transcriptomic response in foliar and root tissues of a drought-tolerant Eucalyptus globulus genotype under drought stress. *Trees - Structure and Function*, *36*(2), 697–709. https://doi.org/10.1007/s00468-021-02241-5

Umami, M., Parker, L. M., & Arndt, S. K. (2021). The impacts of drought stress and phytophthora cinnamomi infection on short-term water relations in two year-old eucalyptus obliqua. *Forests*, *12*(2), 1–14. https://doi.org/10.3390/f12020109

Valdés, A. E., Irar, S., Majada, J. P., Rodríguez, A., Fernández, B., & Pagès, M. (2013). Drought tolerance acquisition in Eucalyptus globulus (Labill.): A research on plant morphology, physiology and proteomics. *Journal of Proteomics*, *79*, 263–276. https://doi.org/10.1016/j.jprot.2012.12.019

Valverde, J. C., Rubilar, R. A., Medina, A., Pincheira, M., Emhart, V., Espinoza, Y., Bozo, D., & Campoe, O. C. (2025). Transpiration and Water Use Efficiency of Mediterranean Eucalyptus Genotypes Under Contrasting Irrigation Regimes. *Plants*, *14*(14). https://doi.org/10.3390/plants14142232

Vicente-Serrano, S. M., Quiring, S. M., Peña-Gallardo, M., Yuan, S., & Domínguez-Castro, F. (2020). A review of environmental droughts: Increased risk under global warming? In *Earth-Science Reviews* (Vol. 201). Elsevier B.V. https://doi.org/10.1016/j.earscirev.2019.102953

Vieira Dos Santos, C., & Rey, P. (2006). Plant thioredoxins are key actors in the oxidative stress response. *Trends in Plant Science*, *11*(7), 329–334. https://doi.org/10.1016/j.tplants.2006.05.005

Villar, E., Klopp, C., Noirot, C., Novaes, E., Kirst, M., Plomion, C., & Gion, J. M. (2011). RNA-Seq reveals genotype-specific molecular responses to water deficit in eucalyptus. *BMC Genomics*, *12*. https://doi.org/10.1186/1471-2164-12-538

Virtuoso, M. C. S., Souza, J. V. O., Zanatto, B., Valente, T. S., Silva, E. H. C., & de Paula, R. C. (2022). Germinative and physiological performance of eucalyptus species under abiotic stress. *Trees, Forests and People*, *10*. https://doi.org/10.1016/j.tfp.2022.100348

Wang, J., Xu, R., & Yang, S. (2009a). Estimation of plant water content by spectral absorption features centered at 1,450 nm and 1,940 nm regions. *Environmental Monitoring and Assessment*, *157*(1–4), 459–469. https://doi.org/10.1007/s10661-008-0548-3

Wang, J., Xu, R., & Yang, S. (2009b). Estimation of plant water content by spectral absorption features centered at 1,450 nm and 1,940 nm regions. *Environmental Monitoring and Assessment*, *157*(1–4), 459–469. https://doi.org/10.1007/s10661-008-0548-3

Wang, L., Hunt, E. R., Qu, J. J., Hao, X., & Daughtry, C. S. T. (2011). Estimating dry matter content of fresh leaves from the residuals between leaf and water reflectance. *Remote Sensing Letters*, *2*(2), 137–145. https://doi.org/10.1080/01431161.2010.503973

Warren, C. R., Aranda, I., & Cano, F. J. (2011a). Responses to water stress of gas exchange and metabolites in Eucalyptus and Acacia spp. *Plant, Cell and Environment*, *34*(10), 1609–1629. https://doi.org/10.1111/j.1365-3040.2011.02357.x

Warren, C. R., Aranda, I., & Cano, F. J. (2011b). Responses to water stress of gas exchange and metabolites in Eucalyptus and Acacia spp. *Plant, Cell and Environment*, *34*(10), 1609–1629. https://doi.org/10.1111/j.1365-3040.2011.02357.x

Wold, S., Esbensen, K., & Geladi, P. (n.d.). *Principal Component Analysis*.

Workman, Jerry., & Weyer, Lois. (2012). *Practical guide and spectral atlas for interpretive near-infrared spectroscopy*. CRC Press.

Xie, Y., Plett, D., & Liu, H. (2021). The Promise of Hyperspectral Imaging for the Early Detection of Crown Rot in Wheat. *AgriEngineering*, *3*(4), 924–941. https://doi.org/10.3390/agriengineering3040058

Ye, N., Zhong, S., Fang, Z., Gao, H., Du, Z., Chen, H., Yuan, L., & Pan, T. (2022). Performance Improvement of NIR Spectral Pattern Recognition from Three Compensation Models' Voting and Multi-Modal Fusion. *Molecules*, *27*(14). https://doi.org/10.3390/molecules27144485

Zade, S. V., & Abdollahi, H. (2024). Evaluation of Classical Least Squares Discriminant Analysis (CLS-DA) as a Novel Supervised Pattern Recognition Technique. *Journal of Chemometrics*. https://doi.org/10.1002/cem.3609

Zahir, S. A. D. M., Omar, A. F., Jamlos, M. F., Azmi, M. A. M., & Muncan, J. (2022). A review of visible and near-infrared (Vis-NIR) spectroscopy application in plant stress detection. In *Sensors and Actuators A: Physical* (Vol. 338). Elsevier B.V. https://doi.org/10.1016/j.sna.2022.113468

Zahra, N., Hafeez, M. B., Kausar, A., Al Zeidi, M., Asekova, S., Siddique, K. H. M., & Farooq, M. (2023a). Plant photosynthetic responses under drought stress: Effects and management. In *Journal of Agronomy and Crop Science*. John Wiley and Sons Inc. https://doi.org/10.1111/jac.12652

Zahra, N., Hafeez, M. B., Kausar, A., Al Zeidi, M., Asekova, S., Siddique, K. H. M., & Farooq, M. (2023b). Plant photosynthetic responses under drought stress: Effects and management. In *Journal of Agronomy and Crop Science*. John Wiley and Sons Inc. https://doi.org/10.1111/jac.12652

Zhu, J. K. (2016). Abiotic Stress Signaling and Responses in Plants. In *Cell* (Vol. 167, Number 2, pp. 313–324). Cell Press. https://doi.org/10.1016/j.cell.2016.08.029

Zhuang, J., Wang, Y., Chi, Y., Zhou, L., Chen, J., Zhou, W., Song, J., Zhao, N., & Ding, J. (2020). Drought stress strengthens the link between chlorophyll fluorescence parameters and photosynthetic traits. *PeerJ*, *8*. https://doi.org/10.7717/peerj.10046

4.9. Supplementary materials

Table S4.1. Species, genotypes, sampling days, number of plants and total HSI obtained during the experimental period. Where C: control plants irrigated continuously and WD: plants subjected to water deficit.

		Sampling days					
		Ramets analysed			Images obtained		
Species	***Genotype***	D3	D7	D10	D3	D7	D10
E. globulus	G1	3C / 3WD	3C / 3WD	3C / 3WD	12C / 12WD	12C / 12WD	12C / 12WD
	G2	3C / 3WD	3C / 3WD	3C / 3WD	12C / 12WD	12C / 12WD	12C / 12WD
***E.* gloni**	G3	3C / 3WD	3C / 3WD	3C / 3WD	12C / 12WD	12C / 12WD	12C / 12WD
	G4	3C / 3WD	3C / 3WD	3C / 3WD	12C / 12WD	12C / 12WD	12C / 12WD
Ramets/images per day		24	24	24	96	96	96
Total Ramets/images			72			288	

Table S4.2. ANOVA analysis, with significance $p<0.05$, of mean masses (g) and mean heights (cm) of seedlings in control condition and seedlings in water deficit stress condition. Comparison between C plants and WD plants on days D3, D7 and D10 for genotypes G1, G2, G3 and G4. Where SS: sum of squares, DF: degrees of freedom and MS: root mean square.

ANOVA table	**SS**	**DF**	**MS**	**P value**
Genotype G1 - Mass				
Sampling Day	1084	2	542.2	P=0,0056
Control-Stress	9339	1	9339	P<0,0001
Genotype G1 - Height				
Sampling Day	21	2	10.5	P=0,0635
Control-Stress	0	1	0	P>0,9999
Genotype G2 - Mass				
Sampling Day	63	2	31.5	P=0,1152
Control-Stress	80.22	1	80.22	P=0,0244
Genotype G2 - Height				
Sampling Day	619	2	309.5	P=0,0384
Control-Stress	5904	1	5904	P<0,0001
Genotype G3 - Mass				
Sampling Day	1024	2	512.1	P=0,0329
Control-Stress	9293	1	9293	P<0,0001
Genotype G3 - Height				
Sampling Day	16.78	2	8.389	P=0,4205
Control-Stress	0.2222	1	0.2222	P=0,8778
Genotype G4 - Mass				
Sampling Day	2172	2	1086	P=0,0001
Control-Stress	8580	1	8580	P<0,0001

Genotype G4 - Height				
Sampling Day	1.333	2	0.6667	P=0,7703
Control-Stress	10.89	1	10.89	P=0,0589

Table S4.3. ANOVA with significance p<0.05, of vegetation indices NDVI, PRI and MCARI. Comparison between C plants and WD plants on days D3, D7 and D10 for genotypes G1, G2, G3 and G4. Where SS: sum of squares, DF: degrees of freedom and MS: root mean square.

ANOVA table	**SS**	**DF**	**MS**	**P value**
Genotype G1 - NDVI				
Sampling Day	0.0008548	2	0.0004274	P=0,4458
Control-Stress	0.00045	1	0.00045	P=0,3588
Genotype G2 - NDVI				
Sampling Day	0.000688	2	0.000344	P=0,6815
Control-Stress	0.0002722	1	0.0002722	P=0,5860
Genotype G3 - NDVI				
Sampling Day	0.001381	2	0.0006905	P=0,1816
Control-Stress	0.0001027	1	0.0001027	P=0,5979
Genotype G4 - NDVI				
Sampling Day	0.007362	2	0.003681	P=0,0176
Control-Stress	0.0002067	1	0.0002067	P=0,5800
Genotype G1 - PRI				
Sampling Day	0.00003879	2	0.00001939	P=0,5523
Control-Stress	0.0001786	1	0.0001786	P=0,0337
Genotype G2 - PRI				
Sampling Day	0.00006758	2	0.00003379	P=0,8041
Control-Stress	0.0006116	1	0.0006116	P=0,0681
Genotype G3 - PRI				
Sampling Day	0.0003202	2	0.0001601	P=0,1359
Control-Stress	0.0001591	1	0.0001591	P=0,1510
Genotype G4 - PRI				
Sampling Day	0.00007683	2	0.00003842	P=0,0961
Control-Stress	0.00008645	1	0.00008645	P=0,0260
Genotype G1 - MCARI				
Sampling Day	0.00956	2	0.00478	P=0,2387
Control-Stress	0.01896	1	0.01896	P=0,0263
Genotype G2 - MCARI				
Sampling Day	0.003816	2	0.001908	P=0,4584
Control-Stress	0.07979	1	0.07979	P<0,0001
Genotype G3 - MCARI				
Sampling Day	0.008031	2	0.004015	P=0,3498
Control-Stress	0.06941	1	0.06941	P=0,0008
Genotype G4 - MCARI				
Sampling Day	0.002269	2	0.001134	P=0,7369
Control-Stress	0.01105	1	0.01105	P=0,1062

Table S4.4. Multiple comparison analysis, Tukey's test, with significance p<0.05, for NDVI, PRI and MCARI vegetation indices of C plants and plants in WD. Where DM: difference of means and Sumary: indicates the significance of the difference in hierarchical levels, a single asterisk (*) indicates a lower level of significance, while two asterisks (**) indicate a higher level of significance.

Tukey's multiple comparisons test	DM	Summary	Adjusted P Value
G3-NDVI			
Day 03:Control plants vs. Day 10:Control plants	-0.071	**	0.0057
Day 10:Control plants vs. Day 10:Stressed plants	0.06933	**	0.0069
G4-NDVI			
Day 03:Stressed plants vs. Day 07:Stressed plants	0.08033	*	0.0204
G4-PRI			
Day 03:Control plants vs. Day 10:Control plants	0.01573	**	0.0021
Day 07:Control plants vs. Day 10:Control plants	0.01149	*	0.0221
Day 07:Stressed plants vs. Day 10:Control plants	0.01474	**	0.0036
Day 10:Control plants vs. Day 10:Stressed plants	0.01676	**	0.0012
G2-MCARI			
Day 03:Control plants vs. Day 03:Stressed plants	-0.1367	*	0.0396
Day 03:Control plants vs. Day 07:Stressed plants	-0.159	*	0.0151
Day 03:Stressed plants vs. Day 10:Control plants	0.1443	*	0.0285
Day 03:Stressed plants vs. Day 10:Control plants	0.1443	*	0.0285
Day 07:Stressed plants vs. Day 10:Control plants	0.1666	*	0.0109
G3-MCARI			
Day 03:Control plants vs. Day 10:Stressed plants	-0.1815	*	0.0255
Day 07:Control plants vs. Day 10:Stressed plants	-0.2135	**	0.0084
Day 10:Control plants vs. Day 10:Stressed plants	-0.2396	**	0.0034

Table S4.5. Confusion matrices and figures of merit of PLS-DA, SVM-DA and KNN classification models. ***Er****:* error rate, ***Ac****:* accuracy, ***Sn****:* sensitivity and ***Sp****:* specificity.

	PLS-DA						***SVM-DA***						***KNN***					
	Training Set			Validation Set			Actual class			Validation Set			Training Set			Validation Set		
	Actual class																	
Predicted	D3	D7	D10	D3	D7	D10	D3	D7	D10	D3	D7	D10	D3	D7	D10	D3	D7	D10
D3	32	0	0	16	0	0	32	0	0	16	0	0	32	0	0	15	0	0
D7	0	32	0	0	16	0	0	32	0	0	16	0	0	31	0	0	16	0
D10	0	0	32	0	0	16	0	0	32	0	0	16	0	1	32	1	0	16
Unassigned	0	0	0	0	0	0	0	0	0	0	0	0	0	0	0	0	0	0
Er	0.00	0.00	0.00	0.00	0.00	0.00	0.00	0.00	0.00	0.00	0.00	0.00	0.00	0.01	0.01	0.02	0	0.02
Ac	1.00	1.00	1.00	1.00	1.00	1.00	1.00	1.00	1.00	1.00	1.00	1.00	1.00	0.99	0.99	0.97	1.00	0.99
Sn	1.00	1.00	1.00	1.00	1.00	1.00	1.00	1.00	1.00	1.00	1.00	1.00	1.00	0.97	1.00	0.94	1.00	1.00
Sp	1.00	1.00	1.00	1.00	1.00	1.00	1.00	1.00	1.00	1.00	1.00	1.00	1.00	1.00	0.98	1.00	1.00	0.97

Figure S4.1. Comparisons between D3, D7 and D10 of mean masses (g) (a) and mean heights (cm) (b) of genotypes G1, G2, G3 and G4 including plants in control condition (C: dark green bars) and plants in water deficit stress condition (WD: light green bars). Letters above the bars indicate groups with significant differences *(p<0.05)*. Data are expressed as mean ± standard error.

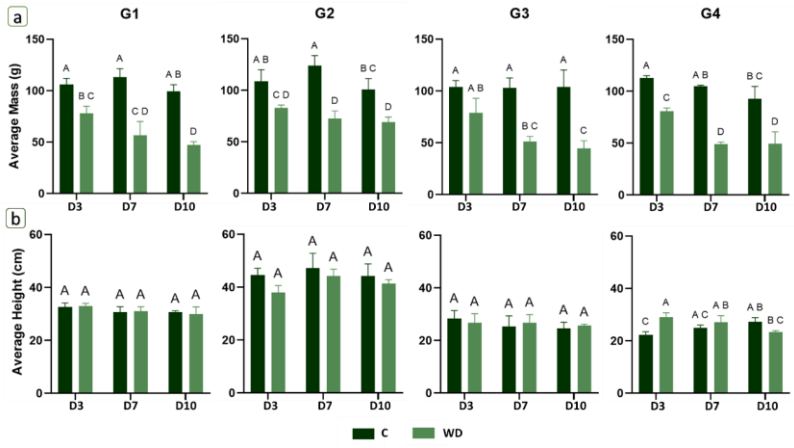

Figure S4.2. Comparisons between D3, D7 and D10 of NDVI (a), PRI (b) and MCARI (c) indices of genotypes G1, G2, G3 and G4 including plants in control condition (C: dark green bars) and plants under water deficit stress condition (WD: light green bars). Letters above the bars indicate groups with significant differences (p<0.05). Data are expressed as mean ± standard error.

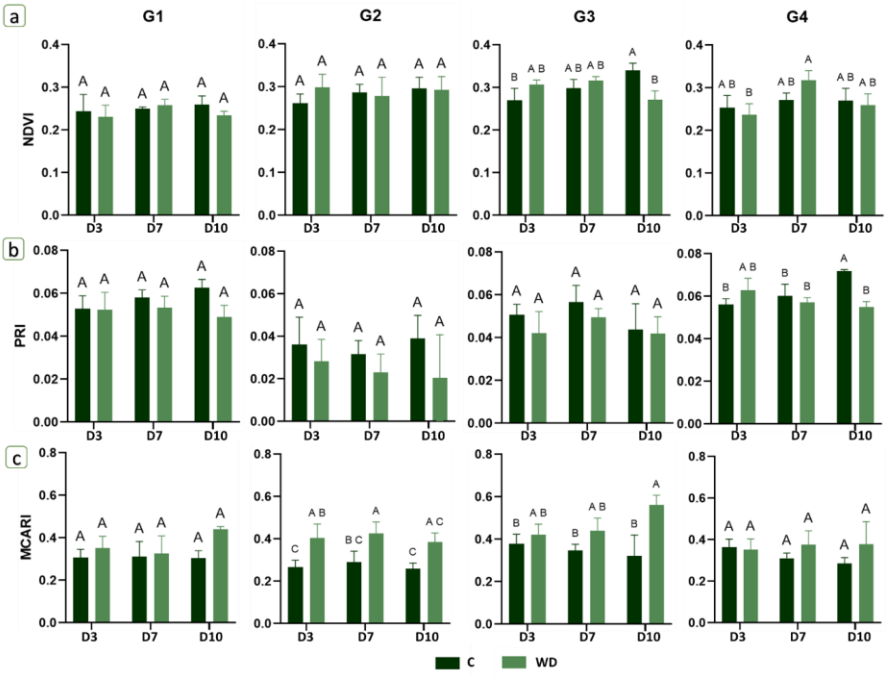

Figure S4.3. PCA of mean spectra of different plant zones (apex, leaves, stem and whole plant) pretreated with second derivative, 11-point window and centered on the mean.

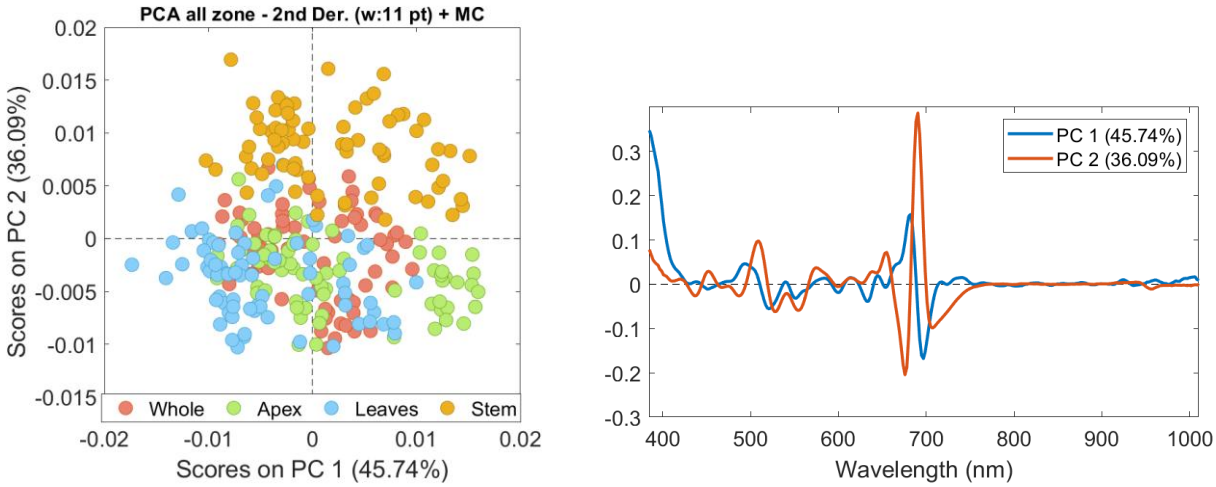

Figure S4.4. Plots of scores and loadings for PCAs corresponding to G1 and G3, pretreated with the second derivative of absorbance, smoothed with a 15-point window and mean center, with higher percentage of variance explained in mean spectra of whole plants, where: A) plot of G1 scores, B) plot of G1 loadings, C) plot of G3 scores and D) plot of G3 loadings.

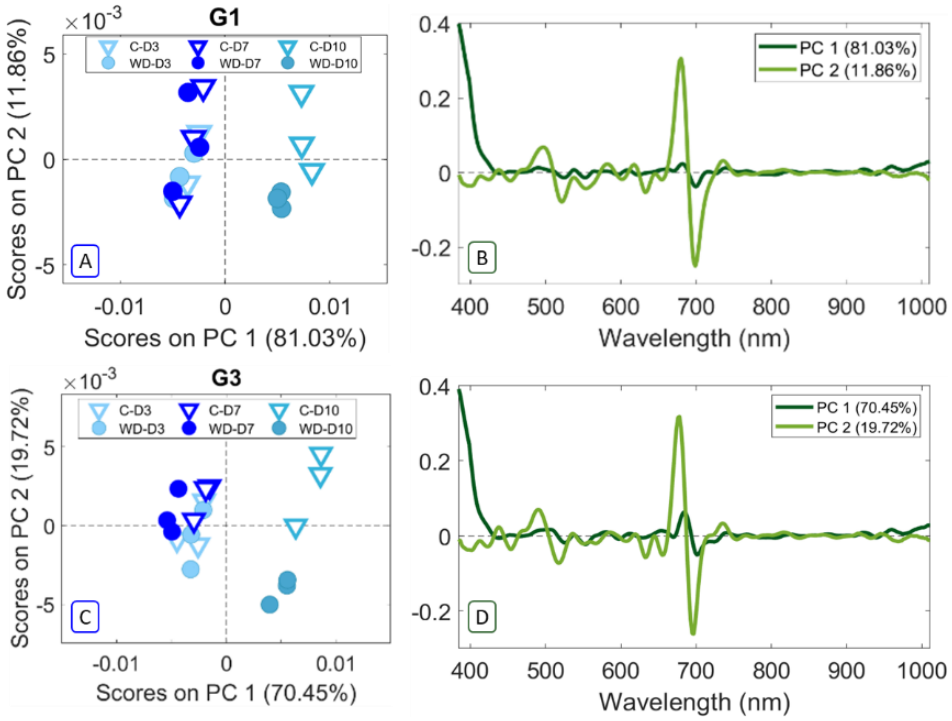

Figure S4.5. PCA of mean spectra of whole-plant matrix clipped wavelengths from 420 to 1010 nm.

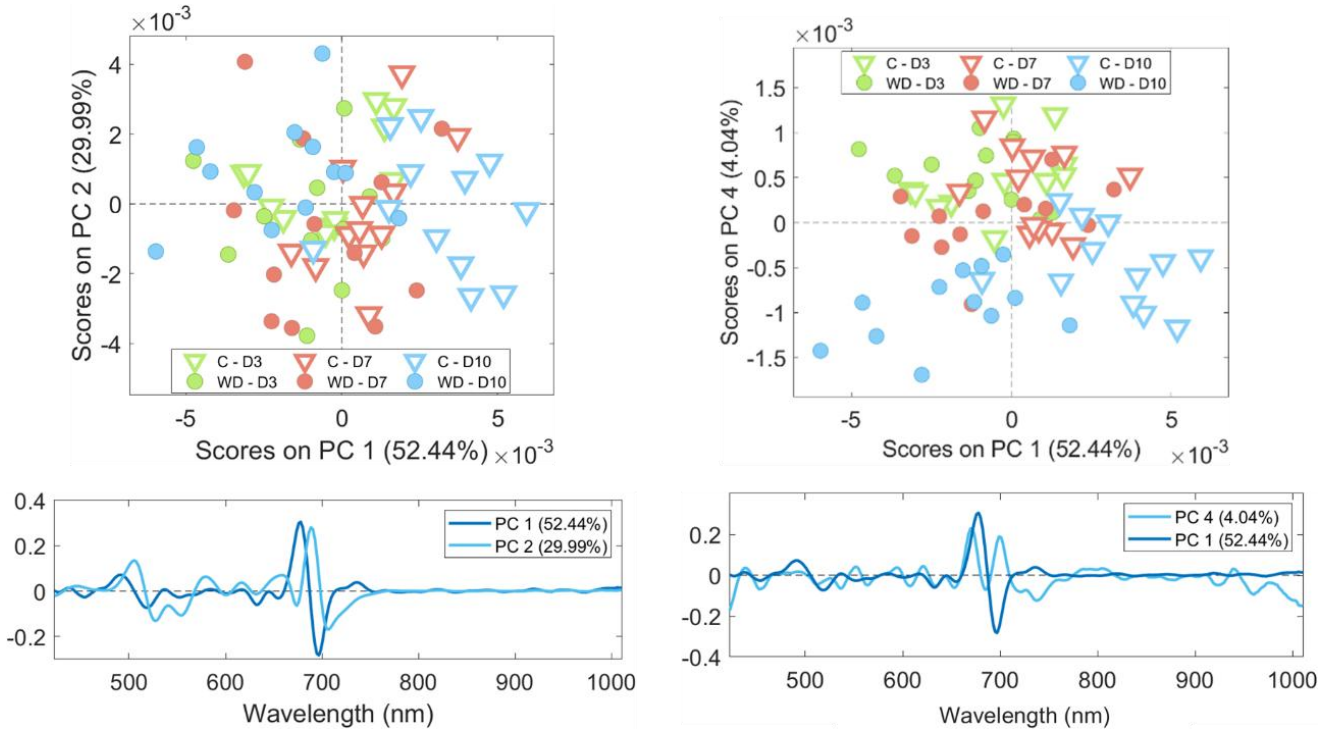

Chapter 5
ASCA-guided hierarchical spectral classification of water deficit in *Eucalyptus* spp. using VIS–NIR hyperspectral imaging and portable NIR spectroscopy

This chapter contributes primarily to Specific Objective 3 and provides partial contributions to Specific Objectives 1 and 2. The expanded experimental assay was used to evaluate complementary spectral information obtained by VIS–NIR hyperspectral imaging and portable NIR spectroscopy (Specific Objective 2), while ANOVA–simultaneous component analysis (ASCA) was used to determine the relative contribution of genotype, sampling day, treatment condition, and experimental replication to spectral variability, thereby supporting the evaluation of the experimental and analytical design (Specific Objective 1). Based on this variance structure, direct and hierarchical supervised classification strategies were developed and externally validated for water-status discrimination and progressive water-deficit classification, directly addressing Specific Objective 3.

This section presents and discusses the results that formed the basis of the manuscript *"ASCA-guided ASCA-guided hierarchical spectral classification of water deficit in Eucalyptus spp. using VIS–NIR hyperspectral imaging and portable NIR spectroscopy"*, submitted to journal Chemometrics and Intelligent Laboratory Systems. Manuscript number: CHEMOLAB-D-26-00968.

These results were presented at the following conferences:

"Spectral evaluation of *Eucalyptus* spp. under water deficit using HSI (VIS-NIR) and near-infrared spectroscopy: an ASCA-based approach." 22nd International Conference on Near Infrared Spectroscopy (NIR2025), 8–12 June 2025, Rome, Italy. Poster presentation.

"Análisis de componentes simultáneos ANOVA (ASCA) y espectroscopía HSI (VIS-NIR) para la clasificación jerárquica de la respuesta de *Eucalyptus* spp. al déficit hídrico." XXXV Jornadas Chilenas de Química, 13–16 January 2026, Concepción, Chile. Poster presentation.

ASCA-guided hierarchical machine learning for spectral water-deficit monitoring in *Eucalyptus* using hyperspectral imaging and portable NIR spectroscopy

Pamela Sanhueza-Novoa[1], Marta Fernández[2], Carolina Hernández-Fuentes[3], José Manuel Amigo[4,5], Jesús Mellado Castro[3], Macarena Rojas-Rioseco[1] and Rosario del P. Castillo[1,*]

[1] Laboratory of Biospectroscopy and Chemometrics, Biotechnology Center & Faculty of Pharmacy, University of Concepción, Chile.

[2] Laboratory of Forest Genomics, Biotechnology Center & Faculty of Forestry Sciences, University of Concepción, Chile.

[3] Bioforest S.A., km 15 road to Coronel, Chile.

[4] Department of Analytical Chemistry, University of the Basque Country UPV/EHU, 48080, Bilbao, P.O. Box 644, Basque Country, Spain.

[5] IKERBASQUE, Basque Foundation for Science, 48011, Bilbao, Spain.

*Corresponding author: rosariocastillo@udec.cl

5.1. Abstract

Drought limits Eucalyptus productivity and adaptation, requiring rapid, non-destructive tools to monitor water-deficit responses in complex plant material. Spectral sensing is promising, but interpretation is often affected by overlapping sources of variation, including genotype, sampling day and irrigation regime. Here, visible–near infrared hyperspectral imaging (VIS–NIR HSI, 400–1000 nm) and portable near-infrared spectroscopy (NIR, 1400–2400 nm) were combined with machine-learning benchmarking and ANOVA–simultaneous component analysis (ASCA) to develop an interpretable workflow for water-deficit monitoring in young *Eucalyptus* plants under controlled environmental conditions.

Six genotypes subjected to control and water-deficit regimes were monitored over four sampling days. Partial least squares-discriminant analysis (PLS-DA), support vector machine classification (SVM-C), Random Forest (RF) and Extreme Gradient Boosting (XGBoost) were benchmarked for binary water-status classification and multiclass stress-progression discrimination. Binary classification was effective for both datasets, whereas direct multiclass performance decreased, indicating spectral overlap among progressive water-deficit stages. ASCA revealed contrasting spectral domains: VIS–NIR HSI variability was dominated by genotype (30.2%), whereas portable NIR was mainly structured by sampling day (40.2%) and treatment condition (10.6%). This variance structure was translated into ASCA-guided hierarchical workflows. For VIS–NIR HSI, the hierarchy incorporated genotype group, water status and stress progression, achieving complete correct classification in external validation (CA = 1.000). For portable NIR, the SVM-C hierarchy provided the most balanced external-validation behaviour, with macro-averaged Sn = 0.778, Sp = 0.861, precision = 0.765 and Err = 0.181. Overall, the proposed workflow supports interpretable spectral decision-making for controlled-environment screening and future precision forestry applications.

Keywords: *Eucalyptus* spp.; Water-deficit monitoring; VIS–NIR hyperspectral imaging; Portable NIR spectroscopy; Interpretable machine learning; ASCA-guided hierarchical classification; Precision forestry.

5.2. Introduction

Water deficit is one of the most critical abiotic stresses limiting forest productivity, particularly under the scenario of climate change, where drought events are predicted to become more frequent and severe (Allen et al., 2010; Hartmann et al., 2025; Vicente-Serrano et al., 2020). *Eucalyptus* spp., widely planted across different regions of the world, exhibit a broad genetic variability in their tolerance to water stress (Ammitzboll et al., 2020; Cursi et al., 2024; Valverde et al., 2025). Understanding and characterizing this variability is essential for breeding programs and for designing sustainable forest management strategies.

From the perspective of smart agricultural and forestry monitoring, water deficit in forest plant material represents a complex multivariate sensing problem. The spectral response of plants is not governed by a single physiological process, but by the simultaneous contribution of water-related absorption features, pigment composition, tissue structure, genotype-dependent traits and time-dependent responses to stress. Therefore, non-destructive spectral sensors must be coupled with data-driven models capable not only of detecting water deficit, but also of identifying whether the observed spectral variation is mainly driven by irrigation condition, genotype, sampling days or their overlap. This distinction is essential for transforming high-dimensional spectral measurements into interpretable decision-support information for controlled-environment screening and future precision forestry applications.

Spectroscopic techniques, such as visible–near infrared (VIS-NIR) reflectance and hyperspectral imaging (HSI), have emerged as powerful, non-destructive tools to monitor physiological and biochemical changes in plants under stress conditions. Their ability to capture subtle variations related to pigments, water content, and structural properties of tissues has been widely demonstrated in agricultural and food systems (Behmann et al., 2014a; Ram et al., 2024). Near-infrared spectroscopy (NIRS), in particular, has been extensively applied in crop quality assessment due to its speed, minimal sample preparation, and environmentally friendly nature (Angel Prieto Lage et al., 2022). Similarly, HSI integrates spectral and spatial information, providing a detailed description of within-leaf and canopy heterogeneity (Sanhueza-Novoa et al., 2026).

VIS–NIR hyperspectral imaging and portable NIR spectroscopy are particularly attractive for smart monitoring because they enable rapid, non-destructive and reagent-free acquisition of high-dimensional spectral fingerprints. VIS–NIR HSI provides spatially resolved information related to pigments, leaf structure and canopy-level heterogeneity, whereas portable NIR spectroscopy offers a simpler and more flexible alternative that is highly sensitive to water-related absorption bands. Recent studies in smart agricultural sensing have demonstrated the feasibility of integrating optical sensors, data processing and machine-learning models for water-stress monitoring. For example, Kuang et al., (2026) systematically compared RF, XGBoost and SVM for water-stress identification using UAV-based multi-source remote sensing data, while Rojek et al., (2023) proposed a multi-sensor imaging system for redundant water-stress detection in greenhouse conditions. These developments indicate that the main challenge is no longer only to acquire spectral data, but to convert sensor outputs into robust, interpretable and operational classification workflows.

Building on this, we previously demonstrated that VIS–NIR HSI can robustly discriminate water-deficit levels in *Eucalyptus* using spectral fingerprints and chemometric modelling (Sanhueza-Novoa et al., 2026). However, moving from discrimination of stress levels to biologically interpretable and transferable phenotyping requires explicitly accounting for additional sources of spectral variability that are intrinsic to forest trees. In practice, the measured response reflects not only water availability, but also species and genotype effects, replicate-to-replicate variability, and time-dependent dynamics during drought imposition. If these components are not quantified, apparent treatment separation can be partially driven by genetic structure or individual heterogeneity, which limits mechanistic interpretation and generalization across plant materials. This issue is particularly relevant in spectral modelling, where high classification accuracy may be obtained even when the underlying spectral separation is influenced by confounding experimental factors. Thus, a robust spectral methodology should not only classify samples correctly but also provide evidence that the discriminant information is associated with the intended source of variation.

These considerations highlight the need for multivariate tools that go beyond predictive accuracy and explicitly reflect the experimental design. Exploratory approaches such as principal component analysis (PCA) summarize dominant directions of variance (Jolliffe & Cadima,

2016), whereas supervised classifiers such as partial least squares-discriminant analysis (PLS-DA) and support vector machine classification (SVM-C) are widely used to discriminate predefined classes in plant spectroscopy and remote sensing applications (El Azizi et al., 2024; Mountrakis et al., 2011; Peerbhay et al., 2013). However, neither strategy directly partitions the spectral response into contributions associated with water treatment, genotype, sampling day and their interactions. Consequently, high classification performance alone does not reveal which experimental factor drives the observed spectral shifts, nor whether those shifts are stable across genotypes and replicates. The central modelling challenge is therefore to complement prediction with a design-aware decomposition of the spectral matrix into interpretable sources of variation.

In parallel, machine-learning benchmarking is necessary to determine whether spectral classification performance depends on the selected algorithm and on the complexity of the prediction task. For this purpose, classifiers representing complementary modelling assumptions were compared: PLS-DA as a linear latent-variable method, SVM-C as a kernel-based approach, and Random Forest (RF) and Extreme Gradient Boosting (XGBoost) as tree-based ensemble methods. RF combines multiple decision trees built from randomized subsets of samples and variables, improving classification robustness and providing estimates of variable importance (Belgiu & Drăgu, 2016; Breiman, 2001). XGBoost is a scalable gradient-boosted tree algorithm designed to capture nonlinear relationships through sequential model optimization (Chen & Guestrin, 2016). Both ensemble approaches have recently been applied in smart agricultural modelling, including water-stress classification and crop-performance prediction using sensor-derived variables (Kuang et al., 2026; Sánchez et al., 2025). Therefore, comparing PLS-DA, SVM-C, RF and XGBoost provides a suitable benchmark to evaluate whether water-status and stress-severity discrimination is model-dependent and whether direct classification remains stable as the number of classes increases.

To address this challenge, the Analysis of Variance–Simultaneous Component Analysis (ASCA) framework has been developed (Jansen et al., 2005). ASCA combines the strengths of ANOVA and component analysis, allowing the decomposition of multivariate data according to the effects of interest while maintaining interpretability of the underlying spectral patterns. Unlike PCA, ASCA explicitly links the factorial structure of the experiment to a multivariate response (here, spectral matrices), enabling variance partitioning into main effects and interactions while

retaining interpretable component patterns. Specifically, it can formally separate the variability in response across the different samples into the various contributions to the experimental design (Bertinetto et al., 2020). Since its introduction, ASCA has been applied in diverse fields including metabolomics, food quality control, and plant science (Ezenarro et al., 2025). For instance, Freitag et al., (2024) demonstrated the ability of NIR coupled with ASCA to disentangle regional and annual effects on wheat composition, highlighting its robustness and sensitivity to preprocessing methods. Therefore, ASCA provides a suitable chemometric framework for analytical studies in which spectral variation is structured by multiple experimental factors and where interpretability is as important as prediction.

A targeted Web of Science screening (2020–2026) using combinations of keywords related to spectral phenotyping, drought, ASCA, HSI, and NIR was used to contextualize the present approach. The retrieved records mainly clustered around plant physiology under water stress, spectroscopy/remote sensing, and multivariate or machine-learning modelling (Figure S1). Within this landscape, studies explicitly combining design-aware variance decomposition (ASCA) with VIS–NIR HSI and portable NIR for drought phenotyping in *Eucalyptus* spp. appear to be scarce. More importantly, most available approaches are based either on spectral classification or on physiological interpretation, whereas fewer studies integrate experimental design decomposition, multimodal spectral acquisition and supervised modelling into a single analytical workflow. This gap limits the development of transferable spectroscopic methodologies for complex biological matrices, where spectral fingerprints are strongly affected by genotype, time and treatment effects.

In the context of forest trees, the integration of ASCA with VIS-NIR HSI and portable NIR spectroscopy provides a rigorous pathway for evaluating spectral responses under water deficit conditions, while explicitly accounting for multifactorial experimental structures. Beyond early stress detection, this framework divides spectral variability into components associated with water deficit, sampling day and variability between genotypes and their replicates, while capturing their interactions, thus revealing which factors robustly drive spectral changes. This design-aware strategy is analytically relevant because it allows the spectral information to be evaluated in terms of variance sources, model interpretability and robustness, rather than relying exclusively on global classification performance.

Accordingly, this study proposes an interpretable spectral machine-learning workflow for non-destructive water-deficit monitoring in young *Eucalyptus* plants under controlled environmental conditions. First, VIS–NIR HSI and portable NIR spectroscopy were used to acquire complementary spectral information from plants subjected to controlled irrigation and water-deficit conditions. Second, four supervised classification models, namely PLS-DA, SVM-C, RF and XGBoost, were benchmarked for binary water-status classification and multiclass stress-severity discrimination. Third, ASCA was used as a design-aware diagnostic tool to identify the dominant sources of spectral variability associated with genotype, sampling day and treatment condition. Finally, the ASCA-derived variance structure was translated into hierarchical classification workflows and compared with direct classification strategies. By integrating spectral sensing, machine-learning benchmarking and ASCA-guided hierarchical modelling, this work aims to support the development of interpretable decision tools for controlled-environment plant screening and future precision forestry applications.

5.3. Materials and methods

5.3.1. Plant material and water deficit assay

The experiment was conducted using 126 six-month-old rooted plants donated by the Scientific Research Center BIOFOREST S.A. Arauco (Chile), one genotype (G1) corresponding to *Eucalyptus globulus*, and the other five (G2, G3, G4, G5 and G6) hybrids between *Eucalyptus nitens* × *Eucalyptus globulus* (GloNi) (Ibarra et al., 2023). Each genotype was represented by eighteen plants that were randomly placed in a tray. The biological assay was designed to generate a structured spectral dataset containing controlled sources of variation associated with genotype, sampling days, replicate variability, and irrigation condition.

Plants were maintained under controlled conditions in a growth chamber, following the parameters evaluated by Fernández et al., (2012) and Sanhueza-Novoa et al., (2026), corresponding to a summer photoperiod of 14 hours of light (>150 µmol photons $m^{-2}s^{-1}$) and 10 hours of darkness, day temperature of 22±1 °C, night temperature of 16±1 °C and humidity of 60-70%. The plants underwent a 30-day acclimation period under constant irrigation. At day 30, the experiment was divided into two treatments: control plants (C), which remained continuously

irrigated, and water-deficit plants (WD), for which irrigation was withheld for the following 12 days (Figure 5.1). Control plants were sampled at day 30 (T0-C), day 34 (T1-C), day 38 (T2-C), and day 42 (T3-C), whereas WD plants were sampled at day 34 (T1-WD), day 38 (T2-WD), and day 42 (T3-WD), corresponding to 4, 8, and 12 days after irrigation withdrawal. T1-WD, T2-WD, and T3-WD were considered to represent mild, moderate, and severe stress levels, respectively. At each sampling point, physiological measurements, multispectral analyses, and image acquisition were performed using three clones per genotype. This factorial structure was subsequently used to guide the chemometric decomposition of spectral variability by ASCA and the development of supervised classification models.

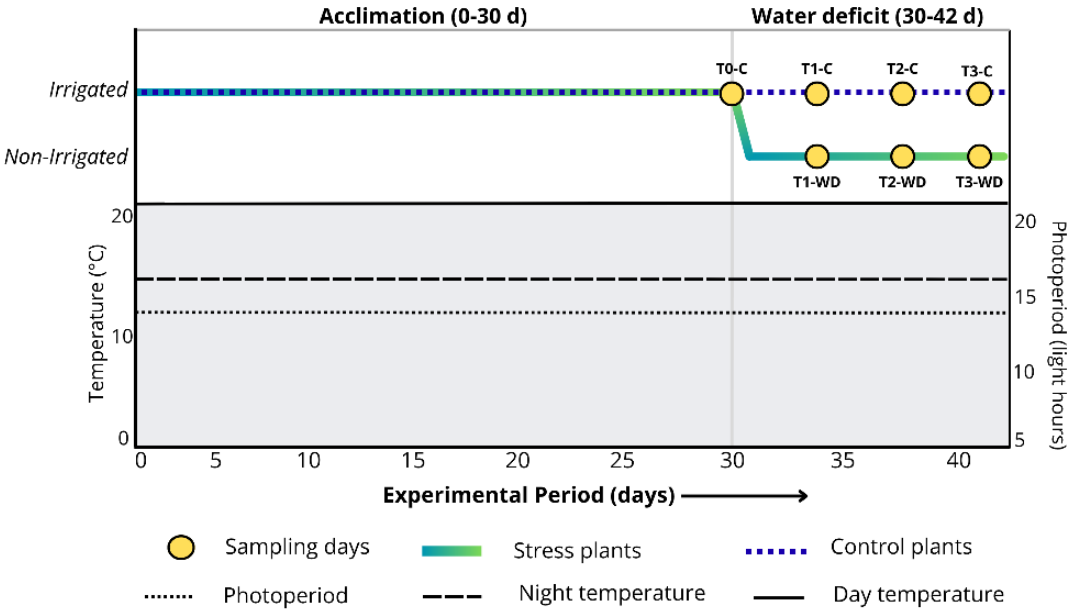

Figure 5.1 Acclimation, irrigation, non-irrigation and sampling stages of control and stressed plants throughout the experimental period. The figure shows the temperature variations during the day and night, as well as the photoperiod and sampling points.

5.3.2. Spectral acquisition and construction of analytical data matrices

During the experiment, HSI were acquired using a Pika-L Resonon hyperspectral camera (Resonon Inc., Bozeman, MT, USA) operating in the spectral range of 400–1000 nm. Images

were collected in diffuse reflectance mode using Spectronon PRO software. Although the raw wavelength vector exported by the acquisition software covered approximately 385–1010 nm and included 300 wavelength variables, only the spectral region within the nominal operating range of the camera was retained for subsequent analysis. After this spectral trimming, 287 wavelength variables were used. The system had a spectral sampling interval of approximately 2.1 nm, a spectral resolution of 2.7 nm, and 900 spatial pixels per line.

Independent hyperspectral images were acquired from whole plants for each genotype (G1–G6) under the two irrigation conditions, well-irrigated control plants (C) and water-deficit plants (WD), at the corresponding sampling days (T0, T1, T2, and T3). A total of 126 hyperspectral images were obtained. For each image, the analytical region corresponding to plant tissue was isolated to avoid the inclusion of background pixels in the spectral matrix. Background removal was performed using an unsupervised k-means clustering algorithm. After defining the regions of interest (ROI), the mean spectrum of each plant was extracted and compiled into the VIS–NIR HSI data matrix (M1), with dimensions of 126 × 287, where rows corresponded to individual plants and columns to the retained wavelength variables. These procedures were performed using the Hyper-Tools v.3.0 graphical user interface (GUI) developed by Mobaraki & Amigo (2018). Thus, M1 represented the whole-plant VIS–NIR hyperspectral dataset, summarizing the average spectral fingerprint of each plant after ROI segmentation and spectral range selection.

In parallel, spectra in the NIR region were acquired from the leaves of the third and/or fourth whorl of each plant using a NanoQuest 2.5 portable spectrometer (Ocean Insight, Orlando, FL, USA). The instrument was connected to an OceanOptics HL-2000-FHSA halogen light source and a fiber-optic reflectance probe. Spectra were collected in diffuse reflectance mode between 1400 and 2400 nm, with a spectral resolution of 8 nm and a scan time of 0.5 s. A total of 1249 spectra were recorded and compiled using NanoQuest software version 6.1 (Ocean Insight Inc.), generating a spectral matrix (M2) with dimensions of 1249 × 118, where rows corresponded to individual spectral measurements and columns to wavelength variables. Unlike M1, which corresponded to whole-plant mean spectra extracted from hyperspectral images, M2 provided point-based leaf-level NIR information, allowing the comparison of two complementary spectral modalities with different spatial and spectral characteristics.

Both spectral datasets (M1 and M2) were transformed from reflectance to pseudo-absorbance according to $pA = -\log_{10}(R)$. This transformation was applied to express the spectral response in an absorbance-like scale and to facilitate the interpretation of bands associated with pigments, water-related absorptions, and tissue composition. Several preprocessing techniques were evaluated for exploratory analyses and supervised model development, including standard normal variate (SNV), multiplicative scatter correction (MSC), first and second derivatives, and mean centering. The preprocessing strategy was selected according to spectral interpretability, exploratory structure, and classification performance. All preprocessing and subsequent analyses were performed in MATLAB R2021a (MathWorks Inc., Natick, MA, USA) using the PLS_Toolbox 8.9.2 (Eigenvector Research Inc., Wenatchee, WA, USA).

5.3.3. Exploratory and design-aware chemometrics analysis

PCA was applied as an unsupervised exploratory tool to matrices M1 and M2 to identify general spectral trends, evaluate sample grouping, and detect possible anomalous observations. In this study, PCA was not used as the main inferential tool, but as an initial diagnostic step to inspect the structure of the spectral matrices before design-based variance decomposition and supervised modelling. Hotelling's T^2 and Q residuals were used to identify extreme or inconsistent observations before subsequent modeling.

ASCA was then applied as a variance-partitioning approach that combines ANOVA with Simultaneous Component Analysis, allowing the interpretation of main effects and interactions in multivariate spectral data. The purpose of ASCA was to decompose the spectral response according to the experimental design and to determine which factors contributed most strongly to the observed spectral variability. Four experimental factors were considered in the model: (F1) genotype, (F2) replicates, (F3) sampling days, and (F4) treatment condition (C or WD). The statistical significance of each effect and its interactions was evaluated by permutation testing (n = 1000), allowing a more robust attribution of variance to the experimental design. The ASCA results were then used to support the selection of relevant classification levels and to guide the construction of hierarchical supervised models.

5.3.4. Machine-learning bechmarking and ASCA-guided hierarchical modelling

To evaluate the predictive potential of both spectral datasets for water-deficit monitoring, four supervised classification algorithms were compared: PLS-DA, SVM-C, RF and XGBoost. These algorithms were selected to represent classical chemometric classification, kernel-based machine learning, and tree-based ensemble learning approaches commonly used for high-dimensional spectral and agricultural sensing data.

Matrices M1 and M2 were divided into calibration and external validation sets using a 70:30 ratio. The same calibration/validation partition was maintained across all classification algorithms to ensure a fair comparison of model performance. For M1, models were built using the mean spectra extracted from whole plants. For M2, the ten-point spectra acquired per leaf were first averaged into a single leaf-level spectrum for each plant and sampling day, and these mean spectra were used for classification.

Two direct classification tasks were evaluated for each spectral dataset. First, a binary water-status classification was performed to discriminate control plants from water-deficit plants. Second, a multiclass classification task was implemented to discriminate stress progression/severity classes. This second task was designed to evaluate whether the models could maintain predictive performance when the classification problem increased from two broad physiological conditions to more subtle and partially overlapping stress stages. In the binary classification tasks, T0-C was considered the reference control class, while T1-WD, T2-WD and T3-WD were grouped into a single WD class. In the multiclass tasks, the models were trained to discriminate four classes: T0-C, T1-WD, T2-WD and T3-WD.

For PLS-DA, the optimal number of latent variables (LVs) was selected by internal cross-validation using the calibration set, according to the minimum classification error. For SVM-C, models were built using the LIBSVM implementation with a C-SVC formulation and a radial basis function (RBF) kernel. The penalty parameter C and kernel parameter γ were optimized individually for each model by internal cross-validation. In multiclass problems, classification followed a one-vs-one strategy.

RF models were built as ensemble classifiers composed of multiple decision trees trained on bootstrap-resampled subsets of the calibration data. At each split, a random subset of spectral variables was considered, reducing correlation among trees and improving model robustness. The main RF parameters included the number of trees, the minimum leaf size, and the number of predictors randomly selected at each split. Out-of-bag prediction was enabled to provide an internal estimate of model behaviour. Variable importance was estimated from the RF model to support the interpretation of relevant spectral regions.

XGBoost models were implemented as gradient-boosted decision tree classifiers. In this approach, trees are sequentially combined to model nonlinear relationships between spectral variables and class labels. The main XGBoost settings included the tree booster, objective function, learning rate, maximum tree depth, number of boosting rounds and evaluation metric. Models were built using using the selected preprocessing strategy for each dataset and task, and were evaluated through internal cross-validation using a Venetian blinds scheme with 10 splits and one sample per blind, followed by external validation.

Model performance was evaluated from the confusion matrix by calculating sensitivity (Sn), specificity (Sp), classification error (Err), accuracy or correct classification rate (CA) and precision, according to Eqs. (1)–(5). (Ballabio & Consonni, 2013; Sokolova & Lapalme, 2009).

$$Sn = \frac{\mathrm{TP}}{\mathrm{TP+FN}} \tag{1}$$

$$Sp = \frac{\mathrm{TN}}{\mathrm{FP+TN}} \tag{2}$$

$$Err = 1 - \frac{(\mathrm{Sn+Sp})}{2} \tag{3}$$

$$CA = \frac{(\mathrm{TP+TN})}{(\mathrm{TP+FP+TN+FN})} \tag{4}$$

$$Precision = \frac{\mathrm{TP}}{\mathrm{TP+FP}} \tag{5}$$

Where true positive (TP) and true negative (TN) represent samples correctly assigned as belonging or not belonging, respectively, to a specific class. False positive (FP) and false negative (FN) represent samples erroneously assigned as belonging or not belonging, respectively, to a specific class (Munera et al., 2018). The final preprocessing strategies, selected model settings and complete class-wise calibration and external-validation metrics for the direct classification benchmark are provided in Table S5.2 of the Supplementary Material.

After direct model benchmarking, ASCA was used as a design-aware diagnostic step to support the construction of hierarchical classification workflows. The hierarchical strategy was intended to translate the experimental structure of the spectral data into sequential classification steps, reducing the complexity of direct multiclass discrimination and improving the interpretability of model decisions. For each spectral dataset, the hierarchy was defined according to the main experimental factors contributing to spectral variability, as identified by ASCA. Hierarchical models were evaluated using the same external validation strategy applied to the non-hierarchical classifiers. Performance was reported both for each individual classification node and as global hierarchical performance. The preprocessing strategies, model settings and selected parameters of the candidate models used to construct the ASCA-guided hierarchical workflows are provided in Table S5.3 of the Supplementary Material.

All statistical and chemometric analyses were performed in MATLAB R2021a (MathWorks, Natick, MA, USA). PCA, ASCA, PLS-DA, SVM-C and XGBoost models were implemented using PLS_Toolbox version 8.9.2 (Eigenvector Research Inc., Wenatchee, WA, USA). RF models were implemented directly in MATLAB using the TreeBagger function.

5.4. Results and discussion

5.4.1. Spectral information

Figure 5.2 (A-C) shows the spectral signatures acquired of M1(400-1000 nm). Figure 5.2A shows minimum reflectance is observed around 445 nm (chlorophylls and carotenoids), a second depression between 585–620 nm corresponding to the transition between carotenoids and chlorophyll b, and a marked absorption feature near 670 nm (Fig. 5.2B) associated with chlorophyll a (Datt, 1993). When comparing all daily control spectra (C) with all water deficit spectra collected during the water deficit period (T1-WD, T2-WD and T3-WD), WD plants (green lines in Fig. 5.2B) tend to show a shallower red absorption feature than C plants (red lines in Fig. 5.2B), with the greatest differences observed in T3-WD (light blue lines in Fig. 5.2C). From a spectral-sensing perspective, these differences indicate that the VIS region was sensitive to stress-induced modifications in the pigment-related spectral fingerprint, particularly around chlorophyll- and carotenoid-associated bands. This behavior is consistent with drought-induced adjustments in the photosynthetic apparatus, where progressive changes in chlorophyll content occur along with changes in protective pigments and leaf structure, which together modulate the depth and shape of the 670 nm band rather than reflecting an abrupt loss of chlorophyll (Kim et al., 2011b; Peñuelas Josep & Filella Iolanda, 1998).

In the NIR region of M1 (750–1000 nm), WD plants exhibited higher reflectance than control plants (Fig. 5.2A). After transformation to pseudo-absorbance, this behavior was expressed as an opposite but consistent spectral trend, reflecting the mathematical relationship between reflectance and $-\log_{10}(R)$ (Fig. 5.2B and 5.2C). This behavior is consistent with the known sensitivity of this spectral domain to leaf water volume and internal structure and may therefore reflect drought-induced changes in leaf hydration and tissue organization, rather than purely pigment-related effects (Cotrozzi et al., 2020; Raymond Hunt & Rock, 1989).

Figure 5.2 (D-F) shows the spectra to M2 (1400–2400 nm) obtained from *Eucalyptus* leaves. Clear differences were observed between C and WD leaves, especially in the water absorption bands near 1450 and 1930 nm (Fig. 5.2D) (Workman & Weyer, 2012), where WD showed higher reflectance than C, indicating a reduction in water content, a typical physiological response under

drought conditions (Bayat et al., 2016; Pivovar et al., 2025; Rojek et al., 2023; Steidle Neto et al., 2017). In the absorbance spectra (Fig. 5.2E), C exhibited higher values in the water absorption bands, consistent with their higher water content, while WD showed reduced absorbance due to water loss and structural changes in the cellular matrix, especially in regions associated with O-H, C-H, and N-H bands from water and organic compounds (Moura Melo et al., 2019). Finally, after applying smoothing and multiplicative scatter correction (MSC), the differences between treatments were enhanced (Fig. 5.2F), particularly in the 1400–1600 nm and 1800–2100 nm regions, reinforcing the diagnostic potential of NIR spectroscopy. These patterns align with recent studies that utilize portable NIR spectroscopy to predict leaf water content in *Eucalyptus* spp. accurately (Zahir et al., 2022).

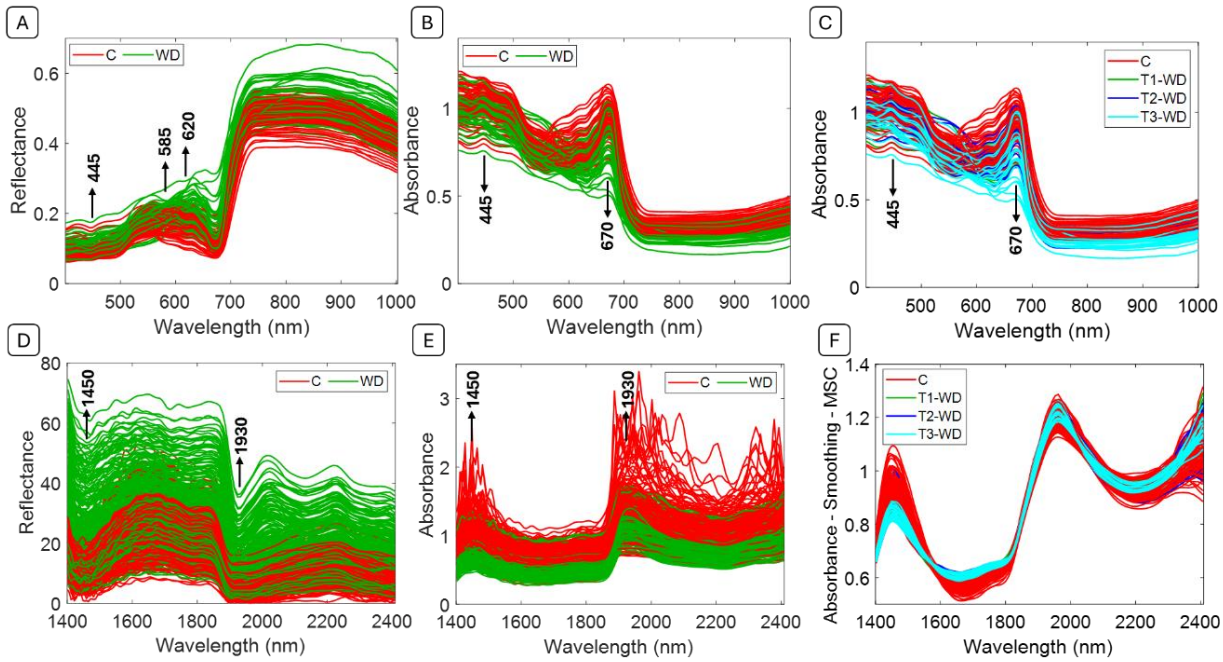

Figure 5.2 Mean spectra obtained from the whole plant for M1 (HSI, 400–1000 nm) and mean spectra obtained from leaves for M2 (NIRS, 1400–2400 nm).

5.4.2. PCA

PCA from VIS-NIR HSI data (M1)

PCA was performed on the M1 matrix to identify potential differences between sampling days and between C and WD conditions. Several pretreatments applied to the VIS-NIR spectra were

tested, but the best result was obtained with the second derivative (polynomial order 2), smoothed with an 11-point window, and mean-centered.

Figure 5.3A shows the distribution of scores according to sampling days (T0, T1, T2, and T3), while Figure 5.3B illustrates the distribution of scores by genotype. In the latter, a general tendency towards separation based on genotypic differences can be observed, although the pattern is not entirely clear. Principal Component 1 (PC1) differentiates G3 from G6, whereas PC2 separates G1 and G6 from G3 and G4. According to the loadings plots (Fig. 3C and 3D), the main contributions correspond to the bands between 500-550 nm and 670-700 nm, which are associated with chlorophyll absorption (Datt, 1993; Gitelson et al., 2003; M. N. Merzlyak*, 2003; Zahir et al., 2022).

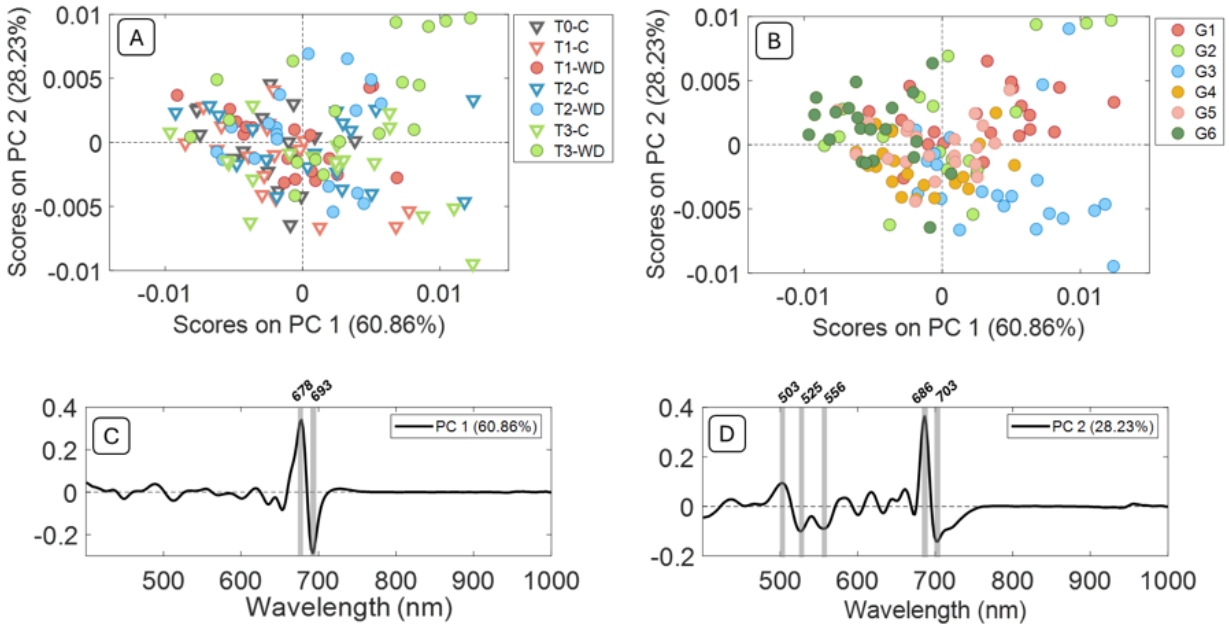

Figure 5.3 Plots of scores (A and B) and loadings (C and D) for all M1 samples at T0, T1, T2 and T3, including C: control samples and WD: water deficit samples, and the six genotypes evaluated.

PCA from NIR data (M2)

An exploratory PCA was performed on matrix M2 to identify differences between sampling days (T0, T1, T2, and T3) and/or between C and WD conditions. Among the preprocessing approaches tested, a Savitzky–Golay smoothing with an 11-point window was selected, combined with multiplicative scatter correction relative to the median and mean-centering on spectra.

Additionally, applying Hotelling's T^2 and Q-residuals greater than 1, a total of 58 spectra were removed (Figure S5.2). Traceability analysis confirmed that these corresponded mainly to spectra from plants in an advanced state of stress (dried leaves) or necrotic leaf regions, as detailed in Table S5.1 and Figure S5.3 of the supplementary material.

Figure 5.4A displays the distribution of PC1 versus PC2 scores from matrix M2, based on 1191 spectra from mature leaves. A clear clustering was observed for samples collected at the beginning of the experimental period (T0-C, T1-C, and T1-WD) on the positive side of PC1. In contrast, samples from T2-C, T3-C, and T2-WD were grouped on the negative side. The corresponding loadings plot (Figure 5.4B) indicates that the main contributions to this separation arise from the bands at 1622 and 1943 nm. The band at 1943 nm is associated with water-related O–H absorption, whereas the contribution near 1622 nm likely reflects a spectral region sensitive to changes in leaf composition and hydration (Schwanninger et al., 2011; Türker-Kaya & Huck, 2017b; L. Wang et al., 2011).

PC2 primarily discriminated T3 samples under both C and WD conditions. WD samples were distributed on the positive side of the component and were mainly associated with the bands at 1677 and 1952 nm (Figure 5.4C), suggesting differences linked to biochemical traits and water-related spectral variation under severe drought. Conversely, the negative side of PC2 was composed mostly of control samples, whose separation was mainly driven by the band at 1454 nm, commonly associated with the first overtone of O–H stretching. Although both 1454 and 1952 nm are water-related bands, their opposite contributions suggest that PC2 captures distinct water-associated spectral responses, possibly reflecting differences in hydration state, water binding, and tissue organization between control and drought-stressed leaves (Beć et al., 2020b; Peguero-Pina et al., 2023; J. Wang et al., 2009b; Workman & Weyer, 2012).

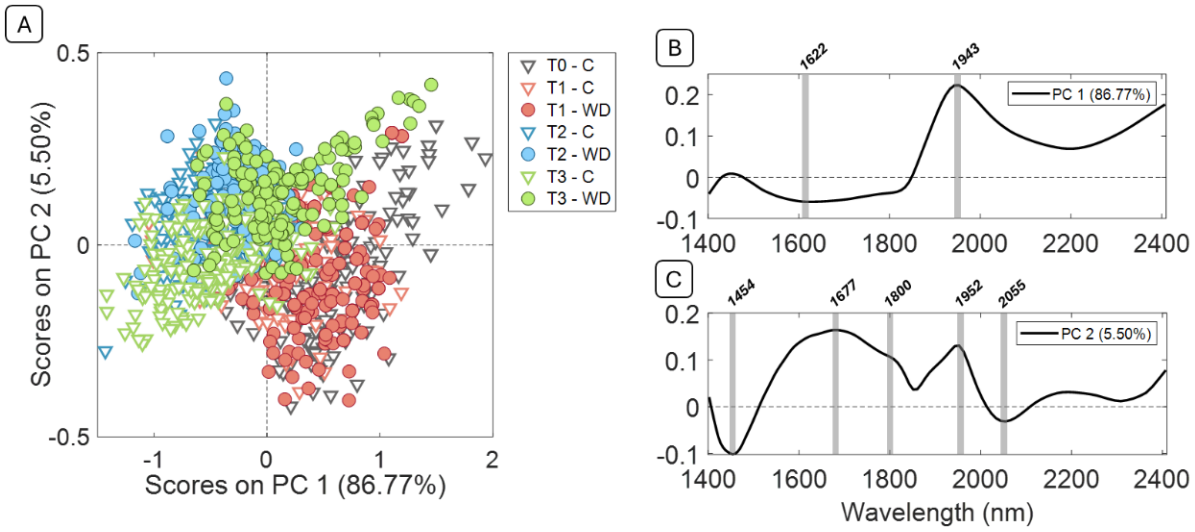

Figure 5.4 Plots of scores (A) and loadings (B and C) for M2 samples at T0, T1, T2 and T3, including C: control samples and WD: water deficit samples

5.4.3. ASCA

ASCA was used to determine how different sources of variability affected the spectral response. Four factors were considered in the model: (F1) genotype, (F2) replicates, (F3) sampling days, and (F4) treatment condition.

Table 5.1 provides an overview of the ASCA decomposition for both spectral datasets (M1 and M2). For each factor, the table reports the effect size (percentage of explained variance), the number of PCs retained to model the effect, the significance level (p-values), and the wavelengths with the highest contributions within each effect model. This summary links the variance decomposition to the interpretation of the scores and loadings discussed below. In addition, Figure 5.5 shows the scores and loadings associated with the factors contributing most strongly in both matrices, allowing visualization of the main separation trends and the spectral regions responsible for these differences, whereas the corresponding plots for the remaining factors are included in the Supplementary Material (Figure S5.4 and S5.5).

Table 5.1 ASCA summary for HSI (400–1000 nm) and portable NIR (1400–2400 nm): effect (% variance), number of PCs, p-values, and top contributing wavelengths.

M1: VIS-NIR HSI – 400 to 1000 nm				
Model effect	**Effect (%)**	**Nums. PC**	**p-values**	**Wavelength (nm)**
Mean	0.0	0		
F1-Genotypes	30.2	5	0.001	449 / 513 / 573 / 607 / 641 / 693
F2-Replicates	0.4	2	0.854	---
F3-Sampling Days	7.0	3	0.001	437 / 457 / 501 / 562 / 609 / 657 / 686
F4-Treatment	6.0	1	0.001	425 / 511 / 570 / 607 / 645 / 695
Residuals	56.5	2		
M2: Portable NIR – 1400 to 2400 nm				
Model effect	**Effect (%)**	**Nums. PC**	**p-values**	**Wavelength (nm)**
Mean	0.0	0		
F1-Genotypes	1.4	5	0.001	1465 / 1649 / 1721 / 1817 / 1952 / 2192
F2-Replicates	0.1	9	0.986	---
F3-Sampling Days	40.2	3	0.001	1448 / 1629 / 1952
F4-Treatment	10.6	1	0.001	1448 / 1551 / 1752 / 1825 / 1952 / 2205
Residuals	47.6	2		

ASCA from VIS-NIR HSI data (M1)

The M1 data, previously transformed from reflectance to pseudo-absorbance, underwent several spectral preprocessing methods to improve factor differentiation and minimize the variance explained by residuals. The optimal preprocessing consisted of a first derivative (second-order polynomial, 11-point smoothing) combined with mean-centering.

Table 5.1 indicates that the largest contribution to spectral variability corresponds to the genotypic factor (F1), which is significant ($p < 0.001$) and explains 30.2% of the variance. This separation is clearly reflected in the F1/PC1 scores (Figure 5.5A), where G1 forms a distinct group relative to the remaining genotypes. This pattern is consistent with the genetic background of the material, as G1 corresponds to *E. globulus*, whereas G2–G6 belong to the *E.* GloNi hybrid group. The spectral features underlying this discrimination are highlighted by the corresponding F1/PC1 loading profile (Figure 5C). Two positive maxima are observed at 513 and 693 nm, associated with carotenoid and chlorophyll absorption, respectively (Blackburn, 2007b; Ge et al., 2008; Gitelson et al., 2006). These features are most strongly expressed in *E. globulus* and in a subset of *E.* GloNi samples (notably G2). In contrast, the negative side of the loadings is

associated with the remaining *E.* GloNi genotypes and is characterized by bands around 573 and 607 nm, located in the green reflectance region and consistent with lower chlorophyll content.

Then, although they explained a smaller proportion of variance than genotype, sampling days (F3) and treatment condition (F4) still had significant effects on the spectral response, accounting for 7% and 6% of the total variance, respectively. By contrast, the replicate factor in M1 was not significant ($p = 0.854$). In this dataset, this factor represents biological replicate variability among individual plants within each genotype treatment sampling day combination, rather than instrumental point measurements. This result indicates that the spectral differences observed in M1 were mainly associated with genotype, sampling day, and treatment condition, while variability among biological replicates had a minor contribution to the total spectral response. From a spectral-sensing perspective, the lack of significance of this factor supports the consistency of the image acquisition and ROI extraction workflow, suggesting that the main spectral patterns were not dominated by random replicate-level variability.

These results demonstrate that genotypic variability is the dominant source of spectral variation within the range of 400-1000 nm, emphasizing the strong influence of the genetic background on pigment composition and photosynthetic traits in *Eucalyptus* spp. The distinct spectral pattern of *E. globulus* compared with *E. GloNi* reflects differences in chlorophyll and carotenoid content, consistent with their known physiological adaptations to water availability and light capture efficiency (Datt, 1999; Humphreys et al., 2008; Josep Peñuelas, 1998). The secondary contributions of sampling days (F3) and treatment condition (F4) suggest that temporal and environmental effects modulate, but do not override the intrinsic spectral signature determined by genotype. This finding highlights that while stress conditions and sampling day influence reflectance intensity and shape, genotypic traits primarily define the overall spectral baseline. Consistency among biological replicates attests to the rigor of the acquisition workflow, indicating that the detected spectral contrasts are attributable to biological responses rather than methodological or sampling influences.

ASCA from NIR data (M2)

For M2 data, which were first transformed from diffuse reflectance to pseudo-absorbance, the four previously described factors were evaluated. To optimize discrimination among them and

minimize the unexplained variance, several spectral preprocessing techniques were tested. The optimal preprocessing was achieved using an 11-point Savitzky–Golay smoothing filter combined with multiplicative scatter correction (MSC) relative to the median and mean centering.

As shown in Table 5.1, the factor explaining the highest proportion of variance (40.2%) and exerting a significant effect on the spectral response was F3 (sampling days), reflecting progressive changes in water stress levels throughout the experiment. This temporal structure is captured by the F3/PC1 scores for M2 (Figure 5.5B), where samples from T0 are located on the positive side of PC1, whereas T2 samples tend to shift toward the negative side. In contrast, T1 and T3 are distributed closer to zero, suggesting an intermediate position along the temporal stress trajectory. However, this pattern should be interpreted with caution, since the T1–T3 groups include both control and water-deficit samples, and the observed overlap likely reflects the coexistence of spectral responses still close to the basal condition together with others more clearly affected by stress. The spectral features driving this separation are indicated by the corresponding F3/PC1 loading profile (Figure 5.5D), with dominant bands at 1448 and 1952 nm, assigned to the first overtone of O–H stretching and the combination band of O–H stretching and deformation, respectively. In addition, the negative side of PC1 is associated with a contribution around 1629 nm, which may reflect changes related to leaf hydration together with modifications in leaf composition and internal structure (Kawamura et al., 2008; Li et al., 2021).

Factors F4 (treatment condition) and F1 (genotypic variability) accounted for smaller but still significant proportions of explained variance (10.6% and 1.4%, respectively; $p < 0.001$). Finally, F2 (instrumental replicates) showed no significant effect ($p = 0.986$), corresponding in this case to the ten spectra acquired from different leaf areas.

These results indicate that temporal variation associated with the progression of water deficit exerted the strongest influence on the spectral response, surpassing the effects of treatment condition and genotypic variability. This finding suggests that changes in leaf water status and related biochemical processes dominate the NIR spectral variability during drought development. At the same time, genetic differences and spatial heterogeneity (instrumental replicates) play comparatively minor roles. This pattern is consistent with previous studies demonstrating the

high sensitivity of the NIR region, particularly the water absorption bands near 1450 and 1950 nm, to fluctuations in leaf moisture and the reorganization of hydrogen bonds in response to dehydration (Workman & Weyer, 2012; Ye et al., 2022). Such dominance of temporal and physiological effects reinforces the potential of NIR spectroscopy as a non-destructive tool for real-time monitoring of drought dynamics and the early detection of stress in *Eucalyptus* spp.

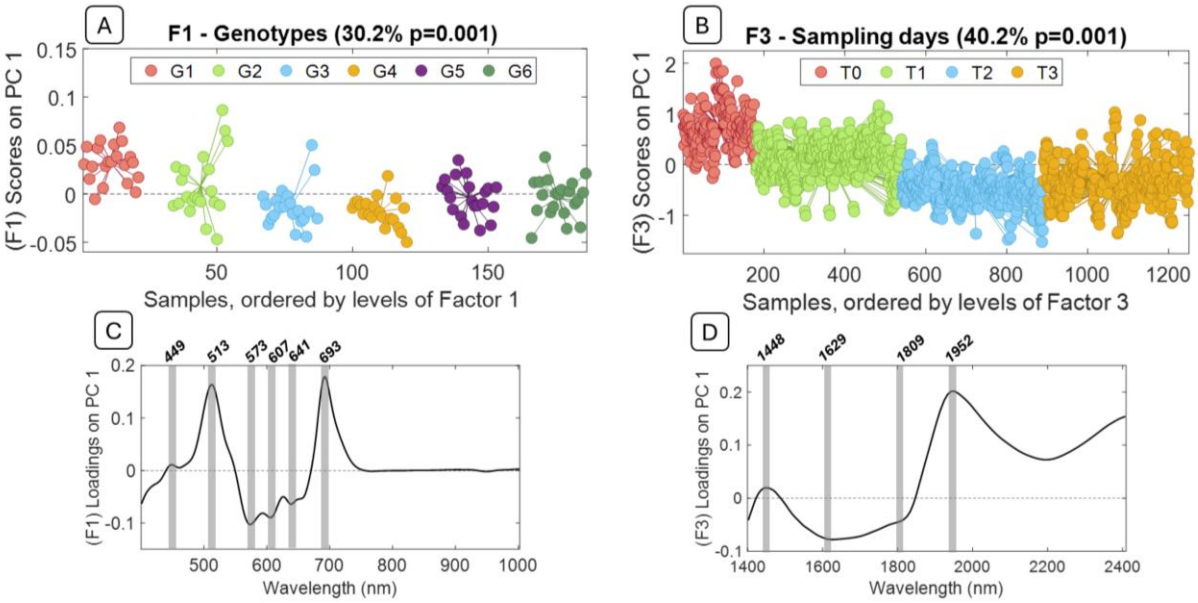

Figure 5.5 ASCA score (A–B) and loading (C–D) plots for the main factors affecting spectral variability. A and C represent genotype effects in VIS–NIR HSI data, whereas B and D represent temporal effects in NIR probe data.

5.4.4. Direct machine-learning benchmarking for binary and multiclass classification

To evaluate the predictive behaviour of both spectral datasets before applying the ASCA-guided hierarchical strategy, four supervised classification models were compared: PLS-DA, SVM-C, RF and XGBoost. Two direct classification tasks were considered: a binary water-status classification task, in which T0-C was discriminated from the pooled WD class, and a multiclass task, in which T0-C, T1-WD, T2-WD and T3-WD were considered as independent classes. This comparison was intended to assess whether model performance was maintained when the classification problem increased from broad water-status discrimination to a more detailed

discrimination of control and progressive water-deficit stages. A summary of the best-performing models for each dataset and classification task is presented in Table 5.2, whereas the complete performance comparison of all evaluated models is provided in Table S5.2 of the Supplementary Material.

For M1, corresponding to VIS–NIR HSI mean spectra, high external-validation performance was obtained for the binary classification task. Among the evaluated models, SVM-C achieved the highest validation accuracy (CA = 0.958), followed by XGBoost (CA = 0.889), PLS-DA (CA = 0.861) and RF (CA = 0.833). However, when the classification problem was extended to four classes, the performance decreased for all models. In this multiclass task, PLS-DA provided the best external-validation performance (CA = 0.792), whereas RF, XGBoost and SVM-C showed lower accuracies. This result suggests that, for VIS–NIR HSI, the main class structure could be effectively captured by a linear latent-variable model when stress progression was explicitly considered.

In the portable NIR dataset (M2), the binary classification task also showed high predictive performance. PLS-DA achieved perfect external-validation accuracy (CA = 1.000), followed by XGBoost (CA = 0.958), SVM-C (CA = 0.875) and RF (CA = 0.833). In contrast, the multiclass classification task again resulted in a decrease in model performance. In this case, XGBoost achieved the highest validation accuracy (CA = 0.792), followed by RF and PLS-DA (CA = 0.667), while SVM-C showed the lowest multiclass performance among the evaluated models. This indicates that the NIR spectral response associated with progressive water deficit may involve nonlinear relationships that were better captured by the gradient-boosted tree model in the direct multiclass setting.

Overall, the benchmarking analysis showed that both spectral modalities were suitable for discriminating control and water-deficit samples, but direct multiclass discrimination of stress progression was more challenging. The decrease in performance from binary to multiclass classification indicates that the spectral differences among progressive WD stages are more subtle and partially overlapping than the broader contrast between control and stressed plants. This finding supports the need for a structured classification strategy capable of decomposing the prediction problem into sequential and interpretable decision steps.

Table 5.2 Best direct machine-learning models selected according to global external-validation accuracy for binary classification (T0-C vs pooled WD) and multiclass classification (T0-C, T1-WD, T2-WD and T3-WD) using M1 and M2 spectral datasets.

Dataset	*Classification task*	*Best model*	*Global CA Val*
M1	Binary	SVM-C	0.958
M1	Multiclass	PLS-DA	0.792
M2	Binary	PLS-DA	1.000
M2	Multiclass	XGBoost	0.792

5.4.5. ASCA-guided hierarchical classification

The direct machine-learning benchmark showed that binary water-status classification was consistently more accurate than direct multiclass classification of water-deficit progression. Therefore, ASCA was used to define a structured hierarchical classification strategy based on the dominant sources of spectral variability in each dataset. This approach aimed to reduce the complexity of the prediction problem by replacing a single non-hierarchical multiclass model with sequential classification steps informed by the experimental design. The hierarchical architectures adopted for both datasets are schematically illustrated in Figure 5.6, where panel A corresponds to M1 (Model A) and panel B to M2 (Model B). The corresponding node-level calibration and external-validation performance metrics are reported in Table S4 of the Supplementary Material.

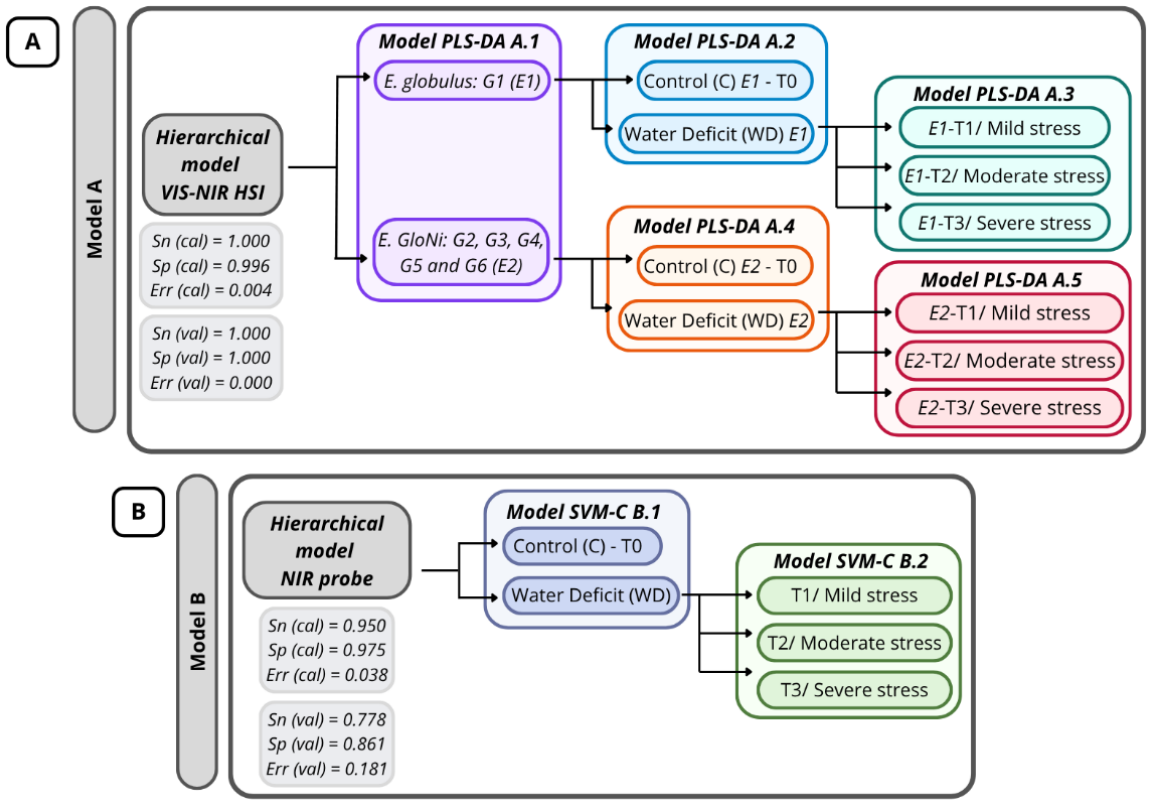

Figure 5.6 Hierarchical structure of supervised models for M1 (VIS–NIR HSI, PLS-DA) and M2 (portable NIR, SVM-C). E1: E. globulus (G1); E2: GloNi hybrids (G2–G6); C: control; WD: water deficit; T0–T3: sampling days.

Hierarchical models from VIS-NIR HSI data (M1)

The hierarchical model for M1 was built using mean spectra extracted from whole-plant hyperspectral images. According to the ASCA results, the first classification step separated *E. globulus* (E1; G1) from the GloNi hybrid group (E2; G2–G6). Subsequently, independent water-status classification models were applied within each genotype group to discriminate T0-C from WD samples. Finally, samples assigned to the WD class were further classified according to stress progression as T1-WD, T2-WD or T3-WD.

The final M1 hierarchical workflow was composed of five PLS-DA submodels and achieved complete correct classification in the external validation set, with global CA = 1.000, Sn = 1.000, Sp = 1.000 and Err = 0.000. This represented an improvement over the best direct multiclass model for M1, which was also based on PLS-DA but reached lower external-validation accuracy

(CA = 0.792; Table 5.2). These results indicate that the spectral structure identified by ASCA could be effectively translated into sequential predictive rules, reducing the complexity of the direct multiclass problem.

The high external-validation performance of the hierarchical HSI model can be attributed to the rich spectral information captured in the VIS–NIR range and to the use of ASCA to define a design-aware classification structure. The use of mean spectra from whole plants likely reduced intra-individual spectral variability and enhanced the representativeness of each genotype–treatment combination. In addition, the strong separability among classes in the hierarchical architecture reflects the sensitivity of VIS–NIR HSI to pigment-related changes, including chlorophylls and carotenoids, as well as structural alterations in leaf tissues associated with progressive water deficit. These results are consistent with previous studies reporting the effectiveness of VIS–NIR hyperspectral data for stress detection and genotype discrimination in *Eucalyptus* and other woody species (Dmitriev et al., 2023; Migacz et al., 2022; Pivovar et al., 2025; Sanhueza-Novoa et al., 2026; Santana et al., 2025). Therefore, under the controlled experimental conditions evaluated, the HSI-based hierarchical framework provided not only accurate classification, but also interpretable decision steps linking genotype-related spectral variability with subsequent water-status and stress-progression discrimination.

Hierarchical models from portable NIR data (M2)

The hierarchical model for M2 (portable NIR, 1400–2400 nm) was built using leaf-level mean spectra obtained from portable NIR measurements. In contrast to M1, the ASCA decomposition indicated that genotype contributed only marginally to the NIR spectral variance, whereas sampling day and treatment condition were the most relevant sources of variability. Therefore, the M2 hierarchy did not include an initial genotype-classification step. Instead, the workflow first discriminated T0-C from WD samples and then classified WD samples according to stress progression as T1-WD, T2-WD or T3-WD.

Both SVM-C and XGBoost were evaluated as hierarchical classifiers for M2. In external validation, their performance was comparable, although SVM-C showed slightly more balanced node-level metrics than XGBoost (Table S5). The SVM-C hierarchy reached macro-averaged Sn = 0.778, Sp = 0.861, Precision = 0.765 and Err = 0.181, whereas the XGBoost hierarchy reached

Sn = 0.733, Sp = 0.850, Precision = 0.752 and Err = 0.208. Therefore, although XGBoost was the best-performing model in the direct multiclass setting, SVM-C provided a slightly more stable hierarchical solution for portable NIR data.

The M2 results highlight the value of the 1400–2400 nm region for drought-related spectral discrimination, particularly because this spectral range contains strong absorption features associated with O–H bonds and leaf water status, especially around 1450 and 1950 nm (J. Wang et al., 2009b; Workman & Weyer, 2012). Although the hierarchical strategy did not produce marked improvement in overall predictive performance compared with the direct multiclass benchmark, it organized the prediction problem into interpretable sequential decisions aligned with the main sources of spectral variability identified by ASCA. This is relevant for smart spectral monitoring because water-status discrimination and stress-progression assessment can be evaluated as connected but distinct decision steps. The performance of the portable NIR models was mainly associated with the sensitivity of the 1400–1600 nm and 1900–2000 nm regions to water-related absorptions, together with additional contributions from spectral regions linked to changes in organic compounds and tissue structure, including O–H, C–H and N–H combinations and overtones (Beć et al., 2020c; Schwanninger et al., 2011; Workman & Weyer, 2012). Compared with VIS–NIR HSI, portable NIR provided a simpler and more targeted spectral response, dominated by temporal and treatment-related variation rather than genotype effects. Therefore, portable NIR spectroscopy represents a complementary sensing modality for monitoring water-deficit progression, whereas VIS–NIR HSI provides broader spectral information suitable for integrating genotype- and stress-related discrimination.

5.4.6. Implications for smart spectral monitoring

The results obtained from the direct and hierarchical classification strategies highlight the complementary roles of VIS–NIR HSI and portable NIR spectroscopy for smart water-deficit monitoring in young *Eucalyptus* plants under controlled environmental conditions. VIS–NIR HSI provided broader spectral information and was particularly effective when genotype-related variability needed to be considered within the classification workflow. This makes HSI suitable for controlled-environment screening scenarios in which both plant material identity and stress progression are relevant. In contrast, portable NIR spectroscopy provided a simpler and more

targeted sensing modality, with spectral variability mainly associated with temporal and water-status changes. Although its multiclass performance was lower than that of HSI, its sensitivity to water-related absorption bands and its simpler acquisition format make it attractive for rapid monitoring of water-deficit progression.

From a modelling perspective, the comparison between direct and ASCA-guided strategies showed that the best-performing algorithm depended not only on the spectral modality, but also on the structure of the classification problem. Direct binary classification was effective for both datasets, indicating that the spectral contrast between control and water-deficit samples was sufficiently strong to be captured by different supervised models. However, direct multiclass classification was more sensitive to class overlap, especially when progressive water-deficit stages were treated as independent categories. The ASCA-guided hierarchical approach addressed this limitation by decomposing the prediction problem into sequential decision steps aligned with the dominant sources of spectral variability.

This design-aware strategy is relevant for smart spectral monitoring because it combines predictive modelling with experimental interpretability. Instead of selecting a classifier only according to global accuracy, the proposed workflow first evaluates the structure of spectral variability and then uses this information to define a more interpretable classification sequence. Under the controlled conditions evaluated in this study, this approach was especially effective for VIS–NIR HSI and provided a structured interpretation of portable NIR data. Future work should validate this workflow under more variable environmental and operational conditions, including larger populations, additional genotypes and independent measurement campaigns, before its implementation as a decision-support tool for precision forestry or large-scale plant-material screening.

5.5. Conclusions

This study demonstrated that combining VIS–NIR HSI, portable NIR spectroscopy, machine-learning benchmarking and ASCA-guided hierarchical modelling provides an interpretable workflow for non-destructive water-deficit assessment in young *Eucalyptus* plants under controlled environmental conditions. By combining VIS–NIR HSI, portable NIR spectroscopy, direct machine-learning benchmarking and ASCA-guided hierarchical modelling, the study

showed that the predictive performance depended strongly on both the spectral modality and the structure of the classification problem. Direct binary classification was effective for both datasets, whereas direct multiclass discrimination of water-deficit progression was more challenging, confirming the spectral overlap among progressive stress stages.

ASCA provided a design-aware interpretation of the spectral data and supported the construction of hierarchical classification workflows. For VIS–NIR HSI, the hierarchy explicitly incorporated genotype-related variability before water-status and stress-progression discrimination, leading to complete correct classification in external validation. For portable NIR spectroscopy, the hierarchical strategy provided a structured and interpretable workflow based mainly on temporal and water-status variation, with SVM-C showing slightly more balanced validation behaviour than XGBoost.

Overall, the proposed workflow demonstrates that combining spectral sensing, machine-learning benchmarking and ASCA-guided hierarchical classification can improve the interpretability of water-deficit assessment in complex plant spectral datasets. Further validation with larger populations, additional genotypes and more variable environmental conditions will be required before operational implementation in precision forestry or large-scale plant-material screening.

CRediT authorship contribution statement

Pamela Sanhueza-Novoa: Conceptualization, Methodology, Software, Validation, Formal analysis, Investigation, Data curation, Visualization, Writing – Original Draft, Writing – Review & Editing. **Marta Fernández:** Writing – Review & Editing. **Carolina Hernández-Fuentes:** Investigation, Writing – Review & Editing. **José Manuel Amigo:** Methodology, Writing – Review & Editing. **Jesús Mellado Castro:** Investigation, Writing – Review & Editing. **Macarena Rojas-Rioseco:** Writing – Review & Editing. **Rosario del P. Castillo:** Supervision, Project administration, Writing – Review & Editing.

Declaration of competing interest

The authors declare that they have no known competing financial interests or personal relationships that could have appeared to influence the work reported in this paper.

Acknowledgements

This work was supported by ANID national doctoral grant No. 21221771, FONDECYT project 1251201, and FONDEQUIP project EQM230094.

Data availability

The datasets and trained models generated and analysed during the current study are not publicly available due to third-party ownership and confidentiality restrictions associated with the industrial plant material and spectral database. Aggregated results, methodological details, model performance metrics and spectral interpretations supporting the conclusions are provided within the article and Supplementary Material. Data may be made available from the corresponding author upon reasonable request and with permission from the data owner.

5.6. References

Abdelaali, B., Taha, D., Hannou, Z., Ayoub, E. H., El Menyiy, N., Bouyahya, A., & Mubarak, M. S. (2023). Bioactive Compounds and Antidiabetic and Other Health Benefits of Eucalyptus globulus. In *Antidiabetic Medicinal Plants and Herbal Treatments* (pp. 469–480). CRC Press. https://doi.org/10.1201/b23347-31

Ahmad, R. S., Imran, M., Ahmad, M. H., Khan, M. K., Yasmin, A., Saima, H., Abbas, K., Chaudhary, R., & Rahim, M. A. (2023). Eucalyptus essential oils. In *Essential Oils* (pp. 217–239). Elsevier. https://doi.org/10.1016/B978-0-323-91740-7.00005-0

Allen, C. D., Macalady, A. K., Chenchouni, H., Bachelet, D., McDowell, N., Vennetier, M., Kitzberger, T., Rigling, A., Breshears, D. D., Hogg, E. H. (Ted), Gonzalez, P., Fensham, R., Zhang, Z., Castro, J., Demidova, N., Lim, J. H., Allard, G., Running, S. W., Semerci, A., & Cobb, N. (2010). A global overview of drought and heat-induced tree mortality reveals emerging climate change risks for forests. *Forest Ecology and Management*, *259*(4), 660–684. https://doi.org/10.1016/j.foreco.2009.09.001

Ammitzboll, H., Vaillancourt, R. E., Potts, B. M., Harrison, P. A., Brodribb, T., Sussmilch, F. C., & Freeman, J. S. (2020). Independent genetic control of drought resistance, recovery, and growth of Eucalyptus globulus seedlings. *Plant Cell and Environment*, *43*(1), 103–115. https://doi.org/10.1111/pce.13649

Amrutha, S., Parveen, A. B. M., Muthupandi, M., Sivakumar, V., Nautiyal, R., & Ghosh Dasgupta, M. (2019). Variation in morpho-physiological, biochemical and molecular responses of two Eucalyptus species under short-term water stress. *Acta Botanica Croatica*, *78*(2), 125–134. https://doi.org/10.2478/botcro-2019-0021

Angel Prieto Lage, M., Barral Martínez, M., Seyyedimansour, S., Manikantan, M. R., Trif, M., & Khaneghah, M. A. (2022). *Recent advancements in NIR spectroscopy for assessing the quality and safety of horticultural products: A comprehensive review*.

Aranjuelo, I., Molero, G., Erice, G., Avice, J. C., & Nogués, S. (2011). Plant physiology and proteomics reveals the leaf response to drought in alfalfa (Medicago sativa L.). *Journal of Experimental Botany*, *62*(1), 111–123. https://doi.org/10.1093/jxb/erq249

Asaari, M. S. M., Mertens, S., Dhondt, S., Inzé, D., Wuyts, N., & Scheunders, P. (2019). Analysis of hyperspectral images for detection of drought stress and recovery in maize plants in a high-throughput phenotyping platform. *Computers and Electronics in Agriculture*, *162*, 749–758. https://doi.org/10.1016/j.compag.2019.05.018

Ballabio, D., & Consonni, V. (2013). Classification tools in chemistry. Part 1: linear models. PLS-DA. *Analytical Methods*, *5*(16), 3790. https://doi.org/10.1039/c3ay40582f

Ballester, C., Zarco-Tejada, P. J., Nicolás, E., Alarcón, J. J., Fereres, E., Intrigliolo, D. S., & Gonzalez-Dugo, V. (2018). Evaluating the performance of xanthophyll,

chlorophyll and structure-sensitive spectral indices to detect water stress in five fruit tree species. *Precision Agriculture*, *19*(1), 178–193. https://doi.org/10.1007/s11119-017-9512-y

Barker, M., & Rayens, W. (2003). Partial least squares for discrimination. *Journal of Chemometrics*, *17*(3), 166–173. https://doi.org/10.1002/cem.785

Bayat, B., van der Tol, C., & Verhoef, W. (2016). Remote sensing of grass response to drought stress using spectroscopic techniques and canopy reflectance model inversion. *Remote Sensing*, *8*(7). https://doi.org/10.3390/rs8070557

Beć, K. B., Grabska, J., & Huck, C. W. (2020a). Near-infrared spectroscopy in bio-applications. In *Molecules* (Vol. 25, Number 12). MDPI AG. https://doi.org/10.3390/molecules25122948

Beć, K. B., Grabska, J., & Huck, C. W. (2020b). Near-infrared spectroscopy in bio-applications. In *Molecules* (Vol. 25, Number 12). MDPI AG. https://doi.org/10.3390/molecules25122948

Beć, K. B., Grabska, J., & Huck, C. W. (2020c). Near-infrared spectroscopy in bio-applications. In *Molecules* (Vol. 25, Number 12). MDPI AG. https://doi.org/10.3390/molecules25122948

Behmann, J., Steinrücken, J., & Plümer, L. (2014a). Detection of early plant stress responses in hyperspectral images. *ISPRS Journal of Photogrammetry and Remote Sensing*, *93*, 98–111. https://doi.org/10.1016/j.isprsjprs.2014.03.016

Behmann, J., Steinrücken, J., & Plümer, L. (2014b). Detection of early plant stress responses in hyperspectral images. *ISPRS Journal of Photogrammetry and Remote Sensing*, *93*, 98–111. https://doi.org/10.1016/j.isprsjprs.2014.03.016

Belgiu, M., & Drăgu, L. (2016). Random forest in remote sensing: A review of applications and future directions. In *ISPRS Journal of Photogrammetry and Remote Sensing* (Vol. 114, pp. 24–31). Elsevier B.V. https://doi.org/10.1016/j.isprsjprs.2016.01.011

Benhizia, R., Phinzi, K., Hateffard, F., Aib, H., & Szabó, G. (2024). Drought Monitoring Using Moderate Resolution Imaging Spectroradiometer-Derived NDVI Anomalies in Northern Algeria from 2011 to 2022. *Environments - MDPI*, *11*(5). https://doi.org/10.3390/environments11050095

Berenguer, H. D. P., Alves, A., Amaral, J., Leal, L., Monteiro, P., de Jesus, C., & Pinto, G. (2018). Differential physiological performance of two Eucalyptus species and one hybrid under different imposed water availability scenarios. *Trees - Structure and Function*, *32*(2), 415–427. https://doi.org/10.1007/s00468-017-1639-y

Bertinetto, C., Engel, J., & Jansen, J. (2020). ANOVA simultaneous component analysis: A tutorial review. In *Analytica Chimica Acta: X* (Vol. 6). Elsevier B.V. https://doi.org/10.1016/j.acax.2020.100061

Blackburn, G. A. (2007a). Hyperspectral remote sensing of plant pigments. *Journal of Experimental Botany*, *58*(4), 855–867. https://doi.org/10.1093/jxb/erl123

Blackburn, G. A. (2007b). Hyperspectral remote sensing of plant pigments. *Journal of Experimental Botany*, *58*(4), 855–867. https://doi.org/10.1093/jxb/erl123

Breiman, L. (2001). *Random Forests* (Vol. 45).

Brockerhoff, E. G., Jactel, H., Parrotta, J. A., & Ferraz, S. F. B. (2013). Role of eucalypt and other planted forests in biodiversity conservation and the provision of biodiversity-related ecosystem services. *Forest Ecology and Management*, *301*, 43–50. https://doi.org/10.1016/j.foreco.2012.09.018

Bustin, S. A., Benes, V., Garson, J. A., Hellemans, J., Huggett, J., Kubista, M., Mueller, R., Nolan, T., Pfaffl, M. W., Shipley, G. L., Vandesompele, J., & Wittwer, C. T. (2009). The MIQE guidelines: Minimum information for publication of quantitative real-time PCR experiments. *Clinical Chemistry*, *55*(4), 611–622. https://doi.org/10.1373/clinchem.2008.112797

Bustin, S. A., Ruijter, J. M., Van den Hoff, M. J. B., Kubista, M., Pfaffl, M. W., Shipley, G. L., Tran, N., Rödiger, S., Untergasser, A., Mueller, R., Nolan, T., Milavec, M., Burns, M. J., Huggett, J. F., Vandesompele, J., & Wittwer, C. T. (2025). MIQE 2.0: Revision of the Minimum Information for Publication of Quantitative Real-Time PCR Experiments Guidelines. In *Clinical Chemistry* (Vol. 71, Number 6, pp. 634–651). Oxford University Press. https://doi.org/10.1093/clinchem/hvaf043

Cen, H., & He, Y. (2007). Theory and application of near infrared reflectance spectroscopy in determination of food quality. *Trends in Food Science and Technology*, *18*(2), 72–83. https://doi.org/10.1016/j.tifs.2006.09.003

Chen, T., & Guestrin, C. (2016). XGBoost: A scalable tree boosting system. *Proceedings of the ACM SIGKDD International Conference on Knowledge Discovery and Data Mining*, *13-17-August-2016*, 785–794. https://doi.org/10.1145/2939672.2939785

Correia, B., Hancock, R. D., Amaral, J., Gomez-Cadenas, A., Valledor, L., & Pinto, G. (2018). Combined Drought and Heat Activates Protective Responses in Eucalyptus globulus That Are Not Activated When Subjected to Drought or Heat Stress Alone. *Frontiers in Plant Science*, *9*. https://doi.org/10.3389/fpls.2018.00819

Correia, B., Pintó-Marijuan, M., Neves, L., Brossa, R., Dias, M. C., Costa, A., Castro, B. B., Araújo, C., Santos, C., Chaves, M. M., & Pinto, G. (2014a). Water stress and recovery in the performance of two Eucalyptus globulus clones: Physiological and biochemical profiles. *Physiologia Plantarum*, *150*(4), 580–592. https://doi.org/10.1111/ppl.12110

Correia, B., Pintó-Marijuan, M., Neves, L., Brossa, R., Dias, M. C., Costa, A., Castro, B. B., Araújo, C., Santos, C., Chaves, M. M., & Pinto, G. (2014b). Water stress and recovery in the performance of two Eucalyptus globulus clones: Physiological and biochemical profiles. *Physiologia Plantarum*, *150*(4), 580–592. https://doi.org/10.1111/ppl.12110

Correia, B., Valledor, L., Hancock, R. D., Jesus, C., Amaral, J., Meijón, M., & Pinto, G. (2016). Depicting how Eucalyptus globulus survives drought: involvement of redox and DNA methylation events. *Functional Plant Biology*, *43*(9), 838. https://doi.org/10.1071/FP16064

Cortes, C., Vapnik, V., & Saitta, L. (1995). Support-Vector Networks Editor. In *Machine Leaming* (Vol. 20). Kluwer Academic Publishers.

Cotrozzi, L., Peron, R., Tuinstra, M. R., Mickelbart, M. V., & Couture, J. J. (2020). Spectral phenotyping of physiological and anatomical leaf traits related with maize water status1[open]. *Plant Physiology*, *184*(3), 1363–1377. https://doi.org/10.1104/pp.20.00577

Cover, T. M., & Hart, P. E. (1952). Approximate formulas for the information transmitted bv a discrete communication channel. In *IEEE TRANSACTIONS ON INFORMATION THEORY* (Vol. 24, Number 1).

Cursi, A. G., Oliveira, F. S., Gouveia, D. G., Oder, J. C., Barrios, W. E. B., Ferreira, G. V., Martins, A. O., Peterle, G., Nunes-Nesi, A., & Araújo, W. L. (2024). Deciphering the importance of morphological aspects in drought tolerance in eucalyptus progenies. *Forest Ecology and Management*, *569*. https://doi.org/10.1016/j.foreco.2024.122198

Cvetković, D., Marković, D., Cvetković, D., & Radovanović, B. (2011). Effects of continuous UV-irradiation on the antioxidant activities of quercetin and rutin in solution in the presence of lecithin as the protective target. *Journal of the Serbian Chemical Society*, *76*(7), 973–985. https://doi.org/10.2298/JSC101123089C

Da Fonseca-Pereira, P., Daloso, D. M., Gago, J., De Oliveira Silva, F. M., Condori-Apfata, J. A., Florez-Sarasa, I., Tohge, T., Reichheld, J. P., Nunes-Nesi, A., Fernie, A. R., & Arajo, W. L. (2019). The Mitochondrial Thioredoxin System Contributes to the Metabolic Responses under Drought Episodes in Arabidopsis. *Plant and Cell Physiology*, *60*(1), 213–229. https://doi.org/10.1093/pcp/pcy194

Datt, B. (1993). Remote Sensing of Chlorophyll a, Chlorophyll b, Chlorophyll ab, and Total Carotenoid Content in Eucalyptus Leaves Recent studies have devel-oped several new vegetation indices based on other visi. In *REMOTE SENS. ENVIRON* (Vol. 66).

Datt, B. (1999). A New Reflectance Index for Remote Sensing of Chlorophyll Content in Higher Plants: Tests using Eucalyptus Leaves. *Journal of Plant Physiology*.

De Angelis, D., Summo, C., Pasqualone, A., Faccia, M., & Squeo, G. (2024). Advancements in food authentication using soft independent modelling of class analogy (SIMCA): a review. *Food Quality and Safety*, *8*. https://doi.org/10.1093/fqsafe/fyae032

Deribe, H. (2025). Review on Effects of Drought Stress on Maize Growth, Yield and Its Management Strategies. *Communications in Soil Science and Plant Analysis*, *56*(1), 123–143. https://doi.org/10.1080/00103624.2024.2404663

Dmitriev, P., Kozlovsky, B., Dmitrieva, A., Lysenko, V., Chokheli, V., Minkina, T., Mandzhieva, S., Sushkova, S., & Varduni, T. (2023). Identification of species of the genus Quercus L. with different responses to soil and climatic conditions according to hyperspectral survey data. *Eurasian Journal of Soil Science*, *12*(1), 37–62. https://doi.org/10.18393/ejss.1183524

Ejaz, I., Li, W., Naseer, M. A., Li, Y., Qin, W., Farooq, M., Li, F., Huang, S., Zhang, Y., Wang, Z., Sun, Z., & Yu, K. (2023). Detection of combined frost and drought stress in wheat using hyperspectral and chlorophyll fluorescence imaging. *Environmental Technology & Innovation*, *30*, 103051. https://doi.org/10.1016/j.eti.2023.103051

El Azizi, S., Amharref, M., Es-Saouini, H., Bernoussi, A. S., & El Abdellaoui, J. E. (2024). Towards a Spectral Library of Medicinal and Aromatic Plant species (MAPs): Plant Discrimination and Wavelength Selection. *Microchemical Journal*, *207*. https://doi.org/10.1016/j.microc.2024.111854

Ezenarro, J., Saouabi, I., García-Pizarro, Á., Schorn-García, D., Mestres, M., Amigo, J. M., Busto, O., & Boqué, R. (2025). NIR-HSI for the non-destructive monitoring of in-bag hazelnut oxidation. *Spectrochimica Acta - Part A: Molecular and Biomolecular Spectroscopy*, *333*. https://doi.org/10.1016/j.saa.2025.125906

Eziz, A., Yan, Z., Tian, D., Han, W., Tang, Z., & Fang, J. (2017). Drought effect on plant biomass allocation: A meta-analysis. *Ecology and Evolution*, *7*(24), 11002–11010. https://doi.org/10.1002/ece3.3630

Farooq, M., Wahid, A., Kobayashi, N., Fujita, D., & Basra, S. M. A. (2009). Plant drought stress: Effects, mechanisms and management. In *Agronomy for Sustainable Development* (Vol. 29, Number 1, pp. 185–212). https://doi.org/10.1051/agro:2008021

Fernández, M., Valenzuela, S., Barraza, H., Latorre, J., & Neira, V. (2012). Photoperiod, temperature and water deficit differentially regulate the expression of four dehydrin genes from Eucalyptus globulus. *Trees - Structure and Function*, *26*(5), 1483–1493. https://doi.org/10.1007/s00468-012-0722-7

Fernández, M., Villarroel, C., Balbontín, C., & Valenzuela, S. (2010). Validation of reference genes for real-time qRT-PCR normalization during cold acclimation in

Eucalyptus globulus. *Trees - Structure and Function*, *24*(6), 1109–1116. https://doi.org/10.1007/s00468-010-0483-0

Freitag, S., Anlanger, M., Lippl, M., Mechtler, K., Reiter, E., Grausgruber, H., & Krska, R. (2024). Simplifying Wheat Quality Assessment: Using Near-Infrared Spectroscopy and Analysis of Variance Simultaneous Component Analysis to Study Regional and Annual Effects. *ACS Measurement Science Au*. https://doi.org/10.1021/acsmeasuresciau.4c00044

Gamon, A., Pe uelas, J., & Field, C. B. (1992). *A Narrow-Waveband Spectral Index That Tracks Diurnal Changes in Photosynthetic Efficiency** (Vol. 41).

Ge, S., Carruthers, R. I., Spencer, D. F., & Yu, Q. (2008). Canopy assessment of biochemical features by ground-based hyperspectral data for an invasive species, giant reed (Arundo donax). *Environmental Monitoring and Assessment*, *147*(1–3), 271–278. https://doi.org/10.1007/s10661-007-0119-z

Gitelson, A. A., Gritz, Y., & Merzlyak, M. N. (2003). Relationships between leaf chlorophyll content and spectral reflectance and algorithms for non-destructive chlorophyll assessment in higher plant leaves. In *J. Plant Physiol* (Vol. 160). http://www.urbanfischer.de/journals/jpp

Gitelson, A. A., Keydan, G. P., & Merzlyak, M. N. (2006). Three-band model for noninvasive estimation of chlorophyll, carotenoids, and anthocyanin contents in higher plant leaves. *Geophysical Research Letters*, *33*(11). https://doi.org/10.1029/2006GL026457

Guigou, M., Moure, S., Bermúdez, F., Clavijo, L., Cabrera, M. N., Xavier, L., Ferrari, M. D., & Lareo, C. (2023). Ethanol Production from Eucalyptus Sawdust Following Sequential Alkaline Thermochemical Pretreatment with Recovery of Extractives. *Bioenergy Research*, *16*(4), 2012–2021. https://doi.org/10.1007/s12155-023-10619-1

Ha, S., Vankova, R., Yamaguchi-Shinozaki, K., Shinozaki, K., & Tran, L. S. P. (2012). Cytokinins: Metabolism and function in plant adaptation to environmental stresses. In *Trends in Plant Science* (Vol. 17, Number 3, pp. 172–179). https://doi.org/10.1016/j.tplants.2011.12.005

Hanin, M., Brini, F., Ebel, C., Toda, Y., Takeda, S., & Masmoudi, K. (2011). Plant dehydrins and stress tolerance: Versatile proteins for complex mechanisms. In *Plant Signaling and Behavior* (Vol. 6, Number 10, pp. 1503–1509). https://doi.org/10.4161/psb.6.10.17088

Hartmann, H., Bastos, A., Das, A. J., Esquivel-Muelbert, A., Hammond, W. M., Martínez-Vilalta, J., Mcdowell, N. G., Powers, J. S., Pugh, T. A. M., Ruthrof, K. X., & Allen, C. D. (2025). Climate Change Risks to Global Forest Health: Emergence of Unexpected Events of Elevated Tree Mortality Worldwide. *Annual Review of Plant Biology*. https://doi.org/10.1146/annurev-arplant-102820

Haynes, R. S., Lucieer, A., Brodribb, T. J., Tonet, V., & Cimoli, E. (2024a). Predicting key water stress indicators of Eucalyptus viminalis and Callitris rhomboidea using high-resolution visible to short-wave infrared spectroscopy. *Plant Cell and Environment*, *47*(12), 4992–5006. https://doi.org/10.1111/pce.15083

Haynes, R. S., Lucieer, A., Brodribb, T. J., Tonet, V., & Cimoli, E. (2024b). Predicting key water stress indicators of Eucalyptus viminalis and Callitris rhomboidea using high-resolution visible to short-wave infrared spectroscopy. *Plant Cell and Environment*, *47*(12), 4992–5006. https://doi.org/10.1111/pce.15083

Humphreys, J. R., O'Reilly-Wapstra, J. M., Harbard, J. L., Davies, N. W., Griffin, A. R., Jordan, G. J., & Potts, B. M. (2008). Discrimination between seedlings of Eucalyptus globulus, E. nitens and their F1 hybrid using near-infrared reflectance spectroscopy and foliar oil content. *Silvae Genetica*, *57*(4–5), 262–269. https://doi.org/10.1515/sg-2008-0040

Hussain, S., Hussain, S., Qadir, T., Khaliq, A., Ashraf, U., Parveen, A., Saqib, M., & Rafiq, M. (2019). Drought stress in plants: An overview on implications, tolerance mechanisms and agronomic mitigation strategies. *Plant Science Today*, *6*(4), 389–402. https://doi.org/10.14719/pst.2019.6.4.578

Ibarra, L., Hodge, G., & Acosta, J. J. (2023). Quantitative Genetics of a Hybrid Population of Eucalyptus nitens × Eucalyptus globulus: Estimation of Genetic Parameters and Implications for Breeding Strategies. *Forests*, *14*(2). https://doi.org/10.3390/f14020381

Jansen, J. J., Hoefsloot, H. C. J., Van Der Greef, J., Timmerman, M. E., Westerhuis, J. A., & Smilde, A. K. (2005). ASCA: Analysis of multivariate data obtained from an experimental design. *Journal of Chemometrics*, *19*(9), 469–481. https://doi.org/10.1002/cem.952

Johnson, J. B. (2023a). Rapid Prediction of Leaf Water Content in Eucalypt Leaves Using a Handheld NIRS Instrument. *Eng*, *4*(2), 1198–1209. https://doi.org/10.3390/eng4020070

Johnson, J. B. (2023b). Rapid Prediction of Leaf Water Content in Eucalypt Leaves Using a Handheld NIRS Instrument. *Eng*, *4*(2), 1198–1209. https://doi.org/10.3390/eng4020070

Jollife, I. T., & Cadima, J. (2016). Principal component analysis: A review and recent developments. In *Philosophical Transactions of the Royal Society A: Mathematical, Physical and Engineering Sciences* (Vol. 374, Number 2065). Royal Society of London. https://doi.org/10.1098/rsta.2015.0202

Jones, H. G. (2007). Monitoring plant and soil water status: Established and novel methods revisited and their relevance to studies of drought tolerance. *Journal of Experimental Botany*, *58*(2), 119–130. https://doi.org/10.1093/jxb/erl118

Josep Peñuelas, I. F. (1998). *Visible and near-infrared reflectance techniques for diagnosing plant physiological status*.

Kawamura, K., Watanabe, N., Sakanoue, S., & Inoue, Y. (2008). Estimating forage biomass and quality in a mixed sown pasture based on partial least squares regression with waveband selection. *Grassland Science*, *54*(3), 131–145. https://doi.org/10.1111/j.1744-697x.2008.00116.x

Kim, Y., Glenn, D. M., Park, J., Ngugi, H. K., & Lehman, B. L. (2011a). Hyperspectral image analysis for water stress detection of apple trees. *Computers and Electronics in Agriculture*, *77*(2), 155–160. https://doi.org/10.1016/j.compag.2011.04.008

Kim, Y., Glenn, D. M., Park, J., Ngugi, H. K., & Lehman, B. L. (2011b). Hyperspectral image analysis for water stress detection of apple trees. *Computers and Electronics in Agriculture*, *77*(2), 155–160. https://doi.org/10.1016/j.compag.2011.04.008

Koag, M. C., Fenton, R. D., Wilkens, S., & Close, T. J. (2003). The binding of maize DHN1 to lipid vesicles. Gain of structure and lipid specificity. *Plant Physiology*, *131*(1), 309–316. https://doi.org/10.1104/pp.011171

Kohzuma, K., Tamaki, M., & Hikosaka, K. (2021). Corrected photochemical reflectance index (PRI) is an effective tool for detecting environmental stresses in agricultural crops under light conditions. *Journal of Plant Research*, *134*(4), 683–694. https://doi.org/10.1007/s10265-021-01316-1

Korek, M., & Marzec, M. (2023). Strigolactones and abscisic acid interactions affect plant development and response to abiotic stresses. In *BMC Plant Biology* (Vol. 23, Number 1). BioMed Central Ltd. https://doi.org/10.1186/s12870-023-04332-6

Kuang, X., Cheng, Q., Chen, D., Fu, W., Li, H., & Chen, Z. (2026). Intelligent Diagnosis of Winter Wheat Water Stress Based on UAV Multi-Modal Remote Sensing. *Smart Agricultural Technology*, 101781. https://doi.org/10.1016/j.atech.2026.101781

Lee, S. C., & Luan, S. (2012). ABA signal transduction at the crossroad of biotic and abiotic stress responses. In *Plant, Cell and Environment* (Vol. 35, Number 1, pp. 53–60). https://doi.org/10.1111/j.1365-3040.2011.02426.x

Li, H., Yang, W., Lei, J., She, J., & Zhou, X. (2021). Estimation of leaf water content from hyperspectral data of different plant species by using three new spectral absorption indices. *PLoS ONE*, *16*(3 March). https://doi.org/10.1371/journal.pone.0249351

M. N. Merzlyak*, A. A. G. O. B. C. A. E. S. and S. I. P. (2003). *Application of Reflectance Spectroscopy for Analysis of Higher Plant Pigments*.

Manley, M. (2014). Near-infrared spectroscopy and hyperspectral imaging: Non-destructive analysis of biological materials. In *Chemical Society Reviews* (Vol. 43, Number 24, pp. 8200–8214). Royal Society of Chemistry. https://doi.org/10.1039/c4cs00062e

Martins, G. S., Freitas, N. C., Máximo, W. P. F., & Paiva, L. V. (2018). Gene expression in two contrasting hybrid clones of Eucalyptus camaldulensis x Eucalyptus urophylla grown under water deficit conditions. *Journal of Plant Physiology*, *229*, 122–131. https://doi.org/10.1016/j.jplph.2018.07.007

McFeeters, S. K. (1996). The use of the Normalized Difference Water Index (NDWI) in the delineation of open water features. *International Journal of Remote Sensing*, *17*(7), 1425–1432. https://doi.org/10.1080/01431169608948714

Merchant, A., Callister, A., Arndt, S., Tausz, M., & Adams, M. (2007). Contrasting physiological responses of six Eucalyptus species to water deficit. *Annals of Botany*, *100*(7), 1507–1515. https://doi.org/10.1093/aob/mcm234

Migacz, I. P., Manfron, J., Farago, P. V., Raman, V., de Muñiz, G. I. B., & Nisgoski, S. (2022). VIS/NIR spectra and color parameters according to leaf age of some Eucalyptus species: influence on their classification and discrimination. *Forest Systems*, *31*(2). https://doi.org/10.5424/fs/2022312-19242

Mobaraki, N., & Amigo, J. M. (2018). HYPER-Tools. A graphical user-friendly interface for hyperspectral image analysis. *Chemometrics and Intelligent Laboratory Systems*, *172*, 174–187. https://doi.org/10.1016/j.chemolab.2017.11.003

Mondal, M., Edida, M., Sharma, N., Lall, B., & Raju, D. (2019). Plants Stress Response Detection by Selecting Minimal Bands of Hyperspectral Images. *2019 9th International Conference on Advances in Computing and Communication (ICACC)*, 230–233. https://doi.org/10.1109/ICACC48162.2019.8986161

Mountrakis, G., Im, J., & Ogole, C. (2011). Support vector machines in remote sensing: A review. In *ISPRS Journal of Photogrammetry and Remote Sensing* (Vol. 66, Number 3, pp. 247–259). https://doi.org/10.1016/j.isprsjprs.2010.11.001

Moura, J. C. M. S., Araújo, P., Brito, M. D. S., Souza, U. R., Viana, J. O. F., & Mazzafera, P. (2012). Validation of reference genes from Eucalyptus spp. under different stress conditions. *BMC Research Notes*, *5*. https://doi.org/10.1186/1756-0500-5-634

Moura Melo, L. de, Dos Santos, A. C., Arteiro da Silva, K., Barbosa, U. do N., De Sena Oliveira, G. F., Alba, E., André Bellé, P., Monteiro Junior, J. J., & Araújo Silva, E. (2019). Spectral Response of Eucalyptus saligna under Water Stress in Southern Brazil. *Journal of Experimental Agriculture International*, 1–8. https://doi.org/10.9734/jeai/2019/v41i430405

Moussa Kourouma, J., Eze, E., Negash, E., Phiri, D., Vinya, R., Girma, A., & Zenebe, A. (2021). Assessing the spatio-temporal variability of NDVI and VCI as indices of crops productivity in Ethiopia: a remote sensing approach. *Geomatics, Natural Hazards and Risk*, *12*(1), 2880–2903. https://doi.org/10.1080/19475705.2021.1976849

Munera, S., Amigo, J. M., Aleixos, N., Talens, P., Cubero, S., & Blasco, J. (2018). Potential of VIS-NIR hyperspectral imaging and chemometric methods to identify similar cultivars of nectarine. *Food Control*, *86*, 1–10. https://doi.org/10.1016/j.foodcont.2017.10.037

Munns, R., James, R. A., Sirault, X. R. R., Furbank, R. T., & Jones, H. G. (2010). New phenotyping methods for screening wheat and barley for beneficial responses to water deficit. In *Journal of Experimental Botany* (Vol. 61, Number 13, pp. 3499–3507). https://doi.org/10.1093/jxb/erq199

Murchie, E. H., & Lawson, T. (2013). Chlorophyll fluorescence analysis: A guide to good practice and understanding some new applications. In *Journal of Experimental Botany* (Vol. 64, Number 13, pp. 3983–3998). https://doi.org/10.1093/jxb/ert208

Okyere, F. G., Cudjoe, D. K., Virlet, N., Castle, M., Riche, A. B., Greche, L., Mohareb, F., Simms, D., Mhada, M., & Hawkesford, M. J. (2024). Hyperspectral Imaging for Phenotyping Plant Drought Stress and Nitrogen Interactions Using Multivariate Modeling and Machine Learning Techniques in Wheat. *Remote Sensing*, *16*(18), 3446. https://doi.org/10.3390/rs16183446

Oliveira, L. A., Cardoso, A. A., Andrade, M. T., Pereira, T. S., Araújo, W. L., Santos, G. A., Damatta, F. M., & Martins, S. C. V. (2022). Exploring leaf hydraulic traits to predict drought tolerance of *Eucalyptus* clones. *Tree Physiology*, *42*(9), 1750–1761. https://doi.org/10.1093/treephys/tpac040

Oliveri, P., Malegori, C., Simonetti, R., & Casale, M. (2019). The impact of signal pre-processing on the final interpretation of analytical outcomes – A tutorial. In *Analytica Chimica Acta* (Vol. 1058, pp. 9–17). Elsevier B.V. https://doi.org/10.1016/j.aca.2018.10.055

Olvera-Carrillo, Y., Campos, F., Reyes, J. L., Garciarrubio, A., & Covarrubias, A. A. (2010). Functional analysis of the group 4 late embryogenesis abundant proteins reveals their relevance in the adaptive response during water deficit in arabidopsis. *Plant Physiology*, *154*(1), 373–390. https://doi.org/10.1104/pp.110.158964

Olvera-Carrillo, Y., Reyes, J. L., & Covarrubias, A. A. (2011). Late embryogenesis abundant proteins: Versatile players in the plant adaptation to water limiting environments. *Plant Signaling and Behavior*, *6*(4), 586–589. https://doi.org/10.4161/psb.6.4.15042

Peerbhay, K. Y., Mutanga, O., & Ismail, R. (2013). Commercial tree species discrimination using airborne AISA Eagle hyperspectral imagery and partial least squares discriminant analysis (PLS-DA) in KwaZulu-Natal, South Africa. *ISPRS Journal of Photogrammetry and Remote Sensing*, *79*, 19–28. https://doi.org/10.1016/j.isprsjprs.2013.01.013

Peguero-Pina, J. J., Sancho-Knapik, D., Ferrio, J. P., López-Ballesteros, A., Ruiz-Llata, M., & Gil-Pelegrín, E. (2023). Reevaluating Near-Infrared Reflectance as a Tool for the Study of Plant Water Status in Holm Oak (Quercus ilex subsp. rotundifolia). *Forests*, *14*(9). https://doi.org/10.3390/f14091825

Peng, Y., Zhang, M., Xu, Z., Yang, T., Su, Y., Zhou, T., Wang, H., Wang, Y., & Lin, Y. (2020). Estimation of leaf nutrition status in degraded vegetation based on field survey and hyperspectral data. *Scientific Reports*, *10*(1). https://doi.org/10.1038/s41598-020-61294-7

Penuelas, J., Pinol, J., Ogaya, R., & Filella, I. (1997). Estimation of plant water concentration by the reflectance Water Index WI (R900/R970). *International Journal of Remote Sensing*, *18*(13), 2869–2875. https://doi.org/10.1080/014311697217396

Peñuelas Josep, & Filella Iolanda. (1998). *Visible and near-infrared reflectance techniques for diagnosing plant physiological status*.

Pita, P., & Pardos, J. A. (2001). Growth, leaf morphology, water use and tissue water relations of Eucalyptus globulus clones in response to water deficit. *Tree Physiology*, *21*(9), 599–607. https://doi.org/10.1093/treephys/21.9.599

Pivovar, M., Näsi, R., Honkavaara, E., Blaženec, M., Škvarenina, J., Modlinger, R., Rožnovský, J., & Jakuš, R. (2025). Spectral signatures discrimination of Norway spruce trees under experimentally induced drought and acute thermal stress using hyperspectral imaging. *Forest Ecology and Management*, *586*. https://doi.org/10.1016/j.foreco.2025.122692

Poblete Hernández, P., Carlos, J., Munita, B., Caselli, J. G., Kahler González, C., Pardo Velásquez, E., Rocha, D. B., Catelicán Vera, L., Pineda, J. H., Celis Cantillana, B., & Recabarren, H. T. (2025). *ANUARIO FORESTAL CHILEAN STATISTICAL YEARBOOK OF FORESTRY 2025*. www.infor.cl

Ram, B. G., Oduor, P., Igathinathane, C., Howatt, K., & Sun, X. (2024). A systematic review of hyperspectral imaging in precision agriculture: Analysis of its current state and future prospects. In *Computers and Electronics in Agriculture* (Vol. 222). Elsevier B.V. https://doi.org/10.1016/j.compag.2024.109037

Raymond Hunt, E., & Rock, B. N. (1989). *Detection of Changes in Leaf Water Content Using Near-and Middle-Infrared Reflectances* (Vol. 30).

Rinnan, Å., Berg, F. van den, & Engelsen, S. B. (2009). Review of the most common pre-processing techniques for near-infrared spectra. In *TrAC - Trends in Analytical Chemistry* (Vol. 28, Number 10, pp. 1201–1222). https://doi.org/10.1016/j.trac.2009.07.007

Rodionova, O. Ye., Oliveri, P., Malegori, C., & Pomerantsev, A. L. (2024). Chemometrics as an efficient tool for food authentication: Golden pillars for building reliable

models. *Trends in Food Science & Technology*, *147*, 104429. https://doi.org/10.1016/j.tifs.2024.104429

Rojas-Rioseco, M., Castillo, R. del P., González-Campos, J., Ipinza, R., Sanhueza, M. I., & Hasbún, R. (2022). Phylogeographic origin authentication of Araucaria araucana (Mol.) K Koch seedlings through the application of spectroscopy techniques in different infrared ranges and chemometric methods. *New Forests*. https://doi.org/10.1007/s11056-022-09933-x

Rojek, L., Möller, M., Richter, M., Bischoff-Schaefer, M., & Hehl, K. (2023). PLANTSENS: A rail-based multi-sensor imaging system for redundant water stress detection in greenhouses. In *Smart Agricultural Technology* (Vol. 4). Elsevier B.V. https://doi.org/10.1016/j.atech.2023.100223

Ryckewaert, M., Gorretta, N., Henriot, F., Gobrecht, A., Héran, D., Moura, D., Bendoula, R., & Roger, J. M. (2021). Potential of high-spectral resolution for field phenotyping in plant breeding: Application to maize under water stress. *Computers and Electronics in Agriculture*, *189*. https://doi.org/10.1016/j.compag.2021.106385

Saadaoui, E., Ben Yahia, K., Dhahri, S., Ben Jamaa, M. L., & Khouja, M. L. (2017). An overview of adaptative responses to drought stress in Eucalyptus spp. *Forestry Studies*, *67*(1), 86–96. https://doi.org/10.1515/fsmu-2017-0014

Saddiq, M. S., Wang, X., Iqbal, S., Bilal Hafeez, M., Khan, S., Raza, A., Iqbal, J., Maqbool, M. M., Fiaz, S., Qazi, M. A., Bakhsh, A., 10, J., Gulshan, A. B., & Yang, S. H. (1934). *Effect of Water Stress on Grain Yield and Physiological Characters of Quinoa Genotypes*. *11*. https://doi.org/10.3390/agronomy

Salazar, C., Hernández, C., & Pino, M. T. (2015). Plant water stress: Associations between ethylene and abscisic acid response. In *Chilean Journal of Agricultural Research* (Vol. 75, pp. 71–79). Instituto de Investigaciones Agropecuarias, INIA. https://doi.org/10.4067/S0718-58392015000300008

Sánchez, J. C. M., Mesa, H. G. A., Espinosa, A. T., Castilla, S. R., & Lamont, F. G. (2025). Improving wheat yield prediction through variable selection using Support Vector Regression, Random Forest, and Extreme Gradient Boosting. In *Smart Agricultural Technology* (Vol. 10). Elsevier B.V. https://doi.org/10.1016/j.atech.2025.100791

Sanhueza-Novoa, P., Fernández, M., Hernández-Fuentes, C., Valenzuela, S., Hayat, M. Q., Ricardo Ramírez, H., & Castillo, R. del P. (2026). Detection of water deficit stress in Eucalyptus spp. through VIS-NIR hyperspectral imaging and chemometric methods. *Spectrochimica Acta Part A: Molecular and Biomolecular Spectroscopy*, *344*, 126675. https://doi.org/10.1016/j.saa.2025.126675

Santana, D. C., Baio, F. H. R., Oliveira, I. C. de, Araújo, F. C. de, Azevedo, G. B. de, Silva, E. V. M., Silva Junior, C. A. da, Teodoro, P. E., & Teodoro, L. P. R. (2025).

From spectral data to species identity: Machine learning and VIS/NIR reflectance in eucalyptus classification. *Remote Sensing Applications: Society and Environment*, *39*. https://doi.org/10.1016/j.rsase.2025.101686

Schwanninger, M., Rodrigues, J. C., & Fackler, K. (2011). A review of band assignments in near infrared spectra of wood and wood components. In *Journal of Near Infrared Spectroscopy* (Vol. 19, Number 5, pp. 287–308). https://doi.org/10.1255/jnirs.955

Shi, Y., Liu, X., Zhao, S., & Guo, Y. (2022). The PYR-PP2C-CKL2 module regulates ABA-mediated actin reorganization during stomatal closure. *New Phytologist*, *233*(5), 2168–2184. https://doi.org/10.1111/nph.17933

Silla, C. N., & Freitas, A. A. (2011). A survey of hierarchical classification across different application domains. In *Data Mining and Knowledge Discovery* (Vol. 22, Numbers 1–2, pp. 31–72). https://doi.org/10.1007/s10618-010-0175-9

Singh, D., Singh, C. K., Taunk, J., Tomar, R. S. S., Chaturvedi, A. K., Gaikwad, K., & Pal, M. (2017). Transcriptome analysis of lentil (Lens culinaris Medikus) in response to seedling drought stress. *BMC Genomics*, *18*(1). https://doi.org/10.1186/s12864-017-3596-7

Smola, A. J., Sch¨olkopf, B., & Sch¨olkopf, S. (2004). A tutorial on support vector regression *. In *Statistics and Computing* (Vol. 14). Kluwer Academic Publishers.

Sobejano-Paz, V., Mikkelsen, T. N., Baum, A., Mo, X., Liu, S., Köppl, C. J., Johnson, M. S., Gulyas, L., & García, M. (2020). Hyperspectral and Thermal Sensing of Stomatal Conductance, Transpiration, and Photosynthesis for Soybean and Maize under Drought. *Remote Sensing*, *12*(19), 3182. https://doi.org/10.3390/rs12193182

Sokolova, M., & Lapalme, G. (2009). A systematic analysis of performance measures for classification tasks. *Information Processing and Management*, *45*(4), 427–437. https://doi.org/10.1016/j.ipm.2009.03.002

Spokevicius, A. V., Tibbits, J., Rigault, P., Nolin, M. A., Müller, C., & Merchant, A. (2017). Medium term water deficit elicits distinct transcriptome responses in Eucalyptus species of contrasting environmental origin. *BMC Genomics*, *18*(1). https://doi.org/10.1186/s12864-017-3664-z

Steidle Neto, A. J., Lopes, D. de C., Silva, T. G. F. da, Ferreira, S. O., & Grossi, J. A. S. (2017). Estimation of leaf water content in sunflower under drought conditions by means of spectral reflectance. *Engineering in Agriculture, Environment and Food*, *10*(2), 104–108. https://doi.org/10.1016/j.eaef.2016.11.006

Stellacci, A. M., Castrignanò, A., Diacono, M., Troccoli, A., Ciccarese, A., Armenise, E., Gallo, A., De Vita, P., Lonigro, A., Mastro, M. A., & Rubino, P. (2012). Combined approach based on principal component analysis and canonical discriminant analysis for investigating hyperspectral plant response. *Italian Journal of Agronomy*, *7*(3), 247–253. https://doi.org/10.4081/ija.2012.e34

T Daughtry, C. S., Walthall, C. L., Kim, M. S., Brown de Colstoun, E., & McMurtrey III, J. E. (1999). Estimating Corn Leaf Chlorophyll Concentration from Leaf and Canopy Reflectance. In *REMOTE SENS. ENVIRON* (Vol. 74).

Taniguchi, M., LaRocca, C. A., Bernat, J. D., & Lindsey, J. S. (2023). Digital Database of Absorption Spectra of Diverse Flavonoids Enables Structural Comparisons and Quantitative Evaluations. *Journal of Natural Products*, *86*(4), 1087–1119. https://doi.org/10.1021/acs.jnatprod.2c00720

Torrion, J. A., Maas, S. J., Guo, W., Bordovsky, J. P., & Cranmer, A. M. (2014). A three-dimensional index for characterizing crop water stress. *Remote Sensing*, *6*(5), 4025–4042. https://doi.org/10.3390/rs6054025

Türker-Kaya, S., & Huck, C. W. (2017a). A review of mid-infrared and near-infrared imaging: Principles, concepts and applications in plant tissue analysis. In *Molecules* (Vol. 22, Number 1). MDPI AG. https://doi.org/10.3390/molecules22010168

Türker-Kaya, S., & Huck, C. W. (2017b). A review of mid-infrared and near-infrared imaging: Principles, concepts and applications in plant tissue analysis. In *Molecules* (Vol. 22, Number 1). MDPI AG. https://doi.org/10.3390/molecules22010168

Ulloa, J. L., Aguayo, P., Conejera, D., Rubilar, R., Balocchi, C., & Valenzuela, S. (2022). Transcriptomic response in foliar and root tissues of a drought-tolerant Eucalyptus globulus genotype under drought stress. *Trees - Structure and Function*, *36*(2), 697–709. https://doi.org/10.1007/s00468-021-02241-5

Umami, M., Parker, L. M., & Arndt, S. K. (2021). The impacts of drought stress and phytophthora cinnamomi infection on short-term water relations in two year-old eucalyptus obliqua. *Forests*, *12*(2), 1–14. https://doi.org/10.3390/f12020109

Valdés, A. E., Irar, S., Majada, J. P., Rodríguez, A., Fernández, B., & Pagès, M. (2013). Drought tolerance acquisition in Eucalyptus globulus (Labill.): A research on plant morphology, physiology and proteomics. *Journal of Proteomics*, *79*, 263–276. https://doi.org/10.1016/j.jprot.2012.12.019

Valverde, J. C., Rubilar, R. A., Medina, A., Pincheira, M., Emhart, V., Espinoza, Y., Bozo, D., & Campoe, O. C. (2025). Transpiration and Water Use Efficiency of Mediterranean Eucalyptus Genotypes Under Contrasting Irrigation Regimes. *Plants*, *14*(14). https://doi.org/10.3390/plants14142232

Vicente-Serrano, S. M., Quiring, S. M., Peña-Gallardo, M., Yuan, S., & Domínguez-Castro, F. (2020). A review of environmental droughts: Increased risk under global warming? In *Earth-Science Reviews* (Vol. 201). Elsevier B.V. https://doi.org/10.1016/j.earscirev.2019.102953

Vieira Dos Santos, C., & Rey, P. (2006). Plant thioredoxins are key actors in the oxidative stress response. *Trends in Plant Science*, *11*(7), 329–334. https://doi.org/10.1016/j.tplants.2006.05.005

Villar, E., Klopp, C., Noirot, C., Novaes, E., Kirst, M., Plomion, C., & Gion, J. M. (2011). RNA-Seq reveals genotype-specific molecular responses to water deficit in eucalyptus. *BMC Genomics*, *12*. https://doi.org/10.1186/1471-2164-12-538

Virtuoso, M. C. S., Souza, J. V. O., Zanatto, B., Valente, T. S., Silva, E. H. C., & de Paula, R. C. (2022). Germinative and physiological performance of eucalyptus species under abiotic stress. *Trees, Forests and People*, *10*. https://doi.org/10.1016/j.tfp.2022.100348

Wang, J., Xu, R., & Yang, S. (2009a). Estimation of plant water content by spectral absorption features centered at 1,450 nm and 1,940 nm regions. *Environmental Monitoring and Assessment*, *157*(1–4), 459–469. https://doi.org/10.1007/s10661-008-0548-3

Wang, J., Xu, R., & Yang, S. (2009b). Estimation of plant water content by spectral absorption features centered at 1,450 nm and 1,940 nm regions. *Environmental Monitoring and Assessment*, *157*(1–4), 459–469. https://doi.org/10.1007/s10661-008-0548-3

Wang, L., Hunt, E. R., Qu, J. J., Hao, X., & Daughtry, C. S. T. (2011). Estimating dry matter content of fresh leaves from the residuals between leaf and water reflectance. *Remote Sensing Letters*, *2*(2), 137–145. https://doi.org/10.1080/01431161.2010.503973

Warren, C. R., Aranda, I., & Cano, F. J. (2011a). Responses to water stress of gas exchange and metabolites in Eucalyptus and Acacia spp. *Plant, Cell and Environment*, *34*(10), 1609–1629. https://doi.org/10.1111/j.1365-3040.2011.02357.x

Warren, C. R., Aranda, I., & Cano, F. J. (2011b). Responses to water stress of gas exchange and metabolites in Eucalyptus and Acacia spp. *Plant, Cell and Environment*, *34*(10), 1609–1629. https://doi.org/10.1111/j.1365-3040.2011.02357.x

Wold, S., Esbensen, K., & Geladi, P. (n.d.). *Principal Component Analysis*.

Workman, Jerry., & Weyer, Lois. (2012). *Practical guide and spectral atlas for interpretive near-infrared spectroscopy*. CRC Press.

Xie, Y., Plett, D., & Liu, H. (2021). The Promise of Hyperspectral Imaging for the Early Detection of Crown Rot in Wheat. *AgriEngineering*, *3*(4), 924–941. https://doi.org/10.3390/agriengineering3040058

Ye, N., Zhong, S., Fang, Z., Gao, H., Du, Z., Chen, H., Yuan, L., & Pan, T. (2022). Performance Improvement of NIR Spectral Pattern Recognition from Three Compensation Models' Voting and Multi-Modal Fusion. *Molecules*, *27*(14). https://doi.org/10.3390/molecules27144485

Zade, S. V., & Abdollahi, H. (2024). Evaluation of Classical Least Squares Discriminant Analysis (CLS-DA) as a Novel Supervised Pattern Recognition Technique. *Journal of Chemometrics*. https://doi.org/10.1002/cem.3609

Zahir, S. A. D. M., Omar, A. F., Jamlos, M. F., Azmi, M. A. M., & Muncan, J. (2022). A review of visible and near-infrared (Vis-NIR) spectroscopy application in plant stress detection. In *Sensors and Actuators A: Physical* (Vol. 338). Elsevier B.V. https://doi.org/10.1016/j.sna.2022.113468

Zahra, N., Hafeez, M. B., Kausar, A., Al Zeidi, M., Asekova, S., Siddique, K. H. M., & Farooq, M. (2023a). Plant photosynthetic responses under drought stress: Effects and management. In *Journal of Agronomy and Crop Science*. John Wiley and Sons Inc. https://doi.org/10.1111/jac.12652

Zahra, N., Hafeez, M. B., Kausar, A., Al Zeidi, M., Asekova, S., Siddique, K. H. M., & Farooq, M. (2023b). Plant photosynthetic responses under drought stress: Effects and management. In *Journal of Agronomy and Crop Science*. John Wiley and Sons Inc. https://doi.org/10.1111/jac.12652

Zhu, J. K. (2016). Abiotic Stress Signaling and Responses in Plants. In *Cell* (Vol. 167, Number 2, pp. 313–324). Cell Press. https://doi.org/10.1016/j.cell.2016.08.029

Zhuang, J., Wang, Y., Chi, Y., Zhou, L., Chen, J., Zhou, W., Song, J., Zhao, N., & Ding, J. (2020). Drought stress strengthens the link between chlorophyll fluorescence parameters and photosynthetic traits. *PeerJ*, *8*. https://doi.org/10.7717/peerj.10046

5.7. Supplementary material

Figure S5.1. Co-occurrence network of terms obtained from a scientometric search in the Web of Science Core Collection (2020–2026). A total of 806 records containing at least one of the following terms in their title, abstract or keywords: physiological, phenotyping, plants, *Eucalyptus*, ASCA, hierarchical models, HSI and NIR, were analyzed using VOSviewer. Nodes represent keywords or index terms, colored by cluster: spectroscopy/multivariate analysis (blue), plant physiology (green) and machine learning (red), and edge thickness indicates co-occurrence strength. No record simultaneously combined all terms related to ASCA, hierarchical models, VIS–NIR HSI and NIR spectroscopy in plants.

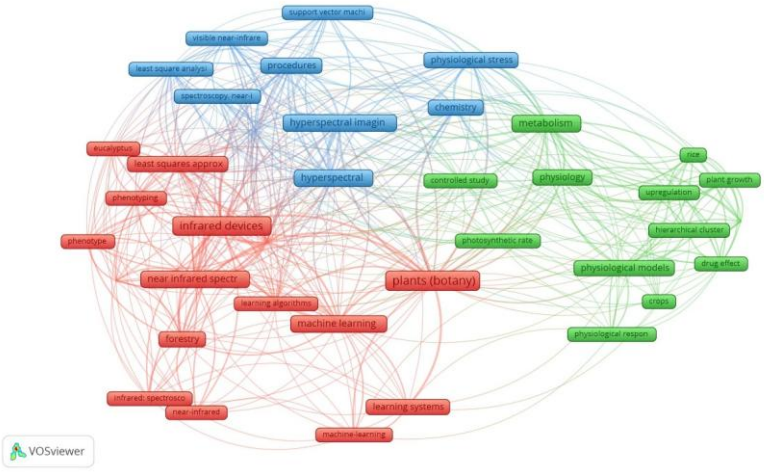

Figure S5.2. Exploratory PCA analysis of the NIR probe dataset (matrix M2) used to detect anomalous samples, where the samples highlighted in pink correspond to outliers identified and subsequently removed from matrix M2. (A) Graph of PC1 (76.84%) vs. PC2 (13.30%) scores showing the distribution of samples according to sampling day and treatment. (B) Graph of loadings corresponding to PC1 and PC2. (C–D) Graphs of Hotelling's T^2 and Q residuals used for the detection of outliers with a confidence level of 95%. (E–F) Raw and preprocessed spectra (smoothing and MSC correction) for control (C) and water deficit (WD) conditions of the selected samples.

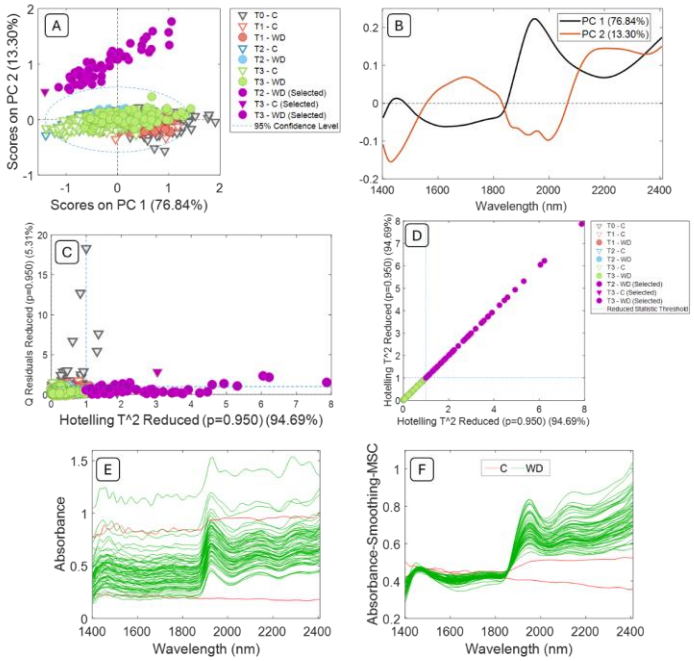

Figure S5.3. Photographs of samples whose spectra were removed from matrix M2 according to the outlier detection criteria described in Table S1. The images show the visual condition of each sample at the time of measurement, corresponding to advanced stress symptoms such as leaf dehydration and necrotic areas.

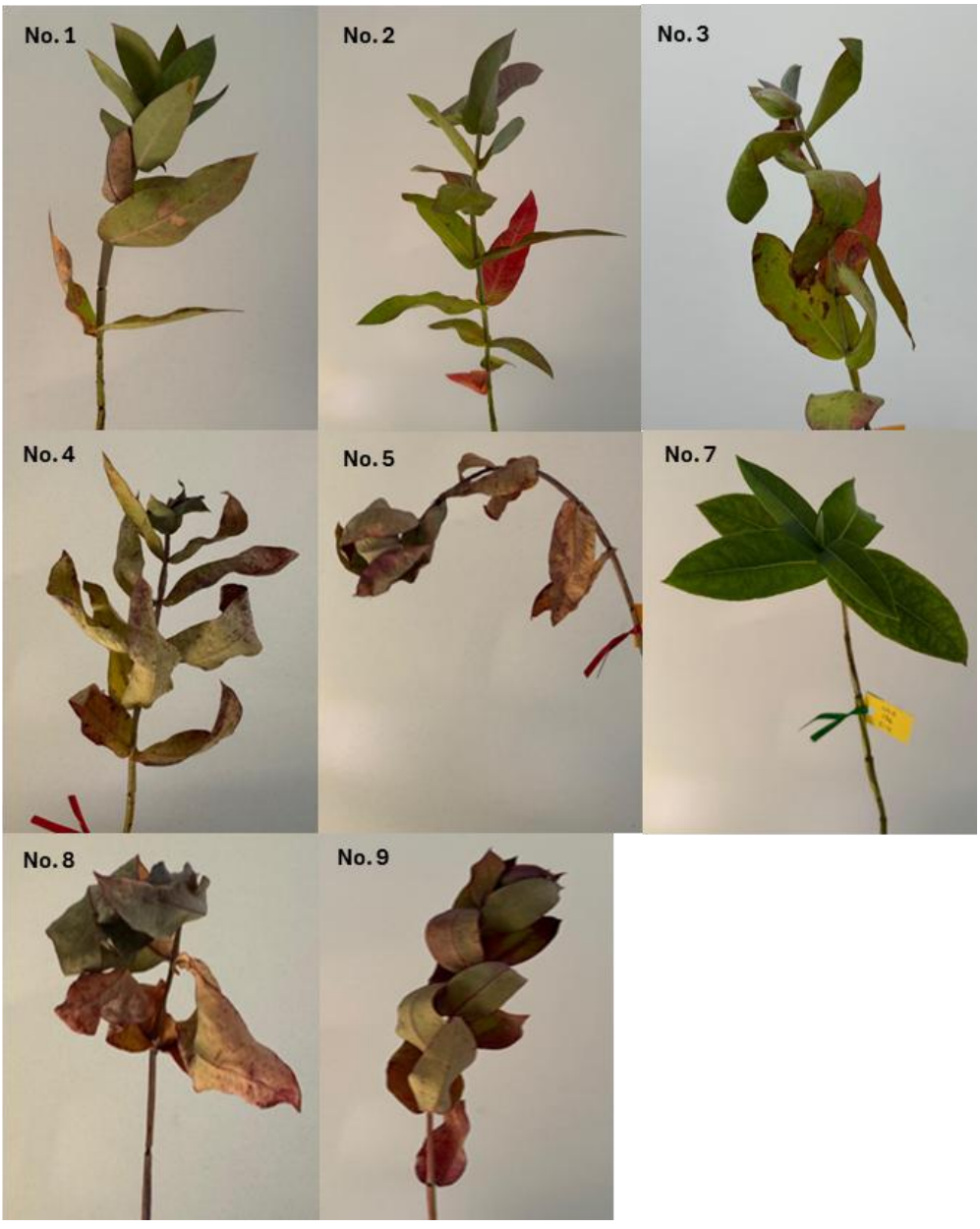

Figure S5.4. ASCA score and loading plots for the remaining factors in matrix M1 that are not shown in Figure 5. Panels include the corresponding score distributions and PC1 loading profiles for factors with lower contribution to the spectral response.

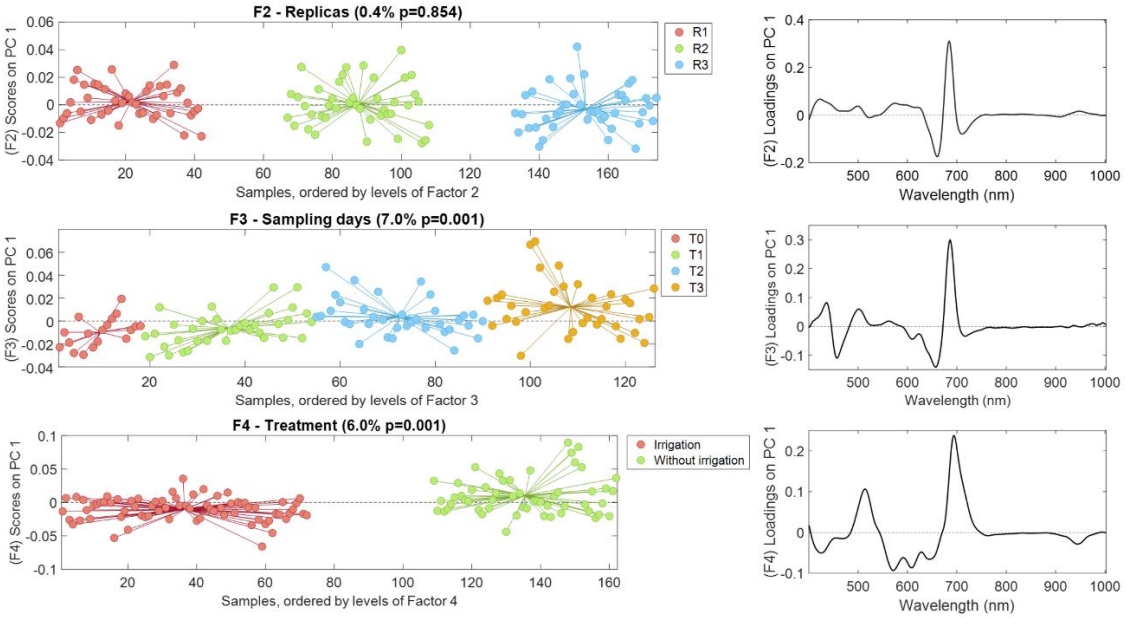

Figure S5.5. ASCA score and loading plots for the remaining factors in matrix M2 that are not shown in Figure 5. Panels include the corresponding score distributions and PC1 loading profiles for factors with lower contribution to the spectral response.

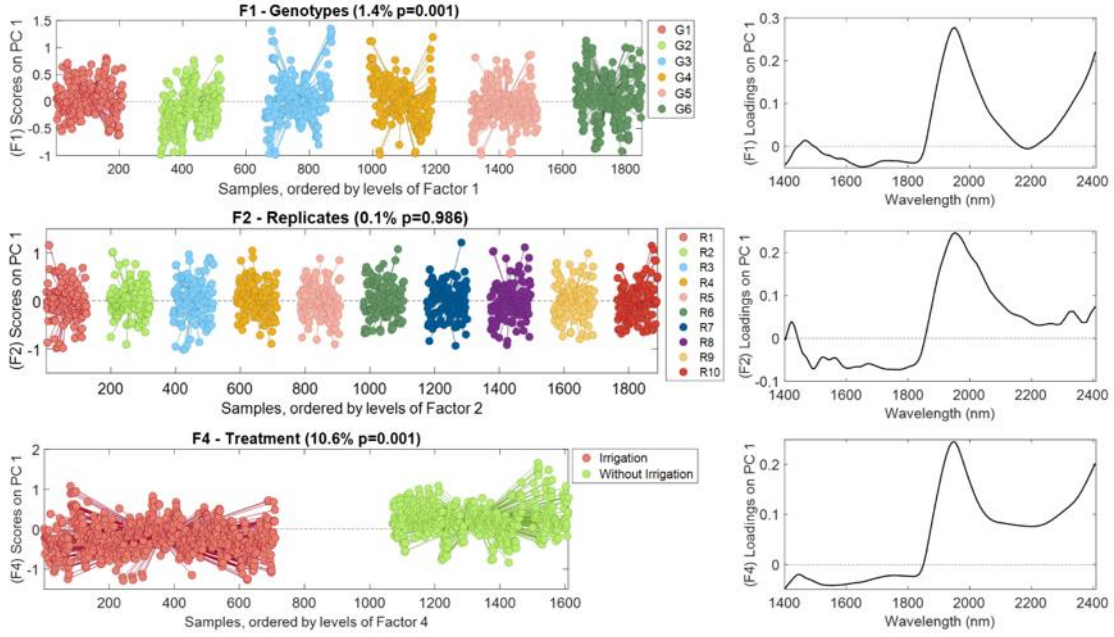

Table S5.1. List of spectra removed from matrix M2 after outlier detection based on Hotelling's T^2 and Q-residuals criteria. The table includes the spectrum identification number, sample number, genotype, treatment condition, sampling day, biological replicate, and instrumental replicate.

Spectra No.	Sample No.	Genotypes	Treatment	Sampling day	Biological replicate No.	Instrumental replicate No.
1	1	G1	C	T0	1	1
2	2	G2	WD	T1	3	7
3	3	G3	WD	T2	3	2
4		G3	WD	T2	3	3
5		G3	WD	T2	3	5
6		G3	WD	T2	3	6
7		G3	WD	T2	3	9
8		G3	WD	T2	3	10
9	4	G3	WD	T2	2	1
10		G4	WD	T2	2	2
11		G4	WD	T2	2	3
12		G4	WD	T2	2	4
13		G4	WD	T2	2	5
14		G4	WD	T2	2	6
15		G4	WD	T2	2	7
16		G4	WD	T2	2	8
17		G4	WD	T2	2	9
18		G4	WD	T2	2	10
19	5	G4	WD	T3	2	1
20		G4	WD	T3	2	2
21		G4	WD	T3	2	3
22		G4	WD	T3	2	4
23		G4	WD	T3	2	5
24		G4	WD	T3	2	6
25		G4	WD	T3	2	7
26		G4	WD	T3	2	8
27		G4	WD	T3	2	9
28		G4	WD	T3	2	10
29	6*	G4	WD	T3	3	1
30		G4	WD	T3	3	2
31		G4	WD	T3	3	3
32		G4	WD	T3	3	4
33		G4	WD	T3	3	5
34		G4	WD	T3	3	6
36		G4	WD	T3	3	8
37		G4	WD	T3	3	10
38	7	G5	C	T3	2	10
39	8	G5	WD	T3	1	1
40		G5	WD	T3	1	2
41		G5	WD	T3	1	3

42		G5	WD	T3	1	4
43		G5	WD	T3	1	5
44		G5	WD	T3	1	6
45		G5	WD	T3	1	7
46		G5	WD	T3	1	8
47		G5	WD	T3	1	9
48		G5	WD	T3	1	10
49	9	G6	WD	T3	1	1
50		G6	WD	T3	1	2
51		G6	WD	T3	1	3
52		G6	WD	T3	1	4
53		G6	WD	T3	1	5
54		G6	WD	T3	1	6
55		G6	WD	T3	1	7
56		G6	WD	T3	1	8
57		G6	WD	T3	1	9
58		G6	WD	T3	1	10

* Sample not found.

Table S5.2. Complete class-wise performance metrics of direct machine-learning models for binary and multiclass classification using M1 and M2 spectral datasets.

M1: HSI (VIS-NIR) - 400 to 1000 nm												
Classification task	**Model**	**Preproces**	**Class**	**Sn (Cal)**	**Sp (Cal)**	**F1-score (Cal)**	**Err (Cal)**	**Sn (Val)**	**Sp (Val)**	**F1-score (Val)**	**Err (Val)**	**CA (Val)**
Binary	RF	SNV-MC	T0-C	1.0000	1.0000	1.0000	0.0000	0.6667	0.8889	0.6667	0.1667	0.8333
			WD	1.0000	1.0000	1.0000	0.0000	0.8889	0.6667	0.8889	0.1667	
Binary	XGBoost	SNV	T0-C	1.0000	1.0000	1.0000	0.0000	0.6667	0.9333	0.6667	0.1111	0.8889
			WD	1.0000	1.0000	1.0000	0.0000	0.9333	0.6667	0.9333	0.1111	
Binary	PLS-DA	2nd-MC	T0-C	0.9167	0.9167	0.8462	0.0833	0.8333	0.8667	0.6667	0.1389	0.8611
			WD	0.9167	0.9167	0.9429	0.0556	0.8667	0.8333	0.9122	0.1389	
Binary	SVM	MSC-MC	T0-C	0.6667	1.0000	0.8000	0.0833	0.8333	1.0000	0.9091	0.0417	0.9583
			WD	1.0000	0.6667	0.9473	0.0833	1.0000	0.8333	0.9730	0.0417	
Multiclass	RF	SNV-MC	T0-C	1.0000	1.0000	1.0000	0.0000	0.6667	0.8889	0.6667	0.1667	0.5833
			T1	1.0000	1.0000	1.0000	0.0000	0.5000	0.8333	0.5000	0.2500	
			T2	1.0000	1.0000	1.0000	0.0000	0.6667	0.8889	0.6667	0.1667	
			T3	1.0000	1.0000	1.0000	0.0000	0.5000	0.8333	0.5000	0.2500	
Multiclass	XGBoost	SNV	T0-C	1.0000	1.0000	1.0000	0.0000	0.6667	1.0000	0.8000	0.0556	0.5417
			T1	1.0000	1.0000	1.0000	0.0000	0.5000	0.7000	0.3333	0.3333	
			T2	1.0000	1.0000	1.0000	0.0000	0.1667	0.8667	0.1818	0.2500	
			T3	1.0000	1.0000	1.0000	0.0000	0.8333	0.6667	0.4762	0.3056	
Multiclass	PLS-DA	2nd-MC	T0-C	1.0000	0.9444	0.9231	0.0417	1.0000	0.9444	0.9231	0.0417	0.7916
			T1	0.6667	0.8889	0.6667	0.1667	0.6667	0.8889	0.6667	0.1667	
			T2	0.5000	0.9444	0.6000	0.1667	0.5000	0.9444	0.6000	0.1667	
			T3	1.0000	0.9444	0.9231	0.0417	1.0000	0.9444	0.9231	0.0417	
Multiclass	SVM	MSC-MC	T0-C	0.9167	0.9722	0.9167	0.0417	0.5000	0.9444	0.6000	0.1667	0.5417
			T1	0.9167	0.9722	0.9167	0.0417	0.5000	0.7778	0.4615	0.2917	
			T2	0.8333	0.9722	0.8696	0.0625	0.5000	0.8889	0.5454	0.2083	
			T3	0.8333	0.9167	0.8000	0.1042	0.6667	0.7778	0.5714	0.2500	
M2: Portable-NIR -1 400 to 2400 nm												
Classification task	**Model**	**Prep**	**Class**	**Sn (Cal)**	**Sp (Cal)**	**F1-score (Cal)**	**Err (Cal)**	**Sn (Val)**	**Sp (Val)**	**F1-score (Val)**	**Err (Val)**	**CA (Val)**
Binary	RF	SNV-MC	T0-C	1.0000	1.0000	1.0000	0.0000	0.3333	0.3330	0.5000	0.1667	0.8333
			WD	1.0000	1.0000	1.0000	0.0000	1.0000	1.0000	0.9000	0.1667	

Binary	XGBoost	MSC	T0-C	1.0000	1.0000	1.0000	0.0000	0.8333	1.0000	0.9091	0.0417	0.9583
			WD	1.0000	1.0000	1.0000	0.0000	1.0000	0.8333	0.9730	0.0417	
Binary	PLS-DA	SavGol-SNV-MC	T0-C	0.9167	0.8889	0.8148	0.1042	1.0000	1.0000	1.0000	0.0000	1.0000
			WD	0.8889	0.9167	0.9275	0.1042	1.0000	1.0000	1.0000	0.0000	
Binary	SVM	MSC-MC	T0-C	1.0000	1.0000	1.0000	0.0000	0.8333	0.8889	0.7692	0.1250	0.8750
			WD	1.0000	1.0000	1.0000	0.0000	0.8889	0.8333	0.9143	0.1250	
Multiclass	RF	SNV-MC	T0-C	1.0000	1.0000	1.0000	0.0000	0.8333	1.0000	0.9091	0.0417	0.6667
			T1	1.0000	1.0000	1.0000	0.0000	0.8333	0.7778	0.6667	0.2083	
			T2	1.0000	1.0000	1.0000	0.0000	0.5000	0.8889	0.5454	0.2083	
			T3	1.0000	1.0000	1.0000	0.0000	0.5000	0.8889	0.5454	0.2083	
Multiclass	XGBoost	MSC	T0-C	1.0000	1.0000	1.0000	0.0000	0.8333	1.0000	0.9091	0.0417	0.7917
			T1	1.0000	1.0000	1.0000	0.0000	1.0000	0.8333	0.8000	0.1250	
			T2	1.0000	1.0000	1.0000	0.0000	0.8333	0.9444	0.8333	0.0833	
			T3	1.0000	1.0000	1.0000	0.0000	0.5000	0.9444	0.6000	0.1667	
Multiclass	PLS-DA	SavGol-SNV-MC	T0-C	1.0000	0.9722	0.9600	0.0208	0.6667	1.0000	0.8000	0.0833	0.6667
			T1	0.7500	0.9167	0.7500	0.1250	0.8333	0.7778	0.6667	0.2083	
			T2	0.5833	0.8611	0.5833	0.2083	0.8333	0.8333	0.7143	0.1667	
			T3	0.6667	0.9167	0.6956	0.1458	0.3333	0.9444	0.4444	0.2083	
Multiclass	SVM	MSC-MC	T0-C	0.9167	1.0000	0.9565	0.0208	0.5000	0.8889	0.5454	0.2083	0.6250
			T1	0.8333	0.9722	0.8696	0.0625	0.6667	0.8333	0.6154	0.2083	
			T2	0.7500	0.9167	0.7500	0.1250	0.6667	0.8889	0.6667	0.1667	
			T3	0.8333	0.8889	0.7692	0.1250	0.6667	0.8889	0.6667	0.1667	

Table S5.3. Performance summary of the individual PLS-DA, SVM and XGBoost models used to construct the hierarchical classification framework based on VIS-NIR HSI data (400–1000 nm) and probe NIR data (1400-2400 nm). The table reports the preprocessing applied, number of latent variables (LVs), support vectors (SVs) or Model complexity, and class-specific figures of merit, including sensitivity (Sn), specificity (Sp), classification error (Err), and cross-validation metrics (CV).

VIS-NIR HSI (400-1000 nm) hierarchical model											
Model	**Preprocessing**	**LV / SVs / Model complexity**	**class**	**Sn (cal)**	**Sp (cal)**	**Sn (CV)**	**Sp (CV)**	**Err (cal)**	**Err (CV)**	**RMSEC**	**RMSECV**
PLS-DA	2nd. Derivative-MC	3	E. globulus	1.000	0.975	0.750	0.925	0.013	0.163	0.218	0.313
			E. gloni	0.975	1.000	0.925	0.750	0.013	0.163	0.218	0.313
SVM	MSC - MC	16	E. globulus	0.583	1.000	0.625	1.000	0.208	0.188	--	--
			E. gloni	1.000	0.583	1.000	0.625	0.208	0.188	--	--
PLS-DA	2nd. Derivative-MC	2	E. globulus Control	1.000	1.000	1.000	1.000	0.000	0.000	0.077	0.091
			E. globulus Stress	1.000	1.000	1.000	1.000	0.000	0.000	0.077	0.091
SVM	MSC - MC	19	E. globulus Control	1.000	1.000	1.000	1.000	0.000	0.000	--	--
			E. globulus Stress	1.000	1.000	1.000	1.000	0.000	0.000	--	--
PLS-DA	2nd. Derivative-MC	4	E. globulus Stress T1	1.000	1.000	1.000	1.000	0.000	0.000	0.051	0.065
			E. globulus Stress T2	1.000	1.000	1.000	1.000	0.000	0.000	0.078	0.105
			E. globulus Stress T3	1.000	1.000	1.000	1.000	0.000	0.000	0.088	0.123
SVM	MSC - MC	32	E. globulus Stress T1	1.000	0.708	0.583	0.667	0.146	0.375	--	--
			E. globulus Stress T2	0.000	1.000	0.250	0.625	0.500	0.562	--	--
			E. globulus Stress T3	1.000	0.792	0.417	0.833	0.104	0.375	--	--
PLS-DA	2nd. Derivative-MC	2	E. gloni Control	1.000	1.000	1.000	1.000	0.000	0.000	0.077	0.091
			E. gloni Stress	1.000	1.000	1.000	1.000	0.000	0.000	0.077	0.091
SVM	MSC - MC	19	E. gloni Control	1.000	1.000	1.000	1.000	0.000	0.000	--	--
			E. gloni Stress	1.000	1.000	1.000	1.000	0.000	0.000	--	--
PLS-DA	2nd. Derivative-MC	4	E. gloni Stress T1	1.000	1.000	1.000	1.000	0.000	0.000	0.051	0.065
			E. gloni Stress T2	1.000	1.000	1.000	1.000	0.000	0.000	0.078	0.104
			E. gloni Stress T3	1.000	1.000	1.000	1.000	0.000	0.000	0.088	0.123
SVM	MSC - MC	32	E. gloni Stress T1	1.000	0.708	0.583	0.667	0.146	0.375	--	--
			E. gloni Stress T2	0.000	1.000	0.250	0.625	0.500	0.562	--	--
			E. gloni Stress T3	1.000	0.792	0.417	0.833	0.104	0.375	--	--
Portable NIR (1400-2400 nm) hierarchical model											

PLS-DA	SavGol-SNV-MC	5	Control	1.000	0.972	0.917	0.944	0.014	0.069	0.235	0.283
			Stress	0.972	1.000	0.944	0.917	0.014	0.069	0.235	0.283
SVM	MSC - MC	21	Control	1.000	1.000	0.917	0.972	0.000	0.056	--	--
			Stress	1.000	1.000	0.972	0.917	0.000	0.056	--	--
XGBoost	MSC	eta:0.5/ depth:1/ round:100	Control	1.000	1.000	0.833	0.967	0.000	0.104	--	--
			Stress	1.000	1.000	0.967	0.833	0.000	0.104	--	--
PLS-DA	SavGol-SNV-MC	3	Stress T1	0.917	0.958	0.833	0.958	0.063	0.104	0.264	0.289
			Stress T2	1.000	0.833	1.000	0.750	0.083	0.125	0.322	0.351
			Stress T3	0.667	0.708	0.667	0.708	0.313	0.313	0.389	0.413
SVM	MSC - MC	32	Stress T1	1.000	1.000	0.833	0.958	0.000	0.104	--	--
			Stress T2	1.000	0.875	0.917	0.833	0.062	0.125	--	--
			Stress T3	0.750	1.000	0.750	0.958	0.125	0.146	--	--
XGBoost	MSC	eta:0.1/ depth:1/ round:300	Stress T1	1.000	1.000	0.833	0.985	0.000	0.083	--	--
			Stress T2	1.000	1.000	0.500	0.708	0.000	0.361	--	--
			Stress T3	1.000	1.000	0.583	0.792	0.000	0.278	--	--

Table S5.4. Node-level calibration and external-validation performance metrics of ASCA-guided hierarchical classification models based on VIS–NIR HSI (M1) and portable NIR (M2) datasets.

	(A) Hierarchical model based on HSI (VIS-NIR) data								
	Calibration set								
Submodels	**Class**	**TP**	**FP**	**FN**	**TN**	**CA**	**Sn**	**Sp**	**Err**
Model A1	*E1*	8	1	0	39	0.889	1.000	0.975	0.013
	E2	39	0	1	8	1.000	0.975	1.000	0.013
Model A2	*E1* / C-*T0*	12	0	0	36	1.000	1.000	1.000	0.000
	E1 / WD	36	0	0	12	1.000	1.000	1.000	0.000
Model A3	*E1* / WD-T1	12	0	0	24	1.000	1.000	1.000	0.000
	E1 / WD-T2	12	0	0	24	1.000	1.000	1.000	0.000
	E1 / WD-T3	12	0	0	24	1.000	1.000	1.000	0.000
Model A4	*E2* / C-*T0*	12	0	0	36	1.000	1.000	1.000	0.000
	E2 / WD	36	0	0	12	1.000	1.000	1.000	0.000
Model A5	*E2* / WD-T1	12	0	0	24	1.000	1.000	1.000	0.000
	E2 / WD-T2	12	0	0	24	1.000	1.000	1.000	0.000
	E2 / WD-T3	12	0	0	24	1.000	1.000	1.000	0.000
Model Average A (cal)	--	--	--	--	--	*0.981*	*1.000*	*0.996*	*0.004*
	Validation set								
Model A1	*E1*	4	0	0	20	1.000	1.000	1.000	0.000
	E2	20	0	0	4	1.000	1.000	1.000	0.000
Model A2	*E1* / C-*T0*	6	0	0	18	1.000	1.000	1.000	0.000
	E1 / WD	18	0	0	6	1.000	1.000	1.000	0.000
Model A3	*E1* / WD-T1	6	0	0	12	1.000	1.000	1.000	0.000
	E1 / WD-T2	6	0	0	12	1.000	1.000	1.000	0.000
	E1 / WD-T3	6	0	0	12	1.000	1.000	1.000	0.000
Model A4	*E2* / C-*T0*	6	0	0	18	1.000	1.000	1.000	0.000
	E2 / WD	18	0	0	6	1.000	1.000	1.000	0.000
Model A5	*E2* / WD-T1	6	0	0	12	1.000	1.000	1.000	0.000
	E2 / WD-T2	6	0	0	12	1.000	1.000	1.000	0.000
	E2 / WD-T3	6	0	0	12	1.000	1.000	1.000	0.000
Model Average A (val)	--	--	--	--	--	*1.000*	*1.000*	*1.000*	*0.000*
	(B) Hierarchical model based on probe NIR data								
	Calibration set								
Submodels	**Class**	**TP**	**FP**	**FN**	**TN**	**CA**	**Sn**	**Sp**	**Err**
Model B1	C-T0	12	0	0	36	1.000	1.000	1.000	0.000
	WD	36	0	0	12	1.000	1.000	1.000	0.000
Model B2	WD-T1	12	0	0	24	1.000	1.000	1.000	0.000
	WD-T2	12	3	0	21	0.800	1.000	0.875	0.063
	WD-T3	9	0	3	24	1.000	0.750	1.000	0.125
ModelAverage B (cal)	--	--	--	--	--	*0.960*	*0.950*	*0.975*	*0.038*
	Validation set								
Model B1	C-T0	5	2	1	16	0.714	0.833	0.889	0.139
	WD	16	1	2	5	0.941	0.889	0.833	0.139
Model B2	WD-T1	6	0	0	12	1.000	1.000	1.000	0.000
	WD-T2	4	3	2	9	0.571	0.667	0.750	0.292
	WD-T3	3	2	3	10	0.600	0.500	0.833	0.333
Model Average B (val)	--	--	--	--	--	*0.765*	*0.778*	*0.861*	*0.181*

Table S5.5. Calibration and external-validation metrics of XGBoost and SVM-C hierarchical classifiers for portable NIR data (M2).

XGBoost – Calibration									
Clase	**TP**	**FP**	**FN**	**TN**	**Sensitivity**	**Specificity**	**Precision**	**F1-score**	**Err**
T0-C	12	0	0	36	1.000	1.000	1.000	1.000	0.000
WD	36	0	0	12	1.000	1.000	1.000	1.000	0.000
T1-WD	12	0	0	24	1.000	1.000	1.000	1.000	0.000
T2-WD	12	0	0	24	1.000	1.000	1.000	1.000	0.000
T3-WD	12	0	0	24	1.000	1.000	1.000	1.000	0.000
Model Average	--	--	--	--	1.000	1.000	1.000	1.000	0.000
XGBoost – Validation									
Clase	**TP**	**FP**	**FN**	**TN**	**Sensitivity**	**Specificity**	**Precision**	**F1-score**	**Err**
T0-C	5	0	1	18	0.833	1.000	1.000	0.909	0.083
WD	18	1	0	5	1.000	0.833	0.947	0.973	0.083
T1-WD	5	2	1	10	0.833	0.833	0.714	0.769	0.167
T2-WD	3	2	3	10	0.500	0.833	0.600	0.545	0.333
T3-WD	3	3	3	9	0.500	0.750	0.500	0.500	0.375
Model Average	--	--	--	--	*0.733*	*0.850*	*0.752*	*0.739*	*0.208*
SVM-C – Calibration									
Clase	**TP**	**FP**	**FN**	**TN**	**Sensitivity**	**Specificity**	**Precision**	**F1-score**	**Err**
T0-C	12	0	0	36	1.000	1.000	1.000	1.000	0.000
WD	36	0	0	12	1.000	1.000	1.000	1.000	0.000
T1-WD	12	0	0	24	1.000	1.000	1.000	1.000	0.000
T2-WD	12	3	0	21	1.000	0.875	0.800	0.889	0.063
T3-WD	9	0	3	24	0.750	1.000	1.000	0.857	0.125
Model Average	--	--	--	--	0.950	0.975	0.960	0.949	0.038
SVM-C – Validation									
Clase	**TP**	**FP**	**FN**	**TN**	**Sensitivity**	**Specificity**	**Precision**	**F1-score**	**Err**
T0-C	5	2	1	16	0.833	0.889	0.714	0.769	0.139
WD	16	1	2	5	0.889	0.833	0.941	0.914	0.139
T1-WD	6	0	0	12	1.000	1.000	1.000	1.000	0.000
T2-WD	4	3	2	9	0.667	0.750	0.571	0.615	0.292
T3-WD	3	2	3	10	0.500	0.833	0.600	0.545	0.333
Model Average	--	--	--	--	*0.778*	*0.861*	*0.765*	*0.769*	*0.181*

Chapter 6
Physiological, molecular, and spectral responses of *Eucalyptus* genotypes during water deficit and recovery

This chapter directly addresses Specific Objectives 2 and 4 and provides the integrative evidence required to address Specific Objective 5. The relationships between VIS–NIR hyperspectral imaging and portable NIR spectroscopy and complementary physiological and molecular measurements were evaluated to determine the biological basis of the spectral response to water deficit (Specific Objective 2). Plant recovery after rewatering was subsequently assessed by monitoring spectral and physiological trajectories during two post-stress sampling stages and determining the extent to which previously stressed plants returned toward their corresponding control conditions (Specific Objective 4). Finally, the combined physiological, spectral, molecular, and recovery responses were evaluated across genotypes to identify contrasting patterns of performance under water deficit and to support the selection of plant material showing the most consistent response to stress and subsequent recovery (Specific Objective 5).

6.1. Introduction

Water deficit is one of the main abiotic constraints on forest productivity because it simultaneously affects plant water relations, stomatal regulation, photosynthetic activity, photochemistry, carbon assimilation, oxidative balance, tissue development, and biomass accumulation. When the intensity or duration of water limitation exceeds the acclimation capacity of the plant, these coordinated alterations may lead to irreversible cellular damage, reduced growth, and even mortality. However, drought responses are not uniform across plant materials. Differences among species, hybrids, clones, and progenies arise from variation in hydraulic regulation, stomatal behaviour, osmotic adjustment, leaf morphology, antioxidant capacity, and molecular pathways involved in stress responses. Consequently, the comparative evaluation of contrasting genotypes is essential for identifying adaptive response patterns and traits potentially associated with improved performance under conditions of limited water availability (Cursi et al., 2024; Farooq et al., 2009; Merchant et al., 2007; Warren et al., 2011).

Drought phenotyping should not be limited to the identification of a single stressed state. A biologically meaningful assessment should consider the rate at which water deficit develops, the extent to which physiological function is impaired, the mechanisms activated to limit damage, and the capacity of the plant to restore its functioning once water availability is re-established. This distinction is particularly relevant in *Eucalyptus*, where considerable genetic variability has been reported in drought resistance, growth maintenance, and post-stress recovery. Genetic analyses in *Eucalyptus globulus* have indicated that drought resistance, recovery, and growth may be under partially independent control. This implies that genotypes selected exclusively from measurements taken at maximum stress are not necessarily those with the greatest capacity for functional recovery (Ammitzboll et al., 2020).

The recovery phase should not be interpreted as a simple reversal of water deficit. Rewatering initiates a new physiological transition in which tissue hydration may improve more rapidly than stomatal reopening, carbon assimilation, photosynthetic electron transport, pigment reorganization, or the repair of oxidative and structural damage. Depending on stress severity and genotype, recovery may be complete, delayed, partial, or absent. Contrasting *E. globulus* clones have shown different physiological and biochemical trajectories after rewatering, including variation in gas exchange, photochemical performance, pigment composition, osmotic

regulation, and antioxidant responses. Therefore, a previously water-stressed plant cannot automatically be considered equivalent to a continuously irrigated control, even when leaf hydration or visual appearance has partially recovered (Correia et al., 2014).

At the molecular level, water deficit activates regulatory and protective pathways associated with cellular dehydration, membrane stabilization, macromolecule protection, osmotic adjustment, and redox homeostasis. Late embryogenesis abundant proteins, commonly known as LEA proteins, constitute a diverse group of predominantly hydrophilic proteins that accumulate during seed desiccation and in vegetative tissues exposed to limited water availability. Their proposed functions include the stabilization of proteins and cellular structures, prevention of molecular aggregation, and protection of membranes and other macromolecular components under conditions of reduced cellular hydration (Olvera-Carrillo et al., 2011).

Dehydrins belong to group II of the LEA protein family and are commonly induced by dehydration, salinity, low temperature, and other environmental stresses. Their conserved sequence segments and intrinsically disordered structure enable them to interact with membranes, proteins, ions, and other cellular components whose stability may be compromised during water loss. In *E. globulus*, genes encoding dehydrins have shown differential regulation in response to water deficit, temperature, and photoperiod, supporting their use as molecular indicators of responses to adverse environmental conditions, although not necessarily as drought-specific markers (Fernández et al., 2012; Hanin et al., 2011).

Thioredoxin-related proteins participate in the regulation of cellular redox status through the modulation of target proteins and the supply of reducing equivalents to different antioxidant systems. Their induction may contribute to maintaining photosynthetic and metabolic functions when stomatal closure, CO_2 limitation, and excess absorbed energy promote the formation of reactive oxygen species. Transcriptomic studies in *E. globulus* subjected to water deficit have identified substantial changes in genes associated with redox regulation, cellular protection, and photosynthetic function, confirming that the molecular response to drought involves mechanisms that protect against dehydration and oxidative stress (Ulloa et al., 2022; Vieira Dos Santos & Rey, 2006).

In this chapter, DHN1, LEA4, and TRDX were selected as markers of complementary components of the molecular response to water deficit. DHN1 was considered mainly in relation to dehydrin-associated protection of membranes and macromolecules; LEA4 was associated with cellular and protein stabilization during dehydration; and TRDX was evaluated as an indicator of redox regulation and oxidative-stress response. The comparison between control plants and plants subjected to water restriction made it possible to assess whether the treatment induced the activation of these molecular pathways and whether this response was consistent with the physiological and spectral changes recorded.

Within this framework, higher relative expression of these genes in plants subjected to water deficit, compared with their respective controls, constitutes molecular evidence that leaf tissues activated mechanisms associated with dehydration, protection of cellular structures, and regulation of redox status. This evidence provides an independent biological basis for interpreting the differences detected using VIS–NIR hyperspectral imaging and portable NIR spectroscopy. In other words, when spectral separation between treatments coincides with reduced physiological performance and induction of genes associated with water-deficit responses, the interpretation that the spectral changes reflect biological modifications caused by water restriction becomes more robust and less likely to be explained solely by instrumental variability or natural differences among genotypes.

Nevertheless, gene expression should be regarded as complementary supporting evidence rather than as an absolute reference standard. Induction of DHN1, LEA4, or TRDX demonstrates transcriptional regulation of stress-associated mechanisms, but it does not by itself determine the magnitude of the protection achieved or the final tolerance of a genotype. High expression may correspond to an intense protective response, but it may also occur in plants experiencing greater dehydration or oxidative load. Therefore, the identification of genotypes with superior performance should consider the intensity of the molecular response together with the maintenance of physiological function during water deficit and the capacity for recovery after rewatering.

The reliability of relative expression estimates also depends on RNA integrity, primer performance, amplification efficiency, normalization strategy, biological replication, and the

stability of reference genes across experimental factors. Reference genes that are stable in one tissue, genotype, developmental stage, or stress condition may vary under other conditions. Studies conducted specifically in *Eucalyptus* have shown that the identity and number of reference genes used can substantially affect normalized expression results and that their validation must be performed for the species and specific experimental conditions under investigation (Fernández et al., 2010; Moura et al., 2012). These principles are consistent with the MIQE (Minimum information for publication of quantitative real-time PCR experiments) guidelines, which emphasize experimental validation and transparent reporting of qPCR procedures (Bustin et al., 2009, 2025).

In the present study, the molecular dataset was smaller and more unbalanced than the physiological and spectral datasets because some samples did not meet RNA quality requirements or were lost during cDNA preparation. In addition, candidate-gene expression was evaluated in selected genotypes and at specific stages of the water-deficit treatment, rather than throughout the entire recovery trajectory. For this reason, the molecular evidence was used primarily to support the occurrence of biological responses associated with the treatment and to explore their correspondence with spectral and physiological signals, without directly extending these associations to all stages or genotypes evaluated.

Spectral analysis provides a complementary, non-destructive approach for monitoring the integrated response of plants to water limitation. Hyperspectral imaging in the visible–near-infrared range combines spatial and spectral information and is particularly sensitive to variation in pigments, colour, red-edge behaviour, leaf surface properties, and tissue structure. Portable NIR spectroscopy extends the analytical range towards absorption bands associated with O–H, C–H, and N–H bonds and is therefore sensitive to water content, hydrogen bonding, dry matter, carbohydrates, and structural organic constituents. Because both techniques can be repeatedly applied to the same plants, they are suitable for longitudinal monitoring during the progression of water deficit and after rewatering.

However, the broad sensitivity of spectral measurements also represents a limitation. A plant spectrum is not generated by a single physiological mechanism but integrates the effects of genotype, developmental stage, water status, pigment composition, leaf anatomy, tissue damage,

leaf orientation, illumination, surface geometry, and instrumental variation. Therefore, spectral separation between control and water-deficit samples cannot by itself determine which biochemical or physiological process caused the observed differences. Integration with independent physiological and molecular measurements is necessary to establish whether spectral variation is consistent with an actual biological response to water deficit.

Physiological variables provide this biological anchor by directly evaluating the functional status of the plant. Net CO_2 assimilation, stomatal conductance, electron transport rate, the effective quantum yield of photosystem II, non-photochemical energy dissipation, leaf temperature, and water potential provide information on stomatal limitation, photosynthetic performance, photoprotection, transpirational cooling, and water availability within plant tissues. Their assessment during water deficit and recovery makes it possible to determine whether changes in spectral profiles are related to functional impairment, acclimation, or partial restoration of physiological activity.

Multivariate analysis is required because spectral, physiological, and molecular datasets are high-dimensional, collinear, and affected by multiple sources of variability. Principal component analysis enables the identification of dominant trends, anomalous samples, and exploratory grouping patterns, although it does not by itself demonstrate statistically significant treatment effects (Wold et al., 1987). Regression models can be used to evaluate the extent to which spectral information can estimate physiological variables or gene-expression levels, whereas correlation analyses can assess whether molecular activation, physiological alteration, and spectral response follow coordinated patterns.

In particular, the predictive ability of the models should be evaluated using cross-validation or independent datasets, rather than solely from calibration performance. An apparently strong spectral relationship in calibration may disappear when predicting samples not used during model development, particularly when the number of biological observations is limited, missing data are present, or between-genotype variability dominates the response. Therefore, spectral relationships with physiological and molecular variables should be interpreted according to their predictive performance and not only according to the goodness of fit obtained for the calibration dataset.

Within this context, the objective of this chapter was to integrate physiological, spectral, and molecular evidence obtained from *Eucalyptus* genotypes subjected to controlled water deficit followed by rewatering. The study addressed four main questions: (i) whether physiological and spectral responses followed a progressive trajectory during water deficit and whether rewatered plants returned to the state of continuously irrigated controls; (ii) which physiological variables could be related to or estimated using VIS–NIR hyperspectral images and portable NIR spectra; (iii) whether the induction of DHN1, LEA4, and TDRX in plants subjected to water deficit provided molecular evidence consistent with the spectral and physiological differences observed; and (iv) to what extent relationships among gene expression, physiology, and spectral information could be generalized considering the limitations of the molecular design and the predictive performance of the models. In this way, the integration of the three sources of information allowed the response to water deficit to be evaluated at complementary levels, distinguishing among spectral detection, functional alteration, molecular activation, and subsequent recovery capacity.

6.2. Materials and methods

6.2.1. Plant material and experimental design

The integrative assay was conducted using 196 six-month-old rooted plants supplied by the BIOFOREST S.A. research centre (Arauco, Chile). Six genotypes were evaluated: one *Eucalyptus globulus* genotype and five hybrids between *Eucalyptus nitens* and *Eucalyptus globulus* (GloNi). The identity and number of plants assigned to each genotype are summarized in Table 6.1; each genotype was represented by thirty-three plants. Plants were randomly distributed within the controlled-environment facility to reduce systematic position effects.

Table 6.1 Genotypes evaluated in the second water-deficit and recovery assay.

Code	***Species***	***Initial n***	***Analytical coverage***
G1	*E. globulus*	33	Physiology, HSI, NIR
G2	GloNi hybrid	33	Physiology, HSI, NIR
G3	GloNi hybrid	33	Physiology, HSI, NIR
G4	GloNi hybrid	33	Physiology, HSI, NIR, qPCR
G5	GloNi hybrid	33	Physiology, HSI, NIR, qPCR
G6	GloNi hybrid	33	Physiology, HSI, NIR, qPCR

Before water withdrawal, plants underwent a 30-day acclimation period under continuous irrigation. Growth-chamber conditions followed the protocol established for the first assay: a 14 h light/10 h dark photoperiod, photon flux density above 150 µmol photons m−2 s−1, day and night temperatures of 22 ± 1 °C and 16 ± 1 °C, respectively, and relative humidity of 60-70%. At the end of acclimation, plants were assigned to a continuously irrigated control treatment (C) or to a water-deficit treatment (WD), for which irrigation was withheld for 12 days. The experimental sequence, including water-deficit induction, rewatering, recovery assessment, and sampling times, is summarized in Figure 6.1.

Measurements were performed at day 0 (T0), 4 days (T1), 8 days (T2), and 12 days (T3) after irrigation withdrawal. T1, T2, and T3 were operationally defined as mild, moderate, and severe water-deficit stages. After T3, irrigation was restored to the WD plants and recovery was evaluated 6 and 13 days after rewatering (T4 and T5, respectively). Three biological replicates per genotype and experimental stage were evaluated in the main analytical workflow. The same experimental labels were used for spectral and physiological data, although the exact number of observations retained in each matrix depended on quality control and data availability.

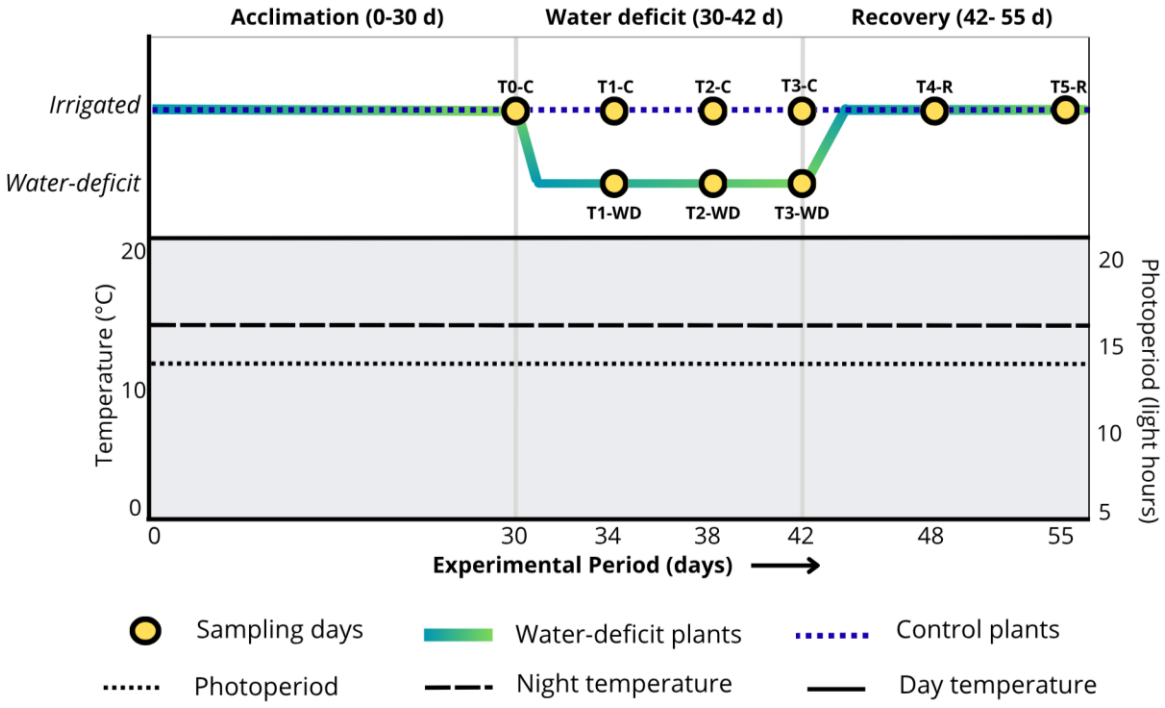

Figure 6.1 Experimental design for water-deficit induction and recovery in *Eucalyptus* plants, including sampling times and controlled environmental conditions.

6.2.2. VIS-NIR hyperspectral image acquisition and processing

Whole-plant hyperspectral images were acquired using a Resonon Pika-L line-scan camera (Resonon Inc., Bozeman, MT, USA) in diffuse reflectance mode. The analytical range used for modelling was 400-1000 nm, comprising 281 spectral channels with an approximate spectral interval of 2.1 nm and spectral resolution of 2.7 nm. Images were acquired using Spectronon PRO software under controlled illumination and geometry. White and dark references were used to convert raw intensity to relative reflectance.

The background was removed by spectral thresholding, and plant regions were retained as regions of interest. Mean spectra were extracted to provide one representative plant-level spectrum for exploratory analysis, regression, ASCA, and plant-level classification. Pixel matrices were retained only for spatial visualization and secondary pixel-level models. Reflectance spectra were transformed to pseudo-absorbance using $A = -\log10(R)$. Smoothing, standard normal variate transformation (SNV), multiplicative scatter correction (MSC), first and second derivatives, normalization, and mean centring were evaluated. Preprocessing was selected separately for each analysis because the transformation that maximizes class separation is not necessarily optimal for physiological regression or variance decomposition.

6.2.3. Portable NIR spectral acquisition and processing

Portable NIR spectra were acquired with a miniaturized Ocean Insight NANOQUEST spectrometer equipped with a reflectance probe. The instrument covered approximately 1300-2500 nm with an 8 nm resolution. To reduce noisy edge regions and maintain comparability with the modelling workflow, analyses were restricted to 1400-2400 nm. Ten-point spectra were collected from leaves located in the third and fourth whorls of each plant and averaged to obtain a leaf-level representative spectrum. This averaging reduced local heterogeneity while preserving the overall hydration and biochemical signal of the measured leaves.

Spectra were converted to pseudo-absorbance and evaluated with smoothing, MSC, SNV, derivatives, and mean centering. An 11-point Savitzky-Golay smoothing filter followed by MSC and mean centering provided a useful representation for several exploratory and ASCA analyses. Hotelling T2 and Q-residual statistics at a 95% confidence level were used to identify anomalous spectra. Observations associated with acquisition failure or severely deteriorated tissue were removed only when supported by both multivariate diagnostics and visual inspection.

6.2.4. Physiological measurements

Physiological measurements were collected at the same sampling stages as the spectral data. The variables used to support the interpretation of the spectral and molecular responses are summarized in Table 6.2. Gas-exchange and chlorophyll-fluorescence measurements were performed using a LI-6800 portable photosynthesis system (LI-COR Biosciences, Lincoln, NE, USA) equipped for simultaneous infrared gas analysis and fluorescence measurements. The recorded variables included net CO_2 assimilation rate (A), stomatal conductance to water vapour (gsw), electron transport rate (ETR), emission-related fluorescence response (Emm), quantum yield associated with CO_2 assimilation (PhiCO_2), effective quantum yield of photosystem II (PhiPS2), non-photochemical quenching (NPQ), photochemical quenching (qP), the fraction of closed PSII reaction centres (1-qL), and leaf energy-balance temperature (TleafEB). Plant height and fresh mass were also determined as complementary growth-related variables. Plant water status was assessed using a Scholander-type Pump-Up pressure chamber (PMS Instruments). Water potential was recorded as the positive balancing pressure in psi; therefore, higher numerical values represent a greater absolute magnitude of negative water potential and, consequently, a more severe plant water deficit.

Table 6.2 Physiological variables used to anchor spectral and molecular interpretation.

Variable	*Definition*	*Biological interpretation*
A	Net CO2 assimilation	Carbon fixation; strongly constrained by stomatal and biochemical limitations
gsw	Stomatal conductance	Stomatal opening and transpiration-related limitation
ETR	Electron transport rate	Photosynthetic electron flow
PhiCO2	Quantum yield of CO2 assimilation	Efficiency of absorbed light use for carbon assimilation
PhiPS2	Effective PSII quantum yield	Photochemical efficiency of PSII
NPQ	Non-photochemical quenching	Thermal dissipation of excess excitation energy

1-qL	Closed PSII reaction-centre fraction	Excitation pressure on PSII
qP	Photochemical quenching	Fraction of open PSII centres under the adopted formulation
TleafEB	Leaf energy-balance temperature	Thermal response linked to transpiration and stomatal closure
Water potential	Pressure magnitude, psi	Severity of plant water deficit; sign convention requires caution

6.2.5. RNA extraction, cDNA synthesis, and qPCR

Leaf tissue was collected from the subset of plants selected for molecular analysis. Initial micro-scale CTAB extraction protocols produced insufficient RNA yield or purity in several drought-stressed *Eucalyptus* samples. The protocol was therefore scaled to approximately 5 mL CTAB extraction buffer per 0.5 g of foliar tissue. RNA quality was evaluated using A260/A280 and A260/A230 absorbance ratios and by inspection of 28S and 18S ribosomal RNA bands on agarose gels. Only samples meeting concentration, purity, and integrity criteria were used for reverse transcription.

cDNA was synthesized from the accepted RNA extracts. The loss of samples during RNA extraction and quality filtering produced an unbalanced molecular dataset in which some genotype × treatment × replicate combinations were underrepresented or absent. This limitation was incorporated explicitly into the interpretation and prevented the molecular block from being treated as a definitive reference method for spectral validation.

Candidate reference genes included IDH, E1F, and EIF1A, whereas the target genes comprised DHN1, LEA4 and TRDX. Primer amplification performance was evaluated using serial cDNA dilution curves consisting of seven dilution levels and no-template control. Quantitative PCR assays were performed using a StepOnePlus Real-Time PCR System with SYBR Green chemistry and ROX as the passive reference dye. For each primer pair, Ct values were plotted against the logarithm of relative cDNA concentration, and the corresponding slope and amplification efficiency were calculated to assess primer suitability for relative gene-expression analysis.

Relative gene expression was calculated using the comparative Ct approach, with the calibrator condition defined according to the objective of each assay. In Assay I, G1, G3, and G4 were evaluated after 7 days of water withdrawal. Water-deficit samples were compared with control samples collected on the same experimental day, allowing the treatment-associated

transcriptional response to be assessed at that sampling stage. In Assay II, G4, G5, and G6 were evaluated after 12 days of water withdrawal, corresponding to the severe water-deficit stage. In this assay, T3-WD samples were compared with the irrigated T0 baseline to quantify the accumulated change in gene expression from the initial condition to severe water deficit. Thus, the two comparison schemes provided complementary information on the molecular response to water restriction: a time-matched treatment comparison in Assay I and a baseline-to-severe-deficit comparison in Assay II.

6.2.6. Statistical and chemometrics analyses

Univariate comparisons and correlations

Control and WD means were compared using Welch's t test when unequal variances were assumed. For genotype-resolved analyses, normality and variance homogeneity were assessed before selecting parametric or rank-based alternatives. Spearman rank correlations were calculated between relative gene expression and physiological variables. Correlations were evaluated for the pooled control-plus-WD dataset, for the WD subset, and descriptively by genotype. Because pooling two strongly separated treatments can generate high correlations even without a continuous within-treatment relationship, pooled correlations were interpreted primarily as evidence of coordinated treatment response rather than as proof of direct gene-to-physiology coupling.

Exploratory spectral analysis and physiological regression

Principal component analysis (PCA) was first applied to the spectral datasets to explore the main sources of variation, identify anomalous observations, and examine possible grouping patterns associated with genotype and sampling stage. Subsequently, separate regression models were developed for each physiological variable using the VIS–NIR HSI and portable NIR spectral matrices as predictor variables (X) and the corresponding physiological measurements as response variables (y). Partial least squares regression (PLS-R) was used to model linear relationships between spectral and physiological data, whereas support vector machine regression (SVM-R) was evaluated as a nonlinear alternative. Model complexity was selected through internal cross-validation. Predictive performance was assessed using the coefficients of

determination and root mean square errors obtained for calibration and cross-validation (R^2cal, R^2CV, RMSEC, and RMSECV). Model robustness was evaluated primarily from cross-validation performance, the agreement between calibration and cross-validation statistics, and the sensitivity of the model to influential observations. Models showing high R^2cal but substantially lower R^2CV, large differences between RMSEC and RMSECV, or a strong dependence on the exclusion of individual samples were considered potentially overfitted and were not interpreted as reliable predictive models.

Spectral-gene regression

Exploratory PLS-R models were developed to examine the relationship between spectral information and the relative expression of DHN1, LEA4, and TRDX. Spectral measurements were matched with the corresponding molecular measurements at the biological-sample level. When multiple instrumental spectra were available for the same sample, they were either averaged or retained as repeated measurements, while keeping all spectra from the same biological sample within the same validation group. Because the number of biological samples with valid paired spectral and molecular data was limited, the resulting models were interpreted as exploratory associations rather than validated predictors of transcript abundance. In the available dataset, some missing molecular values were replaced by the mean of the corresponding observations to obtain complete response vectors. Consequently, model performance was interpreted cautiously, considering that imputed values do not represent independent biological measurements and may affect the variance and covariance structure of the molecular data.

6.3. Results

6.3.1. Physiological response during water deficit and recovery

General physiological response

Water withdrawal produced a coordinated decline in plant physiological performance. As water-deficit severity increased from T1 to T3, previously stressed plants generally showed lower net CO_2 assimilation, stomatal conductance, and effective PSII quantum yield than continuously irrigated controls. These responses were consistent with progressive stomatal limitation, reduced

carbon fixation, and impairment of photochemical activity. However, the magnitude and subsequent reversal of these changes differed among genotypes, indicating that both drought impact and post-drought recovery followed genotype-dependent patterns.

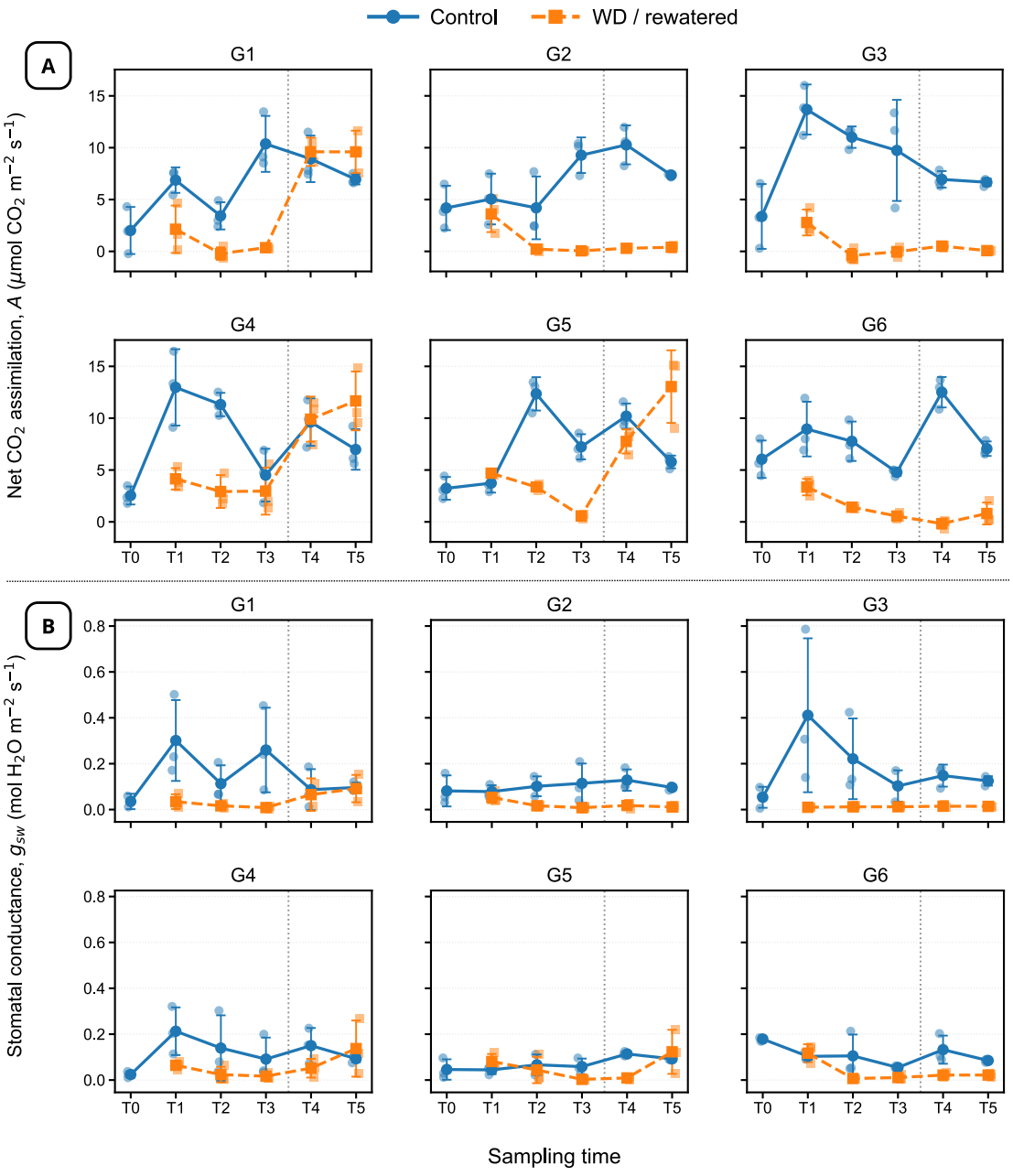

Figure 6.2 Gas-exchange responses of *Eucalyptus* genotypes G1–G6 during water deficit and recovery. (A) Net CO_2 assimilation and (B) stomatal conductance (g_sw) across T0–T5. Symbols show replicates and mean ± SD; the dotted line marks rewatering.

The genotype-resolved trajectories of net CO_2 assimilation and stomatal conductance are shown in Figure 6.2. In all genotypes, the decline in net CO_2 assimilation was accompanied by a reduction in stomatal conductance, supporting an important contribution of stomatal closure to the limitation of photosynthetic carbon uptake under water deficit. At the most severe stress stage (T3), both A and gsw were markedly reduced in water-deficit plants relative to their respective controls.

After irrigation was restored, recovery of gas exchange was clearly genotype dependent. G1, G4, and G5 showed a more evident increase in photosynthetic activity during the recovery period, whereas G2, G3, and G6 maintained comparatively low values. A similar tendency was observed for stomatal conductance, suggesting that restoration of water supply did not necessarily result in immediate stomatal reopening or full recovery of carbon assimilation. Overall, these results indicate that recovery of gas exchange after rewatering was only partial and strongly dependent on genotype.

Photochemical response

The effective quantum yield of PSII also declined during water-deficit development, although its temporal pattern was not identical to that of gas exchange. The genotype-resolved trajectories are shown in Figure 6.3. This distinction suggests that stomatal closure and photochemical limitation developed at different rates. During recovery, PhiPS2 increased in some genotypes but remained strongly altered in others, indicating incomplete restoration of PSII function 13 days after rewatering.

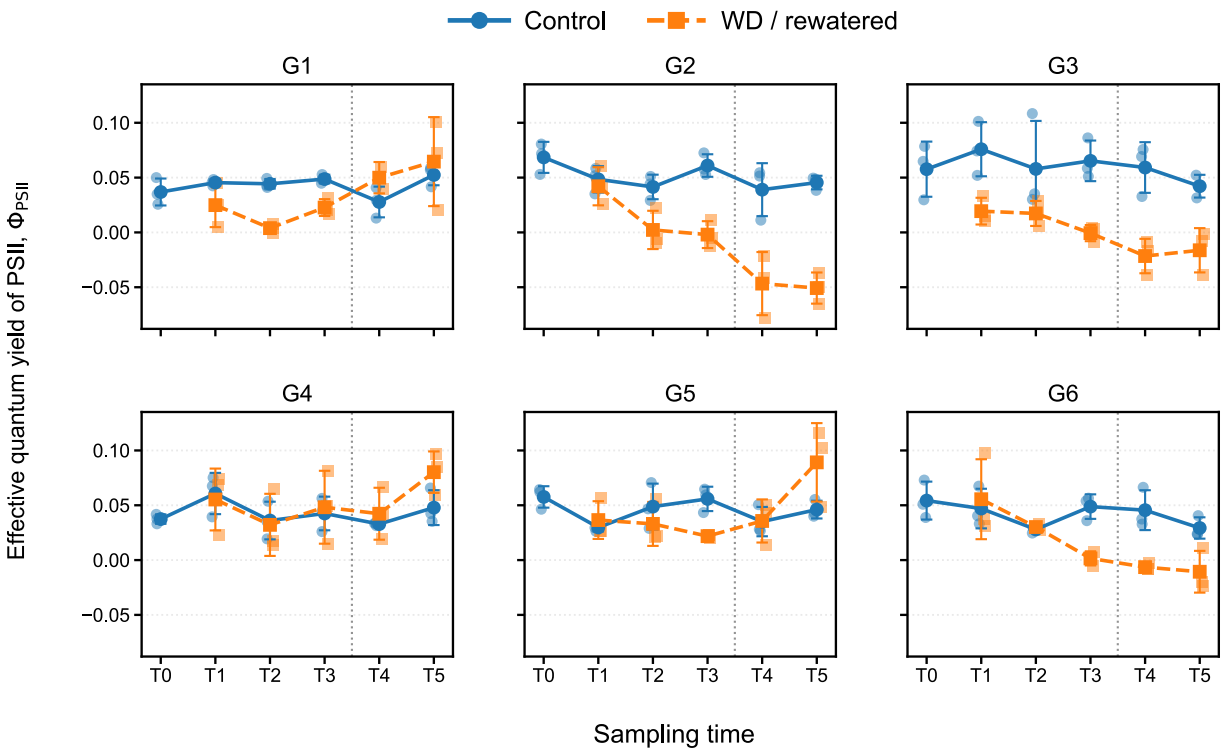

Figure 6.3 Effective quantum yield of photosystem II in *Eucalyptus* genotypes G1–G6 during water deficit and recovery across T0–T5. Symbols show replicates and mean ± SD; the dotted line marks rewatering.

NPQ showed a considerably more heterogeneous response among biological replicates and genotypes. Because non-photochemical energy dissipation can increase as a protective mechanism but may also become unstable under severe tissue deterioration, NPQ was considered complementary rather than primary evidence of recovery. Its complete genotype-resolved trajectories are therefore provided in Figure S6.1 of the Supplementary Material.

Water-potential response

Water potential provided the clearest direct confirmation of severe plant water deficit. At T3, control plants showed water potentials ranging from approximately −0.15 to −0.21 MPa, whereas most water-deficit plants reached the maximum balancing pressure of the pressure chamber (21 bar). These observations were plotted at −2.1 MPa but should be interpreted as $\Psi \leq -2.1$MPa rather than as exact measurements. G4 also exhibited strongly negative water potentials, although its mean value remained slightly above the instrumental limit.

Thirteen days after rewatering, distinct genotype-specific patterns were observed. G1 and G5 showed water potentials approaching those of their corresponding controls, whereas G4 exhibited partial recovery. G6 remained substantially more negative than its control. In contrast, G2 and G3 remained at or beyond the measurement limit of the pressure chamber ($\Psi \leq -2.1$ MPa), indicating little or no measurable restoration of plant water status under the evaluated conditions. Because values beyond this threshold could not be resolved by the instrument, the actual magnitude of the water deficit in these plants may have been greater than that represented in the figure. Overall, the results demonstrate marked genotype-dependent differences in the restoration of plant water status following rewatering (Figure 6.4).

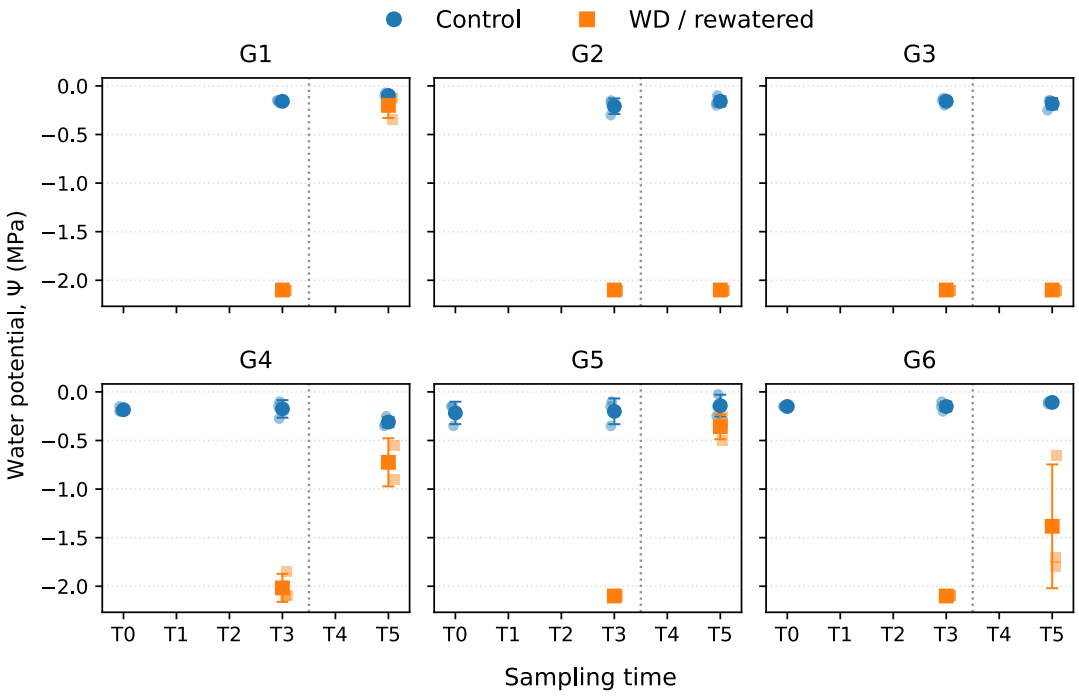

Figure 6.4 Leaf water potential (Ψ) in *Eucalyptus* genotypes G1–G6 at T0, T3, and T5 during water deficit and recovery. Symbols show replicates and mean ± SD; values at −2.1 MPa indicate $\Psi \leq -2.1$ MPa, the pressure-chamber limit.

Complementary whole-plant responses

Fresh mass and plant height were evaluated as complementary indicators of whole-plant response to water deficit and subsequent rewatering (Supplementary Figure S6.2). Fresh mass progressively diverged between continuously irrigated and water-deficit plants during irrigation

withdrawal. At T3, genotype-level mean fresh mass ranged from approximately 94 to 121 g in control plants and from approximately 49 to 66 g in water-deficit plants, indicating a marked reduction in plant hydration and whole-plant fresh mass.

Following rewatering, fresh mass increased in all previously stressed groups. By T5, G4 and G5 reached values similar to or slightly higher than those of their corresponding controls, while G6 also approached the control level. In contrast, G1, G2, and G3 retained lower mean fresh mass than their controls. However, the rapid increase observed after rewatering should not be interpreted exclusively as biomass accumulation, because it likely reflected, at least in part, tissue rehydration.

Plant height showed comparatively smaller and more heterogeneous treatment-related differences. At T5, previously stressed plants of G1, G2, G3, G5, and G6 generally remained shorter than their corresponding controls, whereas G4 showed similar or slightly higher mean values. Because height was measured only at selected stages and displayed considerable variability among biological replicates, particularly in G6, it was considered a complementary rather than a sensitive indicator of short-term recovery.

6.3.2. Molecular response to water deficit

The relative expression of DHN1, LEA4, and TRDX was evaluated in selected genotypes from both assays. Because the experimental designs and calibrator conditions differed, expression magnitudes were interpreted within each assay and were not directly compared between assays

In Assay I, water deficit induced distinct expression patterns among G1, G3, and G4 (Figure 6.5A–C). DHN1 expression increased under water deficit in all three genotypes, indicating that dehydrin-associated mechanisms formed part of the general molecular response to declining water availability. The strongest DHN1 response was observed in G4, which also showed comparatively elevated expression under the control condition. This pattern suggests that G4 maintained relatively high basal activity of a gene associated with membrane and macromolecule protection and further increased this response after water withdrawal. By contrast, LEA4 showed its most pronounced induction in G3, reaching a relative-expression magnitude substantially higher than those recorded in G1 and G4. TRDX followed a similar genotype-dependent pattern,

with the strongest response in G3, an intermediate response in G4, and the lowest expression in G1. Thus, the molecular profile of G3 was dominated by the coordinated induction of genes associated with protein stabilization and redox regulation, whereas G4 showed a response more strongly characterized by DHN1 induction. G1 activated the three molecular components, but generally at a lower magnitude.

The severe water-deficit stage evaluated in Assay II also produced induction of the three candidate genes, although the relative contribution of each response differed among G4, G5, and G6 (Figure 6.5D–F). DHN1 increased in all three genotypes, with the largest expression observed in G5, followed by G4 and G6. LEA4 showed an especially pronounced response in G5. This genotype already exhibited higher LEA4 expression under the irrigated condition than G4 and G6 and showed a marked additional increase under water deficit, reaching a relative-expression level of approximately 1000. G4 and G6 also increased LEA4 expression, but their responses were approximately one order of magnitude lower than that of G5. These results indicate that G5 strongly activated molecular mechanisms associated with the stabilization of proteins and cellular structures during severe dehydration.

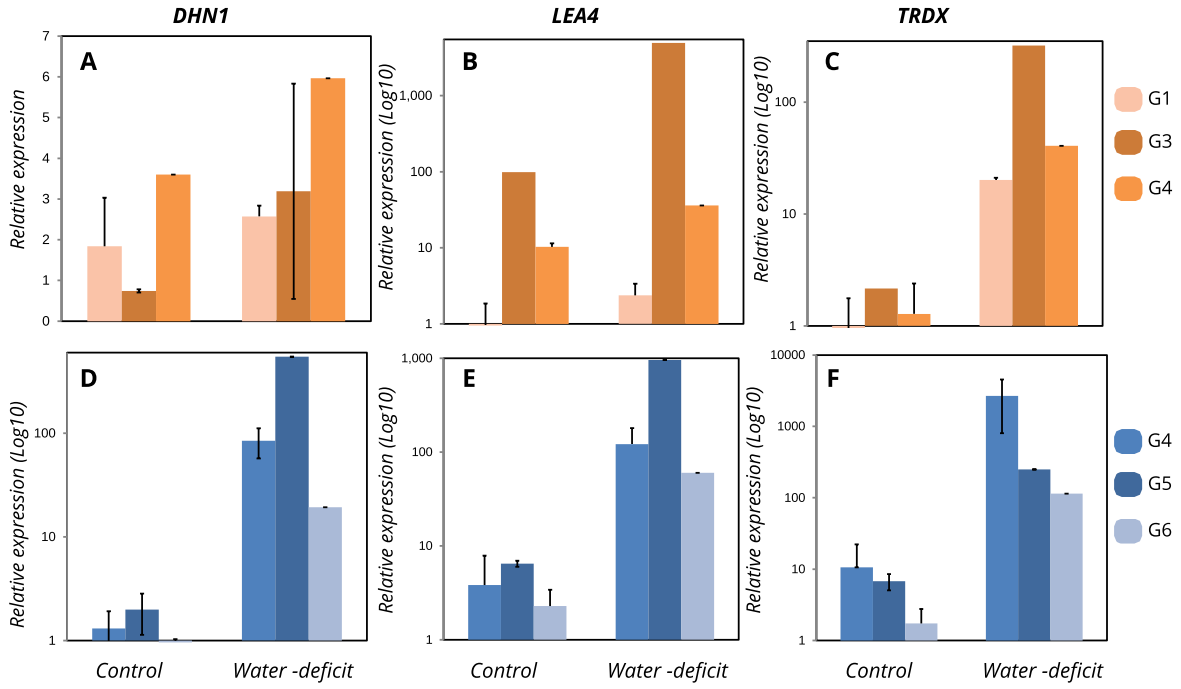

Figure 6.5 Relative expression of DHN1, LEA4, and TRDX in selected *Eucalyptus* genotypes after 7 days (A–C) and 12 days (D–F) of water deficit. Symbols show replicates and mean ± SD; compare values only within each assay.

TRDX showed a different genotype ranking from DHN1 and LEA4. Its largest induction was observed in G4, reaching a relative-expression magnitude of approximately 2500, whereas G5 and G6 showed lower but still substantial responses. The exceptionally high TRDX expression in G4 is consistent with strong activation of redox-regulatory mechanisms. Nevertheless, two alternative interpretations remain possible. The response may represent an effective antioxidant adjustment, but it may also reflect a greater oxidative demand in this genotype. Previous transcriptomic evidence in *Eucalyptus globulus* has similarly shown that greater induction of thioredoxin-related genes does not necessarily occur exclusively in the most drought-tolerant material (Ulloa et al., 2022). Therefore, the TRDX response cannot be interpreted independently as evidence of superior tolerance.

Overall, the two assays demonstrated that water deficit activated molecular pathways associated with dehydration protection, protein stabilization, and redox regulation, but that the relative importance of these mechanisms was strongly genotype dependent. DHN1 showed the most consistent induction across the evaluated materials, supporting its role as a relatively general component of the response to cellular dehydration. LEA4 and TRDX displayed more contrasting genotype-specific responses. In Assay I, G3 showed the strongest coordinated induction of LEA4 and TRDX, whereas G4 was characterized by a comparatively strong DHN1 response. In Assay II, G5 combined high DHN1 and very high LEA4 expression with a more moderate TRDX response, while G4 showed a response strongly dominated by TRDX. G6 activated the same molecular pathways but generally at lower magnitudes.

These patterns indicate contrasting molecular response strategies, but they do not demonstrate that the genotype with the highest transcript accumulation was necessarily the most drought tolerant. Strong induction may represent effective protection, greater stress exposure, or a combination of both processes. The molecular results must therefore be interpreted together with the maintenance of physiological function during water deficit and the capacity for recovery after rewatering. In this context, gene expression provides evidence that the water-deficit treatment activated biologically relevant protective and redox-associated mechanisms, while the

physiological and recovery measurements determine whether this activation was accompanied by improved functional performance.

6.3.3. Spectral relationship with physiological and molecular responses

The relationships among spectral information, physiological performance, and gene expression were examined to determine whether spectral variation detected by VIS–NIR hyperspectral imaging and portable NIR spectroscopy was associated with the biological response to water deficit. Linear relationships between spectral data and physiological variables were explored using PLS-R, whereas SVM-R was used to examine potential nonlinear relationships. These analyses were complemented by correlations between gene expression and physiological status and by exploratory spectral–gene models. Because the analyses differed in sample size, objective, and robustness, their results were interpreted as associations rather than as evidence of validated predictive performance.

Spectral relationships with physiological variables

Separate PLS-R and SVM-R models were developed using the VIS–NIR HSI and portable NIR spectral matrices to explore linear and nonlinear relationships, respectively, between spectral variation and the physiological variables measured during water-deficit development and recovery. The strength of these relationships varied substantially among physiological variables and spectral platforms, indicating that the evaluated processes were reflected with different degrees of consistency in the spectral information.

Although the primary objective was exploratory rather than predictive, cross-validation was used to assess the robustness of the observed relationships. Models were considered more consistent when R^2cal and R^2CV were similar and when RMSECV remained close to RMSEC. In contrast, models showing strong calibration performance but marked deterioration during cross-validation were interpreted as unstable, dataset-dependent, or potentially overfitted.

Table 6.3 Performance of PLS-R and SVM-R models developed to examine relationships between VIS–NIR HSI or portable NIR spectra and physiological variables.

Variable	Technique/Dataset	Model	Preprocessing	R²cal	R²CV	RMSEC	RMSECV
A	HSI/Complete	PLS-R	1st derivative–MC	0.584	0.474	2.40	2.75
PhiCO₂	HSI/Exclude	PLS-R	2nd derivative–MC	0.637	0.532	0.002	0.002
NPQ	HSI/Exclude	SVM-R	SNV–MC	0.940	0.871	2.100	3.020
Water potential	NIR/Complete	SVM-R	MSC-MC	0.735	0.600	68.71	83.25
ETR	NIR/Complete	SVM-R	MSC-MC	0.516	0.464	13.71	14.31
PhiPS2	NIR/Exclude	SVM-R	MSC-MC	0.524	0.469	0.0216	0.0226

The VIS–NIR HSI models showed their strongest relationship with variables associated with photosynthetic regulation and photoprotection. Among these, NPQ showed the strongest and most consistent spectral relationship, indicating that spectral variation in the visible and red-edge regions contained information related to changes in the dissipation of excess absorbed energy. However, because NPQ also showed substantial biological variability among genotypes and replicates, this result should be interpreted as evidence of an association between leaf optical properties and photoprotective adjustment rather than as a universally applicable quantitative relationship.

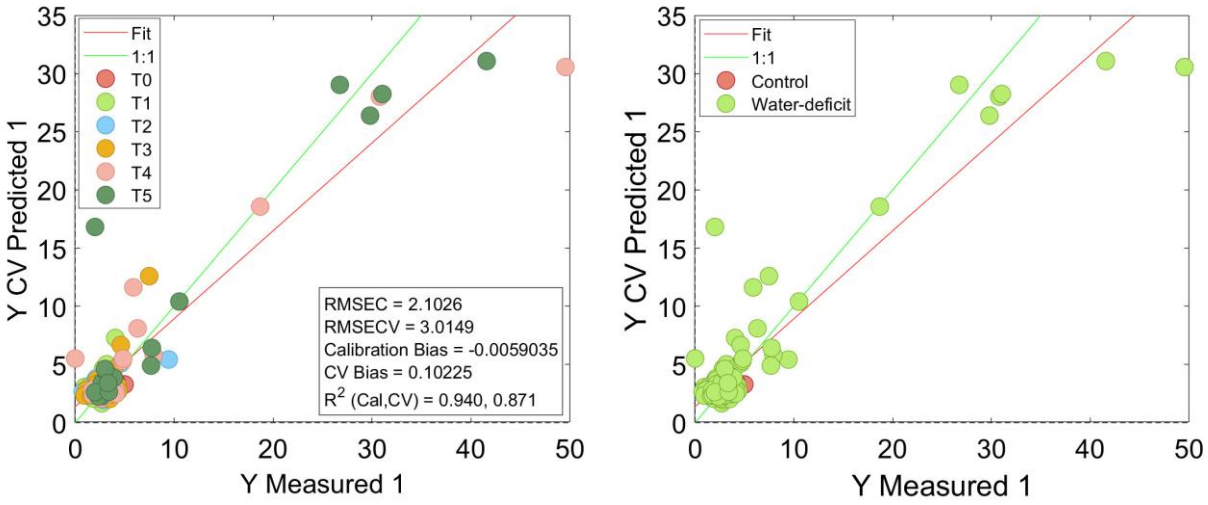

Figure 6.6 Measured versus cross-validated NPQ values for the best spectral model, grouped by sampling stage and treatment. Lines indicate the 1:1 relationship and fitted regression. Model performance: R²cal = 0.940, R²CV = 0.871, RMSEC = 2.10, and RMSECV = 3.02.

Among the evaluated physiological variables, the portable NIR models showed the clearest relationship with plant water status. This result is consistent with the strong contribution of spectral regions associated with O–H absorption, particularly around 1450 and 1940 nm, which are sensitive to changes in water content and hydrogen bonding in plant tissues. The model developed for water potential showed a comparatively consistent agreement between calibration and cross-validation, supporting the capacity of portable NIR spectroscopy to capture variation associated with the severity of plant dehydration.

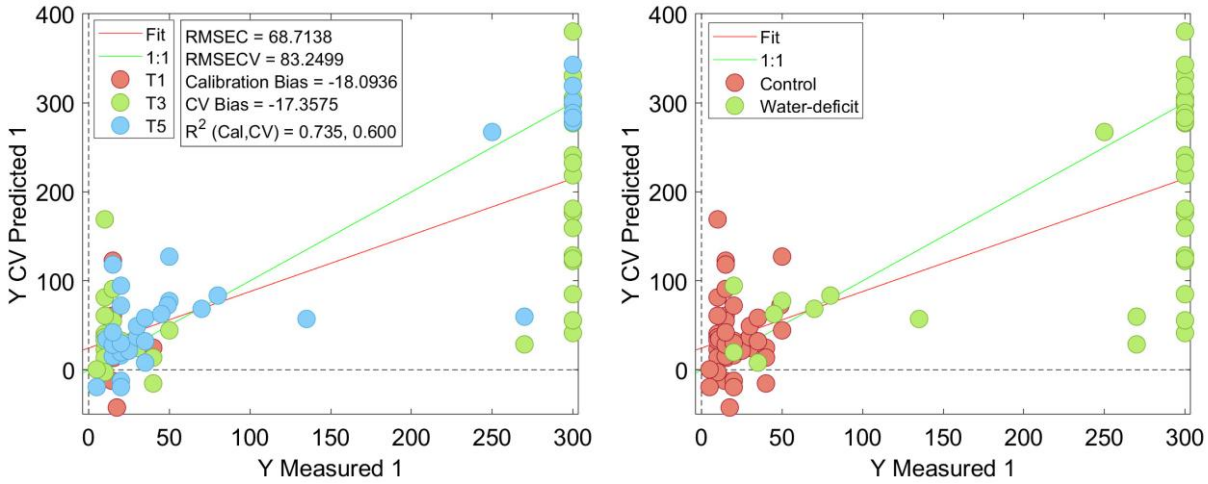

Figure 6.7 Measured versus cross-validated water potential for the best portable NIR model, grouped by time and treatment. higher pressure denotes more negative water potential.

Moderate spectral relationships were also observed for PhiPS2 and ETR using portable NIR data. These variables describe complementary aspects of PSII performance, including photochemical efficiency and electron transport. Because their direct physiological responses occur primarily in the photosynthetic apparatus, their association with the NIR spectra was likely indirect and may reflect coordinated changes in tissue hydration, leaf structure, and biochemical composition during water-deficit development. However, their cross-validation coefficients were lower than those obtained for water potential and NPQ, indicating that these relationships were less consistent across samples.

The remaining physiological variables generally showed weak-to-moderate relationships with the spectral matrices. For A and PhiCO2, cross-validation results indicated that part of their

physiological variation was represented in the spectra, although the models were not sufficiently stable to support a strong quantitative interpretation. For gsw, qP, 1-qL, Emm, and TleafEB, model performance was more limited or showed a marked decrease from calibration to cross-validation (Tables S6.1 and S6.2 in the supplementary material). In some cases, the apparent improvement depended on the exclusion of a small number of observations, further reducing confidence in the generality of the relationship. These results suggest that the models captured partial covariance associated with water-deficit progression, but not a stable spectral representation of each physiological variable.

Overall, the two spectral platforms provided complementary information on the plant response. VIS–NIR HSI showed the strongest association with NPQ and captured additional variation related to photosynthetic activity, pigment-sensitive spectral regions, and leaf optical properties. Portable NIR spectroscopy showed the clearest relationship with plant water status and also contained indirect information associated with photochemical performance. Nevertheless, only a small subset of physiological variables showed sufficiently consistent calibration and cross-validation behaviour to support a robust spectral association. The remaining models were therefore interpreted as exploratory evidence of physiological information embedded in the spectra rather than as validated tools for quantitative estimation.

Associations between gene expression and physiology

Spearman correlation analysis was used to examine whether the expression of DHN1, LEA4, and TRDX followed coordinated patterns with the physiological response to water deficit. In the pooled control-plus-water-deficit dataset, the three genes showed predominantly negative associations with variables related to photosynthetic performance and gas exchange, including A, ETR, PhiCO2, PhiPS2, and gsw, whereas positive associations were observed with TleafEB. These patterns indicate that higher expression of dehydration and redox-responsive genes generally occurred in plants showing lower photosynthetic activity, stronger stomatal limitation, and increased leaf temperature.

However, the pooled correlations must be interpreted cautiously because they may be driven largely by the contrast between treatment conditions. Control plants generally showed lower expression of stress-responsive genes and higher physiological performance, whereas water-

deficit plants showed the opposite pattern. Therefore, a strong pooled correlation does not necessarily demonstrate a continuous within-treatment relationship between gene expression and physiology.

When the analysis was restricted to water-deficit plants, the associations were weaker but more biologically informative. Higher expression of DHN1 and LEA4 was generally associated with lower photosynthetic and photochemical performance, including reduced A, ETR, PhiCO2, and PhiPS2. TRDX showed a negative association with gsw and a positive association with TleafEB, suggesting that stronger redox-related activation occurred in plants with greater stomatal restriction and higher leaf temperature. These results are consistent with stronger induction of the candidate genes in plants showing greater physiological impairment, although they do not establish a causal relationship between gene expression and physiological decline.

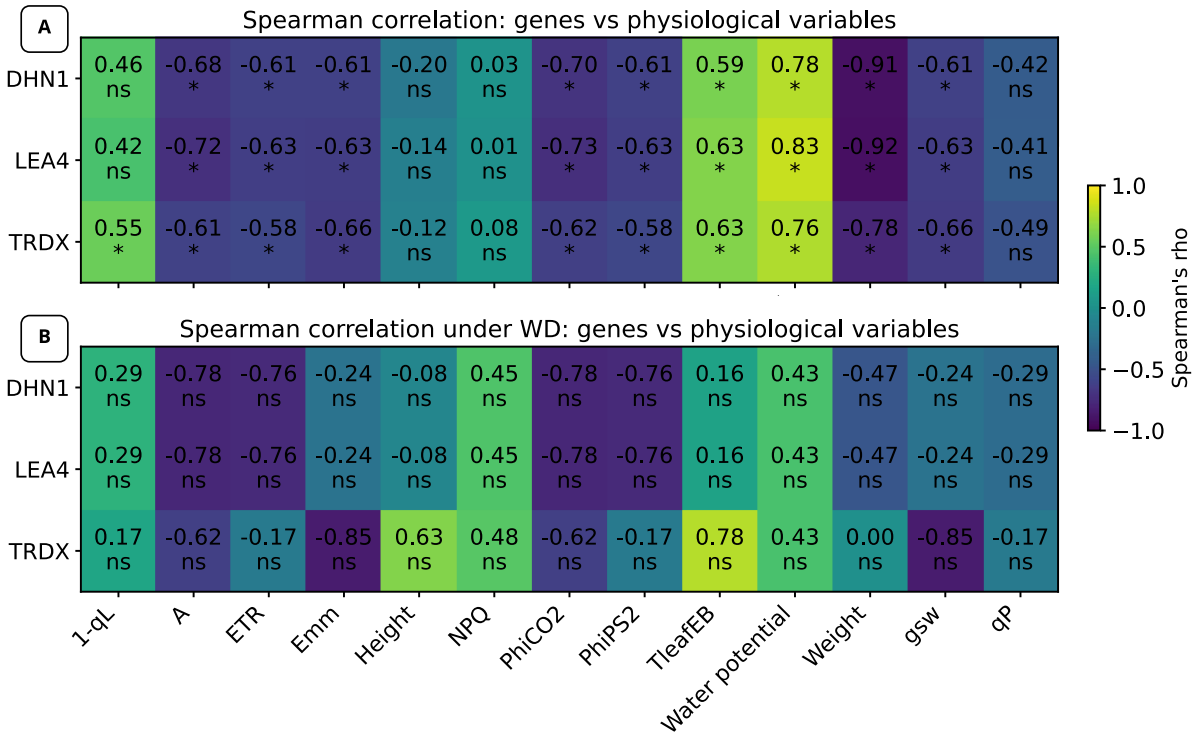

Figure 6.8 Spearman correlation heatmaps between stress-responsive genes and physiological traits in (A) all samples and (B) water-deficit samples. Colors indicate Spearman's rho; asterisks denote FDR-adjusted $p < 0.05$ and "ns" non-significant correlations.

Genotype-resolved analyses showed additional variation in these relationships. G4 exhibited generally weak and non-significant associations between gene expression and physiological

variables, whereas G5 and G6 showed stronger negative correlations between the three candidate genes and variables associated with photosynthesis and gas exchange. Positive associations with TleafEB were also more evident in these genotypes. However, because the number of paired molecular and physiological observations was small, genotype-specific correlations are presented in the Supplementary Material (Figure S6.3).

Overall, the observed molecular–physiological associations suggest that transcriptional activation of dehydration- and redox-related genes accompanied reduced photosynthetic function and stomatal regulation under water deficit. Nevertheless, gene induction appeared to reflect the intensity of the stress response rather than a direct measure of physiological tolerance.

Exploratory spectral associations with gene expression

Exploratory PLS-R and SVM-R models were developed to examine linear and nonlinear multivariate associations, respectively, between VIS–NIR HSI or portable NIR spectra and the relative expression of DHN1, LEA4, and TRDX. Cross-validation was used as an internal assessment of the consistency of these associations rather than as evidence of validated prediction of transcript abundance. Given the limited number of paired molecular–spectral observations, the unbalanced molecular dataset, and the replacement of some missing molecular values by mean values, all models were interpreted as hypothesis-generating.

Table 6.2 summarizes the models showing the highest cross-validation coefficients for each gene, assay, and spectral platform, whereas the complete results are provided in the Supplementary Material (Table S6.3). In Assay I, the strongest association was obtained for DHN1 using VIS–NIR HSI and SVM-R, with $R^2cal = 0.811$ and $R^2CV = 0.550$. The models for LEA4 and TRDX showed lower cross-validation coefficients, despite moderate-to-high calibration fits. This discrepancy indicates that part of the apparent relationship was not maintained when observations were evaluated outside the calibration subsets.

Table 6.4 Best spectral–gene regression models by gene, assay, and platform. LV: latent variables; SV: support vectors; R^2cal and R^2CV: calibration and cross-validation coefficients; RMSEC and RMSECV: corresponding errors.

Assay	*Gene*	*Technique*	*Model*	*R^2cal*	*R^2CV*	*RMSECV*
I	DHN1	VIS–NIR HSI	SVM-R	0.811	0.550	1.214
I	LEA4	VIS–NIR HSI	SVM-R	0.934	0.338	1.036
I	TRDX	VIS–NIR HSI	SVM-R	0.624	0.352	0.91
II	DHN1	VIS–NIR HSI	SVM-R	0.758	0.083	181
II	LEA4	VIS–NIR HSI	SVM-R	1.000	0.482	0.757
II	TRDX	VIS–NIR HSI	SVM-R	0.123	0.047	1.321
II	DHN1	Portable NIR	PLS-R	0.853	0.165	203
II	LEA4	Portable NIR	PLS-R	0.832	0.304	1.455
II	TRDX	Portable NIR	SVM-R	0.348	0.166	1.121

In Assay II, VIS–NIR HSI showed its highest cross-validation result for LEA4 using SVM-R. However, the almost perfect calibration fit was markedly reduced during cross-validation, indicating substantial model instability. The remaining HSI models for DHN1 and TRDX showed weak cross-validation performance. Portable NIR models also produced moderate calibration coefficients for some genes, particularly DHN1 and LEA4, but these relationships weakened considerably during cross-validation.

Overall, some spectral–gene combinations showed apparent multivariate associations, but the large differences between calibration and cross-validation results indicate that these relationships were strongly dataset dependent. The models may have captured spectral variation associated with treatment condition, genotype, tissue hydration, pigment composition, or other coordinated responses to water deficit rather than a direct quantitative relationship with transcript abundance. Therefore, none of the spectral–gene models was considered sufficiently robust for estimating gene expression in unknown samples.

These results nevertheless provide exploratory evidence that spectral and molecular responses changed in a coordinated manner under water deficit. However, the available dataset did not support the development of validated spectral surrogates for transcript abundance, and the models should therefore be interpreted as hypothesis-generating rather than predictive.

6.3.4. Integrative comparison of genotype performance during water deficit and recovery

To provide an integrated comparison of genotype performance, the physiological and whole-plant responses observed during water-deficit development and after rewatering were summarized qualitatively. The comparison considered functional maintenance during water deficit, recovery of plant water status, recovery of photosynthetic function, and recovery of overall plant condition. These dimensions were selected because they were available for all six genotypes and represented complementary aspects of stress response and recovery. The resulting comparison is presented in Table 6.5.

Table 6.5 Qualitative integrative comparison of genotype performance during water deficit and post-rewatering recovery based on physiological and whole-plant responses.

Genotype	*Functional maintenance during WD*	*Recovery of water status*	*Photochemical recovery*	*Recovery of overall plant condition*	*Molecular evidence*	*Integrative interpretation*
G1	✗	✓	✓	~	N/A	Showed substantial deterioration during water deficit but clear physiological recovery after rewatering. It represents favourable plant material because of its recovery capacity.
G2	✗	✗	✗	✗	N/A	Showed very limited recovery of water status and photosynthetic function during the evaluated period.
G3	✗	✗	✗	✗	N/A	Similar to G2, it maintained severe physiological impairment after rewatering.
G4	~	~	✓	✓	~	Showed one of the best relative levels of functional maintenance during stress and clear functional and fresh-mass recovery, although water status recovered only partially. The strong TRDX expression is biologically relevant but remains ambiguous.
G5	✗	✓	✓	✓	✓	Showed the most consistent response among the hybrids, combining recovery of water status, photosynthetic and photochemical function, and fresh mass with coordinated activation of molecular responses.

G6	✗	✗	✗	~	~	Recovered a substantial proportion of its fresh mass but maintained marked impairment of water status and physiological function. This pattern mainly indicates rehydration rather than complete functional recovery.

Note: ✓, favourable response; ~, partial, intermediate, or mixed response; ✗, limited or unfavourable response.

The comparison revealed contrasting genotype-response strategies. G4 showed comparatively favourable functional maintenance during water deficit and clear photosynthetic and whole-plant recovery, although its water status was only partially restored. G5 displayed the most consistent recovery among the evaluated hybrids, combining restoration of water status, photosynthetic function, and overall plant condition. G1 also showed clear physiological recovery after rewatering, despite substantial impairment during water deficit. In contrast, G2 and G3 exhibited limited recovery across the evaluated dimensions, whereas G6 recovered part of its fresh mass but retained marked water-status and photosynthetic impairment. These results demonstrate that maintenance during water deficit and recovery after rewatering represented related but distinct components of genotype performance.

6.4. Conclusions

Water deficit caused a coordinated deterioration of plant physiological performance, expressed as reductions in net CO_2 assimilation, stomatal conductance, PSII efficiency, and plant water status. However, both the magnitude of stress damage and the capacity for recovery after rewatering differed markedly among genotypes. Recovery was therefore not a uniform reversal of stress, but a multidimensional process involving partially independent restoration of water status, gas exchange, photochemical function, and whole-plant hydration.

Among the evaluated materials, G1 and G5 showed the clearest recovery of plant water status, whereas G4 exhibited partial recovery and G6 maintained substantial residual water tension. G2 and G3 showed little or no measurable restoration of water potential within the evaluated recovery period. Fresh-mass recovery did not always coincide with recovery of water potential or gas exchange, confirming that increased mass after rewatering partly reflected tissue rehydration and could not be interpreted alone as functional recovery. Consequently, no single physiological variable was sufficient to establish drought performance, and genotype evaluation required the integration of water status, photosynthetic activity, photochemical behaviour, and post-stress recovery.

Water deficit also activated molecular pathways associated with dehydration protection, protein stabilization, and redox regulation. DHN1 showed the most consistent induction among the evaluated genotypes, whereas LEA4 and TRDX displayed more contrasting genotype-dependent responses. G5 showed a particularly strong induction of DHN1 and LEA4, while G4 exhibited a response dominated by TRDX. Nevertheless, the highest transcript accumulation did not necessarily identify the genotype with the greatest physiological tolerance. Instead, strong gene induction appeared to reflect the intensity and nature of the stress response, and its biological significance could only be interpreted in conjunction with physiological maintenance and recovery.

The spectral platforms captured complementary components of the plant response. VIS–NIR hyperspectral imaging showed its strongest and most consistent association with NPQ, while portable NIR spectroscopy showed the clearest relationship with plant water potential. Moderate relationships were also observed for selected photosynthetic and photochemical variables, but

most physiological models remained exploratory rather than fully validated. These results indicate that spectral variation contained biologically meaningful information related to plant dehydration and photosynthetic regulation, although the strength and robustness of the relationships depended on the physiological variable and on both the spectral range and measurement technique used.

The molecular–physiological correlations further showed that higher expression of stress-responsive genes generally accompanied reduced photosynthetic activity, stomatal limitation, and increased leaf temperature. However, these associations were partly influenced by the contrast between control and water-deficit treatments and did not establish causal relationships. Similarly, the spectral–gene regression models showed unstable cross-validation performance and were not sufficiently robust to estimate transcript abundance in unknown samples. They were therefore considered hypothesis-generating evidence of coordinated spectral and molecular responses rather than predictive tools.

Overall, this chapter demonstrates that the response of *Eucalyptus* genotypes to water deficit and rewatering was genotype dependent, multidimensional, and only partially recoverable within the evaluated period. The integration of physiological, molecular, and spectral information provided a more reliable interpretation than any individual measurement and showed that spectral sensing can support the non-destructive assessment of plant water status and stress-associated physiological changes. However, molecular induction and spectral associations should be interpreted as complementary evidence rather than as independent indicators of drought tolerance.

6.4. References

Ammitzboll, H., Vaillancourt, R. E., Potts, B. M., Harrison, P. A., Brodribb, T., Sussmilch, F. C., & Freeman, J. S. (2020). Independent genetic control of drought resistance, recovery, and growth of Eucalyptus globulus seedlings. *Plant Cell and Environment*, *43*(1), 103–115. https://doi.org/10.1111/pce.13649

Bustin, S. A., Benes, V., Garson, J. A., Hellemans, J., Huggett, J., Kubista, M., Mueller, R., Nolan, T., Pfaffl, M. W., Shipley, G. L., Vandesompele, J., & Wittwer, C. T. (2009). The MIQE guidelines: Minimum information for publication of quantitative real-time PCR experiments. *Clinical Chemistry*, *55*(4), 611–622. https://doi.org/10.1373/clinchem.2008.112797

Bustin, S. A., Ruijter, J. M., Van den Hoff, M. J. B., Kubista, M., Pfaffl, M. W., Shipley, G. L., Tran, N., Rödiger, S., Untergasser, A., Mueller, R., Nolan, T., Milavec, M., Burns, M. J., Huggett, J. F., Vandesompele, J., & Wittwer, C. T. (2025). MIQE 2.0: Revision of the Minimum Information for Publication of Quantitative Real-Time PCR Experiments Guidelines. In *Clinical Chemistry* (Vol. 71, Number 6, pp. 634–651). Oxford University Press. https://doi.org/10.1093/clinchem/hvaf043

Correia, B., Pintó-Marijuan, M., Neves, L., Brossa, R., Dias, M. C., Costa, A., Castro, B. B., Araújo, C., Santos, C., Chaves, M. M., & Pinto, G. (2014). Water stress and recovery in the performance of two Eucalyptus globulus clones: Physiological and biochemical profiles. *Physiologia Plantarum*, *150*(4), 580–592. https://doi.org/10.1111/ppl.12110

Cursi, A. G., Oliveira, F. S., Gouveia, D. G., Oder, J. C., Barrios, W. E. B., Ferreira, G. V., Martins, A. O., Peterle, G., Nunes-Nesi, A., & Araújo, W. L. (2024). Deciphering the importance of morphological aspects in drought tolerance in eucalyptus progenies. *Forest Ecology and Management*, *569*. https://doi.org/10.1016/j.foreco.2024.122198

Farooq, M., Wahid, A., Kobayashi, N., Fujita, D., & Basra, S. M. A. (2009). Plant drought stress: Effects, mechanisms and management. In *Agronomy for Sustainable Development* (Vol. 29, Number 1, pp. 185–212). https://doi.org/10.1051/agro:2008021

Fernández, M., Valenzuela, S., Barraza, H., Latorre, J., & Neira, V. (2012). Photoperiod, temperature and water deficit differentially regulate the expression of four dehydrin genes from Eucalyptus globulus. *Trees - Structure and Function*, *26*(5), 1483–1493. https://doi.org/10.1007/s00468-012-0722-7

Fernández, M., Villarroel, C., Balbontín, C., & Valenzuela, S. (2010). Validation of reference genes for real-time qRT-PCR normalization during cold acclimation in Eucalyptus globulus. *Trees - Structure and Function*, *24*(6), 1109–1116. https://doi.org/10.1007/s00468-010-0483-0

Hanin, M., Brini, F., Ebel, C., Toda, Y., Takeda, S., & Masmoudi, K. (2011). Plant dehydrins and stress tolerance: Versatile proteins for complex mechanisms. In *Plant Signaling and Behavior* (Vol. 6, Number 10, pp. 1503–1509). https://doi.org/10.4161/psb.6.10.17088

Merchant, A., Callister, A., Arndt, S., Tausz, M., & Adams, M. (2007). Contrasting physiological responses of six Eucalyptus species to water deficit. *Annals of Botany*, *100*(7), 1507–1515. https://doi.org/10.1093/aob/mcm234

Moura, J. C. M. S., Araújo, P., Brito, M. D. S., Souza, U. R., Viana, J. O. F., & Mazzafera, P. (2012). Validation of reference genes from Eucalyptus spp. under different stress conditions. *BMC Research Notes*, *5*. https://doi.org/10.1186/1756-0500-5-634

Olvera-Carrillo, Y., Reyes, J. L., & Covarrubias, A. A. (2011). Late embryogenesis abundant proteins: Versatile players in the plant adaptation to water limiting environments. *Plant Signaling and Behavior*, *6*(4), 586–589. https://doi.org/10.4161/psb.6.4.15042

Ulloa, J. L., Aguayo, P., Conejera, D., Rubilar, R., Balocchi, C., & Valenzuela, S. (2022). Transcriptomic response in foliar and root tissues of a drought-tolerant Eucalyptus globulus genotype under drought stress. *Trees - Structure and Function*, *36*(2), 697–709. https://doi.org/10.1007/s00468-021-02241-5

Vieira Dos Santos, C., & Rey, P. (2006). Plant thioredoxins are key actors in the oxidative stress response. *Trends in Plant Science*, *11*(7), 329–334. https://doi.org/10.1016/j.tplants.2006.05.005

Warren, C. R., Aranda, I., & Cano, F. J. (2011). Responses to water stress of gas exchange and metabolites in Eucalyptus and Acacia spp. *Plant, Cell and Environment*, *34*(10), 1609–1629. https://doi.org/10.1111/j.1365-3040.2011.02357.x

Wold, S., Esbensen, K., & Geladi, P. (n.d.). *Principal Component Analysis*.

6.5. Supplementary Material.

Figure S6.1. Genotype-resolved changes in non-photochemical quenching (NPQ) in *Eucalyptus* spp. during water-deficit development and recovery. Responses are shown for genotypes G1–G6. T0 represents the initial well-watered condition; T1–T3 correspond to 4, 8, and 12 days of water deficit, and T4–T5 to 6 and 13 days after rewatering. Small symbols represent biological replicates, whereas larger symbols and error bars indicate mean ± standard deviation. The vertical dotted line marks rewatering between T3 and T4.

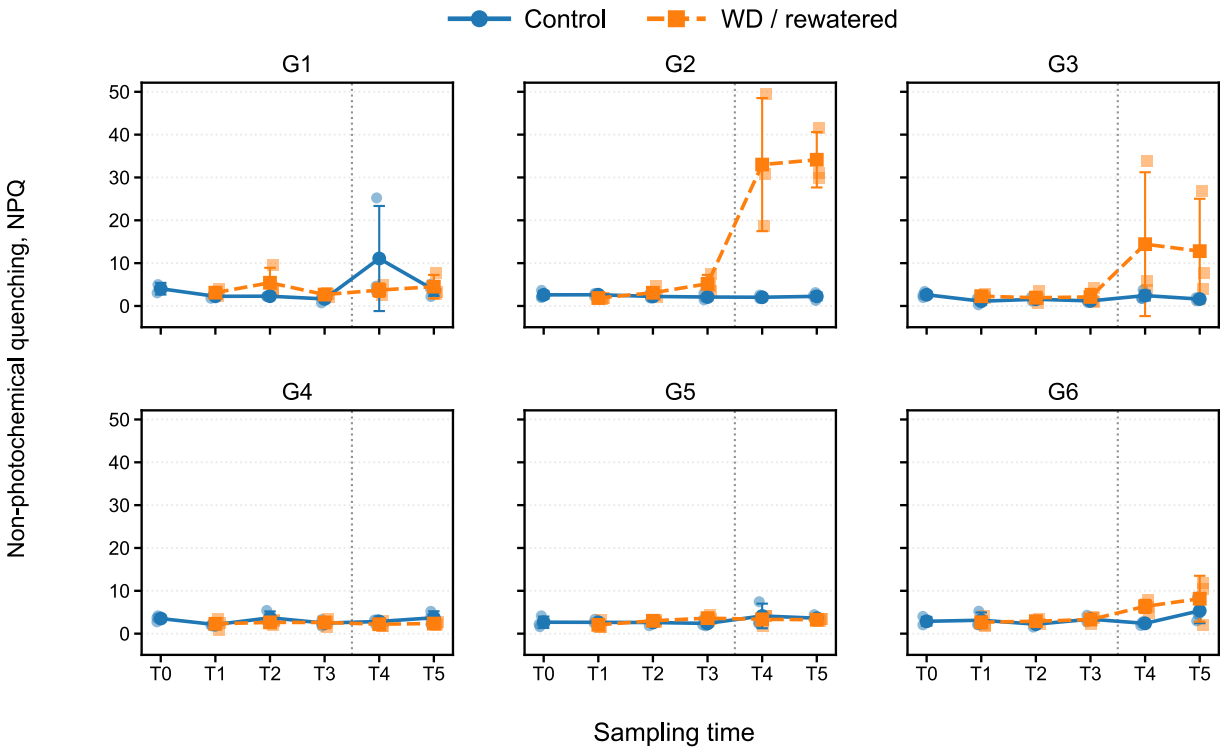

Figure S6.2. Genotype-resolved changes in fresh mass and plant height of *Eucalyptus* spp. during water-deficit development and recovery. (A) Fresh mass and (B) plant height in genotypes G1–G6. T0 represents the initial well-watered condition; T1–T3 correspond to 4, 8, and 12 days of water deficit, whereas T4–T5 correspond to 6 and 13 days after rewatering. Symbols and error bars represent mean ± standard deviation, with individual biological replicates shown as semi-transparent points. The vertical dotted line marks rewatering between T3 and T4. Height was measured only at the sampling stages for which data were available.

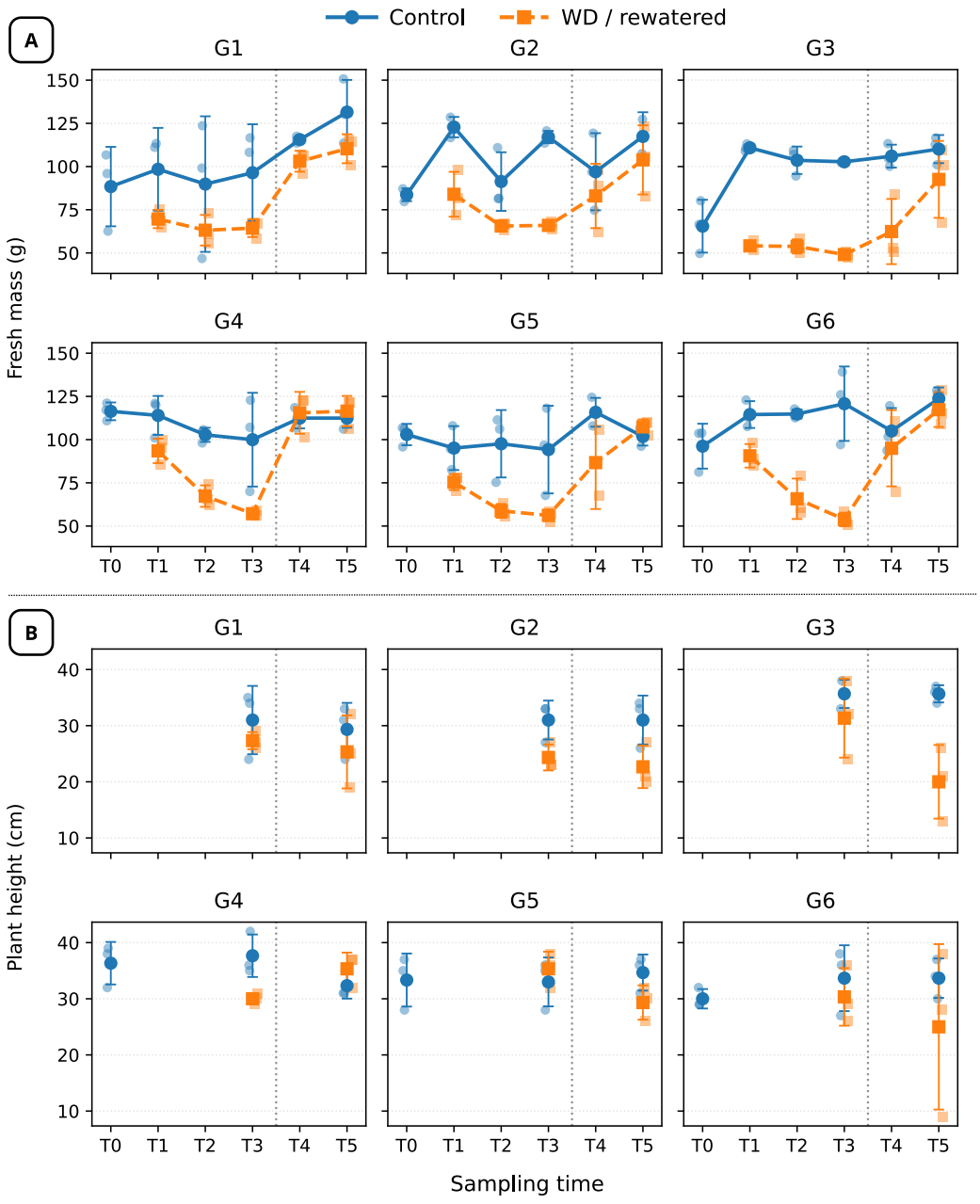

Table S6.1. Performance of PLS-R and SVM-R models developed from VIS–NIR HSI spectra to examine relationships with physiological variables. The table reports the dataset used, spectral preprocessing, RMSEC, RMSECV, R^2cal, and R^2CV for each physiological variable. Results are shown for models developed using the complete dataset and, when applicable, after the exclusion of previously identified anomalous observations. MC: mean centering; SNV: standard normal variate; 1st Der: first derivative; 2nd Der: second derivative.

	PLS-R						***SVM-R***					
	Dataset	***Prepro***	***RMSEC***	***RMSECV***	***R2 (Cal)***	***R2 (CV)***	***Dataset***	***Prepro***	***RMSEC***	***RMSECV***	***R2 (Cal)***	***R2 (CV)***
A	Complete Exclude	1st Der - MC ---	2.40 ---	2.75 ---	0.584 ---	0.474 ---	Complete Exclude	1st Der - MC ---	2.55 ---	2.93 ---	0.597 ---	0.422 ---
ETR	Complete Exclude	SNV - MC ---	16.64 ---	17.36 ---	0.469 ---	0.423 ---	Complete Exclude	SNV - MC ---	13.88 ---	16.11 ---	0.662 ---	0.518 ---
Emm	Complete Exclude	2nd Der - MC ---	0.648 ---	0.715 ---	0.362 ---	0.424 ---	Complete Exclude	1st Der - MC ---	0.700 ---	0.768 ---	0.305 ---	0.144 ---
NPQ	Complete Exclude	SNV - MC SNV - MC	15.38 6.66	16.19 9.97	0.072 0.366	0.010 0.308	Complete Exclude	SNV - MC *SNV - MC*	13.45 2.10	14.69 3.02	0.307 0.940	0.158 0.871
PhiCO2	Complete Exclude	SNV - MC *2nd Der - MC*	3.19 0.002	3.50 0.002	0.078 0.637	0.001 0.532	Complete Exclude	SNV - MC 1st Der - MC	3.32 0.002	3.36 0.002	0.103 0.615	0.082 0.432
PhiPS2	Complete Exclude	SNV - MC 2nd Der - MC	22.23 0.03	24.39 0.03	0.077 0.483	0.001 0.414	Complete Exclude	SNV - MC SNV - MC	23.23 0.021	23.26 0.025	0.186 0.688	0.016 0.517
TleafEB	Complete Exclude	SNV - MC 2nd Der - MC	20.19 0.17	22.15 0.20	0.078 0.261	0.001 0.072	Complete Exclude	SNV - MC 1st Der - MC	21.04 0.183	21.12 0.199	0.237 0.367	0.001 0.132
gsw	Complete Exclude	SNV - MC 2nd Der - MC	3.93 0.04	4.31 0.05	0.077 0.342	0.001 0.230	Complete Exclude	SNV - MC 1st Der - MC	4.09 0.048	4.13 0.051	0.035 0.379	0.080 0.169
qL	Complete Exclude	SNV - MC 2nd Der - MC	2.16 0.43	2.43 0.56	0.121 0.389	0.001 0.066	Complete Exclude	SNV - MC 1st Der - MC	2.27 0.513	2.30 0.528	0.084 0.181	0.021 0.066
qP	Complete Exclude	SNV - MC SNV - MC	2.17 0.52	2.44 0.56	0.127 0.162	0.004 0.050	Complete Exclude	SNV - MC 1st Der - MC	2.30 0.524	2.32 0.538	0.092 0.198	0.037 0.105
Altura (cm)	Complete Exclude	1st Der - MC ---	4.61 ---	5.79 ---	0.408 ---	0.141 ---	Complete Exclude	SNV - MC ---	4.67 ---	5.08 ---	0.322 ---	0.287 ---
Peso freso (g)	Complete Exclude	2nd Der - MC ---	17.17 ---	20.64 ---	0.554 ---	0.369 ---	Complete Exclude	1st Der - MC ---	18.19 ---	23.12 ---	0.507 ---	0.201 ---
Pot. Hídrico (psi)	Complete Exclude	1st Der - MC ---	83.62 ---	95.43 ---	0.571 ---	0.450 ---	Complete Exclude	SNV - MC ---	64.82 ---	94.11 ---	0.642 ---	0.528 ---

Table S6.2. Performance of PLS-R and SVM-R models developed from portable NIR spectra to examine relationships with physiological variables. The table reports RMSEC, RMSECV, R^2cal, and R^2CV for each physiological variable using the complete dataset and, when applicable, after the exclusion of previously identified anomalous observations. All portable NIR models were developed using MSC followed by mean centering.

	PLS					***SVM-R***				
	Dataset	***RMSEC***	***RMSECV***	***R2 (Cal)***	***R2 (CV)***	***Dataset***	***RMSEC***	***RMSECV***	***R2 (Cal)***	***R2 (CV)***
A	Complete Exclude	3.1745 --	3.5539 --	0.461 --	0.339 --	Complete Exclude	3.31779 --	3.47446 --	0.431251 --	0.348035 --
ETR	Complete Exclude	13.1691 --	14.3604 --	0.539 --	0.457 --	Complete Exclude	13.7082 --	14.3111 --	0.515934 --	0.464094 --
Emm	Complete Exclude	3.2226 --	3.5209 --	0.445 --	0.344 --	Complete Exclude	3.31779 --	3.47446 --	0.418543 --	0.360365 --
NPQ	Complete Exclude	10.9391 5.0604	12.435 5.4822	0.175 0.401	0.022 0.306	Complete Exclude	9.4243 1.04199	11.3979 5.01301	0.433412 0.979631	0.111245 0.441545
PhiCO2	Complete Exclude	2.3302 0.0020313	2.6225 0.023188	0.097 0.418	0 0.262	Complete Exclude	2.42663 0.0021050	2.4619 0.0022663	0.0806392 0.400638	0.0026517 0.28451
PhiPS2	Complete Exclude	16.2131 0.020372	18.1503 0.023219	0.097 0.562	0 0.440	Complete Exclude	17.0977 0.021556	17.1021 0.0225924	0.0007177 0.523857	0.0431451 0.468881
TleafEB	Complete Exclude	19.2628 12.4895	21.221 14.1968	0.217 0.375	0.088 0.218	Complete Exclude	13.7825 8.23472	19.626 12.5543	0.624079 0.75828	0.188796 0.377299
gsw	Complete Exclude	2.8392 0.075411	3.2869 0.089608	0.114 0.379	0 0.173	Complete Exclude	3.00561 0.0761873	3.02919 0.0842629	0.02383 0.434791	0.00766 0.249471
qL	Complete Exclude	1.5682 0.035149	1.7811 0.044789	0.152 0.427	0.013 0.16	Complete Exclude	1.63305 0.2514	1.69723 0.297557	0.332516 0.635582	0.0709182 0.132219
qP	Complete Exclude	1.553 0.10298	1.7879 0.13489	0.185 0.306	0.024 0.024	Complete Exclude	1.68093 0.255016	1.70082 0.304475	0.203073 0.631436	0.0875709 0.160888
Altura (cm)	Complete Exclude	4.3554 --	5.4926 --	0.477 --	0.217 --	Complete Exclude	4.85484 --	5.06582 --	0.374419 --	0.310871 --
Peso freso (g)	Complete Exclude	18.8572 --	23.5276 --	0.459 --	0.211 --	Complete Exclude	21.537 --	22.9618 --	0.40917 --	0.249301 --
Pot. Hídrico (psi)	Complete Exclude	70.8525 --	91.6579 --	0.696 --	0.514 --	Complete Exclude	68.7138 --	83.2499 --	0.73512 --	0.5999 --

Figure S6.3. Genotype-specific Spearman correlations between relative gene expression and physiological variables in the combined control and water-deficit dataset. Rows correspond to the expression of DHN1, LEA4, and TRDX for genotypes G4, G5, and G6, whereas columns represent physiological variables. Cell values indicate Spearman's correlation coefficient (ρ). Positive and negative associations are shown according to the colour scale. Asterisks indicate statistically significant correlations ($p < 0.05$), and "ns" denotes non-significant associations.

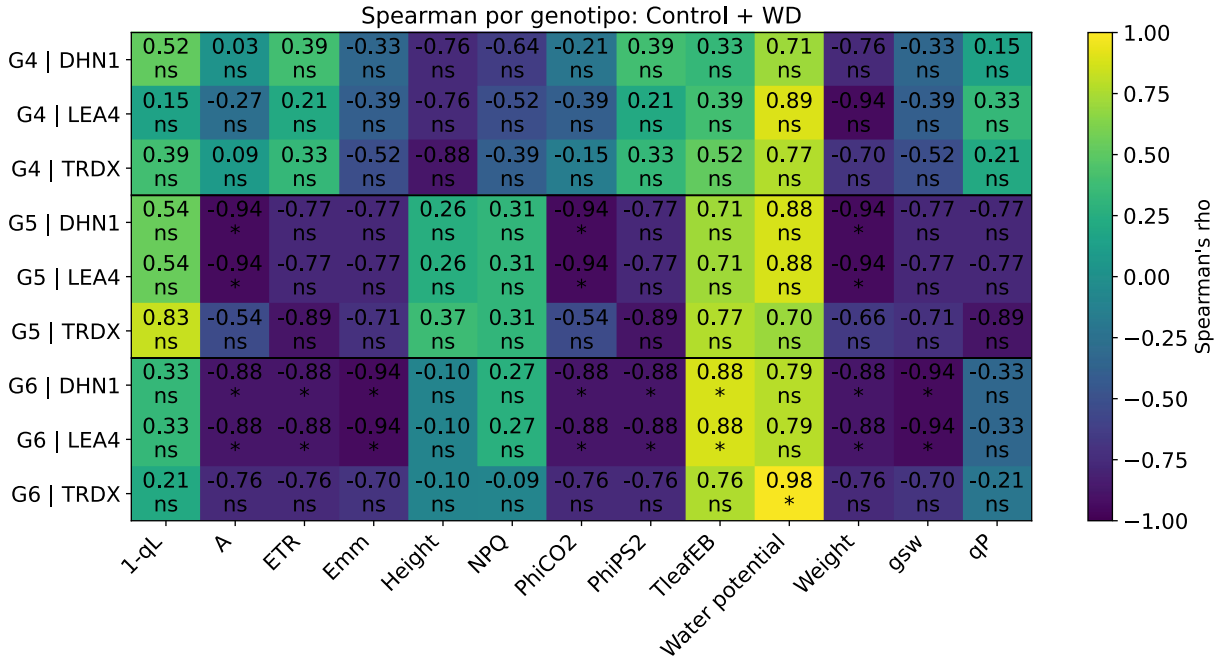

Table S6.3. Summary of the spectral–gene regression models showing the highest cross-validation coefficients for each gene, assay, and spectral platform. PLS-R and SVM-R models were developed to examine linear and nonlinear multivariate associations, respectively, between VIS–NIR HSI or portable NIR spectra and the relative expression of DHN1, LEA4, and TRDX. The table reports model complexity, calibration and cross-validation coefficients of determination, and calibration and cross-validation errors. Models were selected according to R^2CV and were interpreted as exploratory associations rather than validated predictors of transcript abundance. LV: latent variables; SV: support vectors; R^2cal: coefficient of determination in calibration; R^2CV: coefficient of determination in cross-validation; RMSEC: root mean square error of calibration; RMSECV: root mean square error of cross-validation.

Assay	Gene	Technique	Model	LV/SVs	Cost/gamma	R^2cal	R^2CV	RMSEC	RMSECV
I	DHN1	VIS-NIR HSI	PLS-R	3	--	0.6518	0.3249	3.161	3.382
I	LEA4	VIS-NIR HSI	PLS-R	1	--	0.4733	0.3100	1.700	1.733
I	TRDX	VIS-NIR HSI	PLS-R	2	--	0.7300	0.2900	1.204	1.342
I	DHN1	VIS-NIR HSI	SVM-R	18	100/0.316	0.8105	0.5496	0.800	1.214
I	LEA4	VIS-NIR HSI	SVM-R	18	100/0.316	0.9344	0.3379	0.315	1.036
I	TRDX	VIS-NIR HSI	SVM-R	17	100/0.01	0.6239	0.3522	0.753	0.910
II	DHN1	VIS-NIR HSI	PLS-R	5	--	0.7538	0.0392	757	1496
II	LEA4	VIS-NIR HSI	PLS-R	1	--	0.1050	0.0452	1.569	1.588
II	TRDX	VIS-NIR HSI	PLS-R	5	--	0.7438	0.0392	756	1496
II	DHN1	VIS-NIR HSI	SVM-R	17	100/10	0.7580	0.0831	141	181
II	LEA4	VIS-NIR HSI	SVM-R	17	100/0.1	0.9998	0.4820	0.014	0.757
II	TRDX	VIS-NIR HSI	SVM-R	8	0.001/1e-6	0.1227	0.0469	1.301	1.321
II	DHN1	portable NIR	PLS-R	5	--	0.8528	0.1652	106	203
II	LEA4	portable NIR	PLS-R	4	--	0.8317	0.3044	1.304	1.455
II	TRDX	portable NIR	PLS-R	3	--	0.7075	0.0844	1.595	2.000
II	DHN1	portable NIR	SVM-R	8	31.62/0.1	0.3214	0.0973	0.820	0.938
II	LEA4	portable NIR	SVM-R	7	31.62/0.032	0.4144	0.1902	0.815	0.924
II	TRDX	portable NIR	SVM-R	8	10/0.032	0.3479	0.1661	1.135	1.121

Chapter 7
General Conclusions and Future Perspectives

7.1. General Conclusions and Future Perspectives

This Ph.D. thesis demonstrated the potential of visible–near infrared hyperspectral imaging and portable near-infrared spectroscopy, combined with chemometrics and machine-learning methods, for the non-destructive monitoring of water-deficit responses in juvenile *Eucalyptus* plants. The proposed analytical strategy enabled the detection of spectral changes associated with progressive water deficit and provided complementary information on genotype variability, physiological impairment, and recovery after rewatering.

VIS–NIR hyperspectral imaging differentiated water-deficit stages more effectively than the vegetation indices evaluated and preserved spatial information that allowed heterogeneous stress-related responses to be visualized within the plants. Portable NIR spectroscopy also distinguished control and water-deficit conditions and showed particular sensitivity to hydration-related changes. However, classification performance decreased when consecutive stress stages were evaluated simultaneously, indicating that water-deficit progression represents a continuous process with partially overlapping spectral characteristics.

From a chemometric perspective, no universal superiority of linear or nonlinear classification methods was observed. Model performance depended on the spectral modality and on the complexity and structure of the classification problem. In the initial VIS–NIR HSI assay, both linear PLS-DA and nonlinear SVM-DA achieved high performance using mean spectra, although SVM-DA provided the most consistent pixel-level spatial reconstructions. In the expanded assay, the best-performing direct models alternated between linear and nonlinear approaches: SVM-C performed best for binary VIS–NIR HSI discrimination, PLS-DA for multiclass VIS–NIR HSI classification, PLS-DA for binary portable NIR discrimination, and XGBoost for multiclass portable NIR classification. These results indicate that increasing model complexity does not necessarily improve prediction and that model selection should be guided by the spectral domain, classification objective, and independent-validation performance rather than by a priori preference for linear or nonlinear algorithms.

Spectral preprocessing was likewise an important component of model performance, but no single preprocessing strategy was optimal across all datasets and analytical objectives. Derivative-based preprocessing combined with mean centering was particularly effective for

VIS–NIR HSI, where it enhanced subtle spectral features associated with pigments and stress progression. In contrast, portable NIR generally benefited from smoothing and scatter-correction procedures such as MSC or SNV, consistent with the greater influence of scattering and broad overlapping absorption bands in this spectral region. Therefore, future implementations should treat preprocessing and model selection as a joint optimization problem and evaluate candidate pipelines using plant-level cross-validation and independent external validation rather than applying a fixed preprocessing strategy to all spectral platforms.

The application of ANOVA–simultaneous component analysis was essential for identifying the main sources of spectral variability. Genotype was the dominant factor in the VIS–NIR HSI dataset, whereas sampling day and treatment had a greater influence on portable NIR spectra. These results confirmed that the two platforms captured different but complementary dimensions of plant response and that genotype should be explicitly considered during model development rather than treated only as an interfering factor. The ASCA-guided hierarchical models improved the biological interpretation of the classification process, although their transferability must be confirmed using independent experiments and previously unseen genetic material.

Physiological measurements showed that water deficit caused coordinated reductions in plant water status, stomatal conductance, carbon assimilation, and photochemical performance. Spectral regression models reflected part of this physiological variation: VIS–NIR HSI showed its strongest association with non-photochemical quenching, whereas portable NIR spectroscopy showed the clearest relationship with water potential. These associations support the physiological relevance of the spectral information, but they should not be interpreted as direct measurements of isolated physiological variables.

Recovery after rewatering was incomplete and strongly genotype dependent. Restoration of fresh mass did not necessarily imply complete recovery of water status, gas exchange, or photochemical activity. G1 and G5 showed the clearest recovery of water potential, whereas G4 recovered fresh mass but only partially restored its water status. G6 retained considerable water tension despite recovering much of its fresh mass, while G2 and G3 showed limited recovery within the evaluated period. These results demonstrate that recovery is multidimensional and should not be represented as a simple return from a stressed condition to the original control state.

The expression of DHN1, LEA4, and TRDX confirmed the activation of molecular mechanisms associated with dehydration protection, protein stabilization, and redox regulation. Nevertheless, greater gene induction did not necessarily indicate higher tolerance, because it could also reflect more severe physiological disturbance. Among the GloNi hybrids evaluated, G5 showed the most consistent combination of physiological recovery and coordinated molecular response and therefore represents the most promising candidate for further validation under the studied conditions. However, additional evidence from long-term growth, recurrent drought, survival, and field performance is required before it can be considered definitively drought tolerant.

Overall, the central hypothesis of this thesis was supported under controlled experimental conditions. Spectral sensing combined with multivariate analysis enabled early and progressive discrimination of water-deficit responses in *Eucalyptus* and contributed to the identification of contrasting genotype-dependent behaviours. The principal contribution of this work is therefore an integrated and design-aware analytical framework rather than a single universal prediction model. VIS–NIR HSI provides spatially resolved and genotype-sensitive information, portable NIR spectroscopy offers rapid assessment of hydration-related changes, and physiological and molecular measurements provide functional and mechanistic support for spectral interpretation.

The results obtained provide a solid foundation for advancing the application of these analytical tools in forest nurseries and genetic-improvement programs. A key next step will be to validate the developed spectral strategies under operational conditions, including independent experimental campaigns, broader genetic populations, different plant ages, seasonal variation, and environmental conditions representative of commercial nurseries. Standardized acquisition protocols, calibration-transfer procedures, and methods for identifying samples outside the calibration domain will be essential for converting the current analytical framework into a robust tool for routine plant assessment. Within such a workflow, portable NIR spectroscopy could support rapid screening of large plant populations, whereas VIS–NIR HSI could be applied to selected material requiring more detailed genotype-dependent and spatial assessment.

A major projection arising from Chapter 6 and specific objective 5 is the future development of an integrative genotype-performance index combining the three analytical domains evaluated in this thesis. This index could incorporate spectral information derived from validated VIS–NIR

HSI and portable NIR models, physiological indicators of water status, gas exchange, photochemical function, energetic regulation, and whole-plant recovery, together with molecular evidence associated with dehydration protection, protein stabilization, and redox regulation. Physiological variables should be organized into biologically meaningful blocks to avoid overrepresenting strongly correlated measurements, while the relative contribution of each spectral platform should be supported by its independently validated predictive performance. Molecular responses should be incorporated cautiously, considering that high gene induction may represent either effective protection or greater stress intensity.

The biological validity of this integrative index should subsequently be assessed against independent outcomes directly related to plant performance, including survival, growth maintenance, recovery rate, response to recurrent water-deficit cycles, and establishment after transplantation. Once validated, this approach could provide a transparent and reproducible framework for comparing genotypes, prioritizing promising plant material, and supporting decision-making in forest nurseries and breeding programs. For practical implementation in the forestry industry, however, a major challenge will be transferring models developed under controlled experimental conditions to the greater biological and environmental variability encountered in operational nurseries. Differences in genotype, plant age, season, illumination, temperature, leaf orientation, water-deficit history, and instrument response may alter spectral distributions and reduce model transferability. Therefore, initial implementation should be considered as a decision-support workflow rather than as an autonomous diagnostic system. Portable NIR spectroscopy could be used as a first-line, high-throughput screening tool for large plant populations, whereas VIS–NIR HSI could provide a second level of analysis for selected or uncertain material requiring more detailed genotype-dependent or spatial assessment. Successful industrial transfer will require standardized acquisition protocols, calibration-transfer procedures, objective quality-control criteria, identification of samples outside the calibration domain, and progressive expansion of calibration datasets using independent nursery campaigns representative of the genetic, developmental, seasonal, and environmental variability encountered under operational conditions. In this way, the analytical platform developed in this thesis provides a methodological basis for progressing from non-destructive water-deficit detection toward integrated genotype assessment and the future implementation of spectral decision-support tools in precision forestry.

Chapter 8
Appendix

8.1. Productivity during the doctoral program

8.1.1. Participation in scientific articles

Doctoral thesis products

I. January 2026 (Published). Pamela Sanhueza-Novoa, Marta Fernández, Carolina Hernández-Fuentes, Sofía Valenzuela, Muhammad Qasim Hayat, Ricardo Ramírez H. and Rosario del P. Castillo. Detection of water deficit stress in *Eucalyptus spp.* through VIS-NIR hyperspectral imaging and chemometric methods. https://doi.org/10.1016/j.saa.2025.126675

II. July 2026 (Under Review). Pamela Sanhueza-Novoa, Marta Fernández, Carolina Hernández-Fuentes, José Manuel Amigo, Jesús Mellado Castro, Macarena Rojas-Rioseco and Rosario del P. Castillo. ASCA-guided hierarchical machine learning for spectral water-deficit monitoring in *Eucalyptus* using hyperspectral imaging and portable NIR spectroscopy.

III. (In preparation) Pamela Sanhueza-Novoa, Marta Fernández, Carolina Hernández-Fuentes, Rosario del P. Castillo. Genotype-dependent water-deficit recovery in *Eucalyptus* revealed by physiological, spectral, and molecular responses.

Related to the doctoral program

I. August 2025 (Published). Martín Bravo-Arrepol, Eugenio Sanfuentes, José Amigo, Rodrigo Hasbún, Cristian Fuentes, Angella Navarro, Pamela Sanhueza, Rosario del P. Castillo. Early detection of *Fusarium circinatum* in *Pinus radiata* cuttings using VIS-NIR hyperspectral imaging and multivariate analysis. https://doi.org/10.1016/j.saa.2025.126778

II. July 2026 (Published). Cristian A. Fuentes, Esmanur Ilhan, Mariia Ivanova, Macarena Rojas-Rioseco, Pamela Sanhueza-Novoa, Aylin Ozgür Goksu, Mecit Halil Oztop, Leonid Grunin, Rosario del P. Castillo. A multivariate analysis strategy for a comparative study of pectin production methods using time–domain NMR. http://doi.org/10.1016/j.microc.2026.119112

Products From Other Collaborations

I. June 2026 (Published). Yasmin Lima Brasil, Giulia Gorla, Darlei G.D.B. Oliveira, Pamela Sanhueza-Novoa, Fernanda Araujo Honorato, José Manuel Amigo, Douglas Fernandes Barbin. Vegetable Protein Ingredients Using Multispectral Imaging and Chemometrics: a strategy to detect potential minor allergens in bulk materials. https://doi.org/10.1016/j.microc.2026.118639

II. August 2026 (Published). Yasmin Lima Brasil, Giulia Gorla, Darlei G. D. B. Oliveira, Pamela Sanhueza-Novoa, José Manuel Amigo, Douglas Fernandes Barbin. New Approaches for Monitoring Edible Coating Quality Using Hyperspectral Imaging (HSI) and Chemometrics.
https://doi.org/10.1007/s11483-026-10208-7

III.

8.1.2. Congress presentations

Internationals

I. June 2025. 22nd International Conference on Near Infrared Spectroscopy, Rome, Italy. Poster presentation: Spectral evaluation of *Eucalyptus* spp. under water deficit using HSI VIS-NIR and near-infrared spectroscopy: An ASCA-based approach.

II. June 2025. 22nd International Conference on Near Infrared Spectroscopy, Rome, Italy. Poster presentation: Classification of texturized vegetable protein ingredients using hyperspectral and multispectral imaging and chemometrics: Detection of allergenic sunflower proteins.

III. September 2024. XIX Chemometrics in Analytical Chemistry. Santa Fe, Argentina. Poster presentation: Detection of water deficit stress in *Eucalyptus* spp. through VIS-NIR hyperspectral imaging technologies and multivariate analysis.

IV. July 2024. International Association of Spectral Imaging (IASIM). Bilbao, Spain. Oral presentation: Early detection of water deficit stress in *Eucalyptus* spp. through VIS-NIR hyperspectral imaging technologies and multivariate analysis.

Nationals

I. January 2026. XXXV Jornadas Chilenas de Química, Concepción, Chile. Poster presentation: Análisis de componentes simultáneos ANOVA (ASCA) y espectroscopía HSI VIS-NIR para la clasificación jerárquica de la respuesta de *Eucalyptus* spp. al déficit hídrico.

II. January 2024. XXXIV Jornadas Chilenas de Química, Puerto Varas, Chile. Poster presentation: Detección temprana de estrés hídrico en *Eucalyptus* spp. a través de tecnologías de imágenes hiperespectrales VIS-NIR y análisis multivariado.

III. December 2022. III Congreso Chileno de Parasitología. Poster presentation: Efecto de fijadores histológicos comunes en la estructura química de tejidos de *Anisákidos* analizado por imágenes hiperespectrales.

IV. October 2022. XXIV International Symposium on Advances in Extraction Technologies, XV Encuentro de Química Analítica y Ambiental. Iquique, Chile. Poster presentation: Efecto de fijadores histológicos comunes en la estructura química de tejidos de *Anisákidos* analizado por imágenes hiperespectrales.

8.2. Funding and resources awarded during the doctoral program

I. January 2026. "Beca de Doctorado extensión". Agencia Nacional de Investigación y Desarrollo, Chile.

II. July 2024. Complementary benefit "Gastos operacionales del proyecto de tesis doctoral". Agencia Nacional de Investigación y Desarrollo, Chile.

III. July 2024. Complementary Benefit "Pasantía doctoral en el extranjero". Agencia Nacional de Investigación y Desarrollo, Chile.

IV. May 2023. Fund "Proyecto UCO 1866 para la movilidad académica y estudiantil". Universidad de Concepción y Ministerio de Educación, Chile.

V. July 2022. Fund "Proyecto UCO 1866 para la movilidad académica y estudiantil". Universidad de Concepción y Ministerio de Educación, Chile.

VI. March 2022. "Doctorado Nacional" grant number 21221771. Agencia Nacional de Investigación y Desarrollo, Chile.

8.3. Other relevant activities during the doctoral program

8.3.1. International and national training

I. October 2024 – February 2025. Internship at the University of the Basque Country. ANID Supplemental Benefits Grant.

II. July 2024. Pre-conference course: Workshops of Image transformations, Hyperspectral and Multivariate Image Analysis, and Introduction to deep learning on spectral data. Bilbao, Spain.

III. October 2023. Internship at the University of the Basque Country. FOVI Project 220172 Internship Grant.

IV. October 2022. Pre-conference course: Introduction to Multivariate Calibration. Iquique, Chile.

8.3.2. Teaching participation

I. April 2022 - December 2025 Teaching Collaboration in Instrumental Analysis for Marine Biology, Medical Technology, Chemical Analyst, Pharmacy and Biochemistry careers. University of Concepción.

8.3.3. Participation in science communication

I. October 2025. Talk "Deteccion de estrés causado por el déficit hídrico en *Eucalyptus* spp. mediante imágenes hiperespectrales VIS-NIR y análisis multivariado" as part of the "CB-UdeC Chat Series." Biotechnology Center, University of Concepción, Chile.

II. August 2025. Talk "El lenguaje invisible de las plantas: Detectando estrés con luz y matemáticas" al Liceo Bicentenario de Excelencia Domingo Ortiz de Rosas, within the framework of the Science Month, Coelemu, Chile.

III. August 2024. Talk "Explorando la química a través de la interacción luz-materia" at Colegio San Jose Lomas Coloradas, within the framework of the Science Month, San Pedro, Chile.

8.3.4. Project applications and innovation initiatives

I. HydroForest: Early diagnosis of water-deficit stress for *Eucalyptus* nurseries. Project proposal submitted to the VIU Program and currently under evaluation by the National Agency for Research and Development (ANID), Chile. The proposal aims to translate the spectral and chemometric methodologies developed during this Ph.D. thesis into a potential non-destructive tool for the early detection of water deficit in *Eucalyptus* nurseries. The funding decision is expected in August 2026.